CANADIAN THESES ON MICROFICHE

I.S.B.N.

THESES CANADIENNES SUR MICROFICHE

National Library of Canada
Collections Development Branch

Canadian Theses on
Microfiche Service

Ottawa, Canada
K1A 0N4

Bibliothèque nationale du Canada
Direction du développement des collections

Service des thèses canadiennes
sur microfiche

NOTICE

The quality of this microfiche is heavily dependent upon the quality of the original thesis submitted for microfilming. Every effort has been made to ensure the highest quality of reproduction possible.

If pages are missing, contact the university which granted the degree.

Some pages may have indistinct print especially if the original pages were typed with a poor typewriter ribbon or if the university sent us a poor photocopy.

Previously copyrighted materials (journal articles, published tests, etc.) are not filmed.

Reproduction in full or in part of this film is governed by the Canadian Copyright Act, R.S.C. 1970, c. C-30. Please read the authorization forms which accompany this thesis.

THIS DISSERTATION
HAS BEEN MICROFILMED
EXACTLY AS RECEIVED

AVIS

La qualité de cette microfiche dépend grandement de la qualité de la thèse soumise au microfilmage. Nous avons tout fait pour assurer une qualité supérieure de reproduction.

S'il manque des pages, veuillez communiquer avec l'université qui a conféré le grade.

La qualité d'impression de certaines pages peut laisser à désirer, surtout si les pages originales ont été dactylographiées à l'aide d'un ruban usé ou si l'université nous a fait parvenir une photocopie de mauvaise qualité.

Les documents qui font déjà l'objet d'un droit d'auteur (articles de revue, examens publiés, etc.) ne sont pas microfilmés.

La reproduction, même partielle, de ce microfilm est soumise à la Loi canadienne sur le droit d'auteur, SRC 1970, c. C-30. Veuillez prendre connaissance des formules d'autorisation qui accompagnent cette thèse.

LA THÈSE A ÉTÉ
MICROFILMÉE TELLE QUE
NOUS L'AVONS REÇUE

NL-339 (r. 82/08)

Canada

BLOCKAGE EFFECTS IN CLOSED-THROAT WIND TUNNEL TESTING

by

© Philippe P. DesRosiers

A thesis
presented to the School of Graduate Studies
of the University of Ottawa
in partial fulfillment of the
requirements for the degree of
Master of Applied Science
in
Civil Engineering

OTTAWA, Ontario, 1982

UNIVERSITÉ D'OTTAWA
UNIVERSITY OF OTTAWA

A MES PARENTS

LA NATURE AGIT PAR PROGRES. ITUS ET REDITUS, ELLE PASSE ET REVIENT, PUIS VA PLUS LOIN, PUIS DEUX FOIS MOINS, PUIS PLUS QUE JAMAIS, ETC.

BLAISE PASCAL

ABSTRACT

Blockage correction equations for bluff bodies in closed-throat wind tunnel testing have been derived semi-empirically since the 1930's. These blockage correction equations were all designed to correct for the drag coefficient and this in smooth flow only. The range of these equations was not really extended to the lift coefficient (except by Maskell) nor to turbulence in the flow field and were valid for angles of incidence of less than 10 degrees. Furthermore they were not designed to correct for blockage ratios much greater than 15 percent.

This thesis examines some of the better known and accepted blockage correction equations and compares them with one another. It also verifies the validity of these corrections in the case of high blockage ratios (up to 37.2 percent) and in the case of turbulence in the flow. A new blockage correction equation is proposed and ascertained to be equally valid for the correction of either drag or lift either in a smooth or turbulent stream and at any angle of incidence. The effects of turbulence on the flow around a bluff body are also examined.

The proposed blockage correction equation has the form:

$$C_{D_c} = \frac{C_{D_u}}{1 + S/C} \frac{\varepsilon M}{\varepsilon M_o},$$

where C_{D_c} is the corrected drag coefficient,

C_{D_u} is the uncorrected drag coefficient,

S is the projected face area of the model,

C is the wind tunnel test section area,

εM is a base pressure parameter term equal to $1/k^2+1$, where $k^2 = 1 - C_{P_b}$, and where C_{P_b} is the base pressure coefficient, and

εM_o is the base pressure parameter term regressed for zero blockage.

It is found in this thesis that the above blockage correction equation is valid for correcting lift and drag coefficients in either a smooth or turbulent stream and for any blockage ratio. It is also believed that this equation is equally valid for the moment coefficient.

It was also found that contrary to popular belief, turbulence in the flow field does not affect the blockage corrections and that most blockage correction equations are equally suited in turbulence. However, blockage correction equations which take the base pressure into account in one way or another are better suited for correcting lift or drag in a turbulent stream.

ACKNOWLEDGEMENTS

The author wishes to express his deepest gratitude and respect to his advisor Dr. Hiroshi Tanaka for his continuous guidance and encouragement throughout this thesis. Special recognition is due to Mr. Kevin Cooper for his assistance and comments on this research.

The author also wishes to express his appreciation to the following for their help and assistance:

Mr. Mike Burns
Mr. Greg Duchesne
Mr. Claude Lavigne
Miss Gianna Mari
Mrs. Monique Marinier
Mr. William Watson
Miss Nicole Renaud

Finally, the author wishes to extend his gratitude to the National Sciences and Engineering Research Council of Canada for their support without which this work would not have been possible.

CONTENTS

LIST OF FIGURES (In Text)

LIST OF TABLES (In Text)

LIST OF FIGURES (Appendix A)

LIST OF TABLES (Appendix C)

LIST OF FIGURES (Appendix C)

Chapter I

HISTORICAL DEVELOPMENTS IN WIND TUNNEL TESTING

1.1 THE NEED TO EXPERIMENT

Classical hydromechanics began with Daniel Bernoulli (1700-1782). In his treatise "Hydrodynamica", Bernoulli stated his first principle, a fundamental theorem of fluid dynamics as follows: "In the case of steady flow of a fluid that is incompressible and non-viscous, the energy of a unit volume of a fluid is conserved along a streamline. More specifically to be expressed as the algebraic sum of three terms, the pressure, kinetic energy per unit volume and potential energy per unit volume, has a same value at any two points on a streamline."

Although this theory of the potential flow of an incompressible fluid has been well developed by other researchers, it is of limited applicability because, being based on the assumption that the fluid is totally non-viscous, it cannot account for profile drag and other boundary layer effects. While the mathematical theory of boundary-layer flow provides a basis of extrapolation from model to full scale

conditions, it is quite complex and is not readily acceptable for use in routine calculations.

Much theoretical work has been devoted to the motion of an inviscid compressible fluid, and the theory is still being developed. As the theory of boundary layers in compressible fluids contains many intricacies, it has not yet been developed to the same extent as for incompressible fluids. In general, therefore, the theory is incomplete requiring supplementary testing via experimentation. This is achieved most conveniently on a scaled model test in a wind tunnel.

From the point of view of design, such experiments have two principal uses. First, they make it possible to study various designs or variation of designs in a direct and relatively economical manner. The second use of experiments in fluid flow is the gathering of information, usually in conjunction with theoretical work, which either confirms or denies a proposed theory but usually furthers it, thus laying the foundation for future design improvements.

1.2 SIMULATED WIND STUDIES

The 18th century saw experimenters trying to create artificial airflow around their models to simulate the variable nature of natural wind. In 1746, Robins published two papers under the title "Resistance of the Air" and "Experiments Relating to Air Resistance" which described his invention, namely a whirling table or arm apparatus used to measure wind forces as illustrated in Figure 1.2.1.

John Smeaton (1742-1792), the "first civil engineer", improved Robins' whirling arm and with it tested models of windmill sails (Figure 1.2.2). His interest in wind speeds and pressures provided valuable data for builders, bridge designers and architects of that period. It can be noted that engineering literature of the period was flooded by conflicting empirical relations relating wind speeds with wind pressures.

The first wind tunnel to be built is credited to Francis Wenham. A description of the apparatus was published by the Aeronautical Society of Great Britain in their 1871 Annual Report. A fan blower delivered air through a square duct of 3 metre length and 0.5 metre sides. Lift and drag forces on plates were measured by spring deflections.

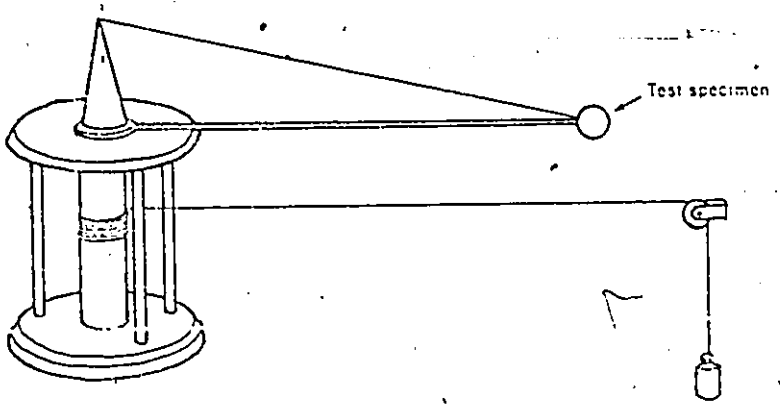

FIGURE 1.2.1 - SKETCH OF THE WHIRLING ARM USED BY ROBINS

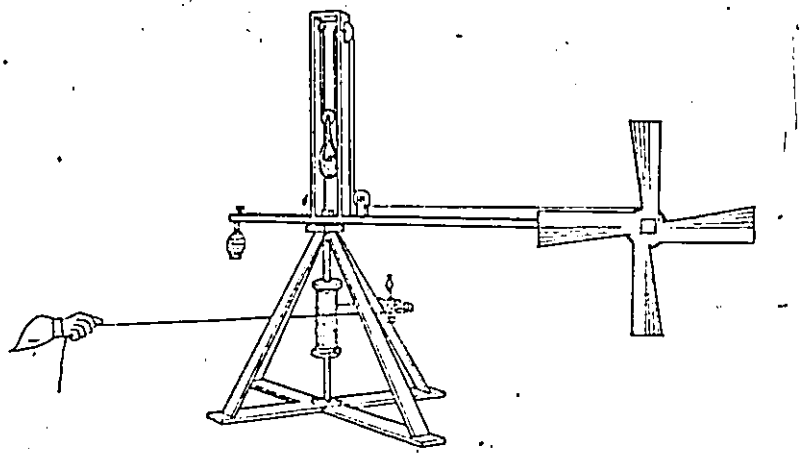

FIGURE 1.2.2 - SMEATON'S ADAPTATION OF ROBINS' WHIRLING ARM FOR WINDMILL TESTS

1.3 EARLY WIND TUNNEL STUDIES

The earliest reference to wind tunnel investigations of wind pressure on a plate appears to be that carried out by J.O.V. Irminger in Denmark. Irminger, head of the Gas Works in Copenhagen decided to use the updraft in one of the smoke stacks as the source for airflow. An opening was made on the side of the chimney and a retangular box 40 inches in length and 4.5 by 9 inches in cross-section was inserted. A shutter was used to control the speed of the air current.

His studies included pressure distribution on flat plates, a model of a bird's wing (probably the first aerofoil tested in a wind tunnel) and building models (Figures 1.3.1 and 1.3.2). The first results of Irminger's experiments were published in 1894 in Denmark and England.

In 1906, a famous civil engineer, Gustave Eiffel built a wind tunnel at the foot of his equally famous tower. With a horizontal test chamber five feet in diameter and powered by the tower's generators, this was probably the biggest wind tunnel in existence in its days. Over the next five years and more than 5000 experiments later, Eiffel had made major contributions to the design of wings and propellers.

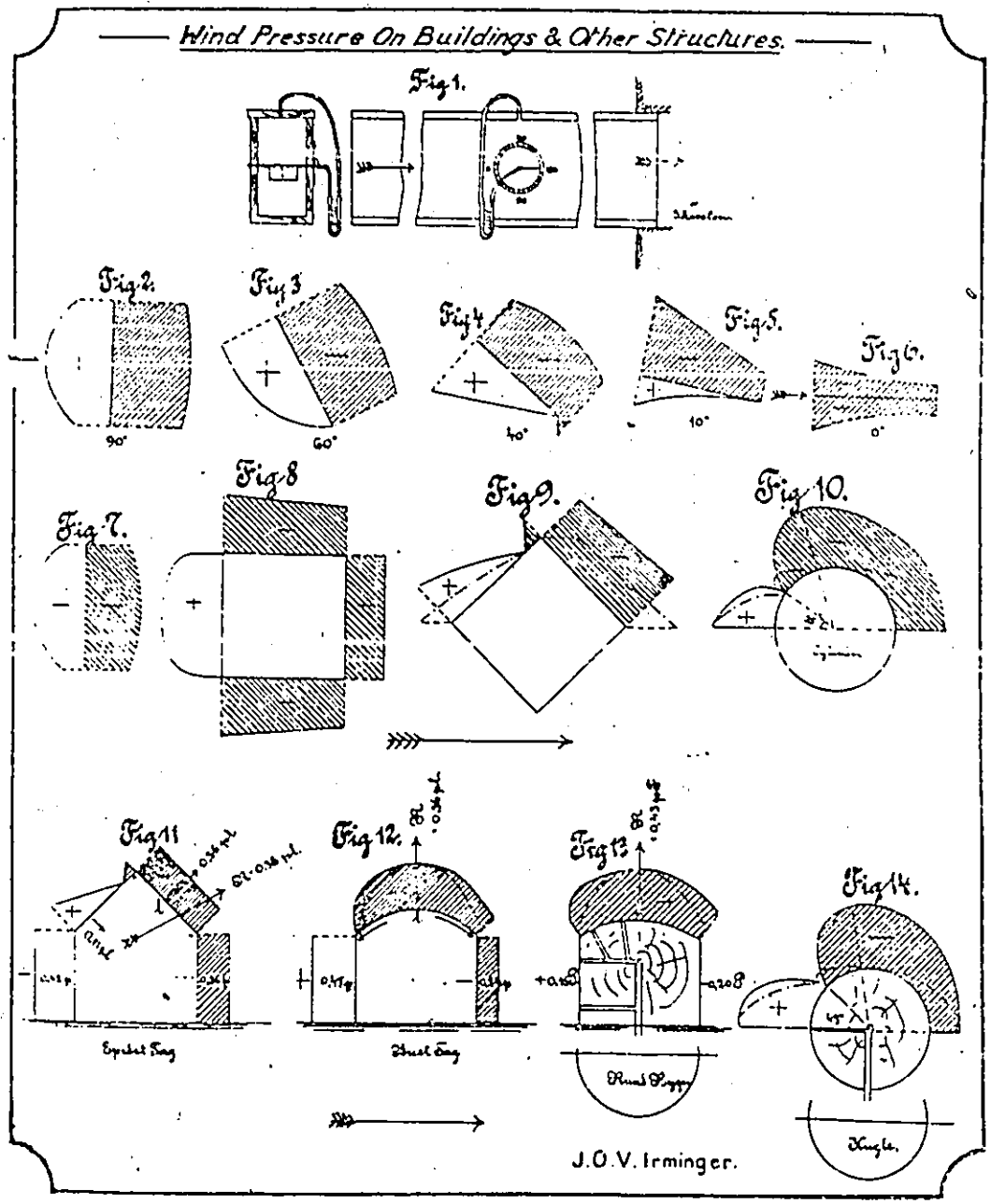

FIGURE 1.3.1 - PRESSURES ON BUILDINGS AFTER IRMINGER

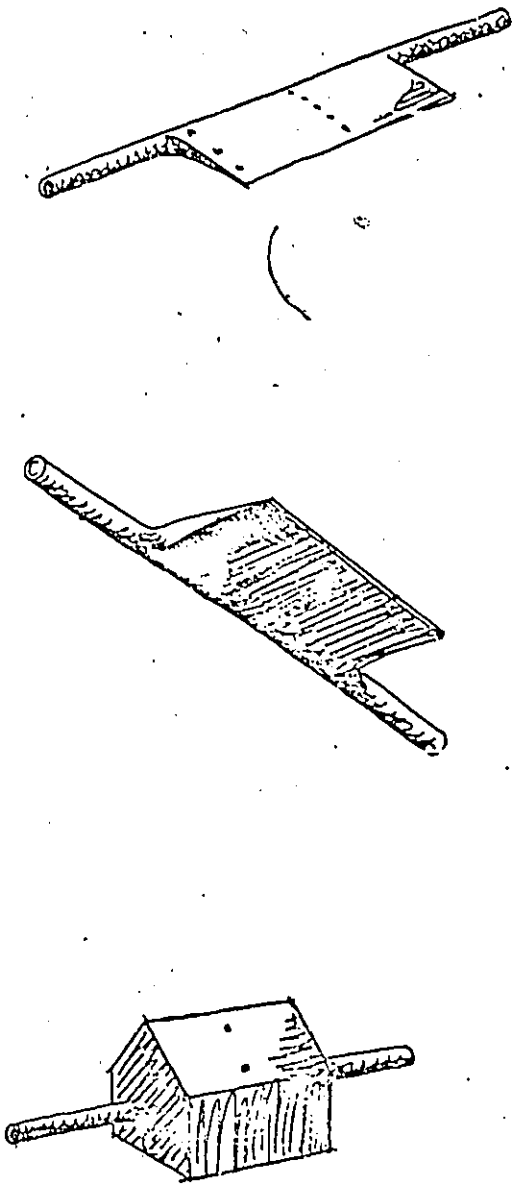

FIGURE 1.3.2 - MODEL OF BIRD'S WING AND BUILDING MODEL TESTED BY IRMINGER

In 1912, Eiffel built another wind-tunnel, in Auteuil. This one was larger and more powerful than the first, having a test chamber 6.5 feet in diameter and a maximum possible wind speed of 71 mph. During the next years, he studied complete scale models of eminent aircraft pioneers. To name but a few: Wright, Blériot, Farman --- even the Allied fighter planes of the First World War were tested at the Laboratoire Eiffel[1].

1.4 WIND TUNNEL INVESTIGATIONS TODAY

Since the first wind tunnel tests of Wenham, much progress has been made. Wind tunnel tests for civil engineering structures have been found to differ greatly in modelling characteristics compared to aeronautical structures. Due to the proximity of the ground to civil structures, there is a turbulent boundary layer which has to be reckoned with. To this effect, Martin Jensen [19, 20] formulated his "Model" law in 1958. "The correct model test for phenomena in the wind must be carried out in a turbulent boundary layer and the model law requires that this boundary layer be to scale

---

[1] The Auteuil laboratory still fuctions with its original equipment, logging an average 10,000 hours of experimental work annually. It is used mostly for stability tests of high-rise structures and automobile wind-stream tests. The German firm Porsche has carried out many tests on its racing cars at Auteuil.

as regards the velocity profile."

With this knowledge, wind tunnel tests today ascertain not only the wind forces to be reckoned with but also give us an indication of the environmental effects this structure will have on its surroundings.

We have indeed made progress since Robins' whirling arm...

1.5 CLOSED-THROAT WIND TUNNEL TESTING PROBLEMS

Although wind tunnel tests are extremely useful, the nature of the model under test as well as the wind tunnel configuration induces experimental problems. In closed-throat wind tunnels the problems stem from wall constraints. Chief among these constraints are the problems of boundary layer flow on the walls and the solid blockage of the flow due to the physical characteristics of the model as well as the wake blockage due to the constraining effects of the walls, floor and ceiling of the test section.

The problem of blockage was first studied by Glauert [16] in 1933. Thom [48], Herriot [49] and Hensel [50] studied the problem in the 1940's and 50's. Maskell [24] and Cowdrey [7, 8] did much research on the problems of solid

and wake blockage in the 1960's. Additional research on this problem was performed by Modi and El-Sherbiny [28], Ranga Raju and Garde [36], Courchesne and Laneville [6] and Hackett and Wilsden [51] in the 1970's.

Some of the contemporary equations for blockage correction will be evaluated in this research and a new blockage correction will be proposed. It is the intent of this study to extend the blockage correction theories from smooth flow to turbulent flow and from low blockage ratios (about 10%) to high blockage ratios (about 40%). This new blockage correction equation will also be valid for any angle of incidence.

Chapter II

THE PROBLEM OF BLOCKAGE IN CLOSED-THROAT WIND TUNNEL TESTING

2.1 BOUNDARY CONSTRAINT

In a closed-throat wind tunnel, the working section has rigid boundaries, namely the side walls, floor and roof of the test section. At the rigid boundaries, the velocity component normal to the walls must be zero. The imposition of this boundary condition causes the flow around a body placed in the working section of the wind tunnel to differ from that of the same body in an unlimited stream.

2.2 SOLID BLOCKAGE AND WAKE BLOCKAGE

The general nature of the interference caused by the rigid boundaries can be visualized in Figure 2.2.1 and 2.2.2. The most obvious effect of the wall constraint is that the lateral expansion of the streamlines in the region of the model will be restricted. This will produce an increased axial velocity in the vicinity of the model. The increase in axial velocity at the model is dependent on the

volume distribution of the body itself, i.e. its partial blocking of the flow in the presence of boundary constraint. This is refered to as solid blockage.

The other interference is wake blockage. Pankhurst and Holder [32] explain the mechanics of this problem in their book on wind tunnel technique.

> The total head of the fluid in the wake of a body is less than that in the region outside since the static pressure in a tunnel is practically constant across any given section normal to the stream (provided this section is not too close to the trailing edge of the model), it follows that the dynamic head, and hence the velocity, in the wake of the model must be lower than in the surrounding stream. In order to satisfy the condition of continuity of mass flow in a closed-throat tunnel, therefore, the velocity of the fluid outside the wake must exceed the velocity far upstream of the model, whereas in free air these velocities are equal. Thus the axial velocity in a closed-throat tunnel gradually increases past the model (except for the reduced velocity inside the wake), and the velocity at the position of the model is correspondingly greater than the tunnel speed. This effect is termed wake blockage.

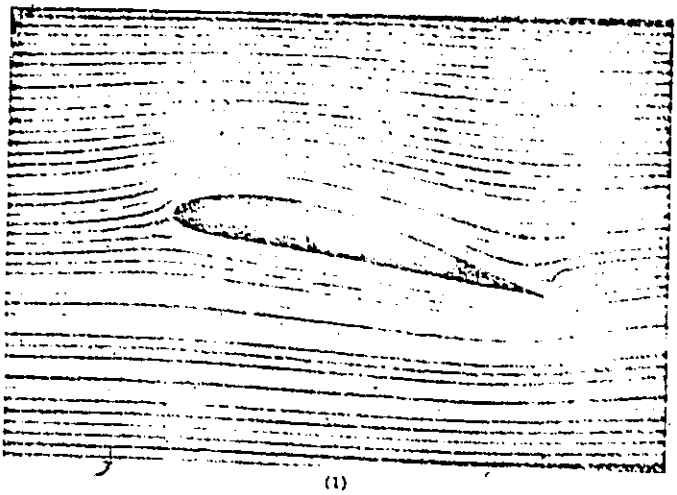

(1)

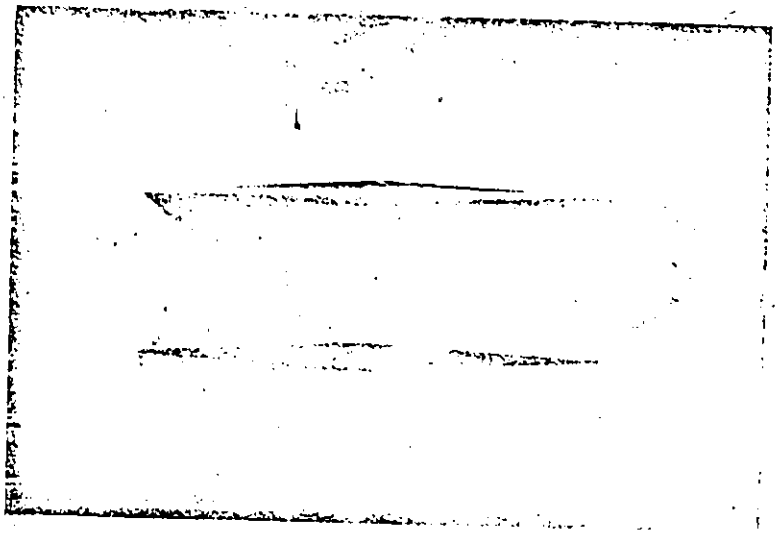

(2)

FIGURE 2.2.1

(1) FLOW AROUND AEROFOIL

(2) SURFACE-WAVE PHOTOGRAPH OF FLOW PAST A PAIR OF DOUBLE-WEDGE AEROFOILS

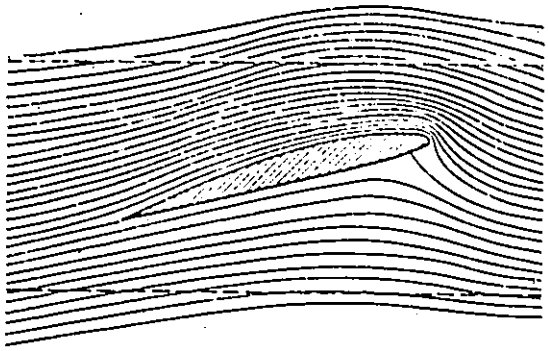

Full Lines are Streamlines in an Unlimited Fluid
Broken Lines are Tunnel Walls (Streamlines of Flow in Tunnel)

FIGURE 2.2.2

WALL CONSTRAINT IN A CLOSED-THROAT WIND TUNNEL

2.3 BLOCKAGE CORRECTION

Little focus has been given to the problem of wall constraint on non-streamline flow past a bluff body since Glauert [16] in 1933. Glauert's approach in the two-dimensional problem seems to have stemmed from the experiments of Fage and Johansen [11, 12] on the flow past an inclined flat plate spanning a wind tunnel. His study of the blockage effect associated with the bluff body wake led Fage and Johansen to test several plates of different sizes and establish the drag coefficient of a two-dimensional flat plate normal to an unlimited stream by extrapolation.

Glauert suggested that for a wing completely spanning a closed-throat wind tunnel, the wake blockage factor ε_ω may be written as:

$$\varepsilon_\omega = \eta \frac{t}{h}$$

where t is the thickness of the wing,
h is the tunnel height, and
η is an empirical factor.

Using his correction factor, Glauert proposed that the ratio of drag in the wind tunnel to its value in an unlimited stream is:

$$\frac{D}{D_c} = \left[1 - \eta \frac{t}{h}\right]^{-2}$$

where D is the drag force and

D_c is the corrected drag force.

The presence of the empirical factor η reduces Glauert's formula to an interpolation between experimental results. These are not sufficiently accurate to support the proposed functional dependence of t/h. Thus the formula was not widely used, the following wake blockage correction equation being prefered to it (see, for example Pankhurst and Holder [32] and Pope [34]):

$$\frac{\Delta q}{q} \doteq \frac{1}{2} C_{D_o} \frac{S}{C}$$

where Δq is the effective increase in dynamic pressure of the undisturbed stream,

q is the dynamic pressure upstream of the model,

S is the face area of the model,

C is the cross-sectional area of the tunnel, and

C_{D_o} is the profile drag coefficient.

The above correction unfortunately holds only for streamline flow, the bluff body problem requiring a different treatment.

Thom [48] expanded the work of Glauert and others to facilitate the estimation of the blockage of streamlined, attached-flow bodies in closed tunnels. Herriot [49] provided tables to cover a much wider range of aerodynamic bodies and wing shapes. For automobile shapes,

$$\frac{q_c}{q} = 1 + \frac{2V}{(2C)^{3/2}} + C_{D_u}\frac{S}{4C}$$

where q_c is the corrected dynamic pressure,

q is the dynamic pressure,

V is the airstream velocity,

S is the test section cross-sectional area,

C is the cross-sectional area of the model and

C_{D_u} is the uncorrected drag coefficient.

Thom and Herriot suggest a wake buoyancy correction to drag that can be expressed by

$$\Delta C_{D_w} = \frac{-2V}{(2C)^{3/2}} C_{D_u}$$

where ΔC_{D_w} is the difference in the wake drag coefficent,

V is the airstream velocity,

C is the model cross-sectional area and

C_{D_u} is the uncorrected drag coefficient.

Hensel [50] developed a velocity ratio method (modified by Wilsden) which uses a single measured velocity increment at the ceiling to determine the interference velocity at the model location due to solid blockage. The ratio of the velocity at the model location to the velocity at the tunnel wall was derived for a line doublet of arbitrary span by Hensel.

The interference velocity is deduced from the computed tunnel-axis-to-ceiling velocity ratio and the measured ceiling-to-uncorrected-approach-flow velocity ratio using

$$\frac{u_A}{V_u} = \frac{u'_c}{V_u} \frac{u_A}{u'_c}$$

where $\frac{u_A}{V_u}$ is the velocity increment at the model location due to the presence of walls,

$\frac{u'_c}{V_u}$ is the measured velocity increment at the ceiling,

$\frac{u_A}{u'_c}$ is the computed tunnel-axis-to-ceiling velocity ratio.

An extension of the method by Hansel to allow computation of the axial distribution of the solid and wake blockage velocities as well as a wake buoyancy correction was devised by Hackett and Wilsden [51]. The procedure requires the measurement of ceiling center-line pressure distribution over the length of the test section with the model both present and absent.

2.4 MASKELL'S BLOCKAGE CORRECTION EQUATION

Interest in the problems of blockage constraint resurfaced in the 1950's when marked differences were noticed in the high lift characteristics of models of a particular aircraft tested in different wind tunnels. From the onset of stall, the different sets of results could only be reconciled through some form of wall interference greater than any explained by the standard correction formulae of the period. The purpose of Maskell's [24, 25] investigation of the problem was to establish the existence of such an interference and to provide adequate corrections for it.

Maskell, in his 1963 report [24] states:

> Since it was evident, from the outset, that the effect was connected with the breakdown of streamline flow over the wing, it seemed worthwhile to concentrate attention, in the first instance, upon the extreme situation concerning a wing-like shape --- for example, a thin flat plate is set normal to the wind stream. The blockage constraint on this type of bluff body flow in a wind tunnel with solid walls is therefore the subject [...] of this paper. A theory is developed which provides an estimate of the effective increase in the dynamic pressure q of the stream, due to the constraint, in the form:

$$\frac{C_D}{C_{D_c}} = \frac{q_c}{q} = \frac{k^2}{k_c^2} = 1 + \frac{C_D}{k_c^2 - 1}\frac{S}{C} = 1 + \varepsilon C_D \frac{S}{C}$$

where $\varepsilon = \dfrac{1}{k_c^2 - 1}$

where $k_c^2 = 1 - C_{p_b}$, C_{p_b} being the base pressure coefficent, and where the suffix c refers to the corrected quantities.

2.5 COWDREY'S BLOCKAGE CORRECTION EQUATION

Maskell, in developing his theory of wind tunnel blockage was primarily interested in the wall interference effects on plates set normal to the wind direction. Cowdrey [7, 8] felt that there was no reason to suppose that the theory could not be applied equally well to other bluff bodies. For this reason, he tested two models of different scale of a power-station boiler house. One had a ratio of model face area to wind tunnel test section area of 7.56 percent while the other had a ratio of 1.88 percent.

While Cowdrey did not advance any new theories, he showed that the required correction was roughly equal to that of a flat plate of the same shape as the front face of the model. Thus Maskell's theory seemed valid for large blockage corrections up to 24 percent.

Cowdrey's correction formula for wind tunnel blockage is similar to Maskell's and is given as:

$$\frac{C_{D_c}}{C_D} = \frac{k_c^2}{k^2} = 1 - m\frac{S}{C}$$

where $m = 3.2 - A/20$

where k is the ratio of the velocity at the wake boundary to the free-stream velocity ($=1-C_{p_w}$),

S is the face area of the model,

C is the wind tunnel cross-sectional area, and

m is the ratio of the cross-sectional area of the wake to the cross-sectional area of the wind tunnel, and

A is the aspect ratio of the face of the model.

2.6 VERIFICATION OF BLOCKAGE THEORIES

It has been found experimentally by Modi and El-Sherbiny [28] and Courchesne and Laneville [6] that Maskell's theory (and therefore Cowdrey's) tends to overestimate the correction for higher blockage ratios (area of model face to area of wind tunnel test section). It is one of the intents of this study to verify these findings using blockage ratios up to 37.2 percent (which is roughly 4.8 times the largest blockage ratio tested by Cowdrey) and to submit a modified blockage correction equation or propose another.

Furthermore, the author intends to extend these theories from smooth flow to turbulent flow and verify the validity of the equations that are in use currently.

Chapter III

THE THEORIES OF E. C. MASKELL AND C. F. COWDREY

3.1 MASKELL'S THEORY

This is the first theory proposed for bluff bodies which attempted to explain the mechanics of blockage due to rigid boundaries and set them in a mathematical equation.

3.1.1 Properties of the Wake Created Behind a Bluff Body

Fail, Lawford and Eyre [13] conducted detailed experiments on the wake characteristics of flat plates normal to an airstream. Although the flow was unsteady, they found a distinct mean flow structure little affected by aspect ratios (ratio of width to height of the plate) or by shape. Fail, Lawford and Eyre state in their report: " As the aspect ratio is increased (from unity), the drag coefficient rises, the base pressure falls and the bubble length decreases. These changes are relatively small up to an aspect ratio of 10; thereafter the changes with aspect ratio are more rapid." and " It became clear from the early measurements of Ref.1 [Fail, Lawford and Eyre] on square, circular

and equilateral-triangular plates that the flow pattern was little affected by the shape." They conclude " The effects of aspect ratio on drag, base pressure and flow pattern are small up to A=10."

Fail, Lawford and Eyre find a tendency towards axial symmetry for the wake further downstream with the drag and base pressure varying slowly at small aspect ratios. Their typical example is the axially symmetric wake formed behind a circular disk (c.f. Figure 3.1.1.1a). Its main feature is a closed "bubble" behind the plate. Figure 3.1.1.1a shows the mean streamlines behind the plate, the closed part being referred to as the "bubble boundary". The "wake boundary", outside of which there is no loss of total head, lies outside the bubble boundary (c.f. Figure 3.1.1.1b). Behind the mid-length of the bubble, the wake spreads and a pressure recovery occurs (c.f. Figure 3.1.1.1c).

Maskell found the classical model of the bluff body wake qualitatively consistent with the above findings as it adequately defines the form of the inner boundary condition on the flow external to the wake, in the neighbourhood of the body. This he deemed sufficient for the purposes of his research.

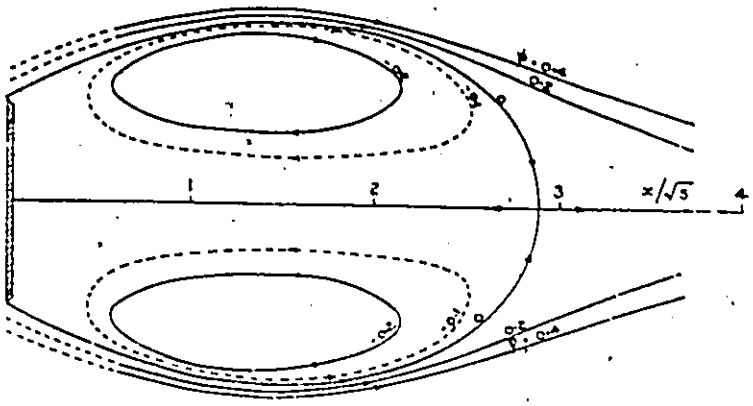

FIGURE 3.1.1.1a - STREAMLINES BEHIND PLATE

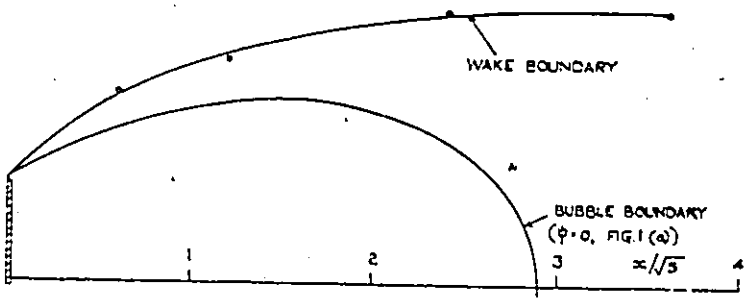

FIGURE 3.1.1.1b - COMPARISON OF BUBBLE AND TOTAL HEAD BOUNDARIES

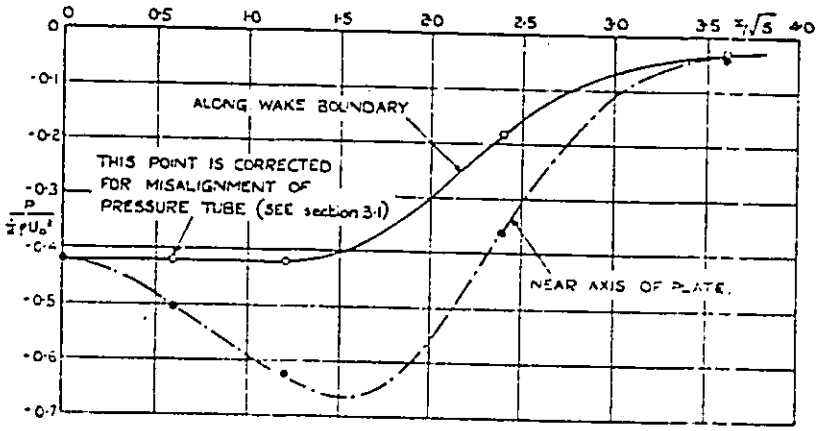

FIGURE 3.1.1.1c - STATIC PRESSURE DISTRIBUTION

Maskell chose to represent the wake by the stream surface illustrated in Figure 3.1.1.2. This extends downstrean from the edge of the body and sustains a constant pressure p as far as station 2 where the cross-sectional area of the wake is maximum. Associated with the constant pressure p is the constant velocity kU where U is the velocity of the undisturbed stream.

Although the shape of the constant pressure surface is unknown and no theory is available to account for the magnitude of the factor k, the essence of the problem is to obtain a quantitative estimate of the effect of wall constraint on k.

3.1.2 Invariance Under Constraint

Maskell's basic assumption was that the wall constraint could be equated to a simple increase in the velocity of the undisturbed stream. This implies that the form of the pressure distribution over the body is invariant under constraint meaning that if p is the pressure at any point (y,z) on the surface of the body, and H is the total pressure of the undisturbed stream, then

$$\frac{p - p_b}{H - p_b} = f(y,z)$$

independent of constraint

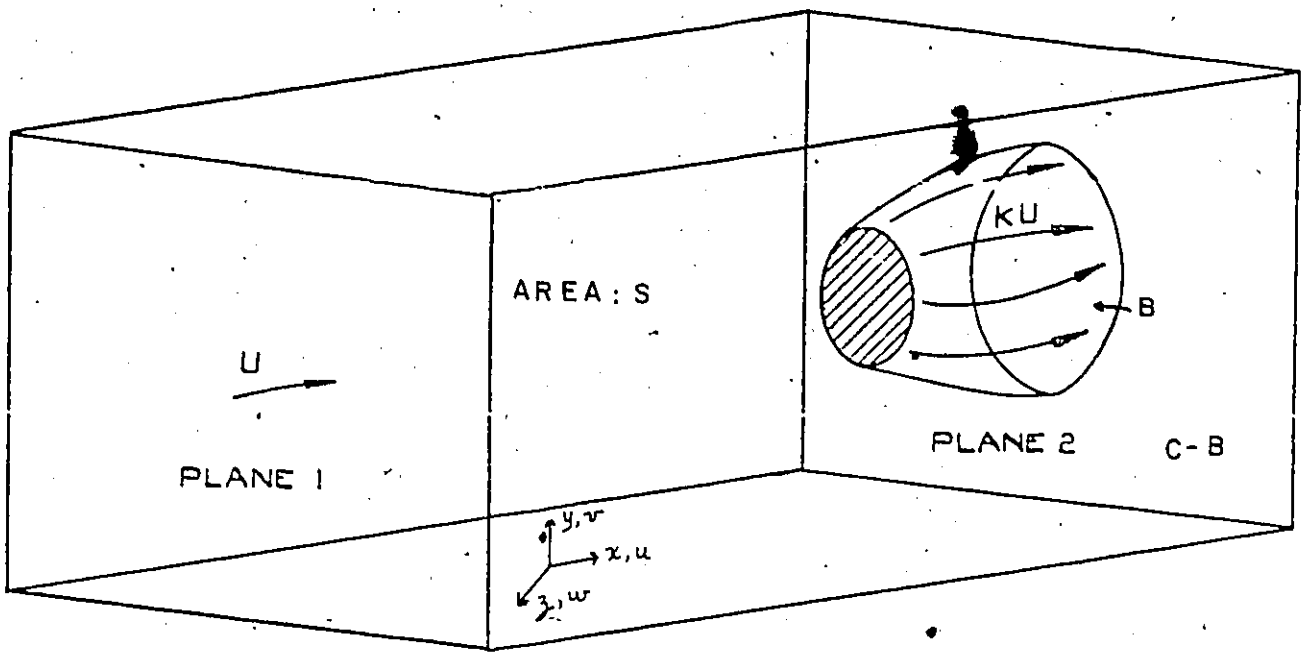

FIGURE 3.1.1.2 MODEL OF FLOW.

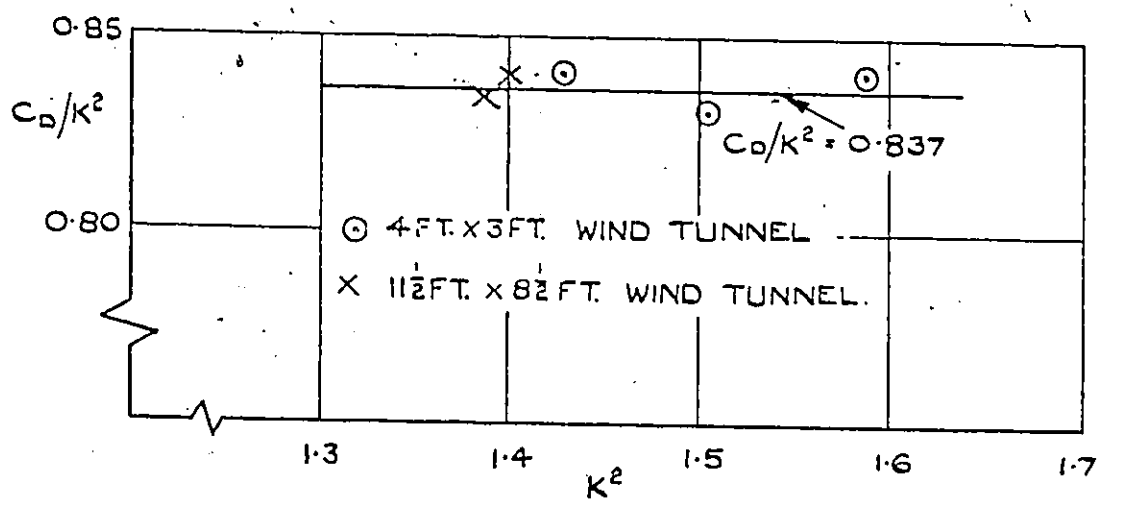

FIGURE 3.1.2.1

INVARIANCE OF THE RATIO C_D/K^2 FOR NON-LIFTING SQUARE PLATES. [REF. 25]

Given that $H-p_b = k^2q$, where $k^2 = 1-C_{p_b}$, C_{p_b} being the base pressure coefficient and q being the dynamic pressure of the undisturbed stream, it follows that

$$\frac{C_D}{k^2} = \text{CONSTANT}$$

Eqn 3.1.2.1

independent of boundary constraint, where C_D is the drag coefficient D/qS, and S is the area of the body perpendicular to the flow. By extension, the corrected velocity U_c of the unlimited stream which gives rise to a pressure distribution identical to that observed is such that $k_cU_c = kU$. Hence

$$\frac{U_c^2}{U^2} = \frac{k^2}{k_c^2} = \frac{C_D}{C_{D_c}}$$

Eqn 3.1.2.2

Maskell tested the validity of the relation given in equation 3.1.2.1 by wind tunnel tests on drag and base pressure on a set of sharp edged square plates. The results found in Maskell's report suggest that

$$\frac{C_D}{k^2} = .837$$

for different sizes of square plates (Figure 3.1.2.1).

This is in agreement with the relation expressed in equation 3.1.2.1 where the ratio of drag coefficient to k^2 is constant. Hence the experiments supported the interpretation of the wall constraint as an effective increase in stream velocity.

3.1.3 Conservation of Momentum

Maskell chose the control surface illustrated in Figure 3.1.1.2 as the control section for the conservation of momentum. The control surface is bounded by the solid walls of the wind tunnel, the face area of the body, the constant pressure surface along the effective wake, and two planes normal to the undisturbed velocity vector --- plane 1 lying upstream of the body, and plane 2 located where the cross-sectional dimensions of the wake bubble are greatest. Choosing u, v and w as orthogonal components of velocity with u in the direction of the undisturbed velocity U and with suffices 1 and 2 respectively, conservation of momentum in the fluid passing through the control surface requires that

$$D + p_b B = \iint_C (p_1 + \rho u_1^2)\, dy\, dz - \iint_{C-B} (p_2 + \rho u_2^2)\, dy\, dz \qquad \text{Eqn 3.1.3.1}$$

where D is the total drag on the body,

C is the cross-sectional area of the wind tunnel and,

B is the cross-sectional area of the effective wake at the downstream plane 2.

Since the fluid is outside the wake, Bernoulli's equation gives

$$p_1 + \frac{1}{2}\rho\,(u_1^2 + v_1^2 + w_1^2) = p_2 + \frac{1}{2}\rho\,(u_2^2 + v_2^2 + w_2^2) = P + \frac{1}{2}\rho U^2$$

where P and U are the pressure and velocity in the undisturbed stream respectively.

Equation 3.1.3.1 may be written as

$$D = (P - p_b)B + \frac{1}{2}\rho U^2 B + \iint_C \frac{1}{2}\rho u_1^2\,dy\,dz - \iint_{C-B} \frac{1}{2}\rho u_2^2\,dy\,dz + \iint_{C-B} \frac{1}{2}\rho (v_2^2 + w_2^2)\,dy\,dz - \iint_C \frac{1}{2}\rho (v_1^2 + w_1^2)\,dy\,dz$$

Eqn 3.1.3.2

Fail, Lawford and Eyre [13] suggest that the wake in the neighbourhood of plane 2 will be fairly axi-symmetric for

most three-dimensional bodies. Hence as plane 1 lies far upstream, the contribution of the last two terms in equation 3.1.3.2 will be negligibly small. The same conclusion holds for two-dimensional bluff body flow therefore equation 3.1.3.2 can be reduced to

$$D = \frac{1}{2}\rho k^2 U^2 B + \iint_C \frac{1}{2}\rho u_1^2 \, dy\, dz - \iint_{C-B} \frac{1}{2}\rho u_2^2 \, dy\, dz \qquad \text{Eqn } 3.1.3.3$$

since $p_b + \frac{1}{2}\rho k^2 U^2 = P + \frac{1}{2}\rho U^2$

Now letting $u_1 = U + u_1'$

$u_2 = U_2 + u_2'$

where $\iint_C u_1' \, dy\, dz = \iint_{C-B} u_2' \, dy\, dz = 0$

so that U is the mean velocity over plane 1 (where the airflow is undisturbed) and U_2 is the mean velocity over plane 2 outside the wake.

Then for continuity,

$$UC = U_2(C-B)$$ Eqn 3.1.3.4

and equation 3.1.3.3 may be written as

$$D = \frac{1}{2}\rho U^2 k^2 B - \frac{1}{2}\rho U^2 B\left(1-\frac{B}{C}\right)^{-1} + \iint_C \frac{1}{2}\rho u_1'^2\, dy\, dz - \iint_{C-B} \frac{1}{2}\rho u_2'^2\, dy\, dz$$ Eqn 3.1.3.5

As we are dealing with smooth flow (i.e. little or no turbulence) and u_1' and u_2' are the velocity fluctuations from their respective mean velocities U and U_2, we can assume that u_1' and u_2' are negligibly small so that the integrals in equation 3.1.3.5 can be neglected. By dividing the drag coefficient in equation 3.1.3.5 by $\rho U^2 S/2$, we obtain the following solution for the drag coefficient C_D.

$$C_D = \frac{B}{S}\left[k^2 \div \frac{1}{1-B/C}\right]$$ Eqn 3.1.3.6

Letting m=B/S, equation 3.1.3.6 becomes

$$C_D = m\left[k^2 - \frac{1}{1-m\frac{S}{C}}\right]$$

$$= m\left[k^2 - 1 - m\frac{S}{C} + \left(m\frac{S}{C}\right)^2\right]$$

Taking $(mS/C)^2$ as being negligibly small, Maskell dismissed it from the equation and thus obtained

$$C_D = m\left[k^2 - 1 - m\frac{S}{C}\right] \qquad \text{Eqn 3.1.3.7}$$

3.1.4 Distortion of the Wake

Setting S/C = 0 in equation 3.1.3.7, a relation between C_D, k_c and m_c appropriate to the equivalent unlimited stream is obtained.

Using equation 3.1.2.2 and 3.1.3.7 we get the following relation

$$\frac{C_D}{k^2} = \frac{C_{D_c}}{k_c^2} = \frac{m}{k^2}\left(k^2 - 1 - m\frac{S}{C}\right)$$

$$= \frac{m_c}{k_c^2}\left(k_c^2 - 1\right) = \text{CONSTANT}$$

$$= \frac{m^*}{k^2}\left(k^2 - 1\right)$$

Eqn 3.1.4.1

The equations 3.1.4.1 are not sufficient to define the blockage effect completely as they do not take into account the distortion of the wake under constraint.

From equations 3.1.4.1, constraint gives rise to distortion of the wake with the pressure distribution over the body and k remaining invariant. This means that m_c takes the value m^* and the blockage velocity is zero. If no distortion were present then

$$m_c = m$$

which when combined in equation 3.1.4.1 gives

$$\frac{C_D}{C_{D_c}} = \frac{k^2}{k_c^2} = 1 + \frac{C_{D_c}}{k_c^2 - 1} \frac{S}{C} \qquad \text{Eqn 3.1.4.2.}$$

Maskell found this last equation to underestimate C_D by 20 percent and thus attempted to set an empirical relationship between m_c and m.

From experimental work, the relationship between m_c, m and m^* seems to be on the order of

$$m_c > m > m^*$$

This inequality is such that all parameters tend to the same value as the ratio $(m - m^*)/(m_c - m^*)$ tends to 1. This last ratio is inferred to behave in the same manner as the contraction ratio (C-B)/C of the external stream in the limit S/C tends to 0.

Thus assuming

$$\frac{m - m^*}{m_c - m^*} = \frac{C - B}{C} = 1 - m\frac{S}{C}$$

and reducing it using equation 3.1.4.1 to

$$\frac{m}{m_c} = 1 - \frac{C_D - C_{D_c}}{(k^2-1)(k_c^2-1)}\frac{S}{C}$$

Eqn 3.1.4.3

neglecting as before the terms of order $(S/C)^2$.

3.1.5 Blockage Correction

From equation 3.1.4.1 and 3.1.4.3, it follows that

$$\frac{k^2}{k_c^2} = 1 + \frac{C_D}{k_c^2 - 1}\frac{S}{C} + \text{TERMS OF ORDER } \left\{\frac{S}{C}\right\}^2$$

Eqn 3.1.5.1

Hence the effect of distortion is to replace C_{D_c} in the correction term of equation 3.1.4.2 by the measured C_D.

An alternative method of expressing this is to write q for the dynamic pressure and using equation 3.1.2.2 to obtain

$$\frac{\Delta q}{q} = \varepsilon C_D \frac{S}{C}$$ Eqn 3.1.5.2

where $\Delta q = q_c - q$ is the effective increase in dynamic pressure of the undisturbed stream due to constraint, $C_D S/C$ is the usual wake blockage parameter, and where

$$\varepsilon = \frac{1}{k_c^2 - 1}$$ Eqn 3.1.5.3

is the blockage factor for the bluff body flow.

In order to find ε, given measured values of k and C_D, it is necessary to find k^2 from equation 3.1.5.1. Maskell found that replacing k_c^2 in equation 3.1.5.3 by k^2 was not sufficient and thus developed an iterative solution of equation 3.1.5.1 using the formula

$$\left(k_c^2\right)_n = k^2\left[1 + \frac{1}{\left(k_c^2\right)_{n-1} - 1} C_D \frac{S}{C}\right]$$

Eqn 3.1.5.4

where $(k_c^2)_n$ is the nth approximation to k_c^2,
and where $(k^2)_0 = k^2$.

Thus the measured values of drag and pressure coefficients can now be corrected to the effective dynamic pressure q_c, according to

$$\frac{1 - C_p}{1 - C_{p_c}} = \frac{C_D}{C_{D_c}} = \frac{k^2}{k_c^2} = \frac{q_c}{q}$$ Eqn 3.1.5.5

Hence from equations 3.1.5.1 and 3.1.5.5

$$\frac{C_D}{C_{D_c}} = 1 + \frac{1}{k_c^2 - 1} C_D \frac{S}{C} = 1 + \varepsilon C_D \frac{S}{C}$$

$$\therefore \quad C_{D_c} = \frac{C_D}{1 + \varepsilon C_D S/C}$$

where varies with the aspect ratio of the model according to Figure 3.1.5.1.

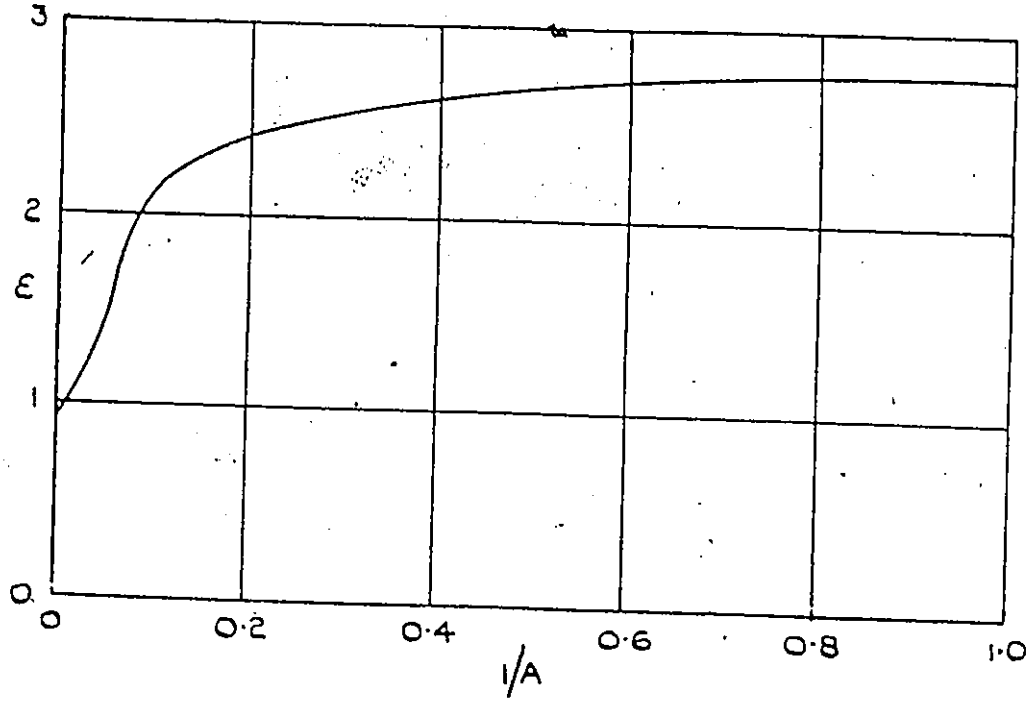

VARIATION OF BLOCKAGE FACTOR WITH ASPECT RATIO FOR NON-LIFTING RECTANGULAR PLATES. ([25])

FIGURE 3.1.5.1

3.2 COWDREY'S THEORY

The theory of wind tunnel blockage developed by Maskell was largely influenced by his interest in the wall interference effects on large delta wings at high angles of incidence. This is the reason why he concentrated mainly on thin flat plates set normal to the wind direction.

As there was no reason to suppose that the theory could not be applied to a broader range of bluff bodies, Cowdrey decided to apply it to large models in the form of rectangular blocks.

The model used by Cowdrey was a scaled down version of a power-station boiler house in various stages of erection. Large blockage corrections on the order of 30 percent were required and seemed to agree with the measurements made on a smaller model as Cowdrey [7] states: "... a re-examination of the theory, together with some measurements on a smaller model of the completed building, showed that the required correction was substantially the same as that required for a flat plate of the same shape as the front face of the model. Furthermore, the same correction applied for angles of incidence up to roughly 10°."

3.2.1 Derivation of the Blockage Equation

The same assumptions as those made by Maskell (c.f. Section 3.1) are used by Cowdrey, namely that for thin flat plates normal to the wind direction, the static pressure is constant and equal to the base pressure over the expanding part of the wake boundary [13].

Thus Cowdrey obtains the following relationship (for more details, see ref. 7):

$$\frac{C_D}{C_{D_c}} = k_w^2 \left(1 - \frac{m}{m_o}\right) + \frac{m}{m_o} \frac{1}{1 - m\frac{S}{C}} \qquad \text{Eqn 3.2.1.1}$$

where k_w^2 is the ratio of the velocity at the wake boundary to the free stream velocity (= 1 - C_{p_w}), m is the ratio of the cross-sectional area of the wake to the cross-sectional area of the model and the suffix $_o$ indicates zero blockage.

3.2.2 Determination of m and m/m_o

As there is no information available concerning the size of the wake shed from bluff bodies of significant depth, the values of m and m/m_o have to be evaluated from an experimental point of view.

If it can be assumed that the size of the wake is little affected by the blockage, i.e. $m/m_o = 1$, then equation 3.2.1.1 would be reduced to a very convenient and compact form of

$$\frac{C_D}{C_{D_c}} = \frac{1}{1 - m\frac{S}{C}} \qquad \text{Eqn 3.2.2.1}$$

This was Maskell's consideration when he used the equation

$$\frac{C_D}{C_{D_c}} = 1 + m\frac{S}{C} \qquad \text{Eqn 3.2.2.2}$$

which is an approximation of equation 3.2.2.1 as the term of order $(mS/C)^2$ is neglected. He compared a calculated value of C_D/C_{D_c} with the value estimated from tests on flat plates of different sizes and found a difference of about 2.5 percent. The inclusion of the $(mS/C)^2$ term in equation 3.2.2.2 would seem to account for most of this error. Thus the distortion of the wake must be negligibly small.

Hence the assumption that $m/m_o = 1$ is reasonable.

Unfortunately, there is no similar evidence available to help in determining the value of m. The term m need not how-

ever be found with great accuracy as S/C is unlikely to be greater than 0.10 according to Cowdrey and, as Maskell has shown, the value of m for flat plates of small aspect ratio is approximately 3.1. Cowdrey further assumed the value of m for large bluff bodies is the same as for a thin flat plate of the same shape as the front of the model.

> ... it seems reasonable to suppose that where the amount of solid in the wake shed from the flat front surface is not too large, the effect upon the width of the wake will not be excessive. This would suggest that the value of m may not be very different from that appropriate to a thin flat plate of the same shape as the front face of the model, namely 3.1.

Good agreement for angles of yaw up to 10° is found when the measured forces are corrected for blockage by multiplying by the factor (1 - 3.1 S/C). This is found in Cowdrey's results.

3.2.3 Variation of $m = C_{D_c}/(k_c^2-1)$ with the Shape of a Flat Plate

Using values of C_{D_c} and C_{p_b} measured by Fail, Lawford and Eyre [13]. Cowdrey calculated the value of m for flat plates of different shapes.

For rectangular plates of aspect ratio less than 20, the value of m_o is represented by the equation

$$m_o = 3.2 - A/20 \qquad \text{Eqn 3.2.3.1}$$

Thus it follows that

$$\frac{C_{D_c}}{C_D} = 1 - \left(3.2 - \frac{A}{20}\right)\frac{S}{C} \; ;$$

Eqn 3.2.3.2

and for aspect ratios A ---> ∞ , the value of m_o tends to 1.7.

For flat plates normal to the wind, the correction to be applied for wind tunnel blockage can be calculated by the equation

$$\frac{C_{D_c}}{C_D} = \frac{k_c^2}{k^2} = 1 - m\frac{S}{C}$$

$$\text{or} \quad C_{D_c} = C_D\left[1 - m\frac{S}{C}\right] \qquad \text{Eqn 3.2.3.3}$$

where m varies with the shape of the model (c.f. Figure 3.2.3.1).

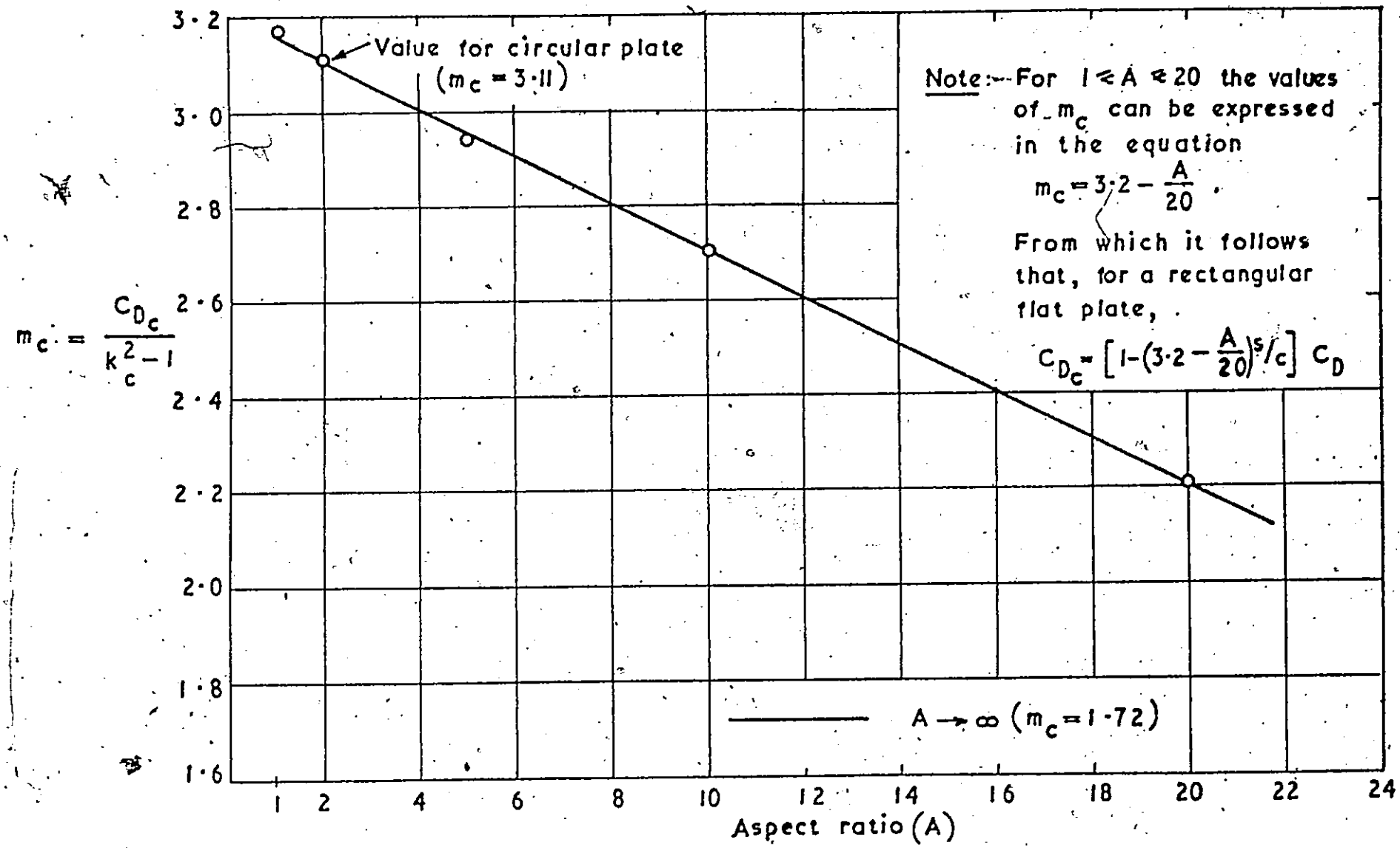

Variation of $m_c \left(= \frac{C_{D_c}}{k_c^2 - 1}\right)$ with the shape of a flat plate

FIGURE 3.2.3.1

(REF. 7)

Chapter IV

AERODYNAMIC DERIVATIVES SUBJECTED TO A BLOCKAGE CONSTRAINT

4.1 MAIN CAUSES OF CHANGES IN AERODYNAMIC FORCES DUE TO WALL CONSTRAINTS

The presence of wind tunnel walls near a body under test causes changes in lift and drag forces as well as on the pitching moment of this body as opposed to one being tested with the rigid wall boundaries being infinitely far away. The changes are mainly due to the following effects:

1. The airstream speed is augmented in the vicinity of the body due to the reduction of test section area in the presence of the model and its wake. The velocity variation increases along the test section and is usually found to be maximum in the immediate vicinity of the model. The speed increase due to the body is called "solid blockage" while that due to the wake is termed "wake blockage". Both cause an increase in the measured aerodynamic forces and moments.
2. The curvature of the streamlines about the body are altered by wall and ceiling proximity. The effects of streamline curvature are not well understood.

3. The static pressures far downstream in the wake drop below the undisturbed free stream value. This produces a wake buoyancy that increases the drag on the body.
4. The boundary layer growth on the rigid boundaries of the test section and the geometry of the wind tunnel test section may result in a longitudinal pressure gradient that can affect drag.

The wall effects are best understood for streamlined shapes where considerable experience was gained primarily by the aeronautical industry which resulted in the availability of well developed and proven correction techniques.

The correction techniques are less well developed for the bluff body shapes that typify most civil engineering structures. In these cases, the potential flow solutions of the aircraft industry are inadequate and more often than not inapplicable.

This thesis research will therefore concentrate on the more complex semi-empirical corrections which have been developed to handle bluff body wall constraint corrections.

4.2 PURPOSE OF THE TESTS

The purpose of the tests was to measure the aerodynamic forces and moments acting on a two-dimensional bluff body of rectangular shape. All force measurements were done using a three-component strain balance (c.f. Appendix A) and drag and lift coefficients were also calculated from pressure measurements. The models tested had a depth-to-width of 0.5 (wide face normal to the flow) and 2.0 (wide face parallel to the flow). Five model sizes were tested with ratios of projected face area to wind tunnel test section area of 4.2 percent to 37.2 percent.

The most common formulae for blockage correction were applied to the test results and a new blockage correction equation was developed and compared to these.

4.3 DESCRIPTION OF TESTS

The tests were carried out in the 2 ft by 3 ft open return wind tunnel at the University of Ottawa. The tunnel has an open circuit system and is of the Eiffel type. This tunnel was designed to have adiabatic airflow at the test section.

The wind tunnel consists of six sections as shown in Figure 4.3.1. These are as follows:

1. Entrance: Four screens are installed at the 3 ft x 8 ft rectangular entrance.
2. Contraction: A contraction area ratio of 4.0 is given at the first 7 ft from the entrance.
3. Working section: The working section is 6 ft long, 4 ft of which has plexiglass panels on both sides, with the sharp rectangular section of 3 ft x 2 ft. Both top and bottom panels of this section can be replaced according to the convenience of the testing.
4. Diffuser: The rectangular cross-section is first converted to a regular octagon for 7 ft 6 in and then changed to a sixteen sided polygon for the length of 3 ft 6 in. The diffusing angle is less than 6.5 degrees.
5. Flexible coupling: This flexible connection is to minimize the vibration of diffuser wall due to the fan.
6. Fan: Buffalo axial flow fan, type S-54C9, 57 inches in diameter. The maximum capacity of the fan is 54 x 10^3 cubic ft/min and rotates at a maximum speed of 1,170 rpm. The induction is controlled by the adjustable speed magnetic drive.

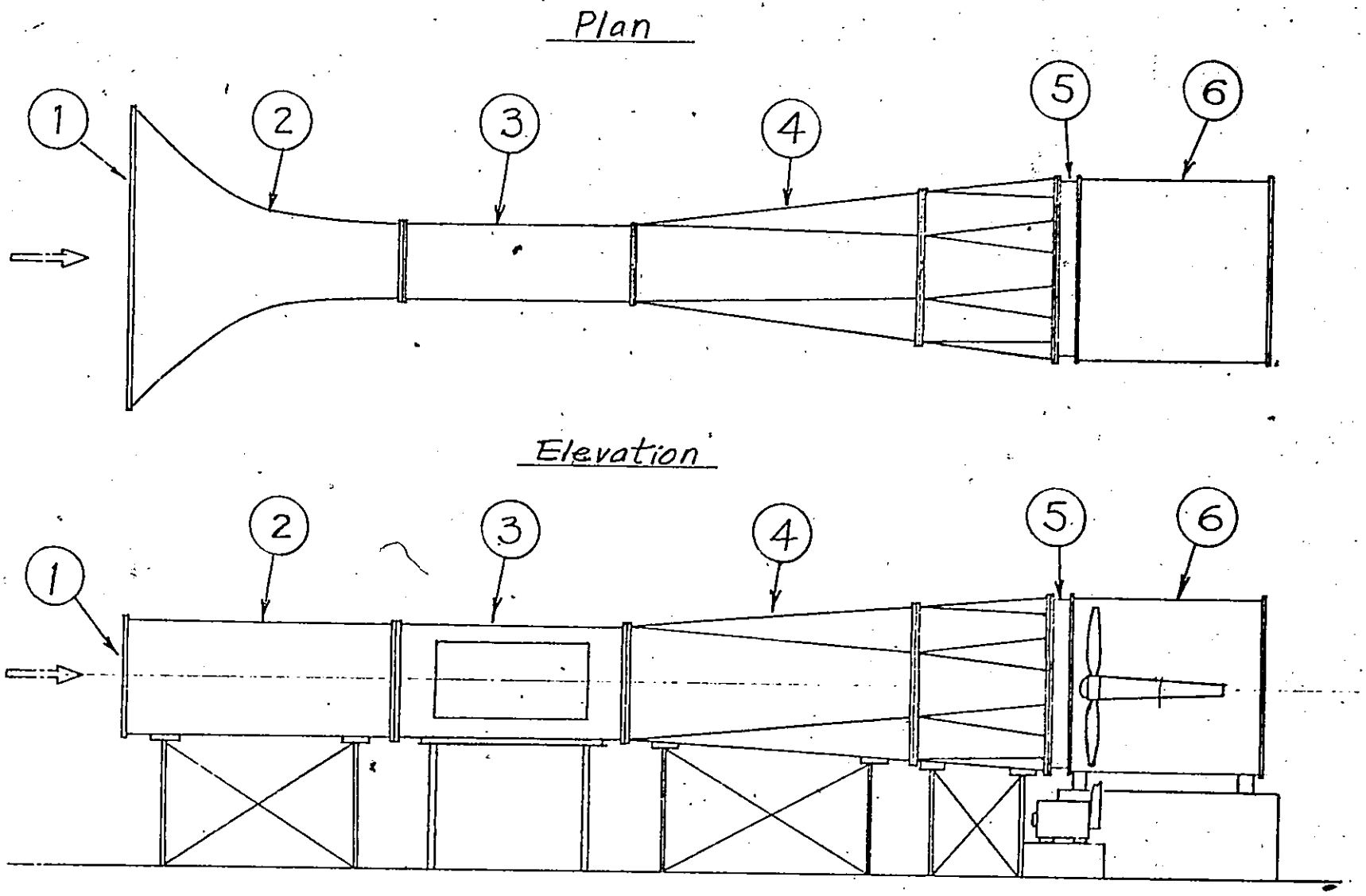

FIGURE 4.3.1 – GENERAL LAYOUT OF THE WIND TUNNEL

(REF. 42)

Although the design speed is up to 150 ft/sec, the maximum speed presently available at the test section is approximately 80 ft/sec because of the drive capacity.

Measurements [42] of mean flow speed were done at different distances from the entrance of the test section and along the wind tunnel center line. The results are summarized in Figures 4.3.2 to 4.3.4. The maximum boundary layer thickness observed in the test section was found to be less than 3 inches. A slight pressure gradient was recognized as existing in the longitudinal direction, but the variation in mean speed is within the range -1.7% at the entrance to +0.7% at the end of the working section. This is shown in Figure 4.3.2.

Horizontal and vertical distributions of mean wind speed are given in Figures 4.3.3 and 4.3.4. As long as the middle quarter of the test section is being used for testing, the mean speed variation is expected not to exceed the order of one percent.

Measurements of turbulence were conducted at the test section of the tunnel [42]. The longitudinal turbulence intensity was found to be 0.4% of the local mean speed.

The production of large scale turbulence in this tunnel is done by the installation of a grid at the entrance of the test section. This should create homogeneous, isotropic turbulence. Two grids were used in the tests; the finest grid giving about 7% turbulence intensity and an integral scale of turbulence of 0.70 inch while the coarsest grid gives about 12% turbulence with an integral scale of turbulence of 0.83 inch. (Figure 4.3.5)

A three-component strain balance (c.f. Appendix A) was mounted on the wind tunnel floor in the test section (c.f. Figure 4.3.6). The models were cantilevered from this strain balance by means of a plate which could rotate on the balance allowing a change in the angle of incidence of the flow at the model (c.f. Figure 4.3.7). The model spanned the full height of the test section except for a gap of 0.6 inches between the top of the model and the wind tunnel ceiling.

Once the model was in place, the strains caused by the wind forces acting on it were measured for five different velocities. The same measurements were repeated for 20 different angles of incidence. In addition to the smooth flow tests, the model was also tested with the fine and coarse grid in place.

The datae were gathered and the lift and drag forces and pitching moment were calculated as well as the lift, drag and pitching moment coefficients. A linear regression was performed on the aforementioned values and a summary of the results is presented in Tables 1 to 9 for a wind speed of 25 ft/sec (17 mph). The lift and drag forces as well as the pitching moment were measured using the coordinate system illustrated in Figure 4.3.8.

The linear regression on the lift, drag and moment forces as well as their respective coefficients was performed to obtain the best line fit of the data. The scatter of the collected data was minimal and the correlation coefficient was typically above 0.96 for the lift and drag and above 0.60 for the pitching moment. This proves that for a given model tested, the drag and lift is independant of the wind speed and the Reynolds number. Thus comparisons can be made between models with flows of different Reynolds number as the drag is independent of it. This is illustrated in Figures Tables 10 to 15 and plotted in Figures 1 to 6.

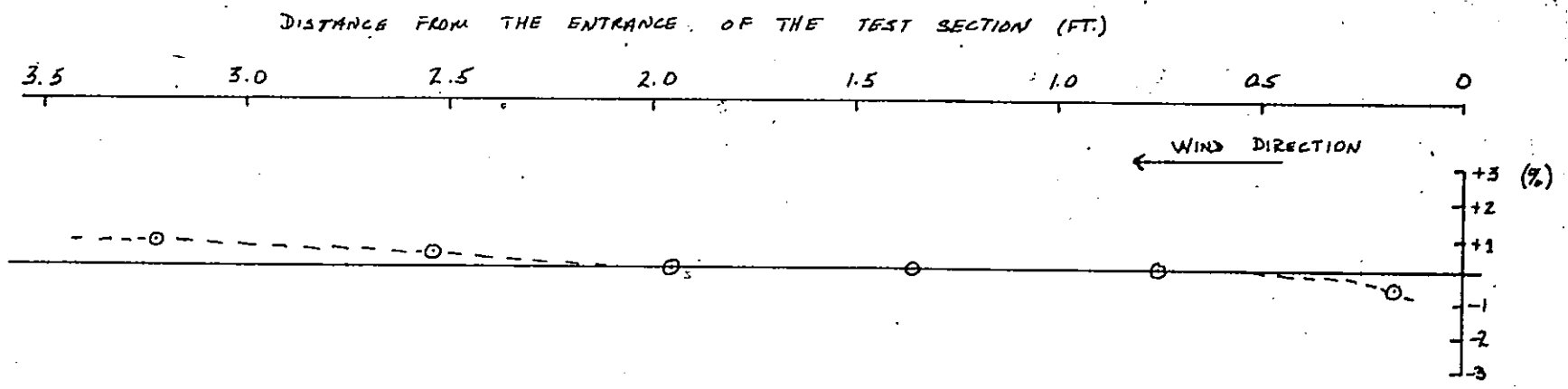

FIG. 4.3.2 LONGITUDINAL DISTRIBUTION OF MEAN WIND SPEED ALONG THE TUNNEL CENTRE LINE

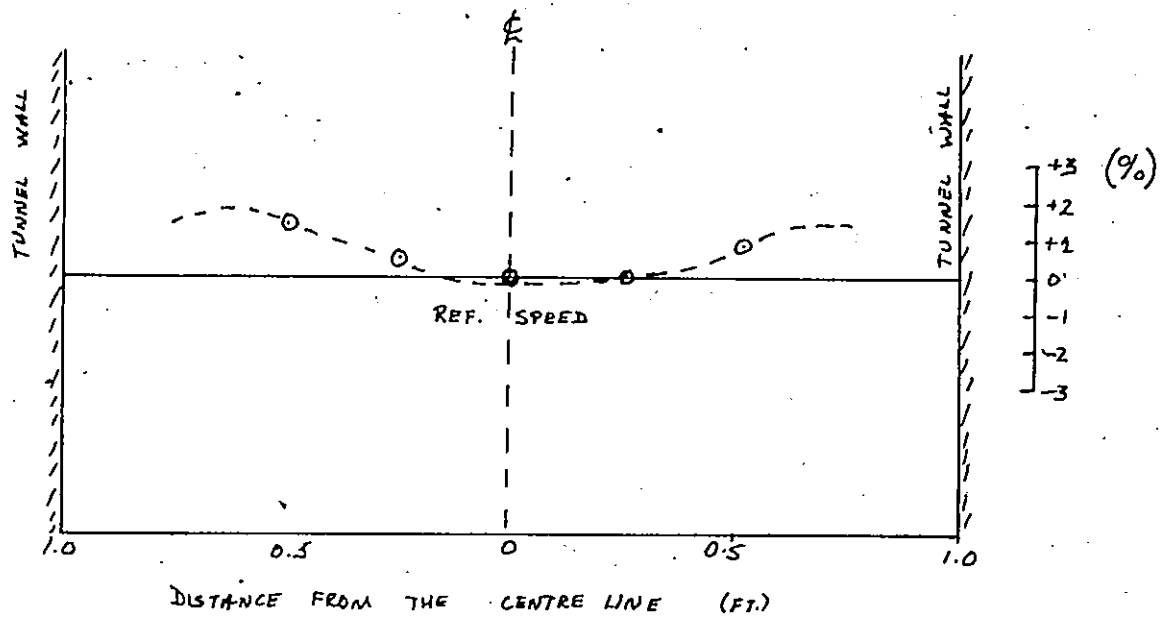

FIGURE 4.3.3 - HORIZONTAL DISTRIBUTION OF MEAN WIND SPEED AT 8 IN. UPSTREAM OF THE MIDDLE SECTION [42]

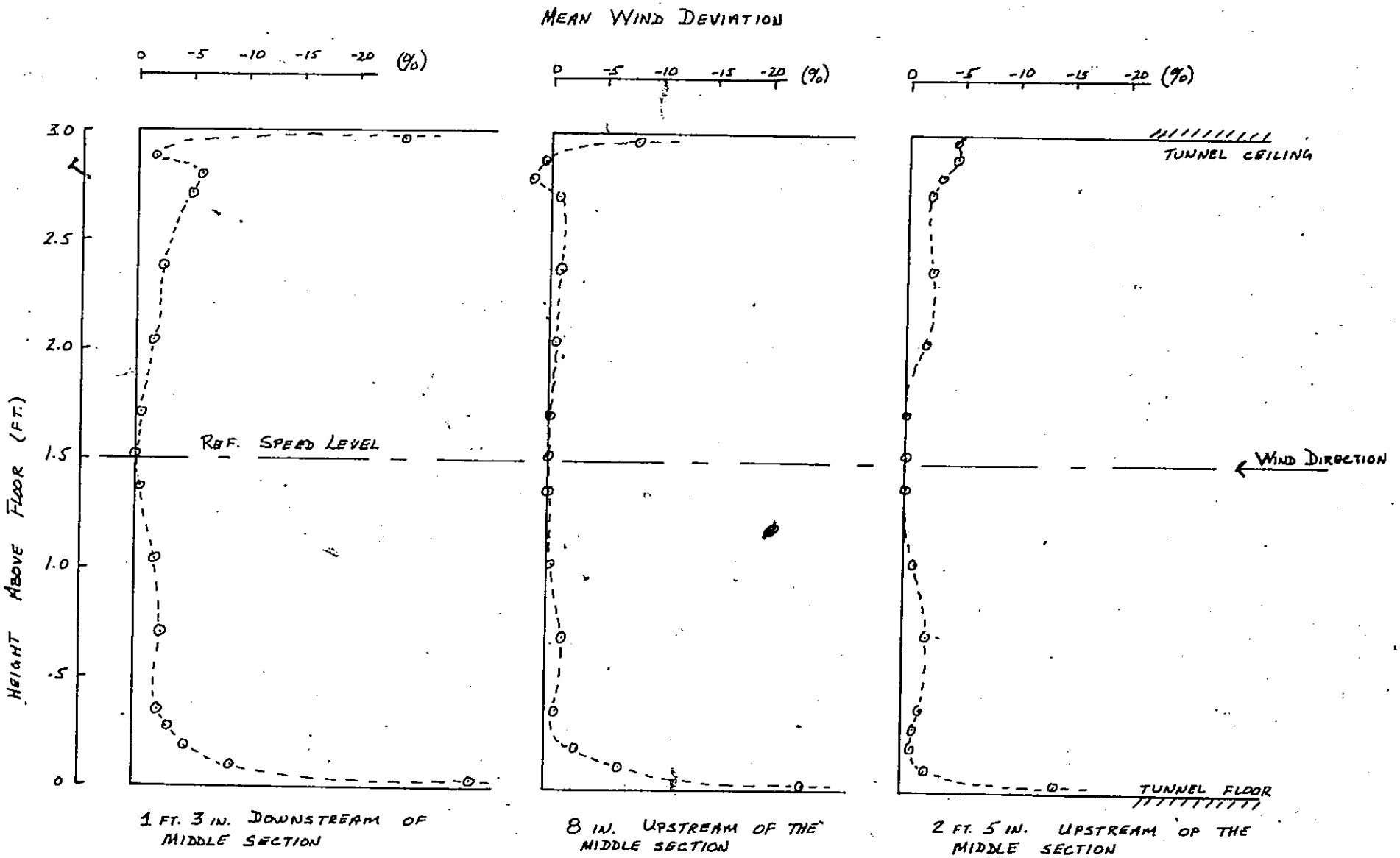

FIGURE 4.3.4 - VERTICAL DISTRIBUTION OF MEAN WIND SPEED [42]

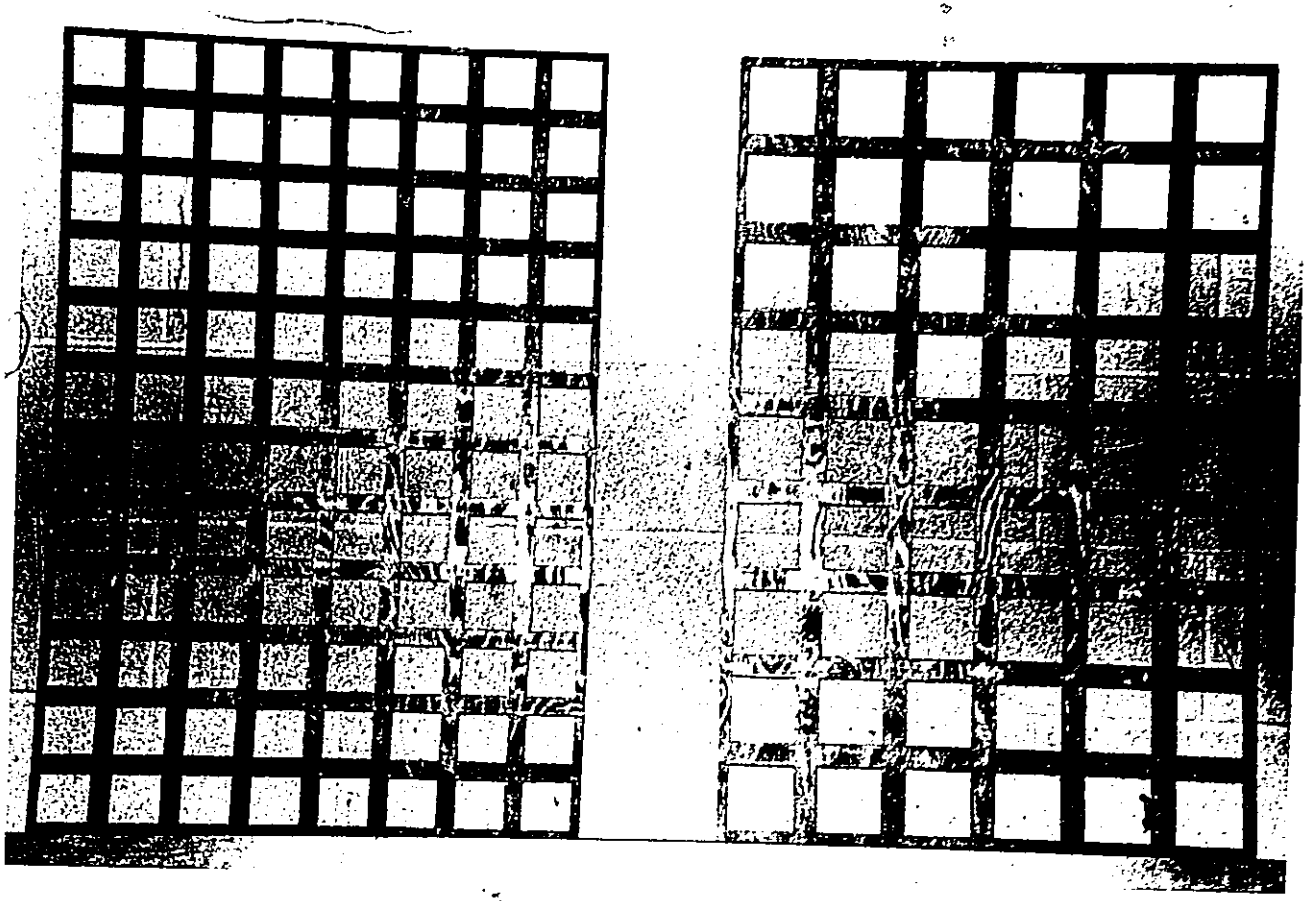

FIGURE 4.3.5 - FINE AND COARSE GRIDS

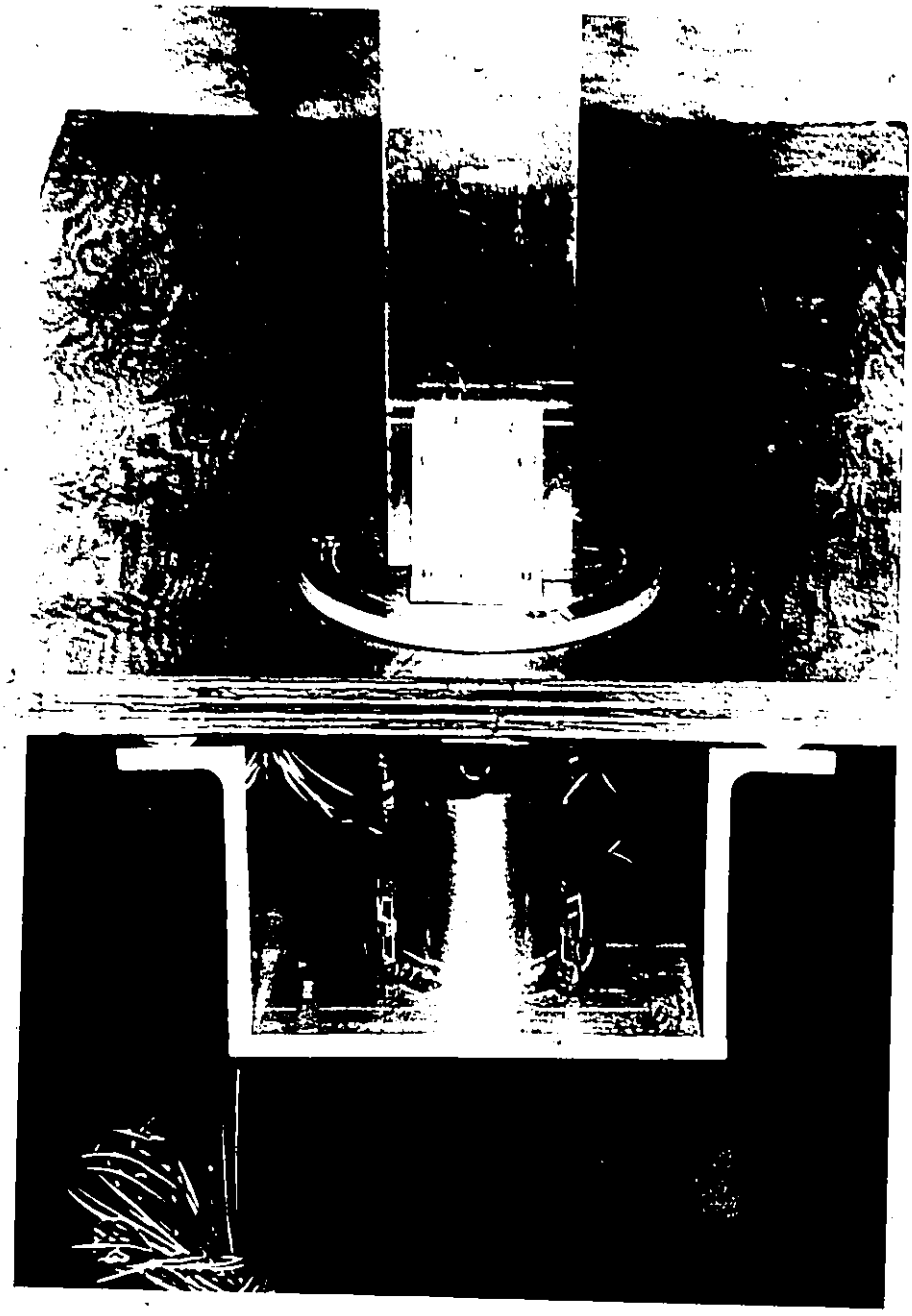

FIGURE 4.3.6 - STRAIN BALANCE MOUNTED ON WIND TUNNEL FLOOR

FIGURE 4.3.7 - MODEL IN WIND TUNNEL TEST SECTION

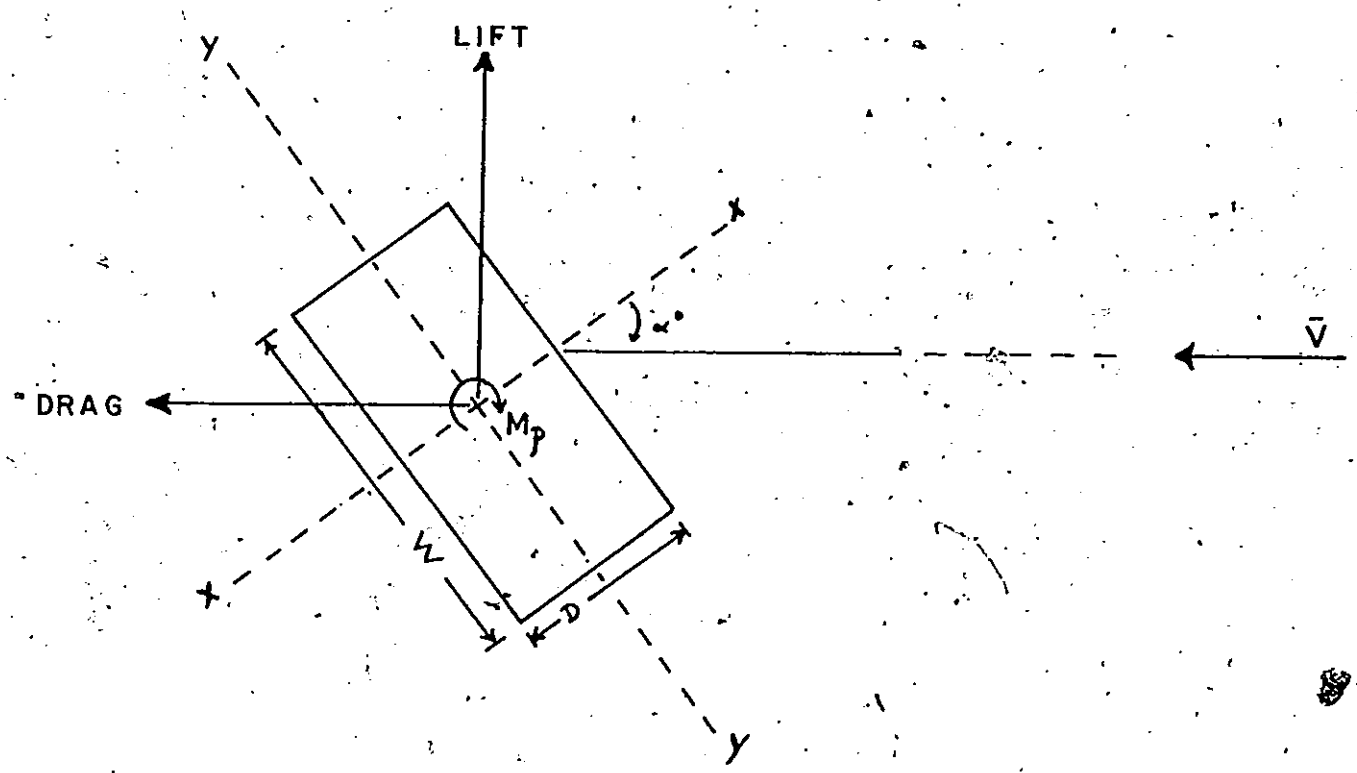

FIGURE 4.3.8 - COORDINATE SYSTEM USED IN DETERMING FORCES ACTING ON THE MODEL

4.4 PRESSURE TESTS

In addition to the strain measurements, pressure measurements were also taken on the models. The experimental configurations were as follows:

AREA RATIO	MODEL ID	SIZE INxIN	GRIDS #	MEASUREMENTS (TYPE)	
0°, 90°				STRAIN	PRESSURE
.083 .042	S36	1x2	0,1,2	*	*
.133 .067	M36	1.5x3	0,1,2	*	
.167 .083	36	2x4	0,1,2	*	*
.250 .125	B36	3x6	0,2		*
.333 .167	---	4x8	0,2		*

The pressure measurements were taken by a ring of pressure taps located at mid-height along the model (c.f. Figures 4.4.1 and 4.4.2). There were 12 pressure taps in total, four on each of the wider sides and two on each of the narrower sides of the model. The accuracy of the pressure measurements for single pressure taps was tested with two models which had pressure taps located the length of the trailing edge of the model. This will be discussed later.

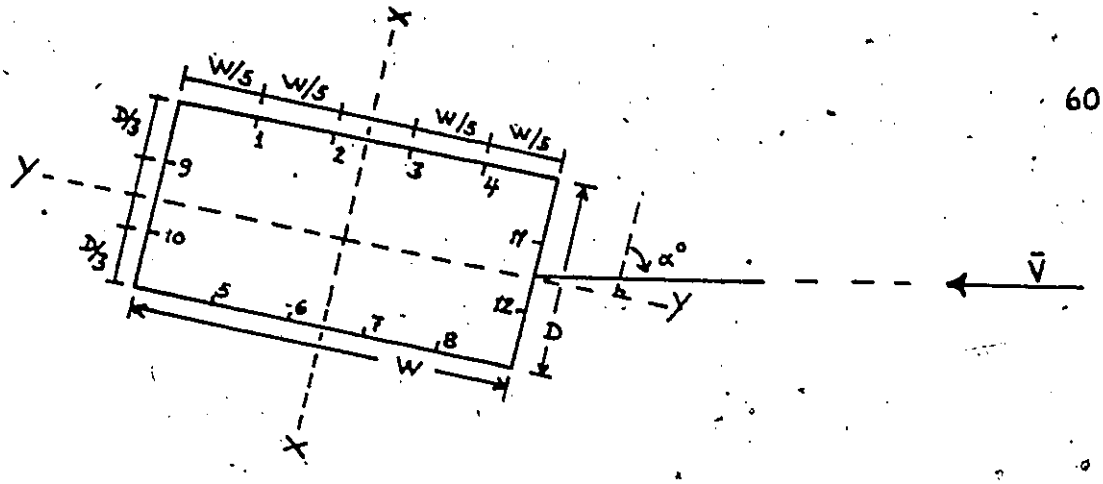

FIGURE 4.4.1

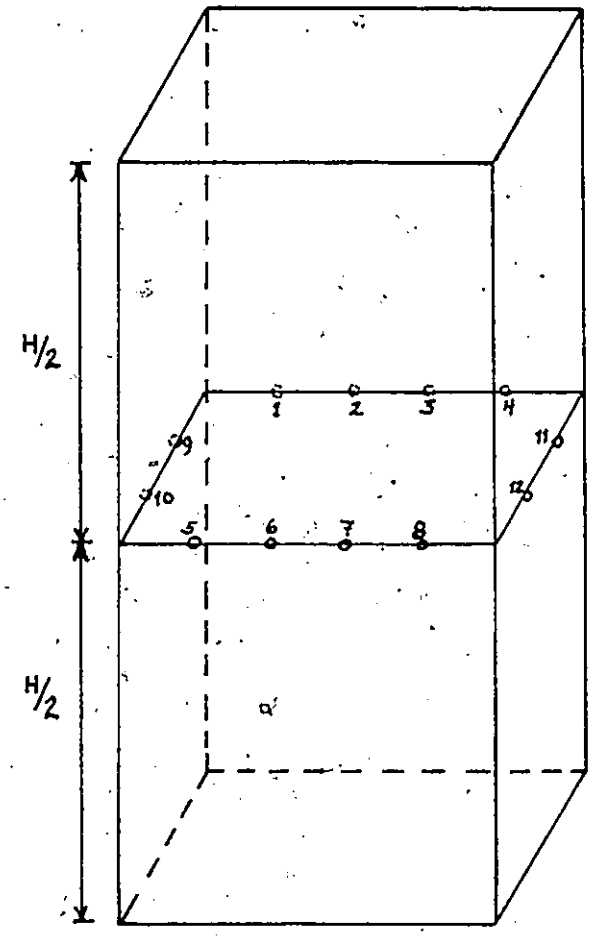

FIGURE 4.4.2

LOCATION OF PRESSURE TAPS ON MODEL

The drag and lift coefficients were calculated from the pressure measurements as well as the base (trailing edge), stagnation and side-face pressure coefficients. The drag and lift coefficients calculated from pressure measurements are summarized in Tables 16 to 21. The stagnation, base and side-face pressure coefficients are tabulated for the different models for angles of incidence of 0, 10, 30, 60, 80 and 90 degrees in Tables 22 and 23 for smooth and turbulent (turbulence intensity 12%) flow respectively. The calculated values of the pressure coefficients for the different models and different angles of incidence are tabulated in Tables 24 to 29 for both smooth and turbulent flow. Figures 7 to 12 illustrate the variation of C with blockage ratio for different angles of attack.

The base pressure was measured the length of the model along the trailing edge to verify the two-dimensionality of the flow distribution. If the model is truly two-dimensional in behaviour, the base pressure distribution will be constant along the trailing edge. The purpose of these measurements was to evaluate the effect of different gap sizes between the tip of the model and the test section ceiling on the two-dimensionality of the flow. The results are summarized in Tables Tables 30 to 34 and are plotted in Figures 13 to 20.

Figures 21 to 24 illustrate the difference between the drag coefficients measured by strain measurements and pressure measurements while Figures 25 to 28 illustrate this for the lift coefficient.

Figures 29 to 31 illustrate the variation in drag coefficients for angles of incidence from 0° to 90° and for three different models each tested in smooth flow and light and strong turbulent flows. Figures 34 to 36 illustrate the same for lift coefficient while Figures 39 to 41 illustrate this for the pitching moment. Figures 32 and 33 illustrate the variation in the drag coefficient with respect to different blockage ratios for various angles of attack. Figures 37 and 38 illustrate the same for the lift coefficient.

Figures 42 to 44 illustrate the variation in drag coefficient with respect to blockage ratio for angles of incidence of 0° and 90°. Figures 45 to 50 illustrate the variation in drag coefficient with respect to blockage ratio for all angles of incidence tested and for smooth flow and turbulent flow conditions. Figures 55 to 57 do the same for the lift coefficient. In addition to these figures based on the strain measurements, Figures 51 to 54 illustrate the variation of drag coefficient determined from pressure measurements versus blockage ratio for all angles of incidence for smooth and turbulent flow.

4.5 ANALYSIS OF THE DATA

The range of available wall correction techniques varies from simple considerations of model and test section geometry to the application of potential flow approximations of the model and its wake. An indication of the wide spectrum of corrections available can be found in the Agard summary [15]. In general, it can be expected that corrections involving measurements taken during the tests will be better than those based on simple geometry.

4.5.1 The Continuity Method

Of all the variable blockage corrections, the simplest is that of continuity where an increase in velocity is proportional to the reduction in the test section area by the presence of the model. The velocity is assumed uniformly distributed over the test section area. The correction has the form:

$$C_{D_c} = C_{D_u}(1 - S/C)^2$$

$$\simeq \frac{C_{D_u}}{1 + 2S/C} \qquad \text{Eqn 4.5.1.1}$$

4.5.2 The Area Ratio Method

A correction similar to that of continuity is given by Pope [34] for use if nothing better is available or known. It is applicable only to streamline flows and assumes that the velocity increase due to blockage is on the order of one quarter that of the average increase over the test section. The correction is:

$$C_{D_c} = C_{D_u}(1 - S/4C)$$

$$\simeq \frac{C_{D_u}}{1 + S/2C} \qquad \text{Eqn 4.5.2.1}$$

and is one quarter that of continuity.

4.5.3 Maskell's Bluff Body Correction

Maskell [24, 25] applies momentum theory and derives a correction applicable to bodies with large separated flows (c.f. Chapter III). The theory assumes that the body's wake becomes axi-symmetric, that the base pressure on the model is uniform and that flow separation on the body is independent of wall constraint. The correction equation is:

$$C_{D_c} = \frac{C_{D_u}}{1 + \varepsilon C_{D_u} S/C} \qquad \text{Eqn 4.5.3.1}$$

where $\varepsilon = \frac{1}{k_c^2 - 1}$

and k_c^2 is determined as in Chapter III.

Strictly speaking, this is valid only for a flat plate perpendicular to the flow, although references 6, 7, 28, 35 and 36 show that the plate and its wake bubble affect the flow in a wind tunnel much like a body which has some depth to it.

4.5.4 Cowdrey's Blockage Correction Equation

Cowdrey [7, 8] extended Maskell's work from flat plates with small blockage ratios to larger bluff bodies with high blockage ratios and devised a similar correction equation as that of Maskell.

The equation is of the form:

$$C_{D_c} = C_{D_u}\left(1 - m\frac{S}{C}\right) \qquad \text{Eqn 4.5.4.1}$$

where $m = 3.2 - A/20$,

and A is the aspect ratio of the model.

The value of m tends to 1.72 as the aspect ratio A tends to infinity.

4.5.5 Modi and El-Sherbiny's Blockage Correction Equation

Modi and El-Sherbiny [27] included the higher order terms which Maskell had left out of his blockage correction equation. Thus Maskell's equation becomes:

$$\frac{C_{D_u}}{C_{D_c}} = 1 + \frac{C_{D_u}}{k_c^2 - 1}\frac{S}{C} + O\left[\left(\frac{S}{C}\right)^2\right] \qquad \text{Eqn 4.5.5.1}$$

Modi and El-Sherbiny remolded this equation into a polynomial of the form

$$\frac{C_{D_u}}{C_{D_c}} = 1 + \sum_{n=1}^{n} A_n \left(C_{D_u}\frac{S}{C}\right)^n \qquad \text{Eqn 4.5.5.2}$$

From their experimental data and with the use of a computer, they found that a straight line fit for drag correction could best be modelled by the following equation:

$$C_{D_c} = C_{D_u}\left(1 - 1.495\frac{S}{C}\right) \qquad \text{Eqn 4.5.5.3}$$

4.5.6 Ranga Raju and Garge's Blockage Correction Equation

Ranga Raju and Garde [35, 36] proposed a blockage equation for two-dimensional flow of the form

$$C_{D_c} = C_{D_u}\left(1 - \frac{h}{D}\right)^n \qquad \text{Eqn } 4.5.6.1$$

where h/D is the ratio of the width of the model to the width of the test section and n is an exponent which varies with t/h, the ratio of model depth to model width as shown in Figure 4.5.6.1.

4.5.7 Laneville and Courchesne's Blockage Correction Equation

Courchesne and Laneville [6] are using the fact that in Maskell's equation $C_{D_c}/(k_c^2-1)$ is constant for a given value of H/D or model width to model depth to express an empirical correction formula in the form:

$$C_{D_c} = C_{D_u}\left(1 - \gamma \frac{S}{C}\right) \qquad \text{Eqn } 4.5.7.1$$

where γ is an empirical constant which when set equal to $C_{D_c}/(k_c^2-1)$ yields Maskell's equation. Values for γ are shown in Figure 4.5.7.1,

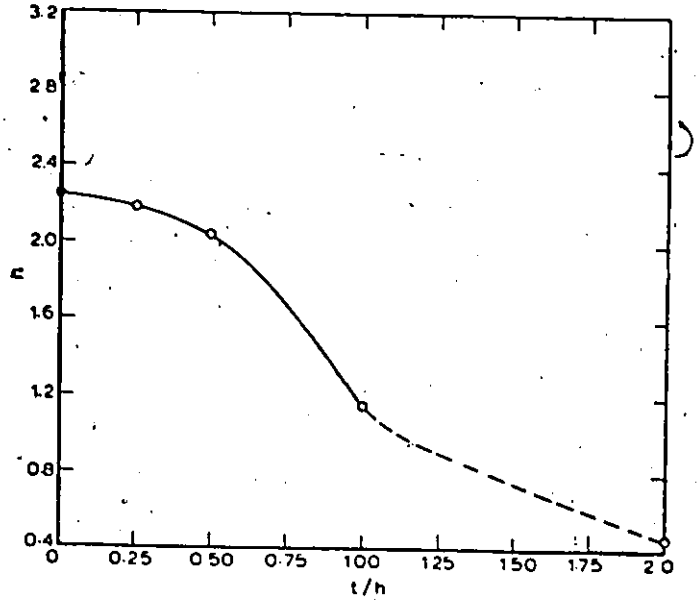

FIGURE 4.5.6.1 - VARIATION OF n WITH t/h AFTER RANGA RAJU FOR TWO-DIMENSIONAL RECTANGULAR PRISMS

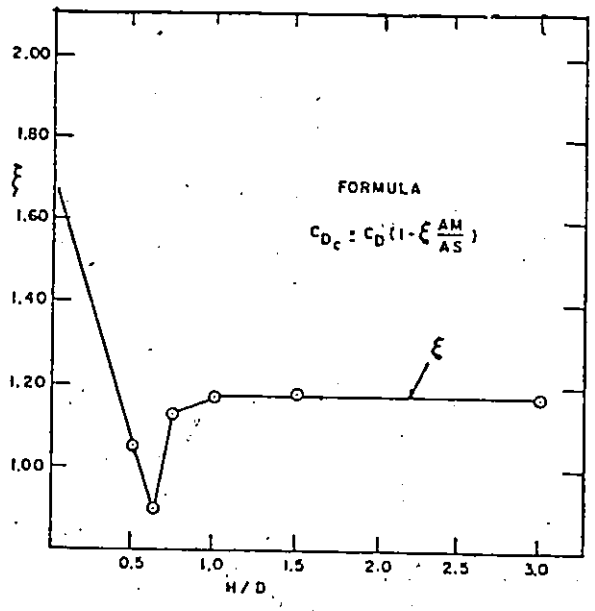

FIGURE 4.5.7.1 - VARIATION OF ξ WITH H/D AFTER COURCHESNE AND LANEVILLE

4.6 INHERENT DISCREPANCIES IN MEASUREMENTS

The accuracy of measured coefficients by strain measurements was tested by comparing them with measurements done by pressure taps along the mid-height perimeter of the model.

It was found that the drag and lift coefficients determined by pressure measurements were higher than those found by strain measurements (c.f. Figures 21 to 24 and 25 to 28). There are two possible causes for this discrepancy, namely that the pressures measured at the mid-height of the model are not representative of the pressures acting along the total height of the model and that there was an insufficient array of pressure taps used.

4.6.1 Accuracy of Perimeter Pressure Measurements at the Mid-Height of the Model

It was decided to check for the discrepancy in drag coefficients measured by strain and pressure readings. To that effect, models were equipped with a piece of tubing along centre of the trailing edge face and the base pressure was measured along the length of the back face of the model by successively moving the tube. The cause of the variance in the representativeness of the center pressures with respect to the whole model was that there was a gap between

the top of the model and the test section ceiling. This gap caused an increase in pressure due to the fact that the flow was behaving in a three-dimensional way at the top of the model. Three gap sizes were tested, namely 0.125, 0.60 and 0.75 inches. The base pressure coefficients are listed in Tables 30 to 34 and are plotted in Figures 13 to 20 for the gap sizes tested. It should be noted that the gap size used for all model tests was 0.60 inches.

Another possible cause for the discrepancy in drag coefficients measured by strain and pressure readings is the possible variation in wind speed in the vertical plane. However it was found by squaring Figure 4.3.4(b) that the mean speed variation was on the order of one percent, typically 1.4%, as was mentioned in section 4.3.

By integrating the base pressure coefficient over the height of the model and relating it to a uniform pressure distribution as was assumed with the center perimeter pressure readings, it was found that the pressure readings at mid-height of the model overestimate the actual pressure due to the non-two-dimensionality of the model.

The results (minus the mean speed variation) are as follows:

MODEL	FLOW CONDITION	% OVER READING OF PRESSURE DUE TO MID-HEIGHT PRESSURE MEASUREMENTS		
		GAP SIZE (INCHES)		
		0.125	0.60	0.75
S36S	SMOOTH	+5	+14	--
S36T2	TURBULENT (GRID 2)	+5	+13	--
36S	SMOOTH	+5	+15	+23
36T2	TURBULENT (GRID 2)	+5	+15	+24
AVERAGE		+5%	+14%	+23%

For an angle of incidence of 90°, there was no noticeable variation in the base pressure coefficient along the height of the model. This is evidenced from the data in Table 34. This is attributable to the shape of the model, i.e. as it is deeper than wide, there is a re-attachment of the wake and the vortex shedding is not as significant on the pressure measurements.

Although there was no variation in the base pressure coefficient measured along the height of the model, it was, as the 0° case, a more positive value than from that measured with the pressure models.

The difference in drag coefficient calculated from strain and pressure measurements is due to the three-dimensional behaviour of the model. The discrepancy in drag and lift coefficients obtained from the strain and pressure measurements between the angles of incidence of 20° and 90° is due to a lack of pressure taps rendering the pressure distribution quite sketchy and very difficult to estimate at large yaw angles.

4.6.2 Estimation of the Variation of the Base Pressure Coefficient between the two-dimensional and three-dimensional models

The relationship between the base pressure coefficient and the variation from two-dimensionality of the model was investigated by plotting the base pressure coefficients versus the normalized gap (ratio of gap width to face width of the model). This is illustrated in Figures 58 and 59 and the data is summarized in Table 35.

The values for the base pressure coefficient for a zero normalized gap (two-dimensional case) obtained from Figures 58 and 59 are summarized in Table 36 and compared with those of the pressure models obtained from Tables 22 and 23. The average difference between the base pressure coefficients obtained from the pressure tests and that regressed from the

normalized gap is 4.6% and 7.2% for an angle of incidence of 0 and 90 degrees respectively. Thus it can be inferred that the data obtained from the non-two-dimensional case and compared with the data of the two-dimensional models.

4.7 ANALYSIS OF THE DRAG COEFFICIENT

The drag coefficients obtained from the strain measurements for three different blockage ratios were corrected using the blockage correction methods explained in Section 4.5 (c.f. references 6, 7, 8, 24, 25, 28 and 36). These are tabulated in Tables 37 to 45. The same was done for the drag coefficients obtained from the pressure measurements (Tables 46 and 47).

The drag coefficients obtained from the strain measurements were increased by 14% to bring the values up to par with the two-dimensional case and make them compatible with the values obtained from the pressure measurements.

4.8 PROPOSED BLOCKAGE CORRECTION EQUATION

It has been noted that in order to correct for blockage, two parameters have to be corrected for: the solid blockage and the wake blockage. The equation proposed corrects for solid blockage by taking the blockage ratio into account and

corrects for wake blockage by taking the base pressure acting on the model into account.

The equation proposed by the author is as follows:

$$C_{D_c} = \frac{C_{D_u}}{1 + S/C} \frac{\varepsilon M}{\varepsilon M_o} \qquad \text{Eqn 4.8.1}$$

applicable to all blockage ratios.

where C_D is the drag coefficient,

S is the projected face area of the model,

C is the test section cross-sectional area,

$\varepsilon M = \frac{1}{k^2+1}$ and $k^2 = 1 - C_{P_b}$

and εM_o is the value of εM regressed for zero blockage ratio.

By plotting $\varepsilon M/(\varepsilon M_o(1+S/C))$ versus blockage ratio, we obtain a straight line with slope Bcor, and x-intercept Delx at a blockage ratio S/C = 0.0. Thus we obtain the following linear relationship:

$$C_{D_c} = C_{D_u}(\text{Delx} + \text{Bcor } S/C) \qquad \text{Eqn 4.8.2}$$

Calculations done using this formula for angles of incidence of 0 and 90 degrees for smooth and turbulent flows for five different model sizes are tabulated in Tables 4.8.1 and 4.8.2. Table 4.8.3 shows the calculations to obtain the correction factors (Bcor and Delx) for blockage and Figure 4.8.1 shows the linear relationship of this blockage correction versus the blockage ratio.

From Figure 4.8.1, the slope of the line was found to be Bcor = -1.88 and the x-intercept was found to be Delx = 1.03 which when substituted in equation 4.8.2 yields the relation

$$C_{D_c} = C_{D_u}(1.03 - 1.88\ S/C) \qquad \text{Eqn } 4.8.3$$

The tabular representation shown in Figure 4.8.5 lists the values of corrected drag coefficient for all models for flows normal to the model faces using the exact form of equation 4.8.1 instead of the regressed form of equation 4.8.2.

TABLE 4.8.1

CALCULATIONS FOR CORRECTED DRAG USING EQUATION DESROSIERS FOR THE SMOOTH FLOW CASE

ANGLE OF INCIDENCE: $\alpha = 0°$

MODEL	C_{D_u}	S/C	C_{p_b}	$\varepsilon M = \frac{1}{k^2+1}$	$\frac{\varepsilon M}{\varepsilon M_o}$	C_D CORRECTED
1X2	2.278	0.083	-1.65	0.274	0.945	1.988
1.5X3	2.607	0.125	-1.88	0.258	0.890	2.062
2X4	2.962	0.167	-2.10	0.244	0.841	2.134
3X6	3.748	0.250	-2.97	0.201	0.693	2.078
4X8	4.730	0.333	-4.00	0.167	0.576	2.044
				$\varepsilon M_o = 0.290$		$\overline{C}_{D_c} = 2.0621 \pm .047$

ANGLE OF INCIDENCE: $\alpha = 90°$

MODEL	C_{D_u}	S/C	C_{p_b}	$\varepsilon M = \frac{1}{k^2+1}$	$\frac{\varepsilon M}{\varepsilon M_o}$	C_D CORRECTED
1X2	1.652	0.042	-0.69	0.372	0.942	1.493
1.5X3	1.821	0.063	-0.71	0.369	0.934	1.600
2X4	1.805	0.083	-0.84	0.352	0.891	1.485
3X6	1.966	0.125	-0.98	0.336	0.851	1.487
4X8	2.162	0.167	-1.19	0.313	0.792	1.467
				$\varepsilon M_o = 0.395$		$\overline{C}_{D_c} = 1.506 \pm .048$

N.B. C_{D_u} OF THE 1.5X3 MODEL WAS OBTAINED FROM THE STRAIN MEASUREMENTS AND INCREASED BY 14%. ALL OTHER VALUES OF C_{D_u} WERE OBTAINED FROM THE PRESSURE MEASUREMENTS.

TABLE 4.8.2

CALCULATIONS FOR CORRECTED DRAG USING EQUATION DESROSIERS FOR THE TURBULENT FLOW CASE (COARSE GRID)

ANGLE OF INCIDENCE: $\alpha = 0°$

MODEL	C_{D_u}	S/C	C_{P_b}	$\varepsilon M = \frac{1}{k^2+1}$	$\frac{\varepsilon M}{\varepsilon M_o}$	C_D CORRECTED
1X2	2.278	0.083	-1.65	0.274	0.945	1.988
1.5X3	3.191	0.125	-2.47	0.224	0.868	2.462
2X4	3.709	0.167	-2.80	0.208	0.806	2.561
3X6	4.080	0.250	-3.45	0.183	0.709	2.315
4X8	5.130	0.333	-4.45	0.155	0.601	2.312
				$\varepsilon M_o = 0.258$		$C_{D_c} = 2.461 \pm .134$

ANGLE OF INCIDENCE: $\alpha = 90°$

MODEL	C_{D_u}	S/C	C_{P_b}	$\varepsilon M = \frac{1}{k^2+1}$	$\frac{\varepsilon M}{\varepsilon M_o}$	C_D CORRECTED
1X2	1.515	0.042	-0.48	0.403	0.983	1.429
1.5X3	1.552	0.063	-0.52	0.397	0.968	1.413
2X4	1.515	0.083	-0.56	0.391	0.954	1.335
3X6	1.673	0.125	-0.65	0.377	0.920	1.367
4X8	1.848	0.167	-0.86	0.350	0.854	1.352
				$\varepsilon M_o = 0.410$		$\bar{C}_{D_c} = 1.377 + .036$

N.B. C_{D_u} OF THE 1.5X3 MODEL WAS OBTAINED FROM THE STRAIN MEASUREMENTS AND INCREASED BY 14%. ALL OTHER VALUES OF C_{D_u} WERE OBTAINED FROM THE PRESSURE MEASUREMENTS.

TABLE 4.8.3

BLOCKAGE CORRECTION FACTOR FOR EQUATION DESROSIERS
(AVERAGE OF SMOOTH AND TURBULENT FLOW)

ANGLE OF INCIDENCE: $\alpha = 0°$

MODEL	S/C	$\left(\frac{\varepsilon M}{\varepsilon M_o}\right)_{avg}$	$\left(\frac{\varepsilon M}{\varepsilon M_o}\right)_{avg} / (1+S/C)$
1X2	0.083	0.942	0.870
1.5X3	0.125	0.879	0.781
2X4	0.167	0.824	0.706
3X6	0.250	0.701	0.561
4X8	0.333	0.594	0.445

ANGLE OF INCIDENCE: $\alpha = 90°$

MODEL	S/C	$\left(\frac{\varepsilon M}{\varepsilon M_o}\right)_{avg}$	$\left(\frac{\varepsilon M}{\varepsilon M_o}\right)_{avg} / (1+S/C)$
1X2	0.042	0.981	0.942
1.5X3	0.063	0.970	0.913
2X4	0.083	0.940	0.868
3X6	0.125	0.902	0.802
4X8	0.167	0.839	0.719

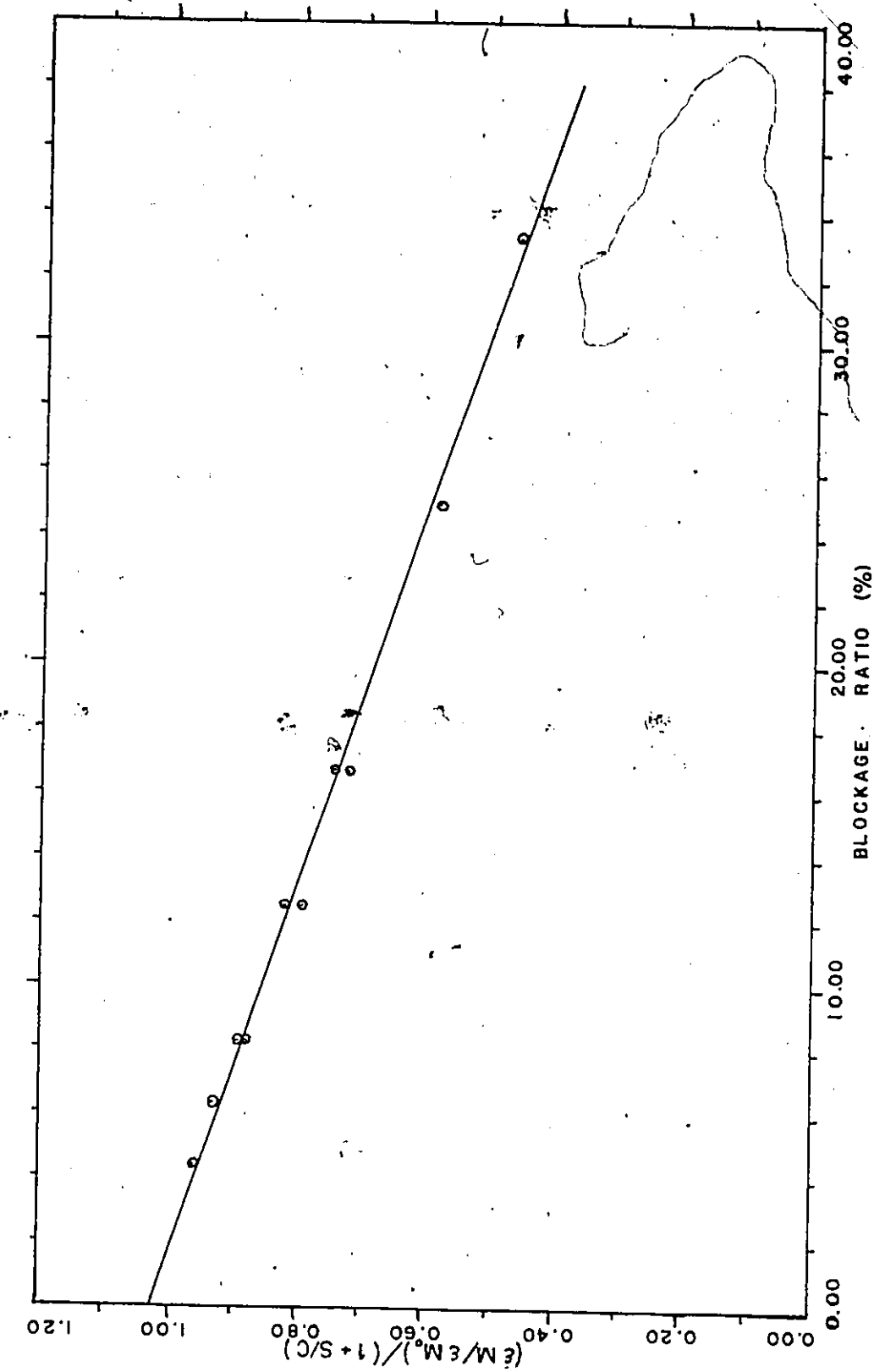

FIGURE 4.8.1 - TOTAL (SOLID & WAKE) BLOCKAGE CORRECTION VERSUS BLOCKAGE RATIO

4.9 CRITICAL COMMENTS ON THE BLOCKAGE CORRECTIONS USED

The values for drag coefficient corrected by the different formulae can be found in Tables 37 to 47. An examination suggests that the equations correct quite well but that some of them have a tendancy towards overcorretion, while others have a tendency towards undercorrection. Bearman and Trueman [4], Nakaguchi, Hashimoto and Muto [29] and the NACA TN 3068 [9] find the following C_D values for bluffness ratios of d/w = 0.5 and d/w = 2.0 for a truly two-dimensional rectangular section:

d/w	DRAG COEFFICIENT C_D			
	NACA	Bearman	Nakaguchi	Mean
.5	2.2	2.3	2.35	2.28
2.0	1.4	1.5	1.55	1.48

The values of corrected drag coefficients as well as the mean drag coefficients and their respective standard devia-

tions can be found in Tables 48 to 51. The means and standard deviations of corrected drag coefficients found by the different blockage correction theories are summarized in Table 4.9.1 for angles of incidence of 0, 30, 60 and 90 degrees. The performance of each of these theories is numbered according to least standard deviation (numbers in circles) and the weighted performance of the equations is summarized in Table 4.9.2.

The blockage corrections applicable to any blockage ratio which correct for standard deviation about the mean corrected drag with little or no over or under-correction are as follows, numbered in order of accuracy (1 being the most accurate, 2 being the second most accurate, etc.).

1. DesRosiers
2. Maskell
3. Modi and El-Sherbiny
4. Cowdrey
5. Ranga Raju
6. Courchesne and Laneville

TABLE 4.9.1

MEANS AND STANDARD DEVIATIONS OF CORRECTED DRAG COEFFICIENTS ACCORDING TO THE DIFFERENT THEORIES

SMOOTH FLOW

ANGLE OF INCIDENCE	MASKELL	COWDREY	MODI & EL-SHERBINY	RANGA RAJU	LANEVILLE COURCHESNE	DESROSIERS
0	1.956±.045	2.054±.065	2.212±.142	2.013±.062	2.525±.356	2.061±.047
30	1.406±.111	1.260±.204	1.339±.169	N/A	N/A	1.378±.127
60	1.703±.184	1.641±.263	1.720±.221	N/A	N/A	1.812±.154
90	1.581±.032	1.558±.034	1.600±.034	1.792±.123	1.653±.056	1.506±.048

TURBULENT FLOW

ANGLE OF INCIDENCE	MASKELL	COWDREY	MODI & EL-SHERBINY	RANGA RAJU	LANEVILLE COURCHESNE	DESROSIERS
0	2.220±.189	2.459±.175	2.639±.085	2.408±.138	2.995±.205	2.461±.134
30	1.923±.138	1.957±.174	2.086±.111	N/A	N/A	2.014±.104
60	2.009±.153	2.075±.192	2.178±.152	N/A	N/A	2.138±.111
90	1.404±.029	1.344±.043	1.380±.033	1.544±.087	1.431±.038	1.379±.036

TABLE 4.9.2

WEIGHTED PERFORMANCE OF THE DIFFERENT BLOCKAGE CORRECTIONS

FLOW TYPE	MASKELL	COWDREY	MODI & EL-SHERBINY	RANGA RAJU	LANEVILLE COURCHESNE	DESROSIERS
SMOOTH	5/4	14/4	13/4	8/2	10/2	8/4
TURBULENT	12/4	17/4	7/4	9/2	10/2	7/4
COMBINED	17/8	31/8	20/8	17/4	20/4	15/8
RATING	2.125	3.875	2.5	4.25	5	1.875

In order of best correction, the theories are:

1. DesRosiers
2. Maskell
3. Modi and El-Sherbiny
4. Cowdrey
5. Ranga Raju
6. Laneville and Courchesne

} Not applicable to angles other than 0 or 90 degrees.

N.B. The correction of DesRosiers is the only one which is uniform in smooth or turbulent flows, hence it is more consistant.

4.9.1 Maskell's Equation

From Tables 37 to 45, it can be seen that Maskell's equation tends to slightly overestimate the drag correction and more so at high blockage ratios, in this case over 15 percent, thus yielding an overcorrected and too small a value for the drag coefficient.

This has been noted by Modi and El-Sherbiny [28] who found that " [Maskell's equation was] inadequate particularly at higher blockage ratios. However modification [of this equation] through inclusion of the the higher order terms improved their applicability." They also found that "... the theory is able to account for the blockage of around 5-10 percent ... It is observed that the validity of the theory is limited to the lower blockage ratio range, as the discrepancy tends to increase with constraint." It can be seen in Figure 4.9.1.1 that including the high order terms in Maskell's equation does not help the overcorrection tendency for high blockage ratios.

Ramamurthy and Ng [35] also find Maskell's equation to overcompensate because the ' Invariance of C_D/k^2 implies that u_j [the velocity on the flow coming off the front face of the model] = u_s =ku [the velocity on the edge of the wake bubble], which denotes a simple increase in the undisturbed

velocity u, provides the necessary adjustments to account for the variations in the drag force due to the blockage effects. However, in blocked flows, dynamic similarity cannot be achieved by a mere change in the velocity scale as the degree of accelerations along the forebodies of bluff shapes near the separation points depend on blockage."

Courchesne and Laneville [6] find that Maskell's equation is valid only for the range $0.5 < d/w < 0.75$ for cylinders. For values of d/w larger than 0.75, Maskell's theory underestimated C_{D_c}. They found that " For cylinders with d/w less than 1 and blockage ratios less than 10 percent, the underestimation of C_{D_c} by Maskell's theory is of the order of 5 percent. For larger blockage ratios and longer after body lengths, Maskell's theory severely underestimates C_{D_c}."

From the data in Tables 48 and 49, it is shown that Maskell's theory underestimates C_{D_c} by a factor of 4 to 9 percent depending on the blockage ratio.

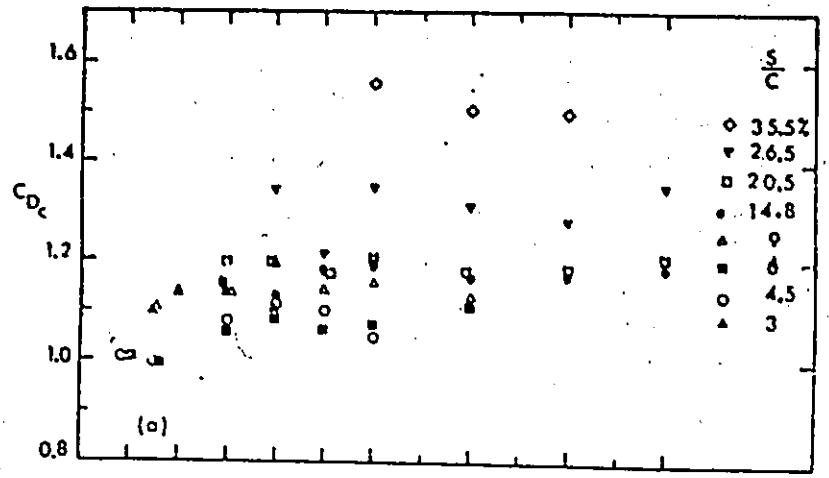

a) DIRECT APPLICATION OF MASKELL'S FORMULA

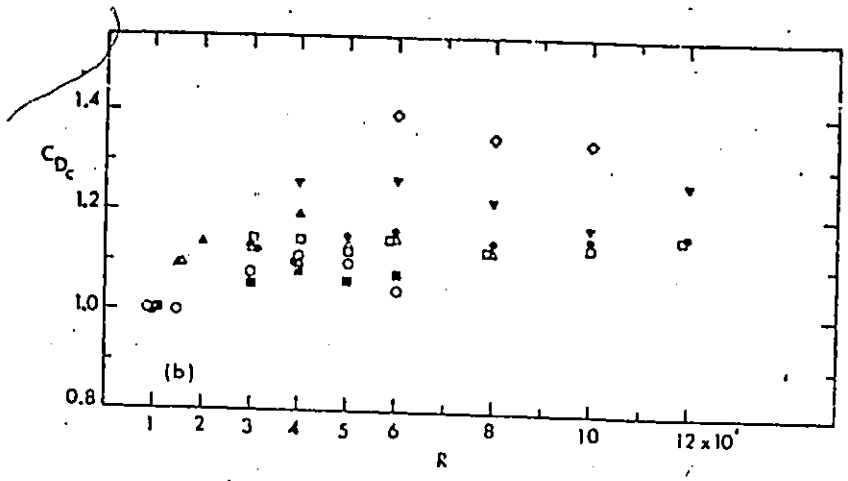

b) USE OF HIGHER ORDER TERMS

FIGURE 4.9.1.1 - INCLUSION OF HIGHER ORDER TERMS IN MASKELL'S FORMULA

4.9.2 Cowdrey's Equation

As Cowdrey's equation is based on Maskell's theory and is basically Maskell's equation written under a slightly different form to take into account higher blockage ratios, it is plausible to assume that it will suffer many of the shortcomings of Maskell's theory. From Tables 37 to 45, it is evident that Cowdrey's theory underestimates C_{D_c} by about 5 percent depending on the blockage ratio. This is mainly due to the fact that Cowdrey devised his equation on the premise that the value of S/C would not be greater than 0.10 (c.f. Section 3.2.2), when in fact we deal with an S/C ratio up to 0.40.

4.9.3 Modi and El-Sherbiny's Equation

In developing a correction formula in a polynomial form based on Maskell's equation and regressing it with their experimental data, Modi and El-Sherbiny obtained a very good relationship for blockage correction. The undercorrection of their formula varies from 1 percent at low blockage ratios to 15 percent at high blockage ratios. Thus it is not applicable for blockage ratios of more than 15 percent.

Courchesne and Laneville [6] observe that " Using Modi and El-Sherbiny's free streamline model for the flat plate

between constraining walls, the prediction of the uncorrected drag coefficient from the base pressure was generally excellent [for blockage ratios of up to 13 percent]. Also their correction of the drag coefficient was ... generally in excellent agreement."

4.9.4 Ranga Raju and Garde's Equation

The empirical formula developed by Ranga Raju and Garde [36, 37] takes only the ratio of model area to test section area and sets it into an equation of an exponential form. The overcorrection of their formula ranges from 5 percent at low blockage ratios to a slight undercorrection at high blockage ratios. The source of this discrepancy lies in the fact that they disregard the contributions of the variations in the base pressure due to blockage. This causes their formula to usually underestimate C_{D_c}.

4.9.5 Courchesne and Laneville's Equation

In basing their correction formula on Maskell's theory, Courchesne and Laneville [6] decided to forego any measurement of the base pressure and have instead set an empirical factor $\gamma - C_{D_c}/(k_c^2-1)$. This factor γ was determined experimentally for different values of d/w. While one of the

advantages of this formula is that it removes the necessity of measuring the base pressure, its drawback is that it is applicable only to blockage ratios up to about 15 percent. Up to this blockage ratio, the formula undercorrects by 12 percent, which is an acceptable value for an empirical formula of this type.

However Laneville and Courchesne realize this equation's drawback and state that "For the range of blockage ratios considered [up to 13%], the ... empirical formula gave very good corrections. Considering the extension to higher blockage (> 13 percent), the linear relation will certainly overestimate the corrected drag coefficient". In fact, at high blockage ratios (over 25%), the equation overestimates the drag coefficient by 50 percent.

4.9.6 Equation DesRosiers

This blockage correction equation, which takes the solid blockage into account with the S/C (blockage ratio) term and the wake blockage into account by relating the base pressure coefficients of the models tested to the base pressure coefficient of a model of with zero blockage, yields very good values of corrected drag. The blockage correction equation proposed by the author corrects within 5 percent at all blockage ratios.

This equation was tested only for two-dimensional models of bluffness aspect ratio d/w=0.5 and d/w=2.0 but there is no reason to suspect why it would not be also applicable to d/w ratios up to 5.0 as it has a built in error compensation residing in the ratio of $\varepsilon M/\varepsilon M_o$. It should also be applicable to bluff body shapes other than rectangular cylinders such as prisms and wedges or other bluff bodies. Furthermore, it is a valid correction for all angles of incidence.

4.9.7 Comments on Blockage Equations

When modelling civil engineering structures in wind tunnel tests the evaluation of the drag coefficient is of great importance if the forces acting on the body are to be determined accurately for design purposes. Of paramount importance is the effect of blockage in wind tunnel testing which increases the apparent drag coefficient and thus overestimates the forces acting on the body. In these cases a correction formula must be applied to correct the measured forces to a realistic value. This is what the previous blockage correction equations have attempted with some being more succesful than others.

It can therefore be concluded that a valid blockage correction formula is very useful in that it allows larger mo-

dels to be used in wind tunnel tests when some details would be lost if the scale of the model was too small. It also allows tests to be run in smaller wind tunnels which results in a lower cost to the user.

4.10 ON THE SIGNIFICANCE OF DRAG

Drag by definition is the force component parallel to the ralative approach velocity, exerted on the body by a moving fluid. The drag force in subsonic aerodynamics is generally recognized to be made up of "friction drag" from the action of the viscosity at the surface and "pressure drag", the streamwise component of the pressure distribution on the body. For slender bodies, the drag is mainly friction drag while for bluff bodies with a certain thickness, the flow separates and the drag is almost entirely due to pressure drag.

In architectural aerodynamics where we deal mostly with bluff bodies with high pressure drag components, the friction drag is negligible.

As the drag force is defined as:

$$D = C_D \, A \, \frac{\rho V^2}{2}$$

where C_D is the drag coefficient,

A is the face area of the body,

ρ is the density of the fluid, and

V is the fluid velocity, we see that by evaluating the drag coefficient of a body, it is very simple to evaluate the drag force acting on it due to a particular body area or fluid velocity.

4.11 ON THE SIGNIFICANCE OF LIFT

Lift by definition is the fluid-force component on a body at right angles to the relative approach velocity. In architectural aerodynamics, lift is as important as drag and causes as many problems. The major problem caused by lift is that it acts as a side force in wind engineering. This side force combined with the drag force creates an overturning moment which must be taken into account when designing tall structures. The lift forces on these structures can be readily predicted by wind tunnel tests, but the scale of the model is important. If the scaled model is too small, many of the details (for example cladding) cannot be modeled properly and the tests are of no use. The problem arises when going to a larger model size and encountering blockage. Thus the lift must also be corrected as was the drag force.

4.11.1 Correction of the Lift Coefficient

Little research was done on how to correct for lift when subjected to blockage problems, however many use the same correction as for the drag and this seems satisfactory. Maskell applies his blockage correction equation to different size models of a Delta wing of aspect ratio 3 and uses it to correct for drag, lift and pitching moment coefficients. This equation is only valid for seperated flow drag and not induced drag or skin friction. It can be seen in Figure 4.11.1.1 that the corrected values of the lift coefficient for models with a blockage ratio of 7 percent and 13 percent fall on the same line. Thus Maskell estimates his correction equation to be valid also for the lift coefficient. The only limitation of his formula lies as was previously noted in the fact that it is not applicable to high blockage ratios (over 15%) and is only valid in the case of seperated flow. Modi and El-Sherbiny [28] from their polynomial correction equation set up two different correction equations; one for drag, the other for lift. Typically their correction for lift coefficient ranged between 2 percent more correction at 5 percent blockage ratio to 15 percent more correction at a blockage ratio of 20 percent. Thus using the drag correction and applying it to lift results in a conservative correction according to Modi and El-Sherbiny's data.

Using the lift coefficient found by the pressure measurements (Tables 16 to 21) and the corresponding values of the base pressure as tabulated in Tables 24 to 29, the lift coefficient measured at different angles of incidence can be corrected for different blockage ratios. The results are shown in Tables 4.11.1.1 and 4.11.1.2 for smooth and turbulent flows.

The blockage correction equations used were Maskell's, Modi and El-Sherbiny's and the proposed equation DesRosiers. The equations are as follows:

Maskell: $C_{L_c} = C_{L_u} / (1 + \varepsilon C_{L_u} S/C)$ Eqn 4.11.1.1

where $\varepsilon = \frac{1}{k_c^2 - 1} = .96$ for two-dimensional models

Modi and El-Sherbiny: $C_{L_c} = C_{L_u} \left(1 - 1.95 \frac{S}{C}\right)$ Eqn 4.11.1.2

DesRosiers: $C_{L_c} = \frac{C_{L_a}}{1 + S/C} \frac{\varepsilon M}{\varepsilon M_o}$ Eqn 4.11.1.3

where $\varepsilon M = \frac{1}{k_c^2 + 1}$

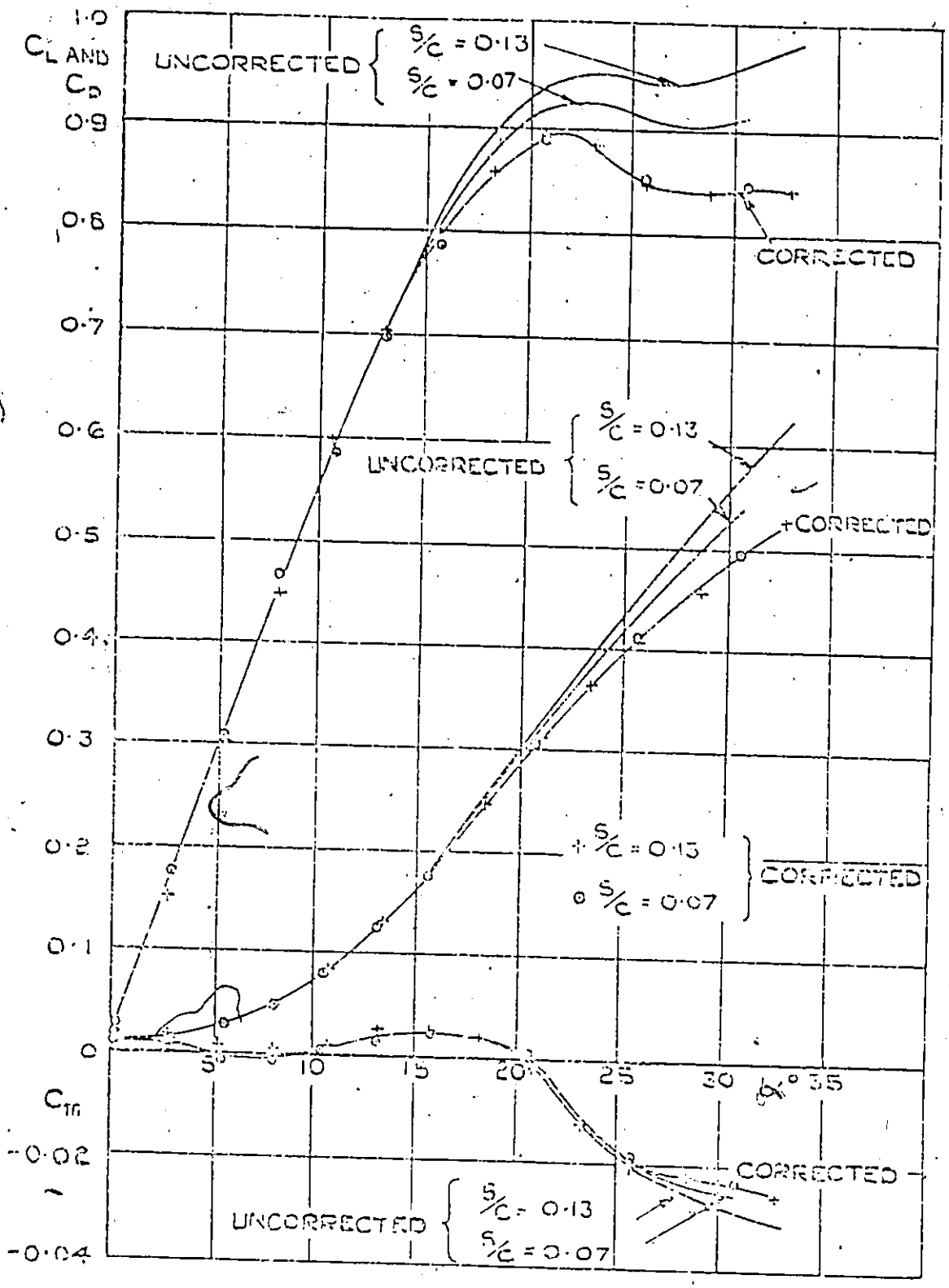

FIGURE 4.11.1.1

APPLICATION OF THE BLOCKAGE CORRECTIONS TO DATA OBTAINED WITH TWO SIZES OF A PARTICULAR WING-BODY COMBINATION.

(DELTA WING OF A=3)

TABLE 4.11.1.1

CORRECTED LIFT COEFFICIENT FOR SMOOTH FLOW FROM PRESSURE TESTS

ANGLE OF INCIDENCE	C_{γ_b}	MODEL	C_{L_u}	CORRECTED C_L MASKELL	MODI	DESROSIERS
10	-1.40	S36S	-0.294	-0.247	-0.237	-0.238
	-1.98	36S	-0.522	-0.355	-0.312	-0.333
	-2.65	B36S	-0.546	-0.292	-0.229	-0.297
20	-1.08	S36S	-0.024	-0.021	-0.020	-0.020
	-1.42	S6S	-0.354	-0.264	-0.213	-0.239
	-2.12	B36S	-0.227	-0.137	-0.098	-0.118
30	-1.08	S36S	-1.037	-0.893	-0.777	-0.877
	-1.35	36S	-0.911	-0.686	-0.499	-0.654
	-1.55	B36S	-1.046	-0.687	-0.373	-0.656
40	-1.16	S36S	-1.475	-1.243	-1.076	-1.230
	-1.39	36S	-1.614	-1.147	-0.815	-1.160
	-1.95	B36S	-1.988	-1.130	-0.615	-1.138
50	-1.13	S36S	-1.553	-1.325	-1.148	-1.313
	-1.35	36S	-1.690	-1.230	-0.882	-1.265
	-1.85	B36S	-2.115	-1.246	-0.695	-1.283
60	-1.13	S36S	-1.689	-1.451	-1.272	-1.461
	-1.25	36S	-1.204	-1.023	-0.711	-0.946
	-1.42	B36S	-1.801	-1.188	-0.700	-1.270
70	-0.98	S36S	-1.199	-1.063	-0.965	-1.048
	-1.15	36S	-1.315	-1.030	-0.827	-1.020
	-1.42	B36S	-1.498	-1.014	-0.701	-1.010
80	-0.72	S36S	-0.102	-0.094	-0.090	-0.091
	-0.86	36S	-0.048	-0.041	-0.037	-0.039
	-1.08	B36S	-0.202	-0.153	-0.132	-0.144

TABLE 4.11.1.2

CORRECTED LIFT COEFFICIENT FOR TURBULENT FLOW (COARSE GRID) FROM PRESSURE TESTS

ANGLE OF INCIDENCE	C_{R_b}	MODEL	C_{L_u}	CORRECTED C_L MASKELL	CORRECTED C_L MODI	CORRECTED C_L DESROSIERS
10	-1.80	S36T2	-0.077	-0.063	-0.063	-0.062
	-2.48	36T2	-0.213	-0.136	-0.134	-0.133
	-3.14	B36T2	-0.392	-0.196	-0.170	-0.200
20	-1.46	S36T2	-0.664	-0.554	-0.514	-0.542
	-1.93	36T2	-0.498	-0.345	-0.292	-0.329
	-2.53	B36T2	-0.957	-0.520	-0.350	-0.511
30	-1.54	S36T2	-1.662	-1.350	-1.185	-1.367
	-1.93	36T2	-1.809	-1.198	-0.871	-1.234
	-2.44	B36T2	-2.125	-1.117	-0.617	-1.191
40	-1.48	S36T2	-1.861	-1.508	-1.319	-1.519
	-1.90	36T2	-2.172	-1.406	-1.019	-1.465
	-2.53	B36T2	-2.651	-1.324	-0.736	-1.434
50	-1.43	S36T2	-1.937	-1.596	-1.393	-1.611
	-1.82	36T2	-2.268	-1.509	-1.102	-1.569
	-2.24	B36T2	-2.536	-1.382	-0.780	-1.473
60	-1.36	S36T2	-2.052	-1.721	-1.509	-1.743
	-1.75	36T2	-2.363	-1.634	-1.217	-1.677
	-1.95	B36T2	-2.459	-1.468	-0.864	-1.549
70	-1.02	S36T2	-1.493	-1.308	-1.181	-1.283
	-1.36	36T2	-1.738	-1.314	-1.044	-1.264
	-1.66	B36T2	-2.041	-1.321	-0.882	-1.284
80	-0.68	S36T2	-0.269	-0.246	-0.236	-0.239
	-0.86	36T2	-0.596	-0.495	-0.439	-0.471
	-1.04	B36T2	-0.765	-0.576	-0.460	-0.541

From Tables 4.11.1.1 and 4.11.1.2, it can be seen that Maskell's correction when applied to the lift coefficient is very accurate, more so in fact than when it is applied to the drag coefficient. Its only drawback is that it requires the drag coefficient to be evaluated in order to correct for the lift.

The blockage correction equation for lift as developed by Modi and El-Sherbiny [28] seems to overcorrect for the lift coefficient. It does so markedly at blockage ratios greater than 15 percent, the reason for this being that it is a polynomial regression based on their data and that it does not take into account the variation in the base pressure due to different blockage ratios. As it underestimates the corrected lift coefficient, this equation should only be used for small blockage ratios, i.e. less than 10 percent, where it seems to perform well.

The proposed equation DesRosiers follows Maskell's correction for lift very closely. As it uses a ratio term M/M for the base pressure coefficient, it is probably slightly more accurate in its values of the corrected lift coefficient and can be used for low to high blockage ratios in the range of about 5 percent to 40 percent. As can be seen in Tables 4.11.1.1 and 4.11.1.2, it corrects very well for smooth and turbulent flows and for all angles of incidence.

4.12 ON THE EFFECTS OF TURBULENCE

The effects of freestream turbulence on boundary layer transition and hence separation is relatively well known. However, the effects of freestream turbulence on the shape of the shear layer shed from a bluff body and therefore the drag has only been recently investigated. It appears that this effect is very significant in the wind loading of structures, not only in terms of mean and fluctuating forces but on the fluctuating pressures near the leading edge of the side face which almost invariably cause the highest pressure on cladding and glazing.

The effects of freestream turbulence have been observed in several apparently contradictory experiments. Bearman [3], Laneville, Gartshore and Parkinson [21], Lee [22] and McLaren, Sherratt and Morton [26] showed how increasing freestream turbulence increased the drag on sharp edged bluff bodies. Vickery [43, 44] and Miyata and Miyazaki [27] showed how increasing freestream turbulence decreased the drag of a square two-dimensional prism. The explanation was shown to lie in the behaviour of the shear layers.

The base pressure (i.e. wake pressure) is a result of the pressure generated by the freestream flow just outside of the shear layer. If the radius of curvature of the shear

layer were to decrease, the velocity just outside the wake would increase and by Bernoulli's equation would give a lower pressure which in turn would result in a lower base pressure and an increase in drag. The radius of curvature of the shear layers are dependent on the rate at which freestream and wake fluid are entrained as shown in Figure 4.12.1.

Notwithstanding the fact that the shear layers roll up into vortices and along with the wake pressures are continually fluctuating, a description of freestream turbulence will be given as though the shear layers are steady. The effect of increasing turbulence is to increase the rate at which the fluid is entrained into the shear layer, which in turn reduces the radius of curvature. In the case of a flat plate the reduced radius of curvature of the shear layer leads to a reduced base pressure and increased drag, but for a square section, for example, it leads to re-attachment on the side faces with increased base pressure and hence lower drag. These effects are described diagrammatically in Figure 4.12.2.

The effect of turbulence and the after-body length on the drag of a rectangular cylinder is illustrated in Figure 4.12.3.

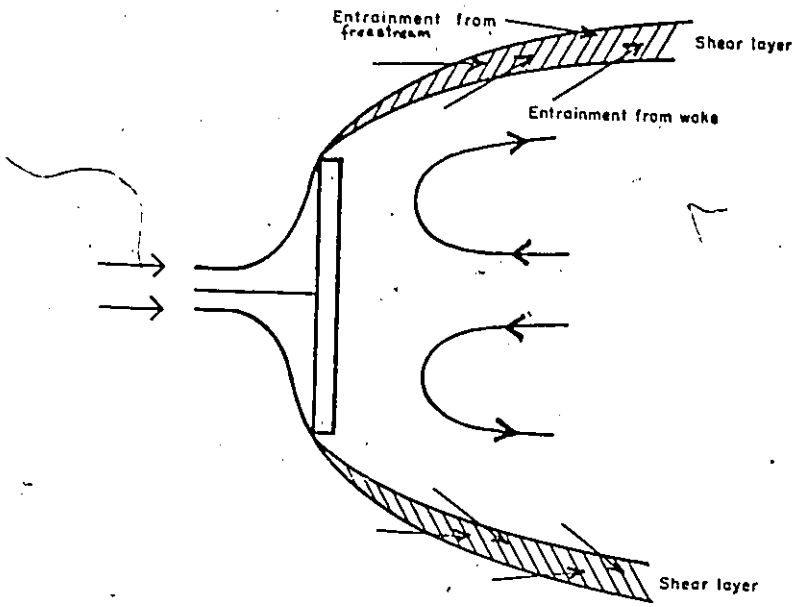

FIGURE 4.12.1 - ENTRAINMENT OF FREESTREAM AND WAKE FLUID INTO THE SHEAR LAYERS

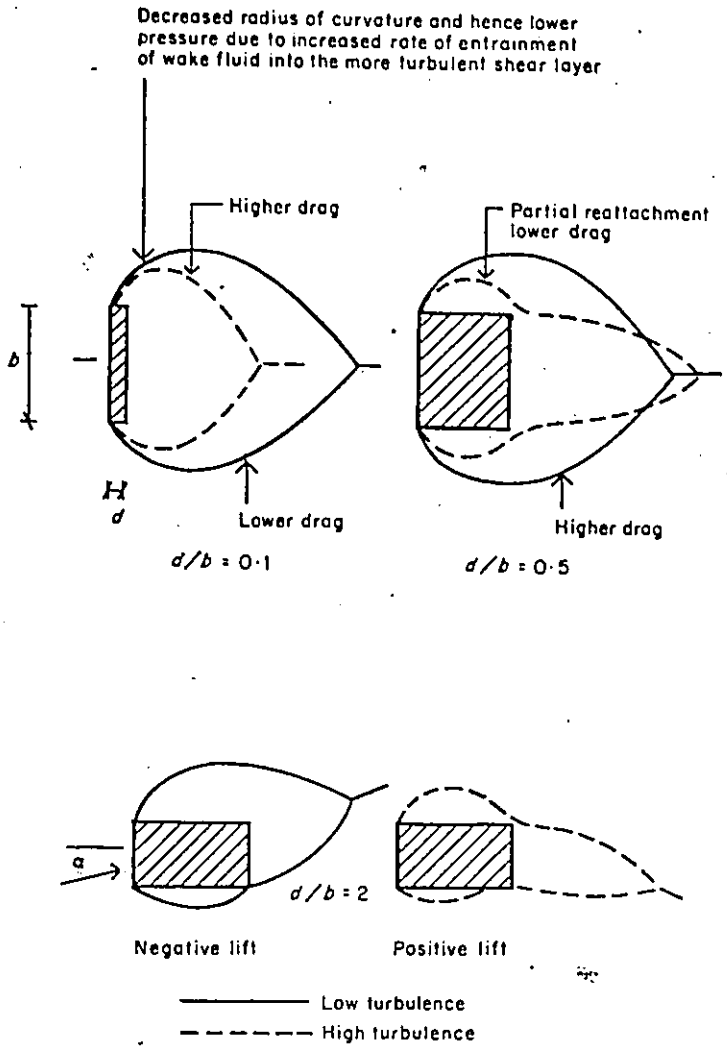

FIGURE 4.12.2 - SKETCHES OF EXPECTED EFFECTS OF TURBULENCE ON DIVIDING STREAMLINES AS IT AFFECTS DRAG AND LIFT OF RECTANGULAR SECTIONS (AFTER GARTSHORE)

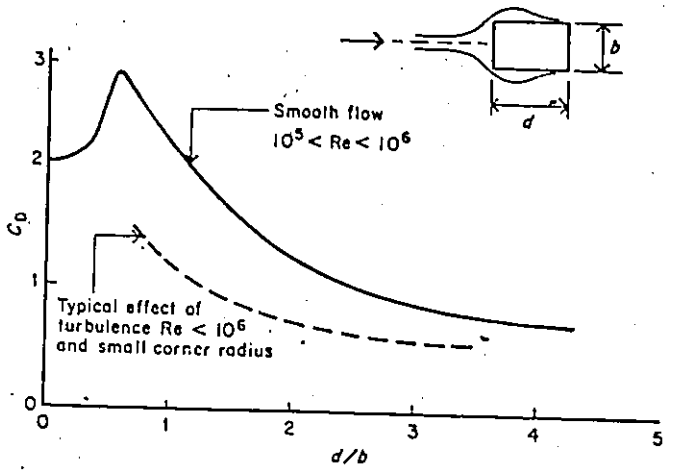

FIGURE 4:12.3 - EFFECT OF TURBULENCE AND AFTER-BODY LENGTH ON THE DRAG OF TWO-DIMENSIONAL CYLINDERS

(AFTER BEARMAN AND VICKERY)

Another most important effect of freestream turbulence is the effect it has on periodicity in the wake. As is previously noted, the shear layers roll up into vortices which are unsteady and continually fluctuating. In the case of smooth flow past a bluff cylinder, the vortices shed alternately and periodically from either side of the cylinder, forming a Von Karman Vortex Street. As the freestream flow becomes more turbulent, the very orderly periodic shedding of vortices starts to break down until eventually the wake contains a broad range of shedding frequencies. The cross-wind oscillations of tall and slender structures tend to be dominated by the wake excitation mechanism.

4.12.1 Effects of Turbulence on Drag

As is reported in the ESDU Data Sheet 71016 [10], the work of McLaren, Sherratt and Morton [26] gives some indication of turbulence scale effects, namely that the drag force is increased due to turbulence. Lee [22] in his paper plots the value of C_D in smooth flow over C_D in turbulent flow for a square cylinder with respect to the turbulence intensity. It is noted that with increasing turbulence, the ratio of drag coefficients of smooth flow to turbulent flow decreases. This is illustrated in Figure 4.12.1.1. Lee states that the "... change of mean drag has been found to be in-

creased influenced by variations in the base pressure alone". This is shown in Figure 4.12.1.2. It can be seen in these two figures that the data does not collapse but nevertheless the trend is to a higher drag coefficient with an increase in turbulence.

As evidenced from Tables 37 to 45, the present drag measurements agree with Mclaren et al and Lee's research for the case where the wide face of the model is normal to the flow. If the model is in its least bluff position, where the narrow face is normal to the flow, the drag coefficient is decreased with turbulence. This is probably due to the fact that there is a reattachment of the seperating shear layers due to turbulence.

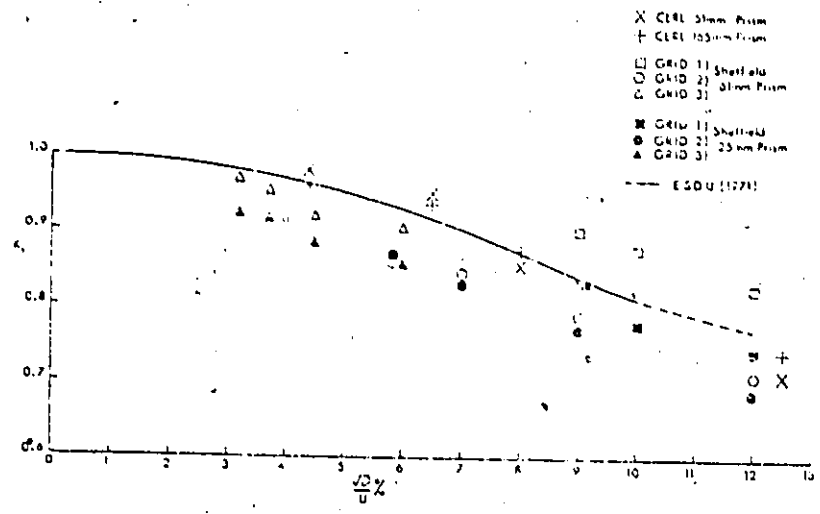

FIGURE 4.12.1.1 - VARIATION OF DRAG RATIO WITH TURBULENCE INTENSITY

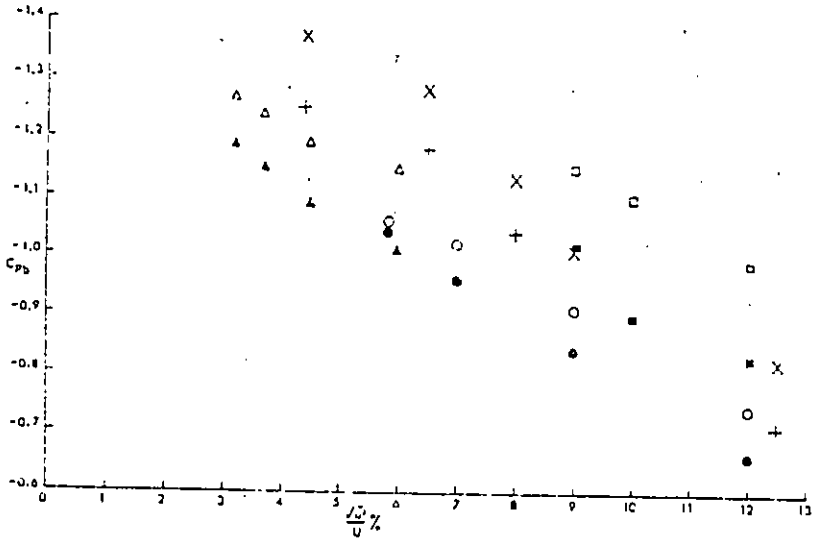

FIGURE 4.12.1.2 - VARIATION OF BASE PRESSURE WITH TURBULENCE INTENSITY

4.12.2 Effects of Turbulence on Lift

Very little research has been done on the effects of turbulence on the lift forces acting on a bluff body, but from data in Tables 1 to 9, it is readily seen that turbulence has a marked effect on the lift, perhaps even more so than on the drag. The main effect of turbulence on the lift is to cause an increase in the magnitude of the lift coefficient for all angles of incidence between 0 and 90 degrees.

This increase in lift is shown as an almost constant offset of the lift curve in Figures 34 to 36. This is attributable to a more negative base pressure which tends to decrease the raduius of curvature of the wake resultuing in a higher drag and higher lift as illustrated in Figure 4.12.2. Partial reattachment of the wake also explains the variation of side pressures on the model, i.e. where the wake reattaches the pressure is of lesser magnitude.

4.12.3 Correcting for Blockage in Turbulent Flow

The main difference between a turbulent flow and a smooth flow is a fluctuation in the fluid velocity about its mean velocity. This however creates many problems resulting in changes in the pressure distribution and alterations in the structure and behaviour of the shear layers.

The freestream turbulence affects the side pressure distribution very strongly when the models have a high bluffness ratio. Figures 4.12.3.1 and 4.12.3.2 illustrate the typical pressure distribution on a model of bluffness ratio 0.5 and 2.0 respectively. From these figures it is seen that the effect of turbulence is to increase the magnitude of the side and base pressures while the frontal or stagnation pressure remains relatively unchanged. When the model has a bluffness ratio of depth to width greater than 1.0, then the side pressure varies in a somewhat triangular pattern from a maximum value near the face of the model to a minimum value near the base of the model. This indicates a tendency of the flow to become reattached to the model and thus reduces the width of the wake as opposed to a model with a depth to width ratio of less than 1.0. This reduction in the width of the wake combined with an increase in the rate of entrainment of the fluid into the shear layers due to reattachment or near reattachment of the flow explains why the base pressure is increased and the drag is reduced in turbulent flow as opposed to smooth flow where there is little reattachment possible.

The variation in the side pressures is explained by the reduced width of the wake and its partial reattachment which results in a greater base pressure and also an increased

side pressure near the frontal face of the model. Near the partial or reattachment points of the shear layers, the side pressure is lessened in magnitude. This explains why the lift is greater in turbulent flow, as in smooth flow the base pressure is lower and there is no reattachment of the wake, thus little variation in side pressures.

The blockage ratio remains unchanged whether in smooth flow or in turbulent flow and creates the same problems, namely a blockage of the flow and a distortion of the wake. However, as was previously explained, the distortion of the wake is not the same in turbulent flow as in smooth flow as there is an increase in the rate of entrainment of the fluid in the shear layers in the presence of freestream turbulence. This results in a decrease in the radius of curvature of the shear layer (c.f. Figure 4.12.1). This reduction in the radius of curvature of the shear layer causes the flow streamlines to be nearer to the streamwise faces of the model leading to a reattachment or near reattachment of the shear layer if the model is deeper than it is wide (typically at least twice as deep as it is wide).

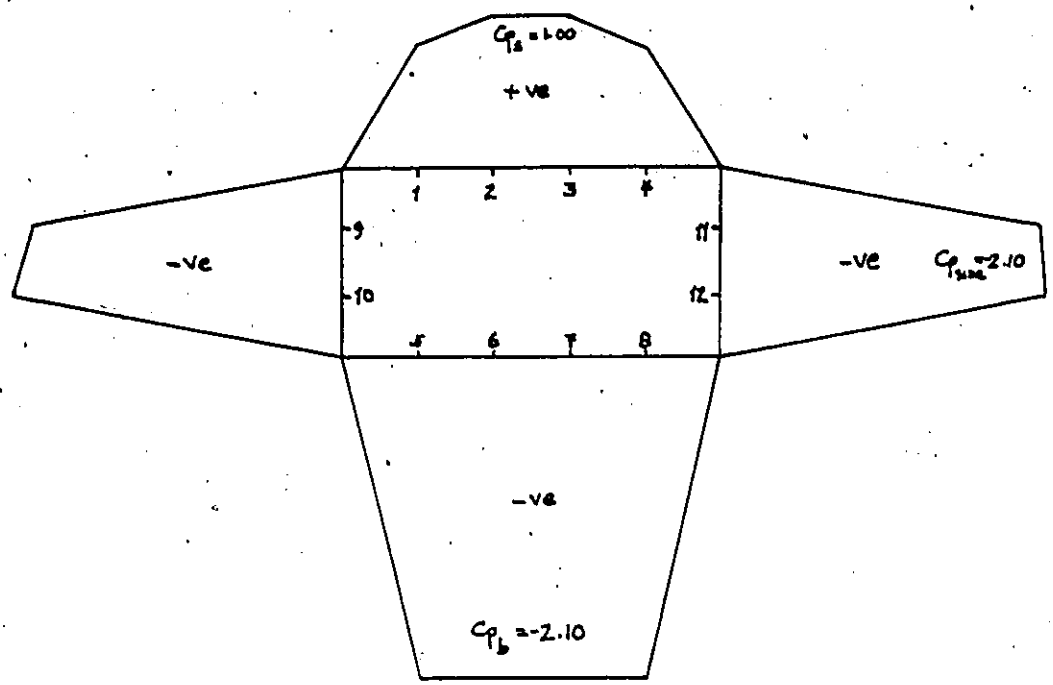

SMOOTH FLOW

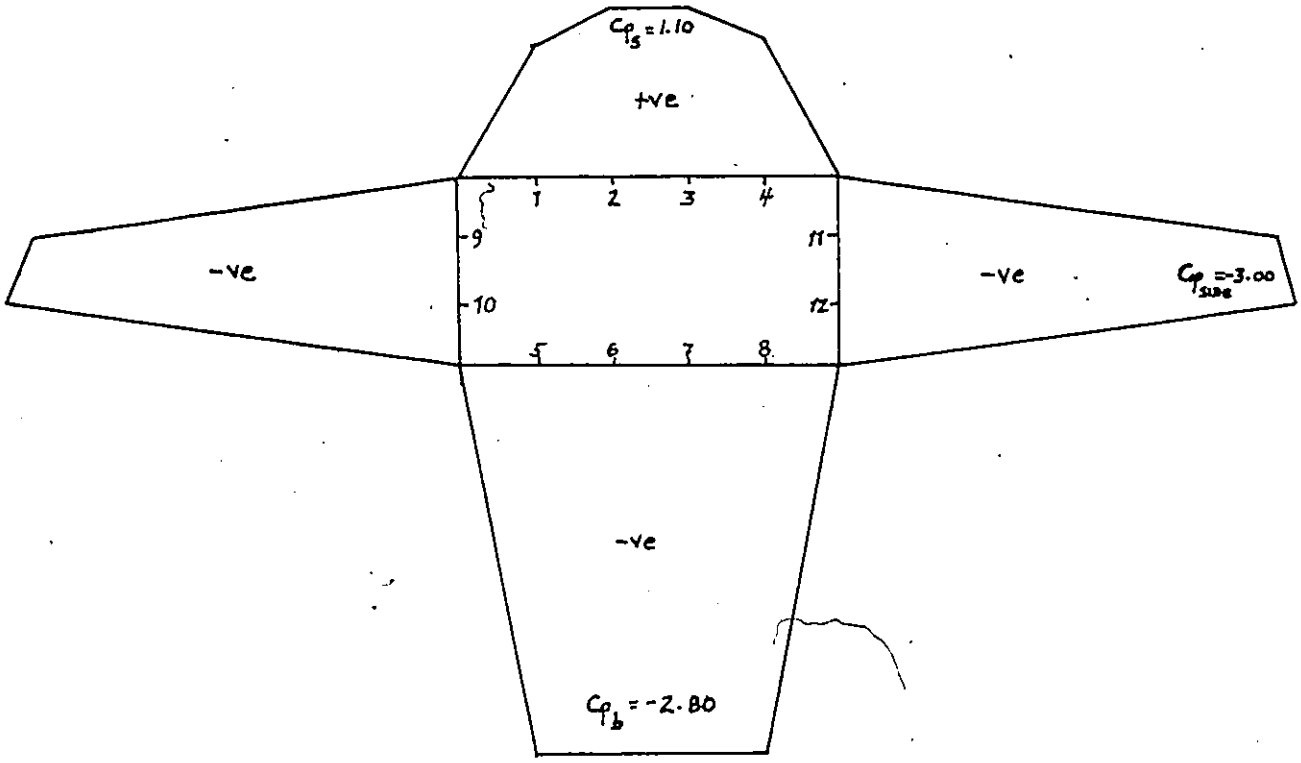

TURBULENT FLOW

FIGURE 4.12.3.1 - TYPICAL PRESSURE DISTRIBUTION FOR A MODEL OF BLUFFNESS RATIO D/W = 0.5 IN SMOOTH AND TURBULENT (GRID 2) FLOW

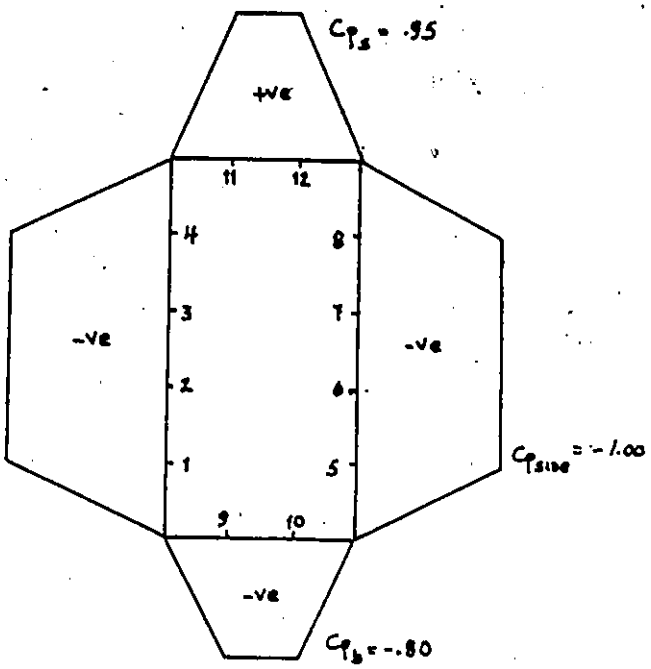

SMOOTH FLOW

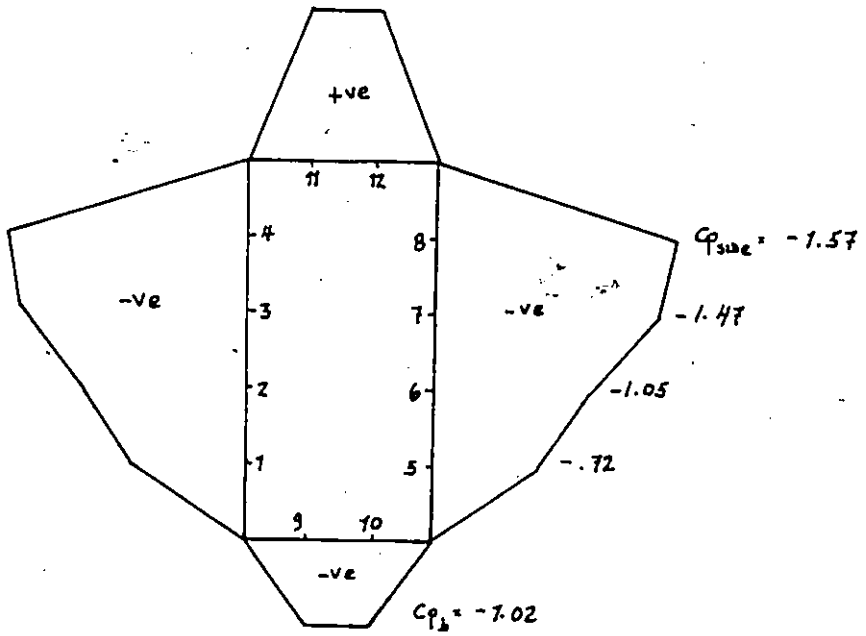

TURBULENT FLOW

FIGURE 4.12.3.2 - TYPICAL PRESSURE DISTRIBUTION FOR A MODEL OF BLUFFNESS RATIO D/W = 2.0 IN SMOOTH AND TURBULENT (GRID 2) FLOW

The reattachment or near reattachment of the shear layer affects the pressure coefficients by reducing the pressure on the streamwise faces and increasing the base pressure. This was also found by Melbourne [47] who states that: "It appears that, for a given blockage, the effect of turbulence parameters is to make the base pressure a little more negative at all angles of attack". This conclusion agrees with the values of the base pressure listed in Tables 22 and 23 and 24 to 29. The stagnation pressure on the front face of the model is little affected by the turbulence in the flow as evidenced in Tables 22 and 23. The small increase in the stagnation pressure is due to the fact that the square of the mean velocity (which is the component used in the calculations) is smaller than the mean square of the velocity.

It is therefore concluded that as the turbulence affects the pressure distribution, these terms should be included in a blockage coreection equation if it is to be valid for turbulent flow. From Tables 38, 39, 40, 42, 44, 45 and 47, it is seen that most blockage corrections are applicable to the drag coefficient in turbulent flow. However, as was noted before in section 4.9, the proposed correction equation by DesRosiers, Maskell and Modi and El-Sherbiny's correction are the preferred equations for drag correction.

Tables 4.11.1.1 and 4.11.1.2 illustrate the corrected values for the lift coefficient according to Maskell, Modi and El-Sherbiny and the proposed DesRosiers blockage correction equations. It is clearly seen that Maskell's equation and the proposed equation DesRosiers are the most accurate for lift correction. Either one can be used but equation DesRosiers is preferred if the blockage ratio is high (over 15%) as it relates the base pressure coefficient of the model tested to a reference standard model of zero blockage.

In conclusion, it can be said that equation DesRosiers is the best all-around blockage correction equation as it not only corrects for drag but also for lift and does so in either smooth or turbulent flow conditions and for all angles of incidence.

4.12.4 Blockage Correction for C_p in Smooth and Turbulent Flow

The past sections have discussed the corrections to be applied to the force measurements, namely the drag and the lift. This section will concentrate on corrections applicable to the pressure forces on the models.

It was previously noted that on the upstream face of the model, there is little effect of the blockage on the pres-

sure distribution. This is also found by Melbourne [47] who states that "On the upstream face even for 20% blockage there is no apparent effect on the pressures in the center of the plate but a distortion of the pressure distribution does occur for the higher blockages towards the edge of the plate". This agrees with the present findings.

Melbourne uses the following formula to correct for the base pressure coefficient:

$$C_{\bar{p}_c} = C_{\bar{p}} - \Delta C_{\bar{p}_c} \qquad \text{Eqn 4.12.4.1}$$

where $C_{\bar{p}_c}$ is the mean corrected base pressure coefficient,

$C_{\bar{p}}$ is the mean base pressure coefficient,

$\Delta C_{\bar{p}_c}$ is the mean base pressure correction,

and $$\Delta C_{\bar{p}_c} = K_b \, C_{D_t} \frac{S}{C}$$

where K_b is an empirical factor determined experimentaly for a particular model/flow/wind tunnel configuration under consideration.

C_{D_t} is the total uncorrected drag acting on the model, and

S/C is the ratio of projected model area to wind tunnel test section area.

The empirical factor K_b is a function of the building height over upstream width expressed as h/b. Some values of K_b are given below for different h/b ratios.

$\frac{h}{b}$	K_b
4	-2.7
2	-2.7
1	-2.7
1/2	-2.7

As yet the author is not aware of any comprehensive study of blockage effects on side pressures. Melbourne [47] in the paper he presented in April 1982 at the Workshop on Wind Tunnel Modelling for Civil Engineering Applications at the National Bureau of Standards in Maryland also states that he "is not aware of any comprehensive study of blockage effects on pressures on streamwise walls" of rectangular bluff bodies. This is on the list of studies to be done and is particularly relevant to designers of large buildings to determine cladding/glazing loads due to peak pressures under reattaching shear layers. As Melbourne states: "This study will be very complex; not only are the reattaching shear

layers and resulting surface pressures sensitive to free-stream turbulence, but it is almost certain that the blockage corrections will be sensitive to turbulence".

It was found however in this study that blockage corrections are not sensitive to turbulence.

Chapter V

DISCUSSION AND CONCLUSIONS

5.1 ON THE DIFFERENT BLOCKAGE CORRECTIONS

No two blockage equations are alike although most of them seem to be derived to some extent using assumptions similar to those of Maskell. Some correct only for solid blockage while others also correct for wake blockage. We are indeed indebted to E. C. Maskell for his blockage correction equation which began an unending cycle of tests on bluff bodies with large blockage ratios. These tests furthered the understanding of the wake distribution behind a bluff body and have also introduced many new blockage correction equations, one of which was introduced in this thesis.

While there is no concensus on which blockage correction formula should be used a priori, a valid blockage correction equation should correct equally well at small blockage ratios (i.e. around 5 percent) as at large blockage ratios (i.e. around 40 percent). Corrected drag values at low blockage ratios and high blockage ratios should be in agreement within 5 percent of each other. This indeed would be an

ideal blockage correction formula. The blockage correction formula proposed by DesRosiers seems to satisfy this criterion as the average standard deviation about the mean corrected drag coefficient values for all models tested whether in smooth or turbulent flow is on the order of 5.2 percent.

5.2 ON THE TWO-DIMENSIONALITY OF THE FLOW

It was discussed previously and shown in Tables 30 to 34 and Figures 13 to 20 that the models tested were not totally two-dimensional in nature as there was a gap between the top of the model and the wind tunnel test section ceiling. Thus the pressure distribution on the trailing edge of the model was not uniform. It was shown that a gap size of 2 percent of the test section height would cause an underestimation of base pressure on the order of 23 percent. Hence, if two-dimensional flow is desired, the top of the model must be flush with the test section ceiling and no leakage must occur around the tip of the model.

This overestimation of forces by pressure measurements is due to the fact that the pressures measured at the mid-height perimeter were assumed to be representative of the pressures along the full height of the model. The actual situation is depicted in Figures 13 to 20 where the base pres-

sure is less at the top of the model due to three-dimensionality of the flow. Hence, to correct the strain-measured forces to equivalent forces on a two-dimensional model, they have to be increased by 14 percent, which was the effect of the 0.60 inch gap of all the models tested.

5.3 CONCLUSIONS

An empirical flat plate type correction (such as Maskell's) should not be used for rectangular cylinders, nor for bluff bodies with a certain depth. Such a procedure will certainly underestimate (i.e. overcorrect) the corrected drag coefficient.

Wind tunnel blockage has a pronounced effect on the drag coefficient as well as on the mean pressure distribution. In particular, the drag coefficient and the magnitude of the base pressure and side pressures and minimum pressure coefficients increase with increasing blockage.

Invariance of C_D / k^2 which denotes a simple increase in the undisturbed stream velocity provides the necessary adjustment to account for the variations in the drag force due to blockage effects. However, in blocked flows, dynamic similarity cannot be achieved by a mere change in the velocity scale as the degree of accelerations along the forebodies of bluff shapes near the separation points depend on blockage.

Free stream turbulence can cause a reduction in wake pressure. It can also promote transition in the boundary layers and free stream layers at lower Reynolds number than in smooth flow. A combination of these effects can cause boundary layer re-attachments not found in smooth flow. The flow around a rectangular cylinder can be altered by the addition of turbulence. Turbulence in the flow, by lowering the wake pressure, increases the drag on the bluff body.

Turbulence in the flow by altering the side pressure distribution, especially when the bluffness ratio is greater than d/w=1.0, causes alternating vortices in the shear layer before reattachment of the flow, resulting in an increase in lift.

A rational and simple method for estimating blockage effects in the case of two-dimensional rectangular prisms has been presented. It has been shown that this equation is suitable in its application from small to large blockage ratios to correct for drag coefficient and lift coefficient because of its ability to relate the base pressure coefficient of the model tested to a reference model of zero blockage.

Most correction equations are applicable only to the drag component but this equation (Equation DesRosiers) is the first simple blockage correction equation which is sui-

table for use for both drag and lift coefficients and for low to high blockage ratios (5% to 40%).

In addition to being valid for smooth flow, this blockage correction equation is equally applicable to turbulent flow cases.

This relation is well suited for other bluff body shapes as it uses a reference term to a zero blockage model to calibrate itself

It was further found that contrary to popular belief, turbulence does not affect the blockage correction problem and that most blockage correction equations currently available can be used satisfactorily in a turbulent flow field. However, it was also found that blockage correction equations which use a base pressure parameter term (such as Des-Rosiers' or Maskell's) yield better corrected values in smooth or turbulent flows, but especially in turbulent flows.

5.4 RECOMMENDATIONS

It is recommended that in further tests the models be set up so as to be flush with the wind tunnel test section ceiling, thereby being more two-dimensional in nature. The only corrections to be added would then be for wall boundary layers.

It is further recommended that a double strain balance be used, i.e. one balance connected at either end of the model and mounted in the floor and ceiling of the wind tunnel test section. This would prevent non-two-dimensionality and also increase the accuracy of the measurements.

All models should be equipped with pressure taps so that all pressures can be readily recorded along with the force and moment measurements by the strain balance.

REFERENCES

1. Awbi, H. R., "Wind-Tunnel-Wall Constraint on Two-Dimensional Rectangular Section Prisms", Journal of Industrial Aerodynamics, Vol. 3, 1978.

2. Aynsley, R. M., Melbourne, W. and Vickery, B. J., Architectural Aerodynamics London (England): Applied Science Publishers Ltd., 1971.

3. Bearman, P. W., "Some Effects of Turbulence on the Flow around Bluff Bodies", N.P.L. Aero Report 1264, April 1968.

4. Bearman, P. W. and Trueman, D. M., "An Investigation of the Flow around Rectangular Cylinders", Aeronautical Quarterly, Vol. XXIII, Part 3, 1972, pp.229-237.

5. Bostok, B. R. and Mair, W. A., "Pressure Distributions and Forces on Rectangular and D-Shaped Cylinders", Aeronautical Quarterly, Vol. XXIII, Part 1, 1972, pp.1-6.

6. Courchesne, J. and Laneville, A., "A Comparison of Correction Methods Used in the Evaluation of Drag Coefficient Measurements for Two-Dimensional Rectangular Prisms", A.S.M.E. Journal of Fluids Engineering, Paper No. 79-WA/FE-3, Aug. 1980.

7. Cowdrey, C. F., "The Application of Maskell's Theory of Wind-Tunnel Blockage to Very Large Solid Models", N.P.L. Aero Report 1247, October 1967.

8. Cowdrey, C. F., "Influence of Small Horizontal Inclinations of the Wind on the Forces on a Model of a Power-Station Boiler House in Various Stages of Erection", N.P.L. Aero Special Report 003, October 1967.

9. Delany, N. K. and Sorensen, N. E., "Low-Speed Drag of Cylinders of Various Shapes", NACA TN 3038, Nov. 1953.

10. E.S.D.U., "Fluid Forces, Pressures and Movements on Rectangular Blocks", Data Sheet 71016, 1971.

11. Fage, A. and Johansen, F. C., "On the Flow of Air Behind an Inclined Flat Plate of Infinite Span", Proceedings Royal Society, A, Vol. 116, 1927.

12. Fage, A. and Johansen, F. C., "The Structure of Vortex Sheets", British A.R.C., R. and M. No. 1143,August 1927.

13. Fail, R., Lawford, J. A. and Eyre, R. C. W., "Low Speed Experiments on the Wake Characteristics of Flat Plates Normal to an Airstream", British A.R.C., R. and M. No. 3120, June 1957.

14. Farell, C., Carrasquel, S., Guven, O. and Patel, V. C., "Effect of Wind Tunnel Walls on the Flow Past Circular Cylinders", A.S.M.E. Journal of Fluids Engineering, Vol. 99, Sept. 1977, pp. 470-479.

15. Garner, H. C., Rogers, E. W. E., Acum, W. E. A. and Maskell, E. C., "Subsonic Wind Tunnel Wall Corrections", AGARDograph 109, Oct. 1966.

16. Glauert, H., "Wind Tunnel Interference on Wings, Bodies and Airscrews", British A.R.C., R. and M. No. 1566, Sept 1933.

17. Guven, O., Patel, V. C. and Farell, C., "A Model for High Reynolds-Number Flow Past Rough-Walled Circular Cylinders", A.S.M.E. Journal of Fluids Engineering, Paper No. 76-WA/FE-14, Sept. 1977.

18. Harris, Joseph, The Tallest Tower, Boston: Houghton Mifflin Co., 1975.

19. Jensen, Martin and Franck, Niels, Model Scale Tests in Turbulent Wind Part I Copenhagen: The Danish Technical Press, 1963.

20. Jensen, Martin and Franck, Niels, Model Scale Tests in Turbulent Wind Part II Copenhagen: The Danish Technical Press, 1965.

21. Laneville, A., Gartshore, I. S. and Parkinson, G. V., "An Explanation of Some Effects of Turbulence on Bluff Bodies", Proceedings of the 4th Int. Conf. on Wind Effects on Buildings and Structures, Heathrow, London, UK, 1975, pp. 333-342.

22. Lee, B. E., "Some Effects of Turbulence Scale on the Mean Forces on a Bluff Body", Journal of Industrial Aerodynamics, Vol. 1, 1975/1976, pp. 361-370.

23. Lee, B. E. and Soliman, B. F., "An Investigation of the Forces on Three-Dimensional Bluff Bodies in Rough Wall Turbulent Boundary Layers", A.S.M.E. Journal of Fluids Engineering, Paper No. 76-WA/FE-1, Sept. 1977.

24. Maskell, E. C., "A Theory of the Blockage Effects on Bluff Bodies and Stalled Wings in a Closed Wind Tunnel", R.A.E. Aero Report 2685, Nov. 1963.

25. Maskell, E. C., "A Theory of the Blockage Effects on Bluff Bodies and Stalled Wings in a Closed Wind Tunnel", British A.R.C., R. and M. No. 3400, 1965.

26. McLaren, F. G., Sherratt, A. F. C. and Morton, A. S., "Effect of Free Stream Turbulence on the Drag Coefficient of Bluff Sharp Edged Cylinders", Nature, 224, 1969.

27. Miyata, Toshio and Miyazaki, Masao, "Turbulence Effects on Aerodynamic Response of Rectangular Cylinders".

28. Modi, V. J. and El-Sherbiny, S., "On the Wall Confinement Effects in Industrial Aerodynamic Studies", Proceedings of Int. Symposium on Vibration Problems in Industry, 1973, Paper no. 116, UK Atomic Energy Authority, Windscale and N.P.L., Teddington.

29. Nakaguchi, H., Hashimoto, K. and Muto, S., "An Experimental Study on Aerodynamic Drag of Rectangular Cylinders", Journal Japan Soc. Aeronaut. Space Sci., Vol. 16, 1968, pp. 1-5.

30. Nakamura, Y. and Tomonari, Y., "The Effect of Turbulence on the Drag of Rectangular Prisms", Journal Japan Soc. Space Sci., Vol. 19, No. 44, 1976.

31. Novak, Milos and Tanaka, Hiroshi, "Effect of Turbulence on Galloping Instability", A.S.C.E. Journal of the Engineering Mechanics Division, Vol. 100, No. EM1, Feb. 1974.

32. Pankhurst, R. C. and Holder, D. W., Wind-Tunnel Technique, London (England): Pitman, 1952.

33. Parkinson, G. V. and Jandali, T., "A Wake Source Model for Bluff Body Potential Flow", Journal of Fluid Mechanics, Vol. 40, 1970, pp. 577-594.

34. Pope, A. and Harper, J. J., Low Speed Wind Tunnel Testing, New-York: John Wiley And Sons, 1966.

35. Ramamurthy, A. S. and Ng, C. P., "Effect of Blockage on Steady Force Coefficients", A.S.C.E. Vol. 99, No. EM4, August 1973, pp. 755-772.

36. Ranga Raju, K. G. and Garde, R. J., "Resistance of an Individual Plate Placed on a Plane Boundary in Two-Dimensional Flow", Transactions A.S.M.E., Journal Basic Engineering, 92, 1970, pp. 21-30.

37. Ranga Raju, K. G. and Singh, V., "Blockage Effects on Drag of Sharp Edged Bodies", Journal of Industrial Aerodynamics, Vol. 1, No. 3, Feb. 1976, pp. 301-309.

38. Roshko, Anatol, "A New Hodograph for Free-Streamline Theory", NACA TN 3168, July 1954.

39. Roshko, Anatol, "On the Drag and Shedding Frequency of Two-Dimensional Bluff Bodies", NACA TN 3169, July 1954.

40. Schuh, H., "The R.A.E. 4-ft x 3-ft Experimental Low-Turbulence Wind Tunnel Part IV", British A.R.C., R. and M. No. 3261, June 1953.

41. Shaw, T. L., "Effect of Side Wall on the Flow Past Bluff Bodies", National Bureau of Standards, Maryland, April 1982. Journal of the Hydraulics Division, A.S.C.E., Vol. 97, No. HY1, Jan. 1971, pp. 65-79.

42. Tanaka, H. and Joshi, V. K., "Measurement of Air Flow Characteristics at Low Speed Wind Tunnel", Aero Report 80-1, Sept. 1980.

43. Vickery, B. J., "on the Flow Behind a Coarse Grid and its Use as a Model of Atmospheric Turbulence in Studies Related to Wind Loads on Buildings", N.P.L. Aero Report 1143, March 1965.

44. Vickery, B. J., "Fluctuating Lift and Drag on a Long Cylinder of Square Cross-Section in a Smooth and in a Turbulent Stream", Journal of Fluid Mechanics, Vol. 25, Part 3, 1966, pp. 481-494.

45. Wind Effects on Buildings and Structures; Proceedings, Vol. I, International Research Seminar, Ottawa, Canada, 11-15 September 1967, Toronto: University of Toronto Press, 1968.

46. Wind Effects on Buildings and Structures; Proceedings, Vol. II, International Research Seminar, Ottawa, Canada, 11-15 September 1967, Toronto: University of Toronto Press, 1968.

47. Melbourne, W. H., "Wind Tunnel Blockage Effects and Corrections", NBS/NSF Workshop on Wind Tunnel Modelling for Civil Engineering Applications, Gaithersburg, Maryland, April 1982.

48. Thom, A., "Blockage Corrections in a Closed High Speed Tunnel", A.R.C., R. and M. 2033, Nov. 1963.

49. Herriot, J. C., "Blockage Corrections for Three-Dimensional Flow in Closed-Throat Wind Tunnels with Considerations of the Effect of Compressibility", NACA TR 995, 1950.

50. Hensel, R. W., "Rectangular Wind Tunnel Corrections Using the Velocity Ratio Method", NACA TN 2372, June 1951.

51. Hackett, J. E. and Wilsden, D. J., "Estimation of Wind Tunnel Blockage from Wall Pressure Signatures: A Review of Recent Work at Lockheed-Georgia", AIAA Paper No. 78-828, April 1978.

Appendix A

THREE-COMPONENT STRAIN BALANCE

A.1 WIND TUNNEL BALANCES

In wind tunnel testing, the direction and the point of action of the wind force is known and thus the balance may be arranged accordingly. The direction and the point of action of the resultant aerodynamic force however, are both unknown and variable during an experiment and the wind tunnel balance must be designed with this in mind.

The resultant force may be replaced by three forces acting along three mutually perpendicular axes, together with three moments acting about the mutually perpendicular axes. The balance is therefore arranged to measure these six components with reference to a known system of axes. The three forces which are measured are usually called lift (L), drag (D) and cross-wind (C) force and the moments are usually called pitching (P), rolling (R) and yawing (Y) moments. These forces and moments are usually expressed in terms of dimensionless coefficients which are a function of the angle of incidence. A system of axis for these six force and moment coefficients is shown in Figure A.1.1.

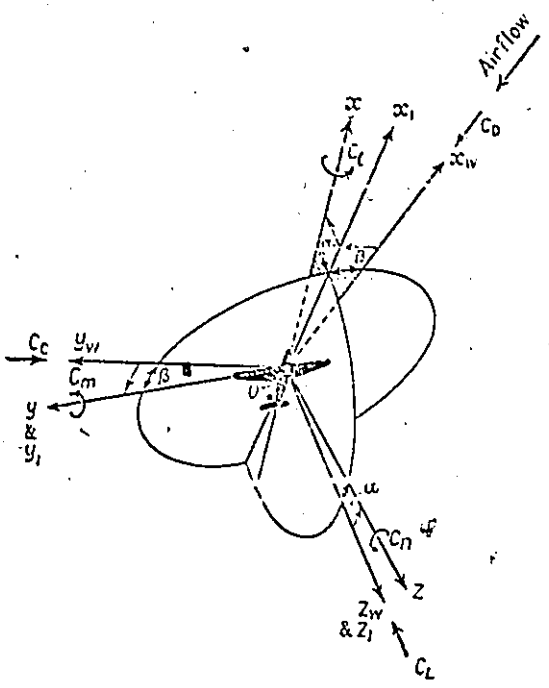

FIGURE A.1.1 - SYSTEM OF AXES
(VIEWED FROM BELOW)

If the angles of yaw and roll are set to zero, then three of the components become zero and it is necessary to measure only the lift, drag and pitching moment. Hence we now only require the use of a three-component balance.

A.2 STRAIN BALANCES

The balance used in the tests is of the strain gauge type, i.e. the applied load is measured as a difference in voltage corresponding to a loading increment. The main advantage of a strain-gauge balance is that it can be small which makes it easy to place in an inaccessible position such as under or inside a model under test.

Supposing that the drag on the model is transmitted via a rigid elastic member and assuming the member deforms under load in accordance with Hooke's law, the drag D is given by the realtion

$$D = E \cdot A \cdot \varepsilon$$

where E is Young's modulus,

A is the cross-sectional area of the member, and

ε is the strain in the member.

The strain of the member can be easily measured by attaching an electrical strain gauge to it and converting the strain into a change of electrical resistance which is measured by a suitable electrical circuit.

A.3 DESCRIPTION OF THE THREE-COMPONENT STRAIN BALANCE

The three-component strain-gauge balance used in the tests is illustrated in Figures A.3.1 to A.3.6. The model is mounted and fastened securely on a rigid top plate. The top plate is anchored to a stiff lower plate by means of four columns set at 45° angles from a perpendicular axis. Strain gauges are mounted on these four columns to measure the strain in the member when the model is subjected to a load.

Extraneous vibrations are dampened by means of a damper plate connected from the top plate to a dashpot mounted on the bottom plate. The dashpot contains STP oil treatment, a very viscous fluid which provides damping on the order of 70 percent.

Finally a hole is made in the wind tunnel floor through which the top plate of the balance is passed and the balance is attached to the wind tunnel floor by means of its side walls which are connected to the bottom plate.

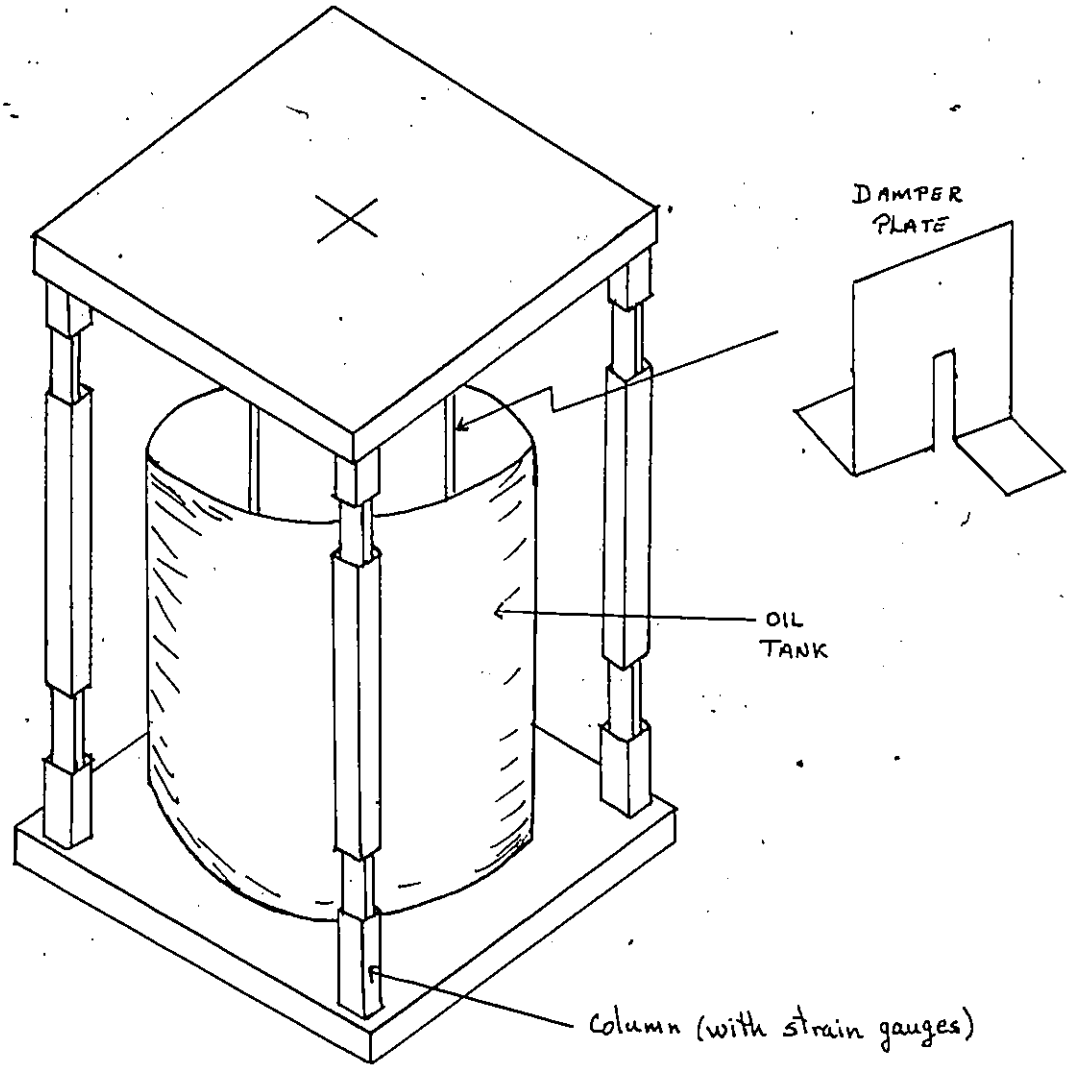

FIGURE A.3.1 - SKETCH OF STRAIN BALANCE

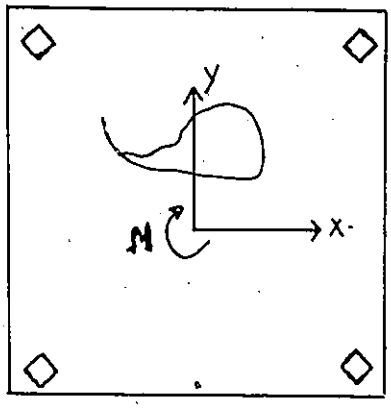

LOCATION OF COLUMNS VIS-A-VIS TOP PLATE

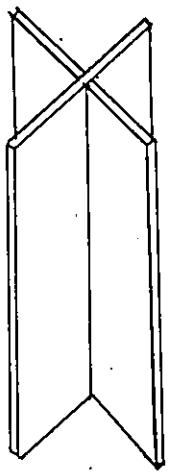

DAMPER VANE

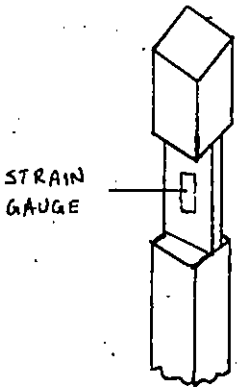

TYPICAL COLUMN

FIGURE A.3.2

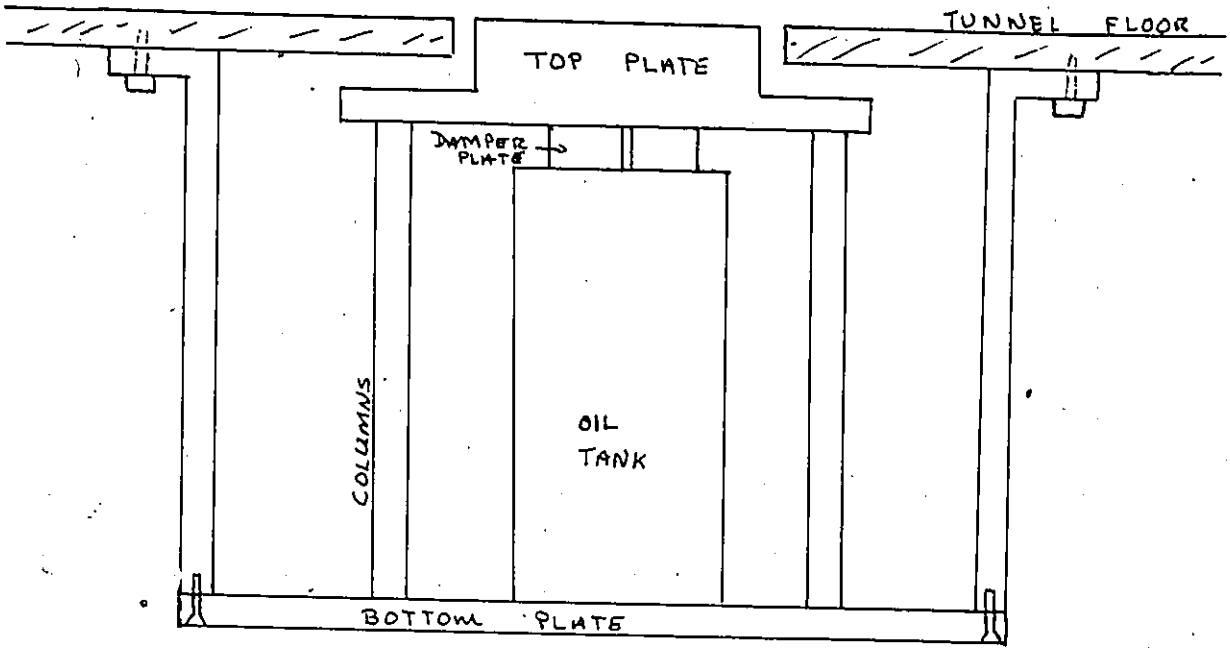

FIGURE A.3.3 - SKETCH OF ASSEMBLY

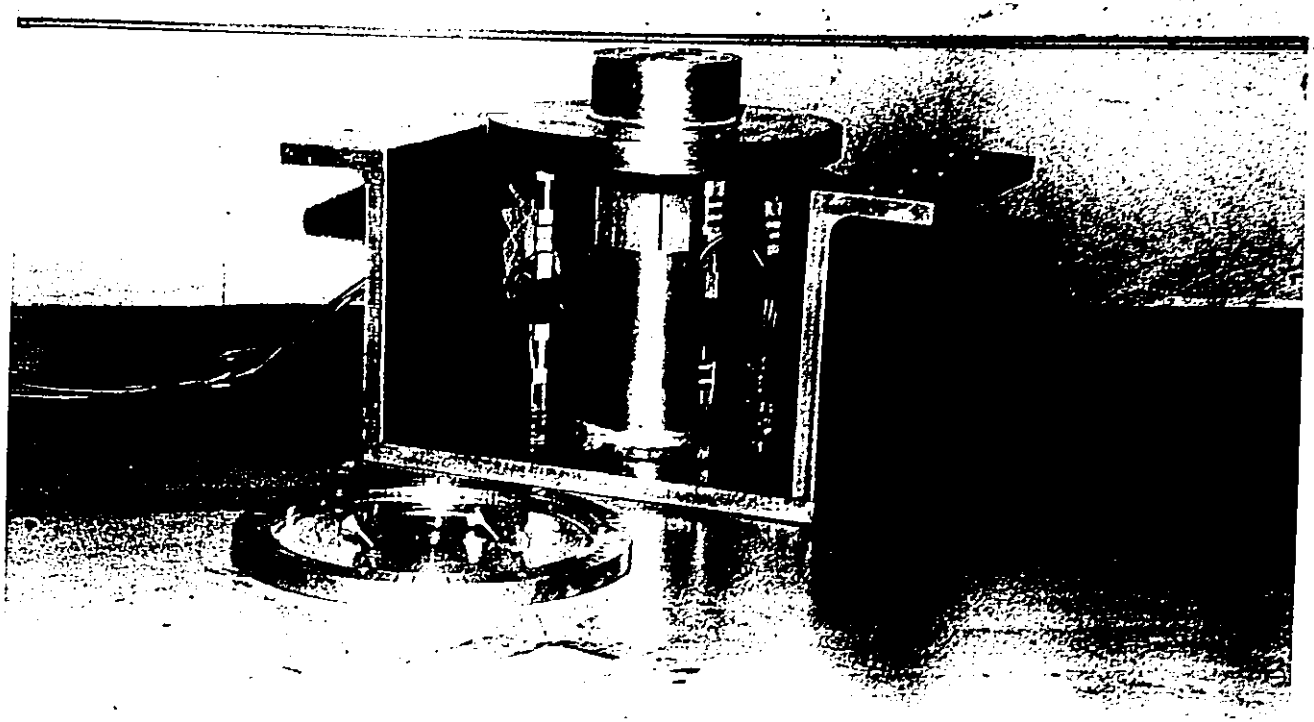

FIGURE A.3.4 - STRAIN BALANCE

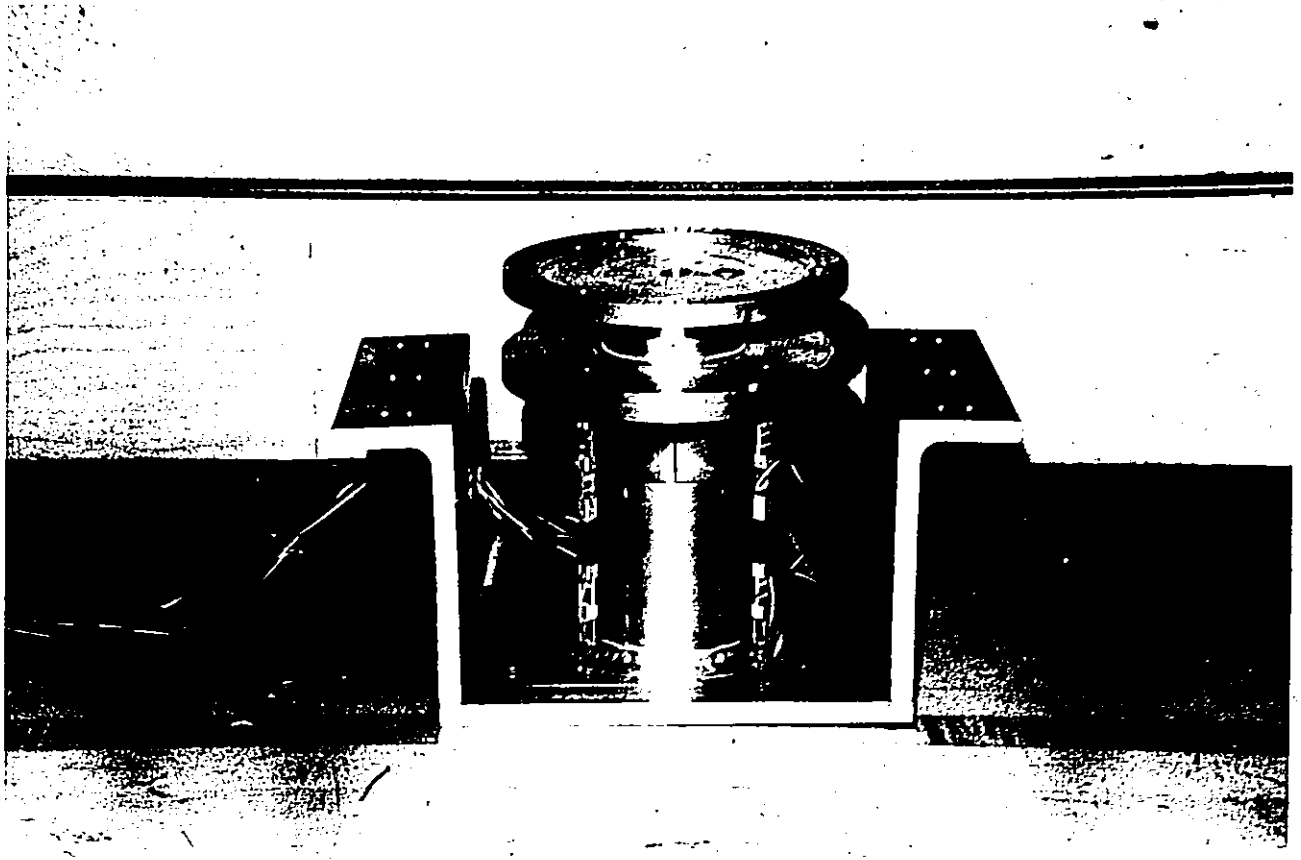

FIGURE A.3.5 - STRAIN BALANCE

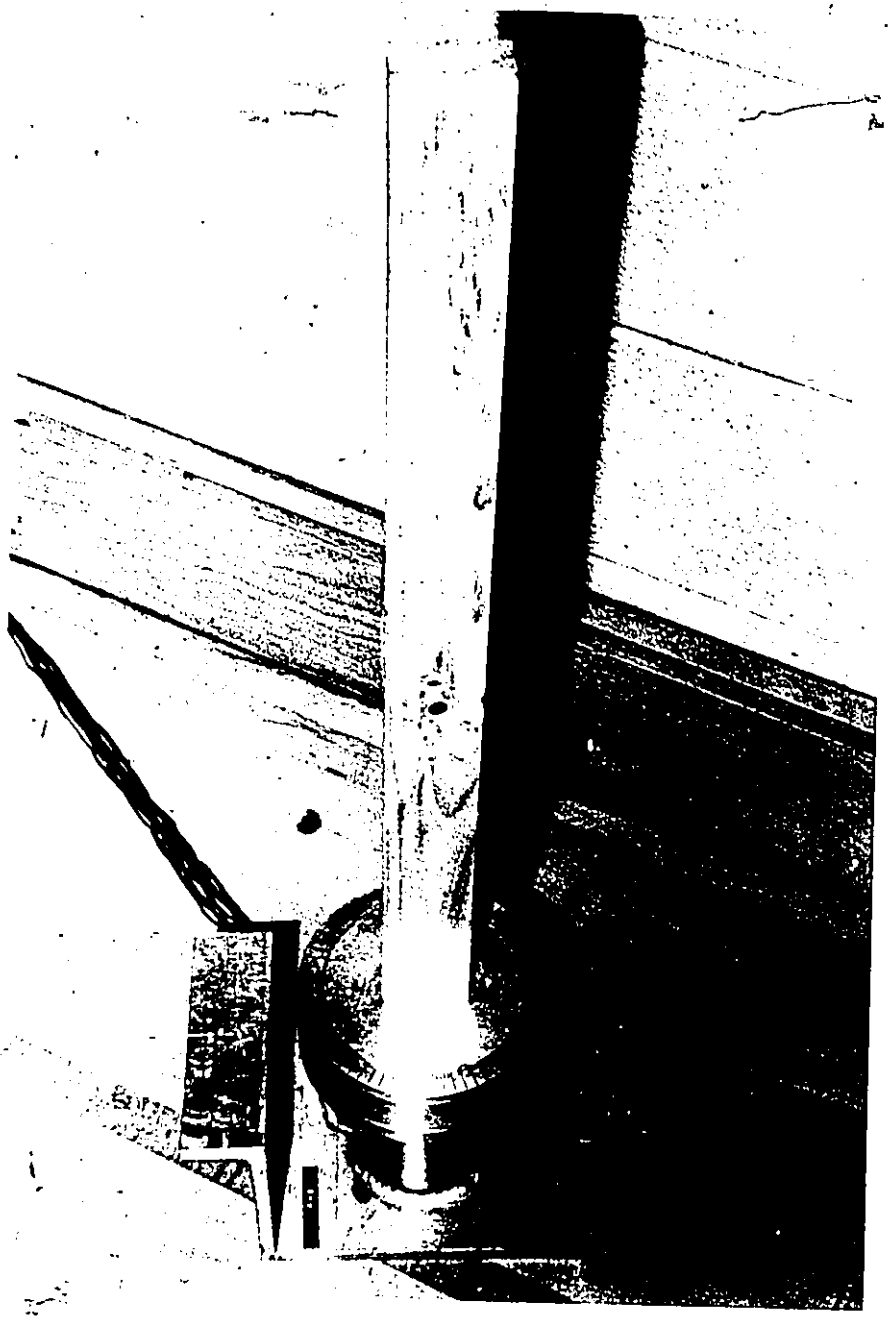

FIGURE A.3.6 - STRAIN BALANCE AND MODEL

Calibration tests were run and strains were measured for known loads and known moments. The calibration factors were found to be:

$f_L = 1.953 \times 10^{-3}$ lbs/micro-strain

$f_D = 1.942 \times 10^{-3}$ lbs/micro-strain

$f_M = 3.425 \times 10^{-4}$ lbs/micro-strain

Lift and drag forces as well as pitching moment are measured by either summing or subtracting the strains measured on the four columns. The direction of the two forces and moment is shown in Figure A.3.7 and taking the displacement direction of the columns as positive, the force and moment equations become:

$$L = f_L (R1 + R2 + R3 + R4)$$

$$D = f_D (-R1 + R2 - R3 + R4)$$

$$M = f_M (-R1 - R2 + R3 + R4)$$

The force and moment coefficients are then calculated by dividing the forces by $\rho V^2 A/2$, where ρ is the air density, V is the wind velocity and A is the effective cross-sectional area of the face of the model.

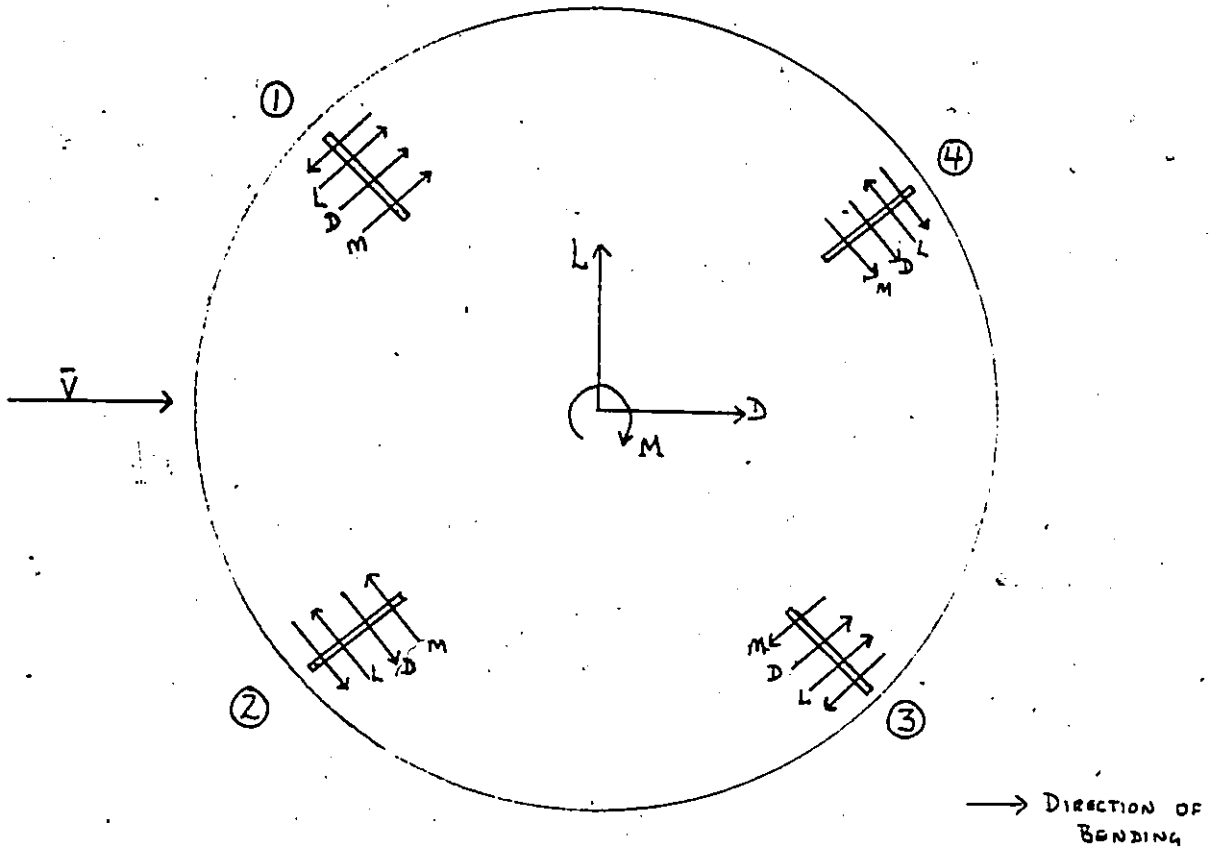

FIGURE A.3.7 - DIRECTION OF FORCES AND MOMENT

Appendix B

NOMENCLATURE

B.1 NOTATION

D	Drag force
L	Lift force
M	Pitching moment
C_D	Drag coefficient ($=D/qs$)
C_L	Lift coefficient
C_M	Moment coefficient
S	Reference area of model
C	Cross-sectional area of wind tunnel
B	Cross-sectional area of wake
U	Velocity of undisturbed stream
P	Static pressure of undisturbed stream
H	Total head of undisturbed stream
q	Dynamic pressure of the undisturbed stream ($=\rho V^2/2$)
p	Static pressure
m	$= B/S$
m^*	Datum value for m
C_p	Pressure coefficients ($=(p-P)/q$)
C_{pw}	Non-dimensional coefficient of the pressure on the wake boundary

C_{p_b}	Non-dimensional coefficient of the pressure on the base of the model
C_{p_s}	Non-dimensional coefficient of the pressure on the side of the model
$C_{p_{stag}}$	Non-dimensional coefficient of the pressure on the front of the model
k	Base pressure parameter
k^2	Ratio of the velocity at the point of separation to the free stream velocity (= $1-C_{p_b}$)
k_w^2	Ratio of the velocity at the wake boundary to the free stream velocity (= $1-C_{p_w}$)
ε	Blockage factor (= $1/(k_c^2-1)$)
εM	Modified blockage factor (=$1/(k^2+1)$)
εM_o	Modified blockage factor regressed to zero blockage
d	Depth of model
w	Width of model
d/w	Bluffness ratio
h	Height of model
h/d	Aspect ratio of model face (= A)
ρ	Air density
u	Velocity component in the free stream direction, outside the wake

suffices

Δ	operator denoting increment due to constraint
u	suffix denoting experimental or uncorrected values
c	suffix denoting effective or corrected values
1	free stream value
2	values at maximum wake area

B.2 MODEL IDENTIFICATION

Example: Model S36T2

The first letter denotes the size of the model:

S - small 1 in. by 2 in. model

M - medium 1.5 in. by 3 in. model

- 2 in. by 4 in. model

B - big 3 in. by 6 in. model

The two digits refer to the height of the model, namely 36 in.

The last letter-digit combination refers to the flow case:

S - smooth flow

T1 - turbulent flow with the fine grid

T2 - turbulent flow with the coarse grid

Appendix C

TABLES AND FIGURES

TABLE 1

RESULTS OF REGRESSED DATA FOR LIFT, DRAG AND MOMENT COEFFICIENTS

MODEL : S36S
WIDTH : 2 IN.
DEPTH : 1 IN.
HEIGHT: 36 IN.

MEAN VELOCITY: 25 FT/SEC
REYNOLDS NO: 3X10**4

ALPHA (DEG.)	LIFT (LBS)	DRAG (LBS)	MOMENT (FT.-LBS)	LIFT COEF.	DRAG COEF.	MOMENT COEF.
0	-0.000	0.754	0.001	-0.022	1.818	0.021
2	-0.027	0.711	-0.002	-0.069	1.753	-0.090
4	-0.070	0.710	-0.001	-0.159	1.693	-0.033
6	-0.088	0.675	0.004	-0.214	1.609	0.139
8	-0.141	0.688	0.002	-0.330	1.568	0.067
10	-0.141	0.704	0.002	-0.343	1.566	0.127
15	-0.205	0.675	-0.000	-0.458	1.505	-0.024
20	-0.323	0.628	0.001	-0.714	1.380	0.027
30	-0.280	0.606	0.002	-0.599	1.297	0.063
40	-0.248	0.628	0.001	-0.542	1.388	0.030
50	-0.250	0.612	0.002	-0.576	1.462	0.040
60	-0.223	0.516	-0.001	-0.570	1.345	-0.035
70	-0.134	0.418	-0.006	-0.366	1.227	-0.197
75	-0.070	0.344	-0.005	-0.192	1.075	-0.148
80	0.070	0.280	-0.007	0.278	0.970	-0.223
82	0.159	0.254	-0.009	0.646	0.969	-0.257
84	0.165	0.261	-0.008	0.709	1.059	-0.227
86	0.157	0.254	-0.005	0.720	1.100	-0.139
88	0.112	0.253	-0.003	0.573	1.129	-0.111
90	0.042	0.292	-0.002	0.244	1.283	-0.087

TABLE 2

RESULTS OF REGRESSED DATA FOR LIFT, DRAG AND MOMENT COEFFICIENTS

MODEL : S36T1
WIDTH : 2 IN.
DEPTH : 1 IN.
HEIGHT: 36 IN.
GRID : FINE

MEAN VELOCITY: 25 FT/SEC
REYNOLDS NO: 3X10**4

ALPHA (DEG.)	LIFT (LBS)	DRAG (LBS)	MOMENT (FT.-LBS)	LIFT COEF.	DRAG COEF.	MOMENT COEF.
0	-0.055	1.021	-0.003	-0.015	2.763	-0.092
2	-0.089	1.036	-0.006	-0.237	2.713	-0.062
4	-0.099	0.992	-0.001	-0.190	2.560	-0.023
6	-0.138	0.965	-0.005	-0.427	2.503	-0.122
8	-0.193	0.948	-0.003	-0.466	2.429	-0.093
10	-0.230	0.918	-0.002	-0.563	2.299	-0.069
15	-0.310	0.768	-0.003	-0.739	1.839	-0.023
20	-0.342	0.722	0.001	-0.780	1.717	0.069
30	-0.298	0.739	-0.001	-0.676	1.738	0.061
40	-0.292	0.723	-0.003	-0.660	1.755	-0.044
50	-0.298	0.667	-0.001	-0.756	1.757	-0.045
60	-0.261	0.535	-0.002	-0.731	1.522	-0.186
70	-0.188	0.458	0.000	-0.636	1.518	-0.109
75	-0.100	0.372	-0.004	-0.324	1.361	-0.206
80	-0.025	0.323	-0.008	-0.032	1.333	-0.314
82	-0.005	0.296	-0.008	0.056	1.258	-0.308
84	0.036	0.288	-0.007	0.273	1.295	-0.297
86	0.037	0.279	-0.006	0.263	1.321	-0.236
88	0.034	0.267	-0.000	0.210	1.292	0.035
90	0.035	0.243	0.002	0.170	1.195	0.051

TABLE 3

RESULTS OF REGRESSED DATA FOR LIFT, DRAG AND MOMENT COEFFICIENTS

MODEL : S36T2
WIDTH : 2 IN.
DEPTH : 1 IN.
HEIGHT: 36 IN.
GRID : COARSE

MEAN VELOCITY: 25 FT/SEC
REYNOLDS NO: 3X10**4

ALPHA (DEG.)	LIFT (LBS)	DRAG (LBS)	MOMENT (FT.-LBS)	LIFT COEF.	DRAG COEF.	MOMENT COEF.
0	-0.098	0.868	-0.002	0.011	2.399	0.145
2	-0.212	0.725	0.015	-0.491	1.921	1.068
4	-0.119	0.800	-0.005	-0.338	2.101	0.580
6	-0.149	0.803	-0.002	-0.351	2.222	0.606
8	-0.195	0.777	0.000	-0.512	2.126	0.711
10	-0.224	0.704	0.001	-0.419	1.821	0.247
15	-0.270	0.596	0.000	-0.712	1.718	-0.260
20	-0.260	0.615	0.005	-0.614	1.490	-0.183
30	-0.263	0.592	0.001	-0.542	1.522	0.227
40	-0.247	0.583	0.005	-0.576	1.549	-0.172
50	-0.248	0.592	-0.003	-1.015	1.897	0.186
60	-0.265	0.519	-0.003	-0.876	1.842	-0.377
70	-0.218	0.421	-0.008	-0.930	1.520	-0.322
75	-0.107	0.355	-0.008	-0.514	1.686	-0.345
80	-0.037	0.297	-0.006	-0.171	1.565	-0.212
82	-0.023	0.310	-0.007	-0.119	1.682	-0.285
84	-0.002	0.305	-0.007	-0.062	1.474	-0.141
86	0.001	0.292	-0.005	0.032	1.590	-0.191
88	0.017	0.266	-0.004	0.126	1.508	-0.134
90	0.023	0.258	-0.001	0.160	1.560	-0.052

TABLE 4

RESULTS OF REGRESSED DATA FOR LIFT, DRAG AND MOMENT COEFFICIENTS

MODEL : M36S
WIDTH : 3 IN.
DEPTH :1.5 IN.
HEIGHT: 36 IN.

MEAN VELOCITY: 25 FT/SEC
REYNOLDS NO: 4.5X10**4

ALPHA (DEG.)	LIFT (LBS)	DRAG (LBS)	MOMENT (FT.-LBS)	LIFT COEF.	DRAG COEF.	MOMENT COEF.
0	-0.010	1.815	-0.003	-0.040	2.287	0.009
2	0.049	1.712	-0.002	0.143	2.366	0.006
4	-0.212	1.769	0.005	-0.522	2.268	0.119
6	-0.205	1.829	0.002	-0.391	2.220	0.047
8	-0.194	1.704	0.001	-0.205	2.189	-0.016
10	-0.359	1.643	0.004	-0.651	2.051	0.005
15	-0.492	1.584	0.005	-0.682	1.937	0.034
20	-0.649	1.295	0.005	-0.849	1.593	0.073
30	-0.574	1.246	0.017	-0.677	1.458	0.196
40	-0.466	1.211	0.016	-0.579	1.518	0.157
50	-0.466	1.221	0.014	-0.522	1.618	0.105
60	-0.398	1.028	0.012	-0.566	1.477	0.204
70	-0.217	0.846	-0.006	-0.367	1.352	-0.042
75	-0.059	0.754	-0.019	-0.147	1.285	-0.345
80	0.246	0.619	-0.018	0.440	1.195	-0.189
82	0.360	0.575	-0.016	0.801	1.205	-0.125
84	0.338	0.600	-0.011	0.840	1.283	-0.144
86	0.222	0.609	-0.003	0.740	1.376	-0.080
88	0.136	0.611	-0.003	0.618	1.474	-0.079
90	0.022	0.625	-0.002	0.123	1.597	-0.077

TABLE 5

RESULTS OF REGRESSED DATA FOR LIFT, DRAG AND MOMENT COEFFICIENTS

MODEL : M36T1
WIDTH : 3 IN.
DEPTH :1.5 IN.
HEIGHT: 36 IN.
GRID : FINE

MEAN VELOCITY: 25 FT/SEC
REYNOLDS NO: 4.5X10**4

ALPHA (DEG.)	LIFT (LBS)	DRAG (LBS)	MOMENT (FT.-LBS)	LIFT COEF.	DRAG COEF.	MOMENT COEF.
0	-0.022	1.578	-0.003	-0.058	2.575	-0.078
2	-0.216	1.546	0.001	-0.390	2.564	0.047
4	-0.142	1.516	0.002	-0.232	2.424	0.031
6	-0.169	1.484	-0.000	-0.277	2.377	0.015
8	-0.252	1.433	0.004	-0.364	2.242	0.036
10	-0.305	1.411	0.003	-0.454	2.116	0.041
15	-0.440	1.261	0.007	-0.674	1.954	0.106
20	-0.558	1.136	0.005	-0.824	1.722	0.094
30	-0.471	1.082	0.010	-0.713	1.660	0.192
40	-0.391	1.123	0.014	-0.592	1.752	0.201
50	-0.424	1.032	0.012	-0.695	1.674	0.110
60	-0.394	0.866	0.007	-0.728	1.609	0.111
70	-0.299	0.692	-0.004	-0.650	1.465	-0.033
75	-0.180	0.578	-0.011	-0.391	1.347	-0.165
80	-0.020	0.505	-0.015	-0.036	1.302	-0.252
82	0.029	0.476	-0.017	0.036	1.325	-0.211
84	0.041	0.447	-0.015	0.070	1.323	-0.184
86	0.067	0.415	-0.010	0.253	1.279	-0.116
88	0.028	0.406	-0.004	0.091	1.233	-0.086
90	0.010	0.408	0.001	0.022	1.327	-0.003

TABLE 6

RESULTS OF REGRESSED DATA FOR LIFT, DRAG AND MOMENT COEFFICIENTS

MODEL : M36T2
WIDTH : 3 IN.
DEPTH :1.5 IN.
HEIGHT: 36 IN.
GRID : COARSE

MEAN VELOCITY: 25 FT/SEC
REYNOLDS NO: 4.5X10**4

ALPHA (DEG.)	LIFT (LBS)	DRAG (LBS)	MOMENT (FT.-LBS)	LIFT COEF.	DRAG COEF.	MOMENT COEF.
0	-0.074	1.588	0.004	-0.070	2.799	0.070
2	-0.114	1.568	0.002	-0.173	2.736	0.078
4	-0.132	1.560	-0.001	-0.196	2.627	0.031
6	-0.213	1.522	0.003	-0.421	2.502	-0.012
8	-0.241	1.460	0.004	-0.429	2.433	-0.043
10	-0.340	1.377	0.004	-0.520	2.204	0.036
15	-0.475	1.270	0.011	-0.723	1.923	0.135
20	-0.465	1.128	0.009	-0.741	1.759	0.125
30	-0.426	1.136	0.013	-0.689	1.763	0.199
40	-0.412	1.126	0.014	-0.700	1.798	0.206
50	-0.441	1.075	0.012	-0.730	1.759	0.172
60	-0.409	0.903	0.008	-0.771	1.700	0.137
70	-0.311	0.724	-0.003	-0.707	1.564	-0.045
75	-0.199	0.610	-0.011	-0.438	1.372	-0.094
80	-0.070	0.506	-0.016	-0.215	1.245	-0.191
82	-0.036	0.479	-0.014	-0.154	1.340	-0.206
84	-0.022	0.453	-0.011	-0.122	1.329	-0.159
86	-0.004	0.416	-0.009	-0.097	1.260	-0.134
88	0.013	0.403	-0.002	0.018	1.297	0.003
90	0.031	0.402	0.003	0.083	1.361	0.057

TABLE 7

RESULTS OF REGRESSED DATA FOR LIFT, DRAG AND MOMENT COEFFICIENTS

MODEL : 36S
WIDTH : 4 IN.
DEPTH : 2 IN.
HEIGHT: 36 IN.

MEAN VELOCITY: 25 FT/SEC
REYNOLDS NO: 6X10**4

ALPHA (DEG.)	LIFT (LBS)	DRAG (LBS)	MOMENT (FT.-LBS)	LIFT COEF.	DRAG COEF.	MOMENT COEF.
0	0.129	3.052	0.003	0.237	3.493	-0.003
2	-0.127	3.489	0.005	-0.188	3.925	-0.059
4	-0.280	3.067	0.013	-0.383	3.431	0.060
6	-0.405	3.066	0.017	-0.558	3.325	0.107
8	-0.540	2.979	0.024	-0.716	3.215	0.113
10	-0.592	3.077	0.028	-0.680	3.190	0.235
15	-0.900	2.716	0.034	-1.005	2.779	0.251
20	-1.157	2.358	0.035	-1.207	2.275	0.203
30	-1.091	2.203	0.049	-1.154	2.167	0.302
40	-0.961	2.212	0.052	-1.036	2.246	0.329
50	-0.964	2.014	0.044	-1.136	2.233	0.284
60	-0.879	1.668	0.035	-1.138	1.953	0.202
70	-0.568	1.261	-0.001	-0.932	1.699	-0.065
75	-0.324	1.051	-0.021	-0.550	1.521	-0.154
80	0.215	0.885	-0.041	0.265	1.476	-0.287
82	0.406	0.823	-0.036	0.419	1.417	-0.248
84	0.499	0.818	-0.022	0.886	1.468	-0.106
86	0.324	0.845	-0.016	0.540	1.596	-0.080
88	0.146	0.851	-0.010	0.180	1.674	-0.067
90	-0.018	0.830	0.002	-0.176	1.666	0.040

TABLE 8

RESULTS OF REGRESSED DATA FOR LIFT, DRAG AND MOMENT COEFFICIENTS

MODEL : 36T1
WIDTH : 4 IN.
DEPTH : 2 IN.
HEIGHT: 36 IN.
GRID : FINE

MEAN VELOCITY: 25 FT/SEC
REYNOLDS NO: 6X10**4

ALPHA (DEG.)	LIFT (LBS)	DRAG (LBS)	MOMENT (FT.-LBS)	LIFT COEF.	DRAG COEF.	MOMENT COEF.
0	0.072	3.168	0.011	0.095	3.938	0.091
2	-0.177	3.196	0.008	-0.229	3.905	0.034
4	-0.302	3.150	0.009	-0.365	3.769	0.059
6	-0.426	3.129	0.008	-0.508	3.667	0.038
8	-0.559	3.026	0.004	-0.661	3.517	0.021
10	-0.601	2.929	0.016	-0.688	3.350	0.119
15	-0.974	2.580	0.018	-1.091	2.862	0.163
20	-1.127	2.198	0.035	-1.245	2.416	0.270
30	-0.900	2.086	0.051	-0.974	2.265	0.377
40	-0.901	2.068	0.045	-1.039	2.351	0.319
50	-0.936	1.862	0.047	-1.122	2.205	0.352
60	-0.890	1.523	0.039	-1.194	2.001	0.292
70	-0.652	1.175	0.008	-0.972	1.740	0.053
75	-0.439	0.966	-0.014	-0.721	1.572	-0.111
80	-0.144	0.781	-0.034	-0.302	1.408	-0.238
82	-0.063	0.725	-0.039	-0.162	1.370	-0.272
84	0.041	0.657	-0.035	0.072	1.317	-0.259
86	0.033	0.615	-0.026	0.046	1.284	-0.183
88	0.024	0.593	-0.019	0.022	1.316	-0.135
90	-0.029	0.588	-0.002	-0.110	1.419	-0.017

TABLE 9

RESULTS OF REGRESSED DATA FOR LIFT, DRAG AND MOMENT COEFFICIENTS

MODEL : 36T2
WIDTH : 4 IN.
DEPTH : 2 IN.
HEIGHT: 36 IN.

MEAN VELOCITY: 25 FT/SEC
REYNOLDS NO: 6X10**4

ALPHA (DEG.)	LIFT (LBS)	DRAG (LBS)	MOMENT (FT.-LBS)	LIFT COEF.	DRAG COEF.	MOMENT COEF.
0	-0.172	3.295	0.016	-0.278	4.445	0.201
2	-0.207	3.416	0.008	-0.213	4.476	0.071
4	-0.305	3.347	0.005	-0.327	4.301	0.063
6	-0.487	3.201	0.006	-0.526	4.077	0.055
8	-0.598	3.047	0.006	-0.694	3.814	0.072
10	-0.588	2.826	0.004	-0.712	3.478	0.033
15	-1.057	2.391	0.050	-1.183	2.845	0.352
20	-1.027	2.110	0.068	-1.196	2.447	0.483
30	-0.783	2.396	0.026	-0.941	2.718	0.240
40	-0.845	2.316	0.030	-0.972	2.717	0.230
50	-0.965	2.093	0.029	-1.171	2.585	0.229
60	-0.964	1.690	0.030	-1.265	2.314	0.218
70	-0.698	1.272	0.005	-1.153	2.029	0.051
75	-0.452	1.033	-0.019	-0.768	1.776	-0.135
80	-0.228	0.850	-0.037	-0.404	1.618	-0.297
82	-0.198	0.780	-0.037	-0.377	1.529	-0.261
84	-0.189	0.712	-0.033	-0.361	1.487	-0.263
86	-0.171	0.661	-0.025	-0.370	1.468	-0.186
88	-0.130	0.604	-0.016	-0.293	1.433	-0.130
90	-0.018	0.604	-0.002	-0.010	1.555	0.004

TABLE 10 - DRAG COEFFICIENT AND REYNOLDS NUMBER FOR THE 1 X 2 MODEL AND AN ANGLE OF INCIDENCE OF 0 DEGREES

MODEL	ASPECT RATIO	MEAN VELOCITY FT/SEC	REYNOLDS NO. X10**4	C_{D_u} UNCORRECTED FOR 3-D EFFECTS
S36S	.083	9.82	1.06	1.932
		15.53	1.68	1.803
		20.84	2.26	1.789
		25.99	2.81	1.817
		31.39	3.40	1.829
S36T1	.083	6.43	0.70	1.503
		11.74	1.27	2.480
		16.81	1.82	2.474
		22.58	2.44	2.650
		27.03	2.93	2.701
S36T2	.083	5.25	0.57	2.818
		9.82	1.06	2.415
		14.85	1.61	2.536
		19.47	2.11	2.541
		24.34	2.63	2.412

TABLE 11 - DRAG COEFFICIENT AND REYNOLDS NUMBER FOR THE 1 X 2 MODEL AND AN ANGLE OF INCIDENCE OF 90 DEGREES

MODEL	ASPECT RATIO	MEAN VELOCITY FT/SEC	REYNOLDS NO. X10**4	C_{D_u} UNCORRECTED FOR 3-D EFFECTS
S36S	.042	16.60	0.90	0.902
		21.49	1.16	1.279
		26.25	1.42	1.262
		30.72	1.66	1.382
		34.33	1.86	1.767
S36T1	.042	7.42	0.40	1.691
		11.74	0.64	1.353
		18.37	0.99	1.012
		23.03	1.25	1.230
		27.28	1.48	1.336
S36T2	.042	7.87	0.43	---
		13.38	0.72	1.387
		16.81	0.91	1.320
		21.33	1.15	1.366
		26.38	1.43	1.339

TABLE 12 - DRAG COEFFICIENT AND REYNOLDS NUMBER FOR THE 1.5 X 3 MODEL AND AN ANGLE OF INCIDENCE OF 0 DEGREES

MODEL	ASPECT RATIO	MEAN VELOCITY FT/SEC	REYNOLDS NO. X10**4	C_{D_u} UNCORRECTED FOR 3-D EFFECTS
M36S	.125	11.14	1.81	2.087
		21.00	3.41	2.113
		30.39	4.93	2.355
		39.64	6.44	2.637
		48.26	7.83	2.739
M36T1	.125	5.25	0.85	4.133
		11.14	1.81	2.755
		16.81	2.73	2.676
		23.33	3.79	2.663
		28.76	4.67	2.668
M36T2	.125	4.91	0.80	2.576
		10.50	1.70	2.912
		15.53	2.52	2.877
		22.43	3.64	2.759
		27.41	4.45	2.744

TABLE 13 - DRAG COEFFICIENT AND REYNOLDS NUMBER FOR THE 1.5 X 3 MODEL AND AN ANGLE OF INCIDENCE OF 90 DEGREES

MODEL	ASPECT RATIO	MEAN VELOCITY FT/SEC	REYNOLDS NO. X10**4	C_{D_u} UNCORRECTED FOR 3-D EFFECTS
M36S	.063	8.30	0.67	1.503
		20.67	1.68	1.600
		28.99	2.35	1.626
		38.76	3.15	1.655
		48.26	3.92	1.690
M36T1	.063	6.43	0.52	2.004
		12.59	1.02	1.438
		18.00	1.46	1.343
		24.20	1.96	1.308
		29.58	2.40	1.373
M36T2	.063	6.43	0.52	1.002
		12.59	1.02	1.568
		17.61	1.43	1.336
		24.06	1.95	1.324
		29.58	2.40	1.325

TABLE 14 - DRAG COEFFICIENT AND REYNOLDS NUMBER FOR THE 2 X 4 MODEL AND AN ANGLE OF INCIDENCE OF 0 DEGREES

MODEL	ASPECT RATIO	MEAN VELOCITY FT/SEC	REYNOLDS NO. X10**4	C_{D_u} UNCORRECTED FOR 3-D EFFECTS
36S	.167	8.30	1.80	3.382
		15.75	3.41	3.256
		22.12	4.79	3.747
		29.70	6.43	3.434
		33.62	7.28	3.533
36T1	.167	6.43	1.39	3.757
		12.31	2.66	3.791
		18.19	3.94	3.757
		26.51	5.74	4.067
		28.03	6.07	3.925
36T2	.167	6.43	1.39	3.382
		11.74	2.54	3.832
		17.01	3.68	3.999
		21.96	4.75	4,670
		26.77	5.79	4.249

TABLE 15 - DRAG COEFFICIENT AND REYNOLDS NUMBER FOR THE 2 X 4 MODEL AND AN ANGLE OF INCIDENCE OF 90 DEGREES

MODEL	ASPECT RATIO	MEAN VELOCITY FT/SEC	REYNOLDS NO. X10**4	C_{Du} UNCORRECTED FOR 3-D EFFECTS
36S	.083	9.09	0.98	1.315
		17.01	1.84	1.664
		25.99	2.81	1.771
		34.02	3.68	1.758
		39.81	4.31	1.833
36T1	.083	7.42	0.80	1.409
		13.38	1.45	1.561
		19.99	2.16	1.360
		25.72	2.78	1.432
		31.61	3.42	1.399
36T2	.083	6.95	0.75	0.644
		11.74	1.27	1.353
		18.19	1.97	1.456
		23.48	2.54	1.550
		28.76	3.11	1.522

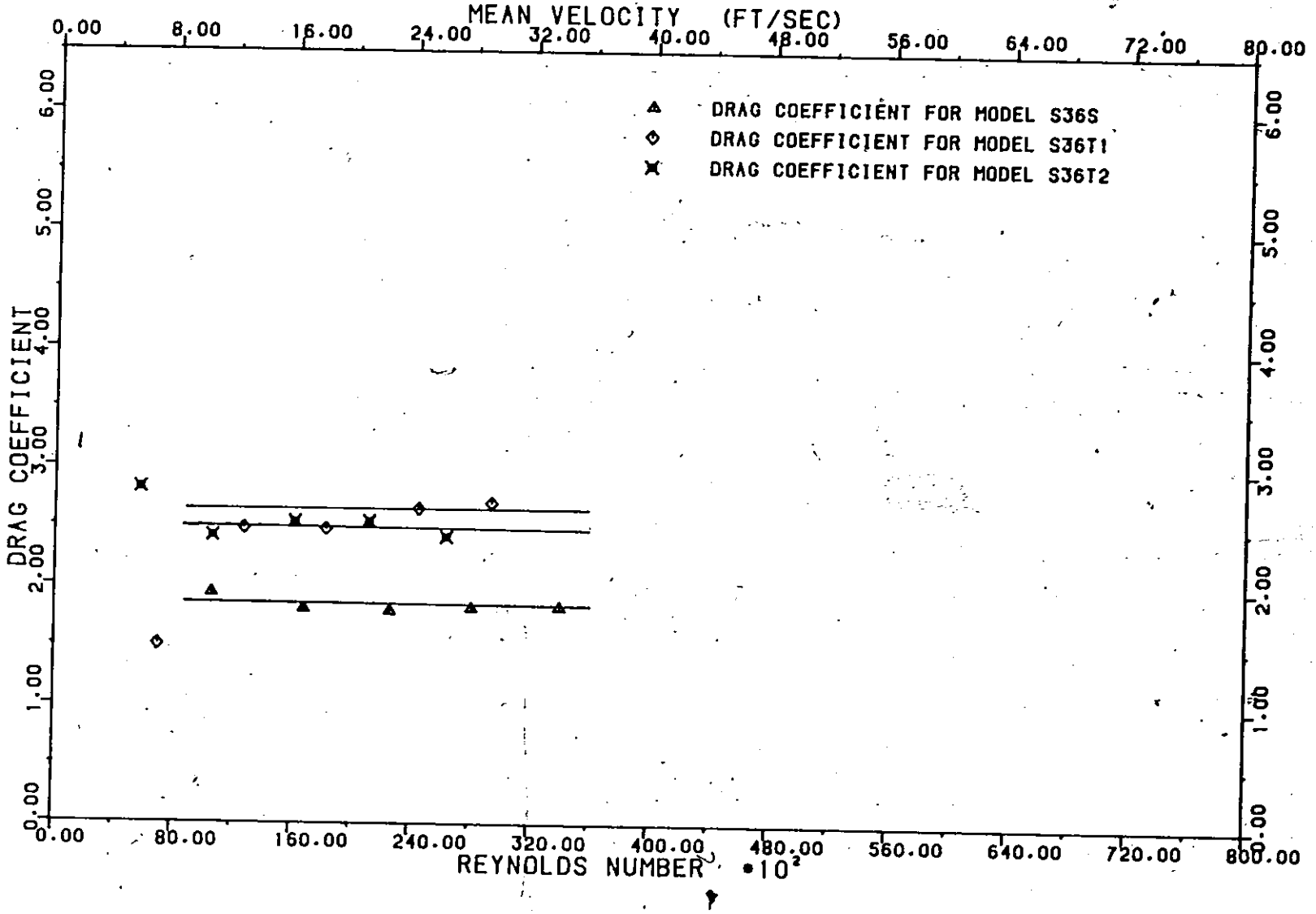

FIGURE 1 - DRAG COEFFICIENT VERSUS REYNOLDS NUMBER FOR MODELS S36S, S36T1 AND S36T2 FOR AN ANGLE OF INCIDENCE OF 0 DEGREES

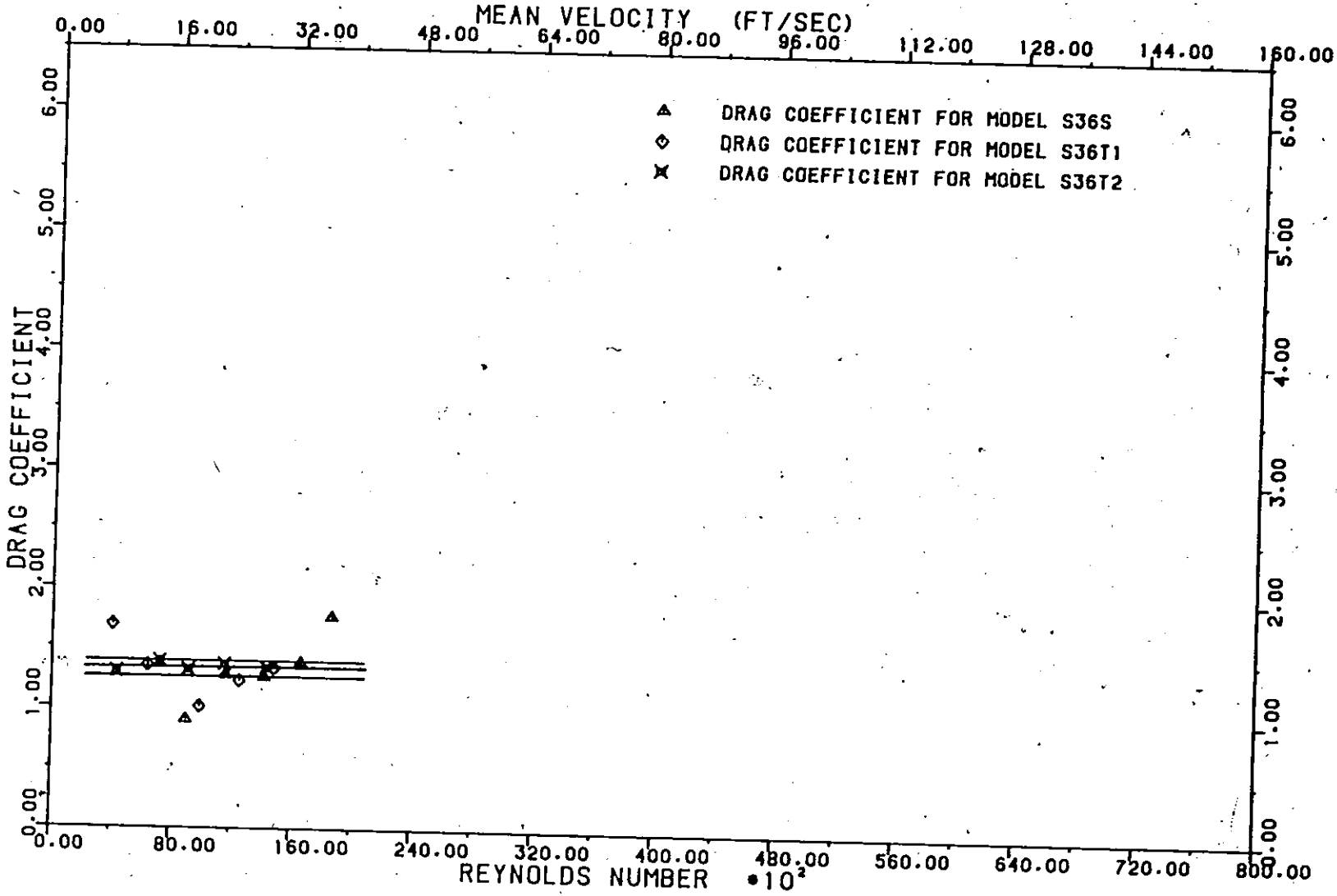

FIGURE 2 - DRAG COEFFICIENT VERSUS REYNOLDS NUMBER FOR MODELS S36S, S36T1 AND S36T2 FOR AN ANGLE OF INCIDENCE OF 90 DEGREES

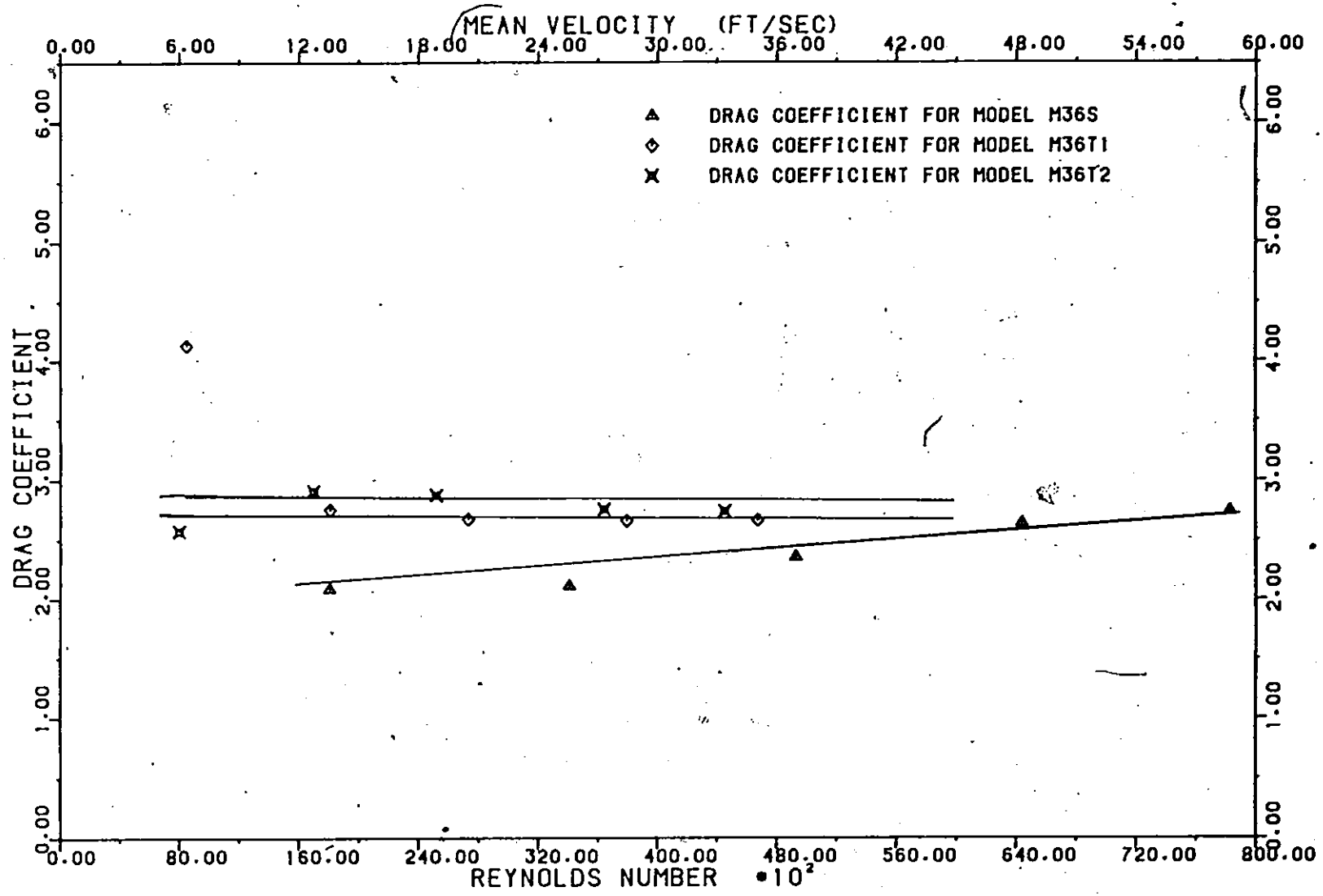

FIGURE 3 - DRAG COEFFICIENT VERSUS REYNOLDS NUMBER FOR MODELS M36S, M36T1 AND M36T2 FOR AN ANGLE OF INCIDENCE OF 0 DEGREES

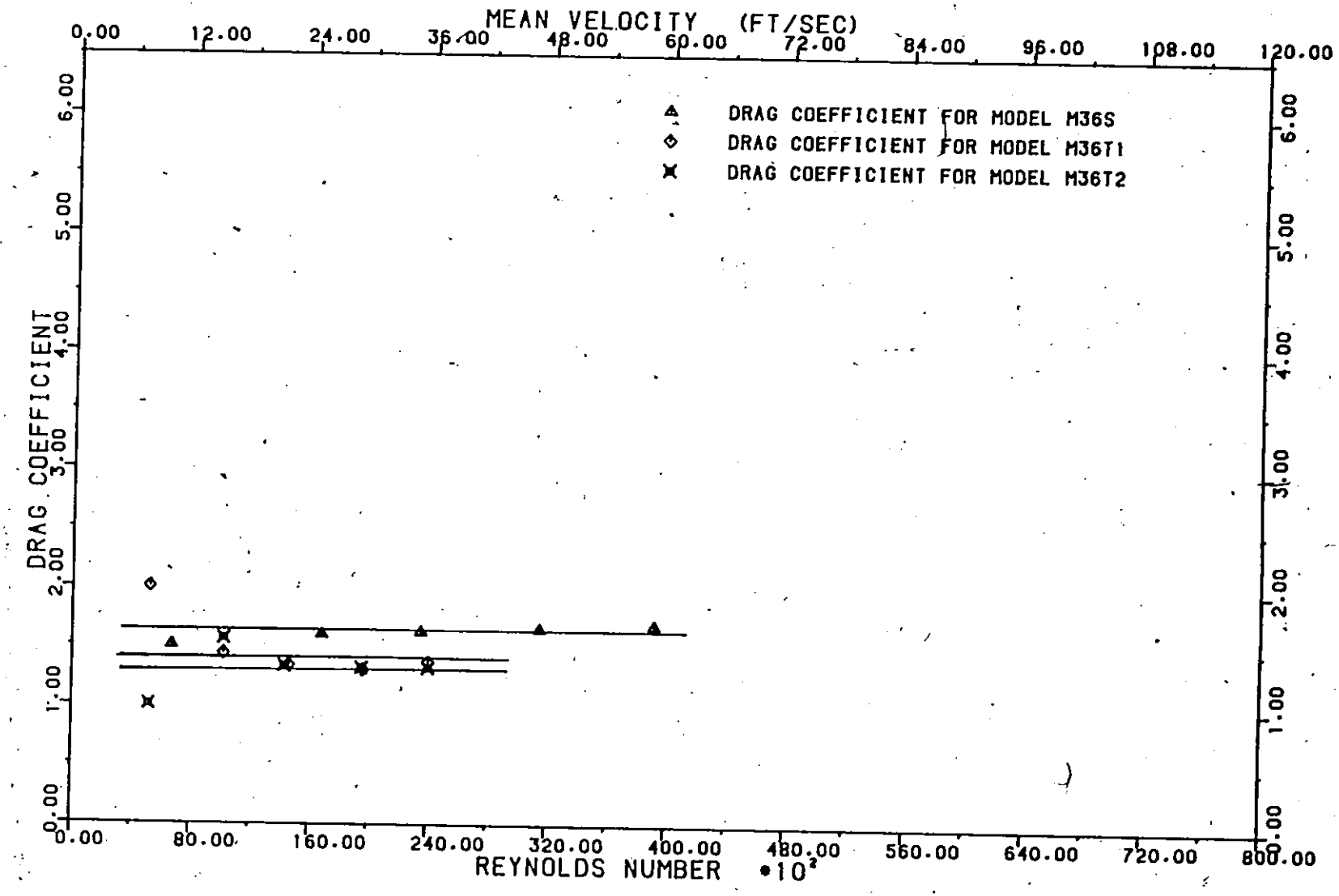

FIGURE 4 - DRAG COEFFICIENT VERSUS REYNOLDS NUMBER FOR MODELS M36S, M36T1 AND M36T2 FOR AN ANGLE OF INCIDENCE OF 90 DEGREES

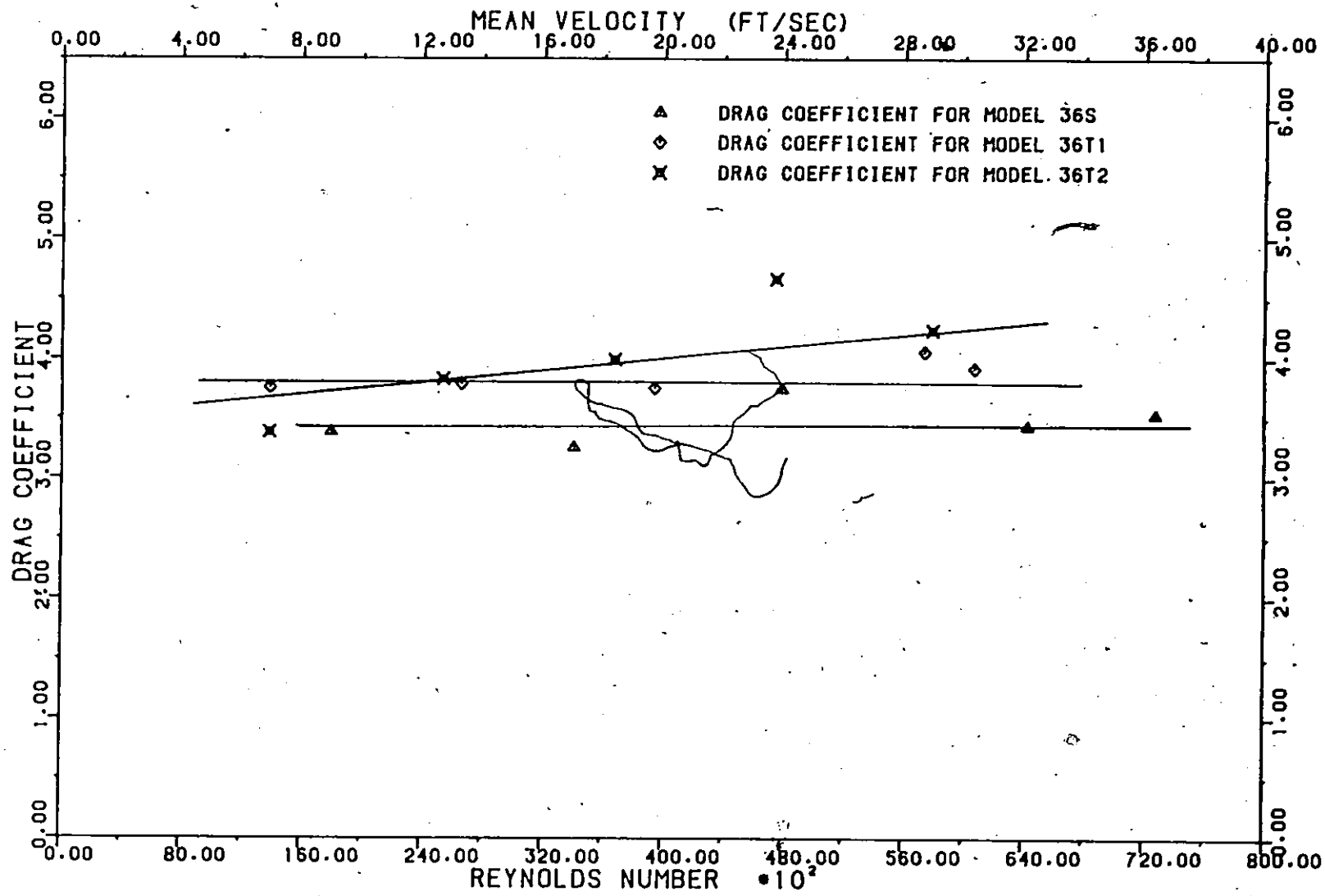

FIGURE 5 - DRAG COEFFICIENT VERSUS REYNOLDS NUMBER FOR MODELS 36S, 36T1 AND 36T2 FOR AN ANGLE OF INCIDENCE OF 0 DEGREES

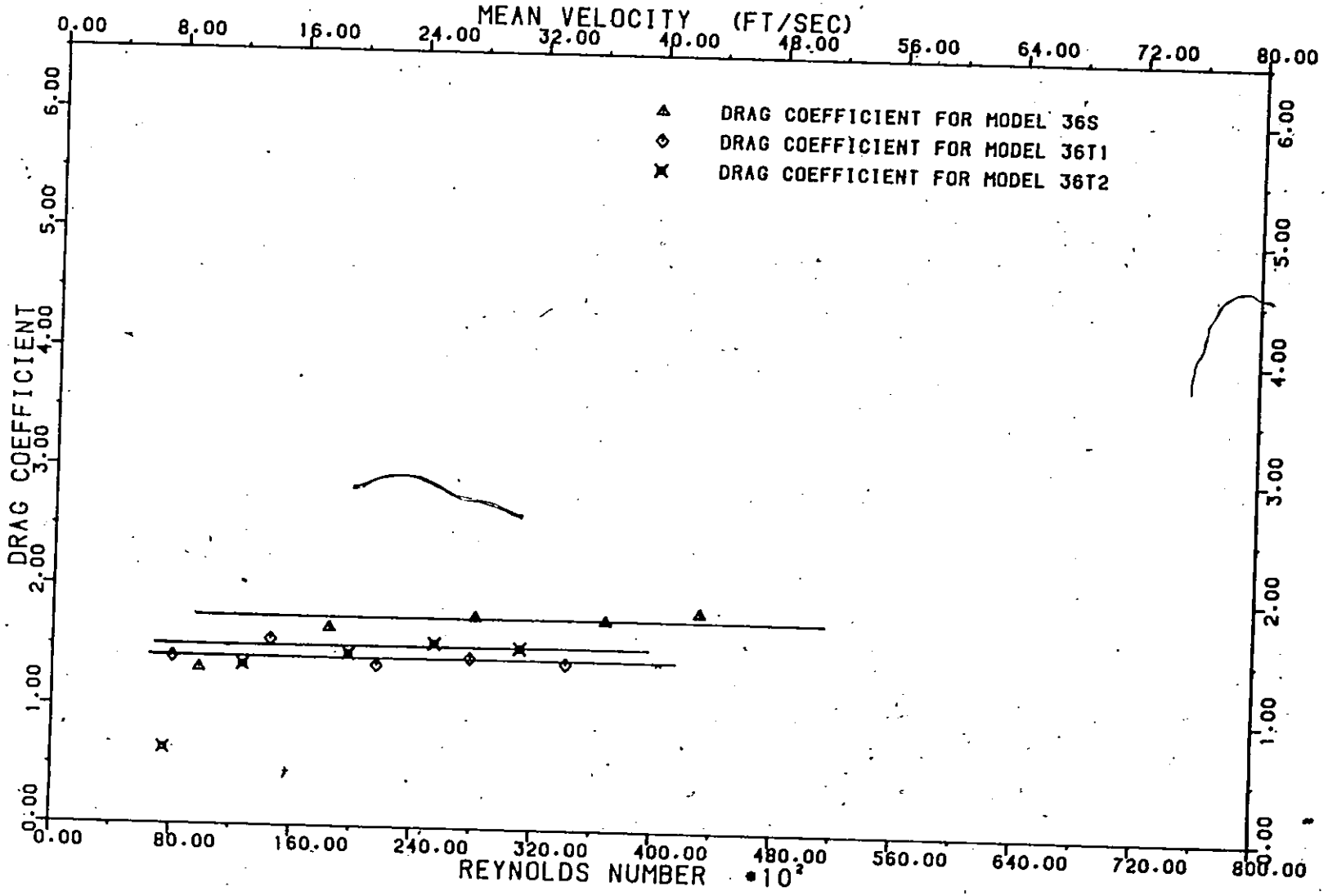

FIGURE 6 - DRAG COEFFICIENT VERSUS REYNOLDS NUMBER FOR MODELS 36S, 36T1 AND 36T2 FOR AN ANGLE OF INCIDENCE OF 90 DEGREES

TABLE 16

DRAG AND LIFT COEFFICIENTS FOR MODEL S36S
AS DETERMINED BY PRESSURE READINGS

HEIGHT OF MODEL: 36 IN.
WIDTH OF MODEL: 2 IN.
DEPTH OF MODEL: 1 IN.
GRID IN USE: NONE

ANGLE	CD	CL
-2	2.587	-0.041
0	2.278	0.039
2	2.582	-0.127
4	2.586	-0.165
6	2.543	-0.273
10	2.222	-0.294
20	1.568	-0.024
30	1.803	-1.037
40	2.142	-1.473
50	2.095	-1.553
60	2.197	-1.689
70	1.961	-1.199
80	1.570	0.102
86	1.657	0.013
88	1.730	-0.006
90	1.652	-0.092
92	1.647	-0.139

TABLE 17

DRAG AND LIFT COEFFICIENTS FOR MODEL 36S
AS DETERMINED BY PRESSURE READINGS

HEIGHT OF MODEL: 36 IN.
WIDTH OF MODEL: 4 IN.
DEPTH OF MODEL: 2 IN.
GRID IN USE: NONE

ANGLE	CD	CL
-2	2.958	-0.077
0	2.962	0.012
2	2.944	-0.125
4	2.926	-0.209
6	2.867	-0.298
10	2.752	-0.522
20	1.927	-0.354
30	1.837	-0.911
40	2.340	-1.614
50	2.279	-1.690
60	1.185	-1.204
70	2.128	-1.315
80	1.729	-0.048
86	1.705	0.190
88	1.743	0.090
90	1.805	-0.058
92	1.712	-0.165

TABLE 18

DRAG AND LIFT COEFFICIENTS FOR MODEL B36S
AS DETERMINED BY PRESSURE READINGS

HEIGHT OF MODEL: 36 IN.
WIDTH OF MODEL: 6 IN.
DEPTH OF MODEL: 3 IN.
GRID IN USE: NONE

ANGLE	CD	CL
-2	3.628	-0.125
0	3.748	-0.015
2	3.742	-0.161
4	3.694	-0.265
6	3.614	-0.406
10	3.370	-0.546
20	2.474	-0.227
30	1.954	-1.046
40	2.910	-1.988
50	2.834	-2.115
60	2.302	-1.801
70	2.452	-1.498
80	1.979	-0.202
86	1.866	0.326
88	1.923	0.252
90	1.966	0.046
92	1.873	-0.119

TABLE 19

DRAG AND LIFT COEFFICIENTS FOR MODEL S36T2
AS DETERMINED BY PRESSURE READINGS

HEIGHT OF MODEL: 36 IN.
WIDTH OF MODEL: 2 IN.
DEPTH OF MODEL: 1 IN.
GRID IN USE: COARSE

ANGLE	CD	CL
-2	3.195	-0.091
0	3.064	0.052
2	3.171	0.023
4	3.044	-0.017
6	2.932	-0.128
10	2.696	-0.077
20	2.225	-0.664
30	2.592	-1.662
40	2.687	-1.861
50	2.607	-1.937
60	2.577	-2.052
70	2.176	-1.493
80	1.746	-0.727
86	1.581	-0.269
88	1.517	-0.139
90	1.515	0.050
92	1.562	0.170

TABLE 20

DRAG AND LIFT COEFFICIENTS FOR MODEL 36T2
AS DETERMINED BY PRESSURE READINGS

HEIGHT OF MODEL: 36 IN.
WIDTH OF MODEL: 4 IN.
DEPTH OF MODEL: 2 IN.
GRID IN USE: COARSE

ANGLE	CD	CL
-2	3.720	-0.301
0	3.709	-0.071
2	3.598	-0.140
4	3.672	-0.214
10	3.274	-0.213
20	2.499	-0.498
30	2.859	-1.809
40	3.129	-2.172
50	3.066	-2.268
60	2.988	-2.363
70	2.484	-1.738
80	1.906	-0.596
86	1.649	-0.177
88	1.612	-0.056
90	1.515	0.045
92	1.545	0.142

TABLE 21

DRAG AND LIFT COEFFICIENTS FOR MODEL B36T2
AS DETERMINED BY PRESSURE READINGS

HEIGHT OF MODEL: 36 IN.
WIDTH OF MODEL: 6 IN.
DEPTH OF MODEL: 3 IN.
GRID IN USE: COARSE

ANGLE	CD	CL
-2	4.108	-0.249
0	4.080	-0.155
2	4.205	-0.167
4	4.168	-0.260
10	3.898	-0.392
20	3.157	-0.957
30	3.367	-2.125
40	3.842	-2.651
50	3.393	-2.536
60	3.014	-2.459
70	2.794	-2.041
80	2.060	-0.765
86	1.907	-0.289
88	1.694	-0.172
90	1.673	-0.087
92	1.666	0.132

TABLE 22

PRESSURE COEFFICIENTS FOR
DIFFERENT ANGLES OF INCIDENCE
(SMOOTH FLOW)

MODEL	ANGLE OF INCIDENCE	C (STAG.)	C (BASE)	C (SIDE)
S36S	0	1.02	-1.65	-1.65
	10	0.88	-1.40	-1.44
	30	0.72	-1.08	-1.10
	60	0.73	-1.13	-1.12
	80	0.95	-0.72	-0.76
	90	0.96	-0.69	-0.84
36S	0	0.99	-2.10	-2.12
	10	0.83	-1.98	-2.04
	30	0.67	-1.35	-1.27
	60	0.82	-1.27	-1.29
	80	0.94	-0.86	-0.89
	90	0.98	-0.84	-1.04
B36S	0	0.95	-2.97	-2.88
	10	0.79	-2.66	-2.74
	30	0.51	-1.55	-1.54
	60	0.52	-1.40	-1.42
	80	0.95	-1.08	-1.11
	90	1.00	-0.98	-1.30
4X8S	0	0.91	-4.00	-3.90
	90	0.99	-1.19	-1.63

TABLE 23

PRESSURE COEFFICIENTS FOR
DIFFERENT ANGLES OF INCIDENCE
(TURBULENT FLOW)

MODEL	ANGLE OF INCIDENCE	C (STAG.)	C (BASE)	C (SIDE)
S36T2	0	1.04	-2.14	-2.31
	10	1.02	-1.80	-2.21
	30	0.82	-1.54	-1.66
	60	0.75	-1.34	-1.32
	80	1.01	-0.68	-1.05
	90	1.04	-0.48	-1.19
36T2	0	1.03	-2.80	-2.94
	10	0.94	-2.48	-2.66
	30	0.72	-1.93	-2.10
	60	0.66	-1.71	-1.75
	80	1.03	-0.86	-1.12
	90	1.01	-0.56	-1.48
B36T2	0	0.93	-3.45	-3.72
	10	0.89	-3.14	-3.48
	30	0.68	-2.44	-2.76
	60	0.52	-1.86	-1.95
	80	0.98	-1.04	-1.33
	90	1.02	-0.65	-1.64
4X8T2	0	0.93	-4.45	-5.06
	90	0.99	-0.86	-1.98

TABLE 24

PRESSURE COEFFICIENTS

MODEL 1 X 2 (SMOOTH)

ANGLE	CP1	CP2	CP3	CP4	CP5	CP6	CP7	CP8	CP9	CP10	CP11	CP12
-2	0.90	0.98	1.02	0.92	-1.63	-1.65	-1.65	-1.63	-1.63	-1.61	-1.65	-1.69
0	0.83	0.94	0.96	0.87	-1.37	-1.41	-1.45	-1.35	-1.43	-1.35	-1.47	-1.39
2	0.87	0.98	1.00	0.92	-1.61	-1.61	-1.67	-1.69	-1.67	-1.67	-1.63	-1.63
4	0.82	0.98	1.00	0.94	-1.70	-1.66	-1.64	-1.64	-1.64	-1.64	-1.66	-1.64
6	0.79	0.92	0.96	0.94	-1.67	-1.63	-1.63	-1.69	-1.69	-1.63	-1.63	-1.65
10	0.72	0.91	0.95	0.95	-1.36	-1.38	-1.42	-1.44	-1.44	-1.42	-1.53	-1.48
20	0.63	0.84	0.92	0.96	-1.08	-1.08	-1.06	-1.08	-1.13	-1.13	-1.80	-1.78
30	0.44	0.68	0.81	0.93	-1.08	-1.06	-1.08	-1.10	-1.10	-1.10	-0.96	-0.21
40	0.22	0.48	0.66	0.82	-1.18	-1.16	-1.16	-1.16	-1.16	-1.20	0.26	-0.04
50	-0.02	0.23	0.41	0.57	-1.13	-1.13	-1.13	-1.13	-1.13	-1.13	0.59	0.25
60	-0.25	0.0	0.15	0.28	-1.13	-1.13	-1.13	-1.15	-1.12	-1.13	0.87	0.59
70	-0.40	-0.16	-0.06	-0.50	-0.98	-1.02	-1.02	-1.00	-0.98	-0.98	0.94	0.76
80	-0.83	-1.10	-1.36	-1.36	-0.76	-0.76	-0.76	-0.74	-0.74	-0.70	0.96	0.93
86	-0.89	-0.89	-0.89	-0.87	-0.76	-0.76	-0.76	-0.74	-0.69	-0.69	0.98	0.98
88	-0.90	-0.88	-0.88	-0.88	-0.84	-0.84	-0.84	-0.81	-0.73	-0.71	1.02	1.00
90	-0.79	-0.81	-0.77	-0.79	-0.88	-0.88	-0.88	-0.87	-0.69	-0.69	0.96	0.96
92	-0.74	-0.74	-0.74	-0.74	-0.95	-0.95	-0.95	-0.91	-0.68	-0.68	0.96	0.98

TABLE 25

PRESSURE COEFFICIENTS

MODEL 2 X 4 (SMOOTH)

ANGLE	CP1	CP2	CP3	CP4	CP5	CP6	CP7	CP8	CP9	CP10	CP11	CP12
-2	0.78	0.99	0.93	0.73	-2.12	-2.12	-2.12	-2.12	-2.07	-2.12	-2.12	-2.12
0	0.77	0.99	0.99	0.79	-2.10	-2.10	-2.10	-2.10	-2.03	-2.15	-2.08	-2.12
2	0.72	0.96	0.99	0.79	-2.10	-2.08	-2.10	-2.12	-2.10	-2.12	-2.08	-2.10
4	0.68	0.94	1.02	0.85	-2.05	-2.03	-2.15	-2.10	-2.08	-2.08	-2.05	-2.08
6	0.63	0.92	0.97	0.82	-2.08	-2.05	-2.05	-2.08	-2.08	-2.08	-2.05	-2.08
10	0.57	0.89	0.96	0.89	-1.93	-1.98	-2.03	-1.98	-2.08	-2.08	-2.00	-1.98
20	0.46	0.79	0.93	0.93	-1.41	-1.44	-1.41	-1.41	-1.44	-1.46	-1.78	-1.81
30	0.25	0.63	0.83	0.95	-1.37	-1.37	-1.34	-1.34	-1.37	-1.37	-1.55	-0.79
40	-0.04	0.39	0.65	0.87	-1.37	-1.39	-1.39	-1.39	-1.39	-1.41	0.26	-0.17
50	-0.25	0.14	0.37	0.57	-1.35	-1.33	-1.35	-1.35	-1.35	-1.35	0.49	0.16
60	-0.44	-0.10	0.08	0.24	-1.28	-1.30	-1.28	-1.28	-1.26	-1.28	-0.78	-0.44
70	-0.59	-0.30	-0.13	-0.40	-1.13	-1.15	-1.15	-1.15	-1.15	-1.17	0.95	0.70
80	-0.66	-1.14	-1.47	-1.45	-0.91	-0.87	-0.89	-0.87	-0.85	-0.87	0.96	0.93
86	-1.13	-1.17	-1.17	-1.13	-0.85	-0.83	-0.83	-0.83	-0.78	-0.76	0.98	0.95
88	-1.08	-1.08	-1.06	-1.06	-0.93	-0.93	-0.91	-0.91	-0.79	-0.79	0.96	0.95
90	-1.02	-1.00	-1.00	-0.96	-1.04	-1.08	-1.06	-1.04	-0.84	-0.82	0.98	0.96
92	-0.89	-0.89	-0.85	-0.85	-1.08	-1.12	-1.10	-1.10	-0.76	-0.76	0.96	0.96

TABLE 26

PRESSURE COEFFICIENTS

MODEL 3 X 6 (SMOOTH)

ANGLE	CP1	CP2	CP3	CP4	CP5	CP6	CP7	CP8	CP9	CP10	CP11	CP12
-2	0.71	0.93	0.91	0.62	-2.97	-2.80	-2.80	-2.83	-2.75	-2.83	-2.80	-2.78
0	0.71	0.95	0.95	0.71	-2.97	-2.82	-2.88	-3.03	-2.88	-2.88	-2.88	-2.85
2	0.67	0.91	0.94	0.74	-2.93	-2.82	-2.89	-3.09	-2.86	-2.93	-2.86	-2.86
4	0.64	0.93	0.96	0.74	-2.88	-2.75	-2.94	-3.04	-2.88	-2.91	-2.88	-2.88
6	0.61	0.90	0.96	0.77	-2.78	-2.72	-2.88	-2.97	-2.81	-2.81	-2.75	-2.78
10	0.52	0.84	0.96	0.84	-2.61	-2.58	-2.73	-2.70	-2.73	-2.75	-2.73	-2.75
20	0.46	0.85	1.00	0.97	-2.13	-2.13	-2.10	-2.10	-2.16	-2.22	-2.98	-2.95
30	0.12	0.49	0.65	0.76	-1.55	-1.55	-1.55	-1.53	-1.53	-1.55	-1.48	-0.83
40	-0.07	0.39	0.65	0.86	-1.95	-1.95	-1.95	-1.95	-1.95	-1.95	-0.09	-0.44
50	-0.37	0.14	0.32	0.58	-1.85	-1.85	-1.85	-1.85	-1.88	-1.85	0.25	0.05
60	-0.47	-0.16	0.02	0.18	-1.42	-1.42	-1.42	-1.42	-1.40	-1.40	0.65	0.37
70	-0.68	-0.40	-0.24	-0.84	-1.48	-1.44	-1.42	-1.42	-1.42	-1.42	1.00	0.74
80	-0.82	-1.20	-1.60	-1.58	-1.14	-1.14	-1.12	-1.12	-1.08	-1.08	0.98	0.92
86	-1.44	-1.46	-1.61	-1.52	-1.07	-1.04	-1.02	-1.02	-0.91	-0.91	1.00	0.98
88	-1.39	-1.52	-1.41	-1.39	-1.13	-1.13	-1.09	-1.07	-0.94	-0.94	1.00	1.00
90	-1.30	-1.40	-1.34	-1.28	-1.28	-1.32	-1.28	-1.24	-0.98	-0.96	0.98	1.00
92	-1.20	-1.20	-1.17	-1.13	-1.35	-1.37	-1.37	-1.35	-0.91	-0.91	0.96	0.98

TABLE 27

PRESSURE COEFFICIENTS

MODEL 1 X 2 (GRID 2)

ANGLE	CP1	CP2	CP3	CP4	CP5	CP6	CP7	CP8	CP9	CP10	CP11	CP12
-2	0.95	1.06	1.06	0.95	-2.16	-2.24	-2.28	-2.16	-2.43	-2.43	-2.47	-2.43
0	0.93	1.04	1.04	0.93	-2.07	-2.11	-2.14	-2.07	-2.28	-2.24	-2.31	-2.31
2	0.91	1.04	1.08	0.98	-2.22	-2.22	-2.22	-2.12	-2.25	-2.32	-2.42	-2.42
4	0.92	1.05	1.08	1.02	-2.10	-2.10	-2.10	-1.97	-2.23	-2.13	-2.39	-2.36
6	0.86	1.02	1.12	0.99	-2.01	-1.98	-1.98	-1.95	-2.11	-2.14	-2.33	-2.27
10	0.89	1.02	1.08	1.08	-1.80	-1.80	-1.84	-1.77	-2.00	-2.00	-2.56	-2.26
20	0.72	0.90	1.06	1.06	-1.47	-1.47	-1.50	-1.40	-1.59	-1.65	-2.03	-1.28
30	0.48	0.80	0.96	1.05	-1.60	-1.57	-1.50	-1.47	-1.60	-1.73	-0.64	-0.45
40	0.24	0.55	0.73	0.88	-1.55	-1.49	-1.46	-1.43	-1.61	-1.64	0.21	-0.06
50	0.0	0.33	0.48	0.68	-1.48	-1.46	-1.40	-1.37	-1.46	-1.48	0.62	0.24
60	-0.15	0.12	0.27	0.45	-1.43	-1.37	-1.34	-1.31	-1.28	-1.40	0.89	0.62
70	-0.36	-0.18	-0.12	-0.12	-1.22	-1.19	-1.19	-1.13	-1.01	-1.04	1.07	0.80
80	-0.39	-0.36	-0.59	-0.95	-1.01	-1.07	-1.07	-1.04	-0.68	-0.68	1.07	0.95
86	-0.50	-0.71	-1.04	-1.43	-0.89	-1.07	-1.13	-1.28	-0.50	-0.50	1.07	1.07
88	-0.62	-0.80	-1.19	-1.37	-0.86	-1.07	-1.22	-1.22	-0.48	-0.48	1.04	1.04
90	-0.83	-1.01	-1.19	-1.31	-0.65	-0.98	-1.19	-1.34	-0.48	-0.48	1.04	1.04
92	-0.86	-1.07	-1.10	-1.28	-0.53	-0.80	-1.10	-1.40	-0.50	-0.50	1.07	1.04

TABLE 28

PRESSURE COEFFICIENTS

MODEL 2 X 4 (GRID 2)

ANGLE	CP1	CP2	CP3	CP4	CP5	CP6	CP7	CP8	CP9	CP10	CP11	CP12
-2	0.85	1.10	1.10	0.85	-2.69	-2.76	-2.83	-2.80	-3.12	-3.19	-2.94	-3.01
0	0.81	1.10	1.10	0.92	-2.76	-2.80	-2.76	-2.69	-2.94	-3.08	-2.94	-2.94
2	0.76	1.04	1.04	0.86	-2.69	-2.73	-2.80	-2.62	-2.90	-3.04	-2.93	-2.97
4	0.74	1.10	1.13	0.92	-2.76	-2.76	-2.80	-2.66	-2.87	-3.08	-3.01	-3.01
10	0.66	1.00	1.10	1.00	-2.52	-2.55	-2.45	-2.38	-2.62	-2.69	-3.11	-2.93
20	0.49	0.95	1.08	1.08	-1.97	-1.97	-1.90	-1.87	-2.10	-2.16	-3.02	-2.03
30	0.20	0.69	0.89	1.08	-1.97	-1.97	-1.93	-1.84	-2.07	-2.13	-1.15	-0.69
40	-0.10	0.46	0.75	0.95	-1.97	-1.93	-1.84	-1.84	-2.03	-2.13	0.10	-0.23
50	-0.32	0.22	0.42	0.64	-1.89	-1.85	-1.79	-1.76	-1.89	-1.98	0.58	0.13
60	-0.51	-0.03	0.16	0.38	-1.85	-1.79	-1.69	-1.66	-1.73	-1.85	0.86	0.45
70	-0.61	-0.27	-0.09	0.0	-1.46	-1.43	-1.40	-1.37	-1.31	-1.40	1.00	0.73
80	-0.56	-0.48	-0.71	-1.43	-1.10	-1.16	-1.13	-1.10	-0.86	-0.86	1.07	0.98
86	-0.62	-0.77	-1.37	-1.63	-0.92	-1.19	-1.31	-1.31	-0.62	-0.62	1.04	1.01
88	-0.67	-0.91	-1.49	-1.67	-0.82	-1.19	-1.40	-1.40	-0.58	-0.58	1.03	1.03
90	-0.77	-1.07	-1.48	-1.57	-0.68	-1.01	-1.46	-1.57	-0.56	-0.56	0.89	1.01
92	-0.91	-1.19	-1.39	-1.27	-0.54	-0.82	-1.36	-1.61	-0.57	-0.57	0.96	0.99

TABLE 29

PRESSURE COEFFICIENTS

MODEL 3 X 6 (GRID 2)

ANGLE	CP1	CP2	CP3	CP4	CP5	CP6	CP7	CP8	CP9	CP10	CP11	CP12
-2	0.75	0.97	0.93	0.62	-3.10	-3.36	-3.45	-3.41	-3.63	-3.63	-3.50	-3.54
0	0.66	0.93	0.93	0.58	-3.27	-3.45	-3.41	-3.27	-3.63	-3.72	-3.50	-3.54
2	0.68	0.96	0.96	0.73	-3.46	-3.46	-3.42	-3.28	-3.60	-3.69	-3.60	-3.65
4	0.68	1.00	1.05	0.77	-3.42	-3.37	-3.37	-3.19	-3.56	-3.69	-3.69	-3.60
10	0.59	0.96	1.09	0.91	-3.28	-3.14	-3.14	-3.01	-3.37	-3.51	-3.83	-3.60
20	0.53	0.93	1.02	1.02	-2.57	-2.57	-2.57	-2.39	-2.74	-2.83	-3.41	-2.21
30	0.17	0.64	0.86	1.03	-2.54	-2.49	-2.45	-2.28	-2.71	-2.84	-1.68	-1.12
40	-0.08	0.46	0.71	0.96	-2.63	-2.63	-2.46	-2.38	-2.71	-2.84	-0.38	-0.42
50	-0.38	0.12	0.38	0.65	-2.38	-2.27	-2.19	-2.11	-2.23	-2.42	0.19	-0.04
60	-0.50	-0.08	0.08	0.35	-2.03	-1.96	-1.92	-1.88	-1.80	-1.92	0.65	0.38
70	-0.65	-0.35	-0.19	-0.12	-1.84	-1.73	-1.69	-1.73	-1.61	-1.69	0.92	0.69
80	-0.65	-0.50	-0.65	-1.54	-1.31	-1.34	-1.34	-1.31	-1.04	-1.04	1.04	0.92
86	-0.69	-0.88	-1.38	-2.15	-1.27	-1.50	-1.61	-1.54	-0.88	-0.84	1.04	1.04
88	-0.69	-0.95	-1.53	-1.93	-1.09	-1.42	-1.56	-1.56	-0.69	-0.69	1.02	0.98
90	-0.73	-1.16	-1.60	-1.82	-0.95	-1.31	-1.67	-1.75	-0.65	-0.65	1.02	1.02
92	-0.96	-1.35	-1.56	-1.70	-0.81	-1.13	-1.56	-1.74	-0.67	-0.67	0.99	0.99

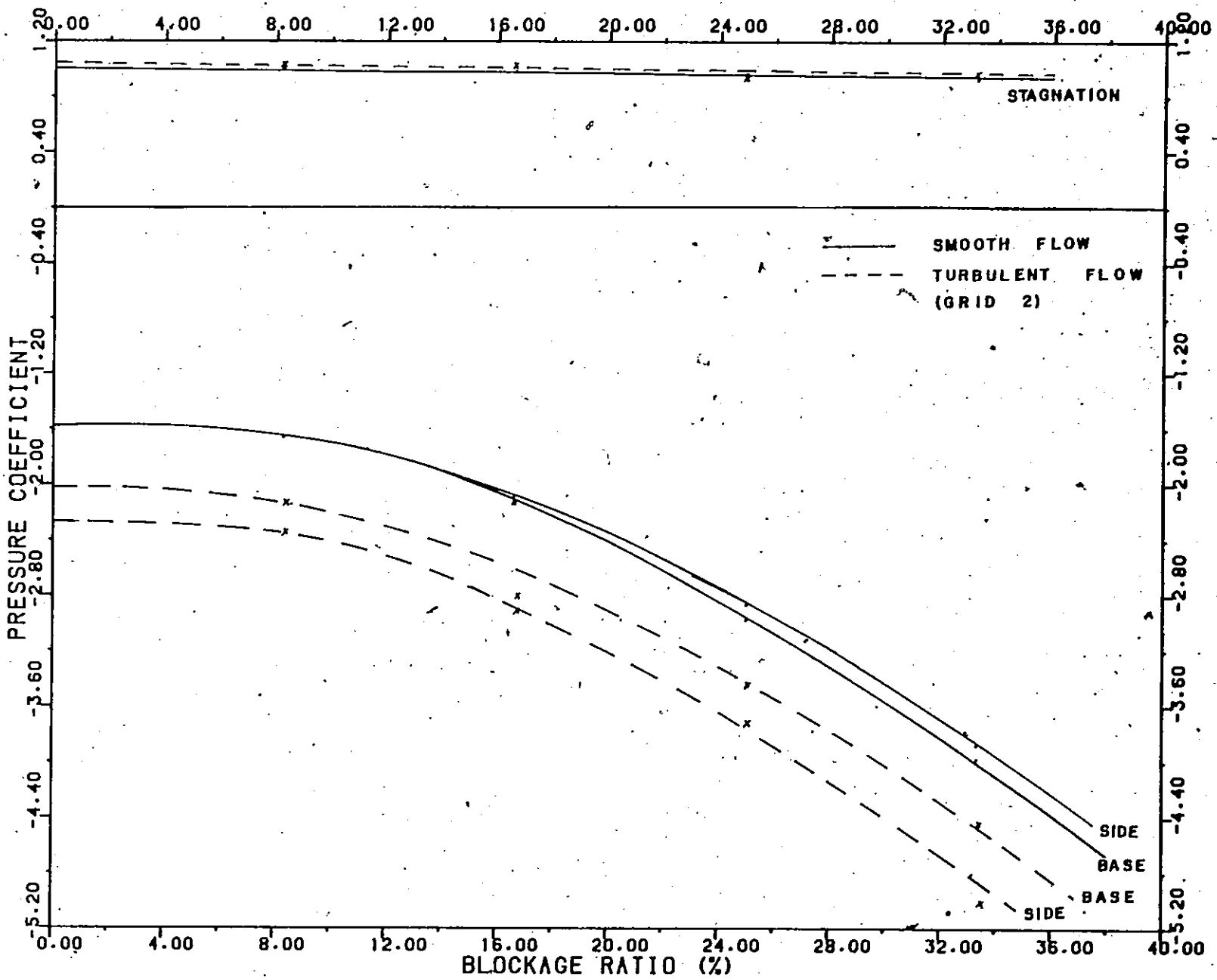

FIGURE 7 - BASE, SIDE AND STAGNATION PRESSURE COEFFICIENTS VERSUS BLOCKAGE RATIO FOR AN ANGLE OF INCIDENCE OF 0 DEGREES

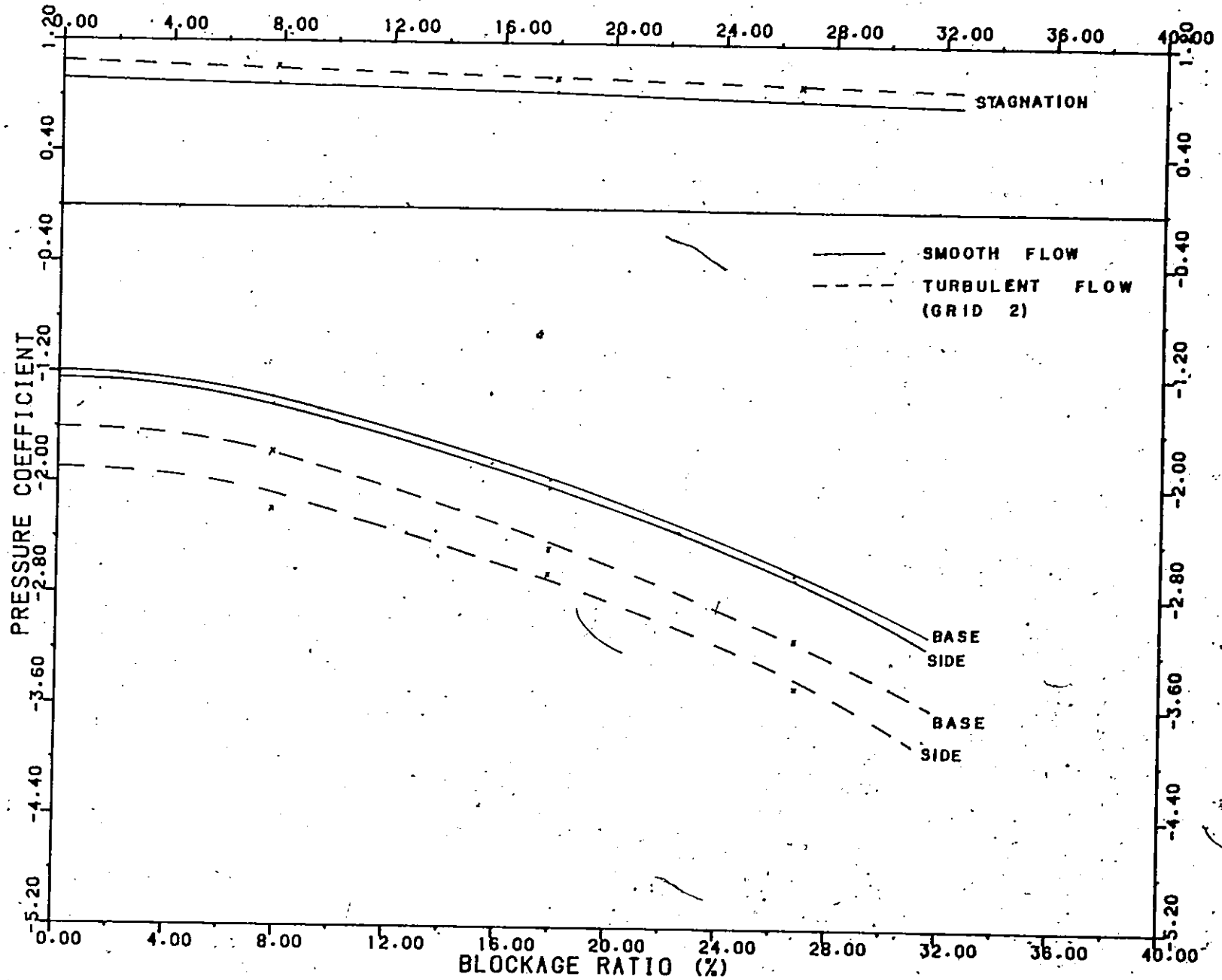

FIGURE 8 - BASE, SIDE AND STAGNATION PRESSURE COEFFICIENTS VERSUS BLOCKAGE RATIO FOR AN ANGLE OF INCIDENCE OF 10 DEGREES

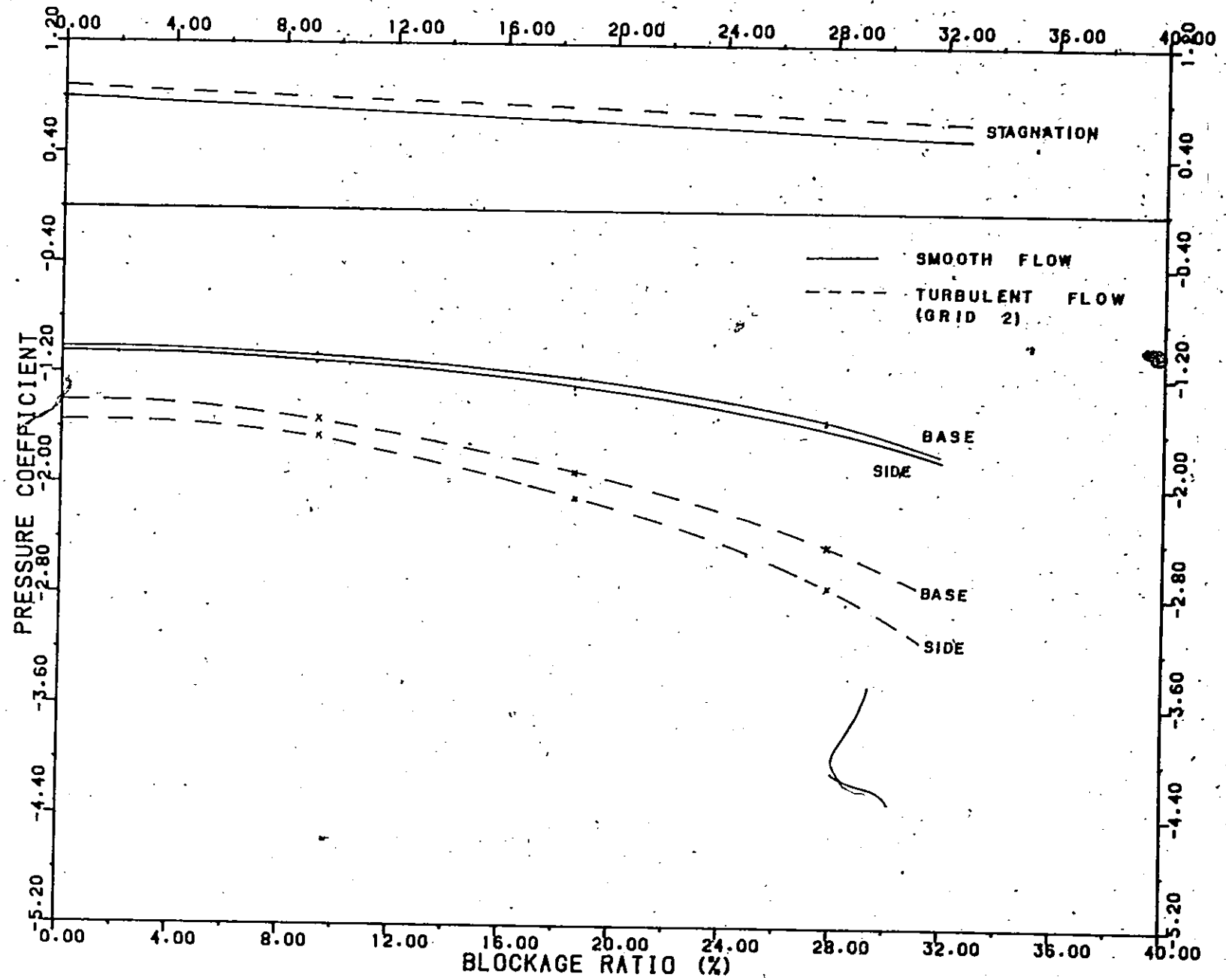

FIGURE 9 - BASE, SIDE AND STAGNATION PRESSURE COEFFICIENTS VERSUS BLOCKAGE RATIO FOR AN ANGLE OF INCIDENCE OF 30 DEGREES

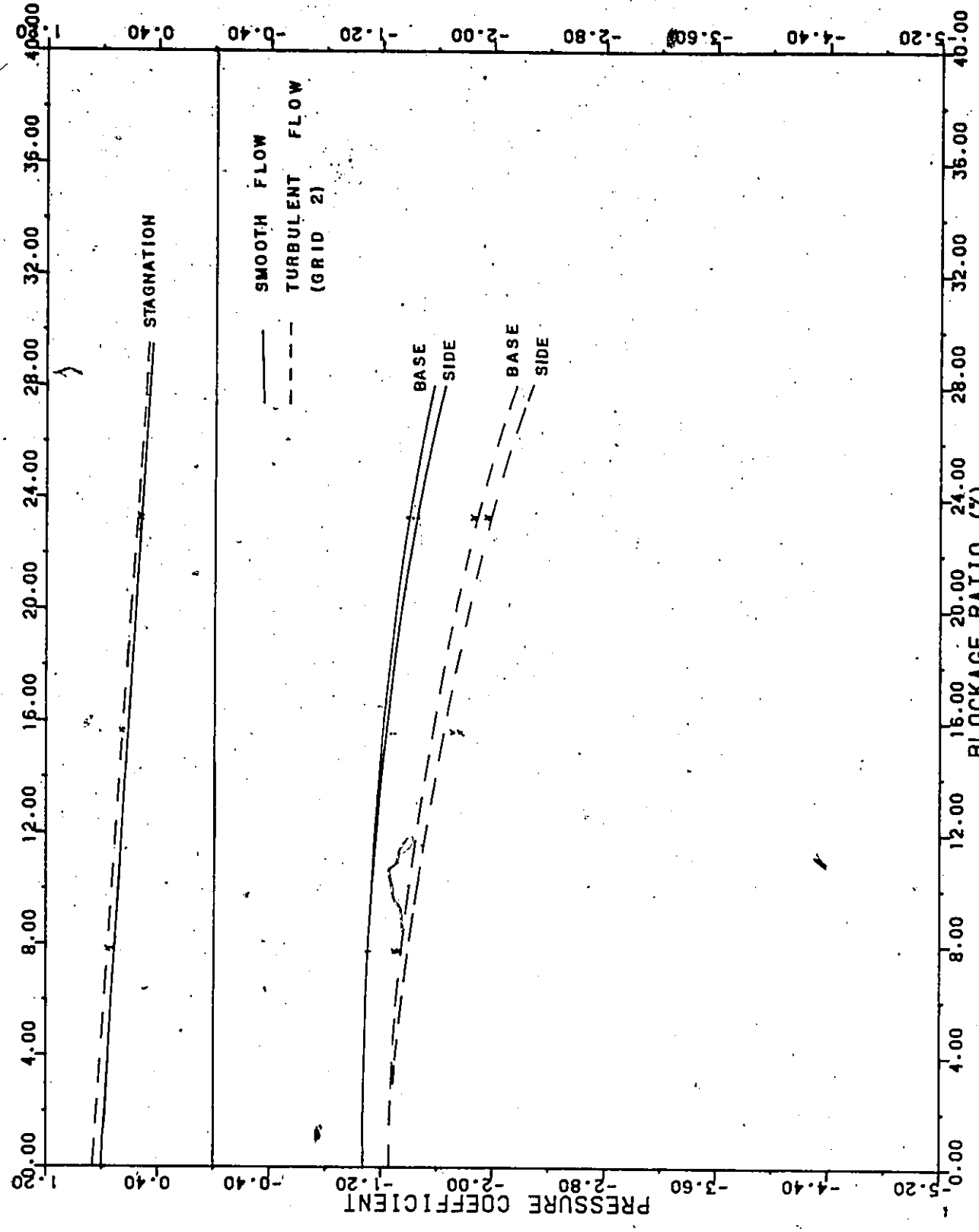

FIGURE 10- BASE, SIDE AND STAGNATION PRESSURE COEFFICIENTS VERSUS BLOCKAGE RATIO FOR AN ANGLE OF INCIDENCE OF 60 DEGREES

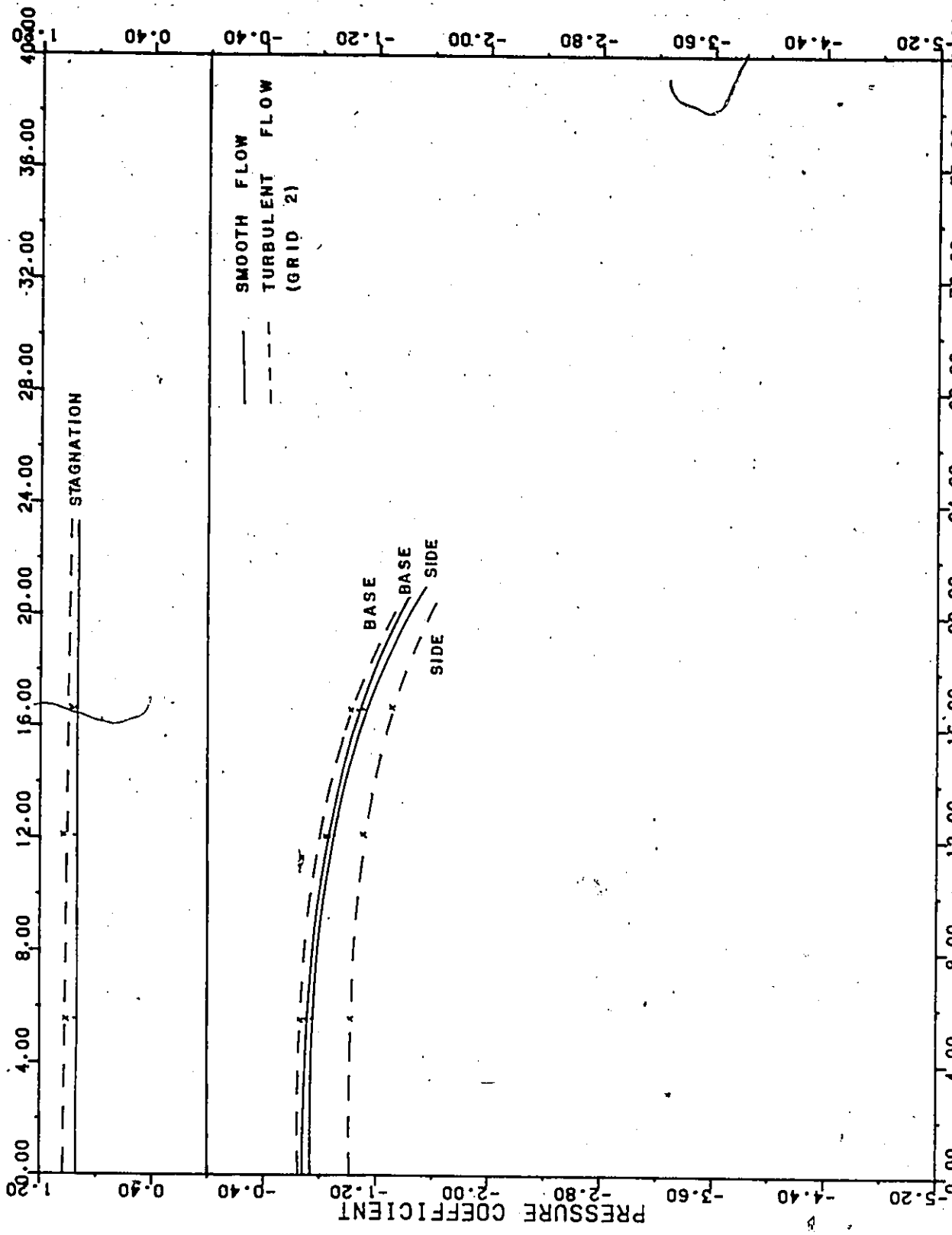

FIGURE 11 - BASE, SIDE AND STAGNATION PRESSURE COEFFICIENTS VERSUS BLOCKAGE RATIO FOR AN ANGLE OF INCIDENCE OF 80 DEGREES

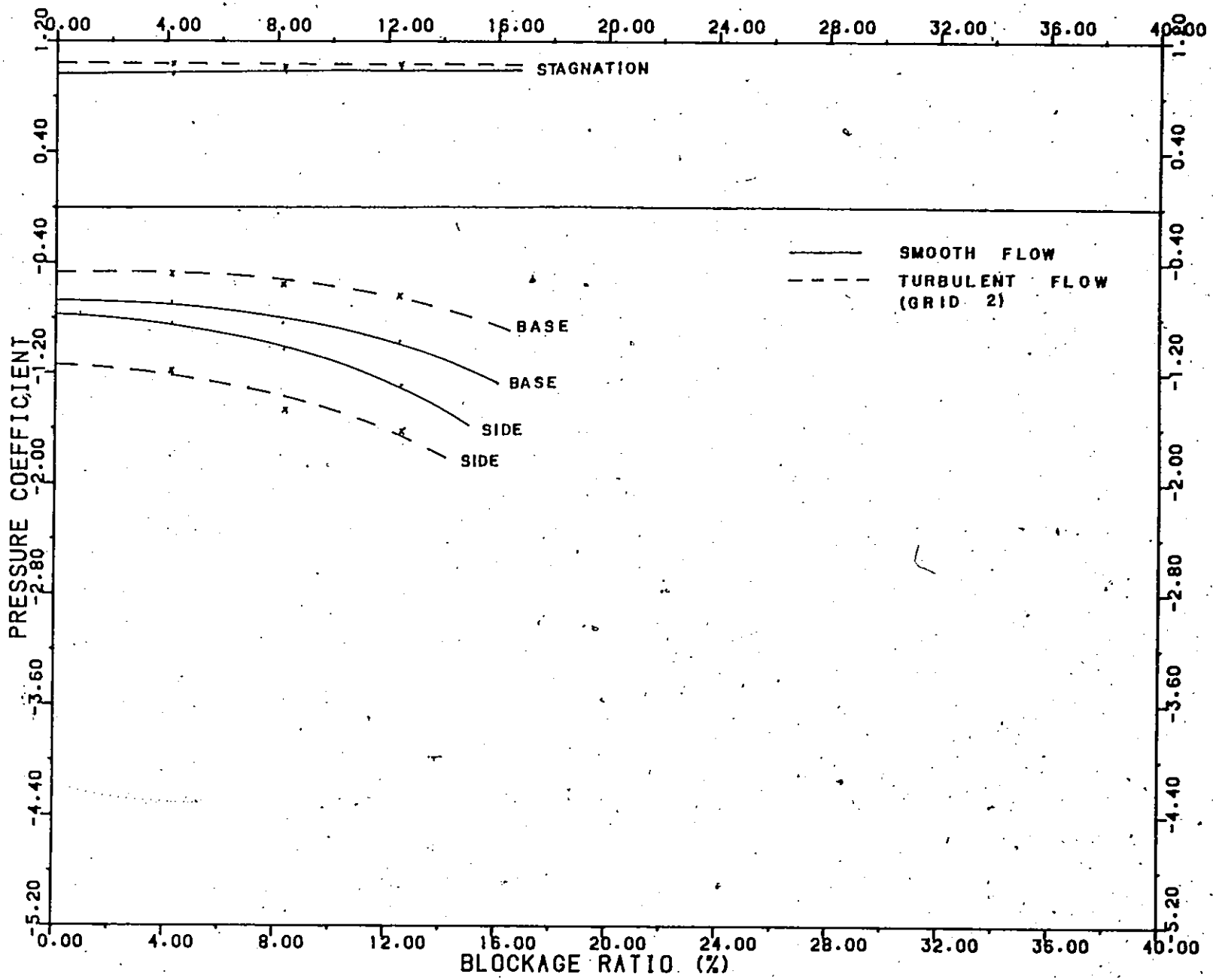

FIGURE 12 - BASE, SIDE AND STAGNATION PRESSURE COEFFICIENTS VERSUS BLOCKAGE RATIO FOR AN ANGLE OF INCIDENCE OF 90 DEGREES

TABLE 30

BASE PRESSURE COEFFICIENTS FOR THE 1X2 MODEL IN SMOOTH FLOW WITH $\alpha = 0°$

HEIGHT ALONG MODEL (IN.)	C_p (BASE) GAP: 0.125 IN.	GAP: 0.60 IN.	GAP: 0.75 IN.
35	-1.25	-1.16	-1.14
34	-1.23	-1.14	-1.11
33	-1.27	-1.18	-1.18
32	-1.37	-1.25	-1.21
30	-1.37	-1.28	-1.23
28	-1.42	-1.28	-1.23
26	-1.42	-1.32	-1.28
24	-1.47	-1.32	-1.28
22	-1.54	-1.37	-1.28
20	-1.54	-1.37	-1.33
18	-1.54	-1.42	-1.33
16	-1.54	-1.42	-1.37
14	-1.54	-1.47	-1.35
12	-1.58	-1.47	-1.38
10	-1.56	-1.49	-1.31
8	-1.51	-1.51	-1.28
6	-1.47	-1.44	-1.26
4	-1.42	-1.39	-1.14
3	-1.37	-1.35	-1.11
2	-1.30	-1.30	-1.16
MEAN	-1.44	-1.35	-1.25
MEAN OF MIDDLE THIRD	-1.54	-1.41	-1.33

TABLE 31

BASE PRESSURE COEFFICIENTS FOR THE 1X2 MODEL IN TURBULENT FLOW (GRID II) WITH $\alpha = 0°$

HEIGHT ALONG MODEL (IN.)	C_p (BASE) GAP: 0.125 IN.	GAP: 0.60 IN.	GAP: 0.75 IN.
35	-1.88	-1.42	-1.38
34	-1.75	-1.34	-1.29
33	-1.75	-1.34	-1.29
32	-1.88	-1.46	-1.33
30	-1.96	-1.59	-1.42
28	-2.09	-1.75	-1.50
26	-2.17	-1.92	-1.59
24	-2.17	-1.92	-1.72
22	-2.30	-1.96	-1.72
20	-2.30	-1.96	-1.72
18	-2.30	-2.00	-1.80
16	-2.38	-2.00	-1.85
14	-2.38	-2.09	-1.93
12	-2.46	-2.05	-1.80
10	-2.30	-2.09	-1.89
8	-2.21	-1.96	-1.80
6	-2.13	-1.92	-1.72
4	-2.05	-1.83	-1.72
3	-2.05	-1.75	-1.63
2	-2.09	-1.71	-1.63
MEAN	-2.13	-1.79	-1.64
MEAN OF MIDDLE THIRD	-2.33	-2.00	-1.79

TABLE 32

BASE PRESSURE COEFFICIENTS FOR THE 2X4 MODEL IN SMOOTH FLOW WITH $\alpha = 0°$

HEIGHT ALONG MODEL (IN.)	C_p (BASE) GAP: 0.125 IN.	GAP: 0.60 IN.	GAP: 0.75 IN.
35	-1.69	-1.34	-1.20
34	-2.01	-1.15	-1.23
33	-2.01	-1.23	-1.19
32	-2.01	-1.23	-1.23
30	-2.05	-1.34	-1.23
28	-2.10	-1.46	-1.35
26	-2.10	-1.50	-1.43
24	-2.10	-1.54	-1.50
22	-2.14	-1.54	-1.54
20	-2.14	-1.65	-1.62
18	-2.23	-1.77	-1.66
16	-2.32	-1.88	-1.85
14	-2.42	-1.88	-1.81
12	-2.51	-2.00	-1.85
10	-2.60	-2.03	-1.81
8	-2.64	-2.15	-1.85
6	-2.64	-2.11	-1.81
4	-2.60	-2.07	-1.77
3	-2.55	-1.96	-1.70
2	-2.47	-1.92	-1.74
MEAN	-2.27	-1.69	-1.57
MEAN OF MIDDLE THIRD	-2.27	-1.75	-1.69

TABLE 33

BASE PRESSURE COEFFICIENTS FOR THE 2X4 MODEL IN TURBULENT FLOW (GRID II) WITH $\alpha = 0°$

HEIGHT ALONG MODEL (IN.)	C_p (BASE) GAP: 0.125 IN.	GAP: 0.60 IN.	GAP: 0.75 IN.
35	-1.70	-1.49	-1.40
34	-1.70	-1.49	-1.25
33	-1.70	-1.54	-1.25
32	-1.70	-1.60	-1.30
30	-2.09	-1.70	-1.97
28	-2.20	-1.86	-2.27
26	-2.53	-2.02	-2.52
24	-2.53	-2.12	-2.58
22	-2.53	-2.34	-2.77
20	-2.58	-2.55	-2.95
18	-2.69	-2.61	-2.95
16	-2.80	-2.55	-3.01
14	-2.80	-2.55	-3.07
12	-2.97	-2.61	-3.14
10	-3.03	-2.61	-3.01
8	-2.80	-2.61	-3.01
6	-2.69	-2.45	-2.83
4	-2.50	-2.34	-2.71
3	-2.20	-2.23	-2.71
2	-2.04	-2.08	-2.46
MEAN	-2.39	-2.17	-2.46
MEAN OF MIDDLE THIRD	-2.70	-2.48	-2.92

TABLE 34

BASE PRESSURE COEFFICIENTS FOR THE MODELS IN SMOOTH FLOW WITH $\alpha = 90°$ FOR THE REAR CENTER TAPS

MODEL	C_{p_b} (BASE) GAP: 0.125 IN.	GAP: 0.60 IN.	GAP: 0.75 IN.
1X2	-0.62	-0.56	-0.58
2X4	-0.73	-0.68	-0.70

BASE PRESSURE COEFFICIENTS FOR THE MODELS IN TURBULENT FLOW (GRID II) WITH $\alpha = 90°$ FOR THE REAR CENTER TAPS

MODEL	C_{p_b} (BASE) GAP: 0.125 IN.	GAP: 0.60 IN.	GAP: 0.75 IN.
1X2	-0.50	-0.50	-0.46
2X4	-0.58	-0.56	-0.60

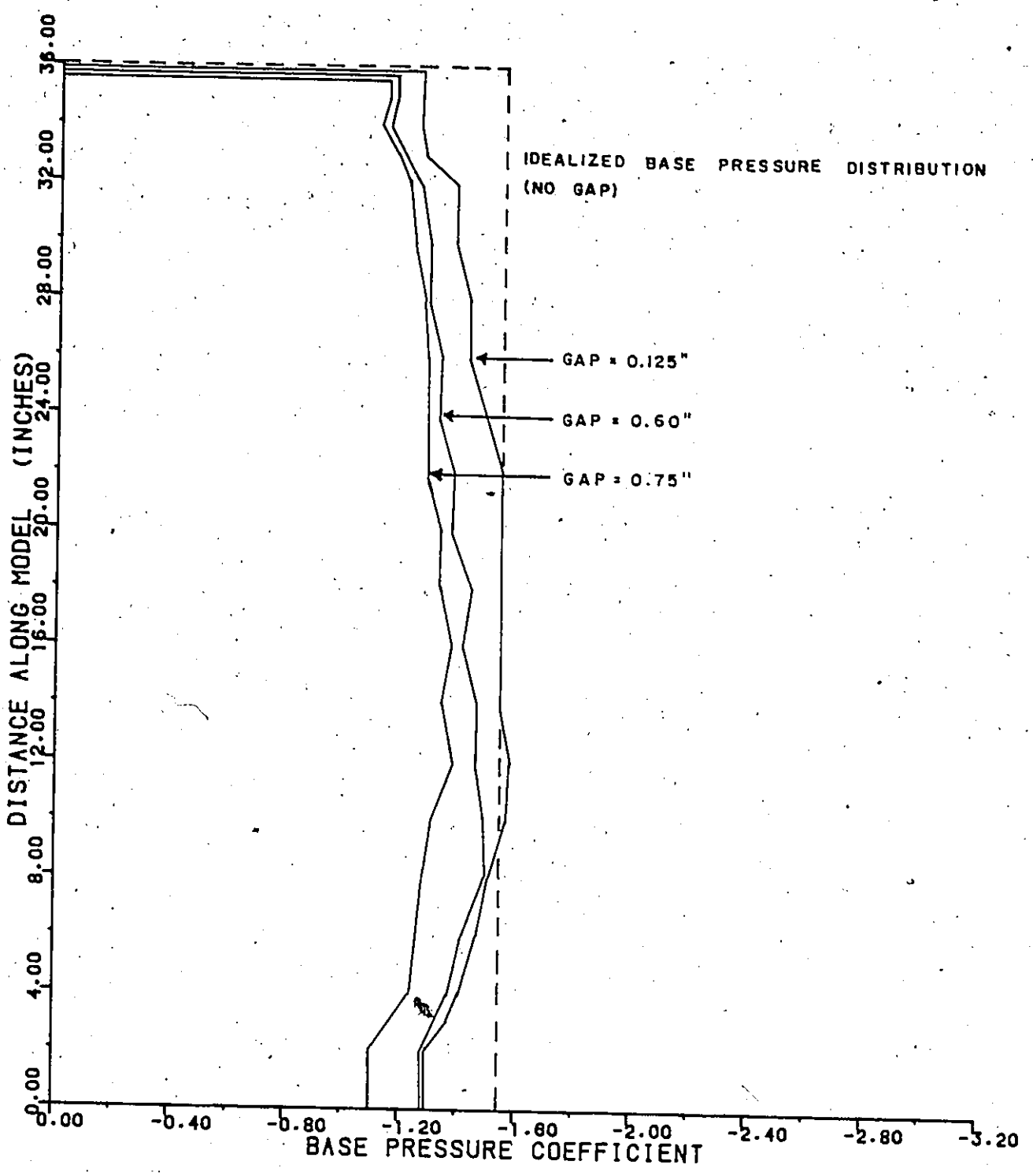

FIGURE 13 - VARIATION OF THE BASE PRESSURE COEFFICIENT FOR MODEL S36S FOR DIFFERENT GAP SIZES WITH AN ANGLE OF INCIDENCE OF 0 DEGREES

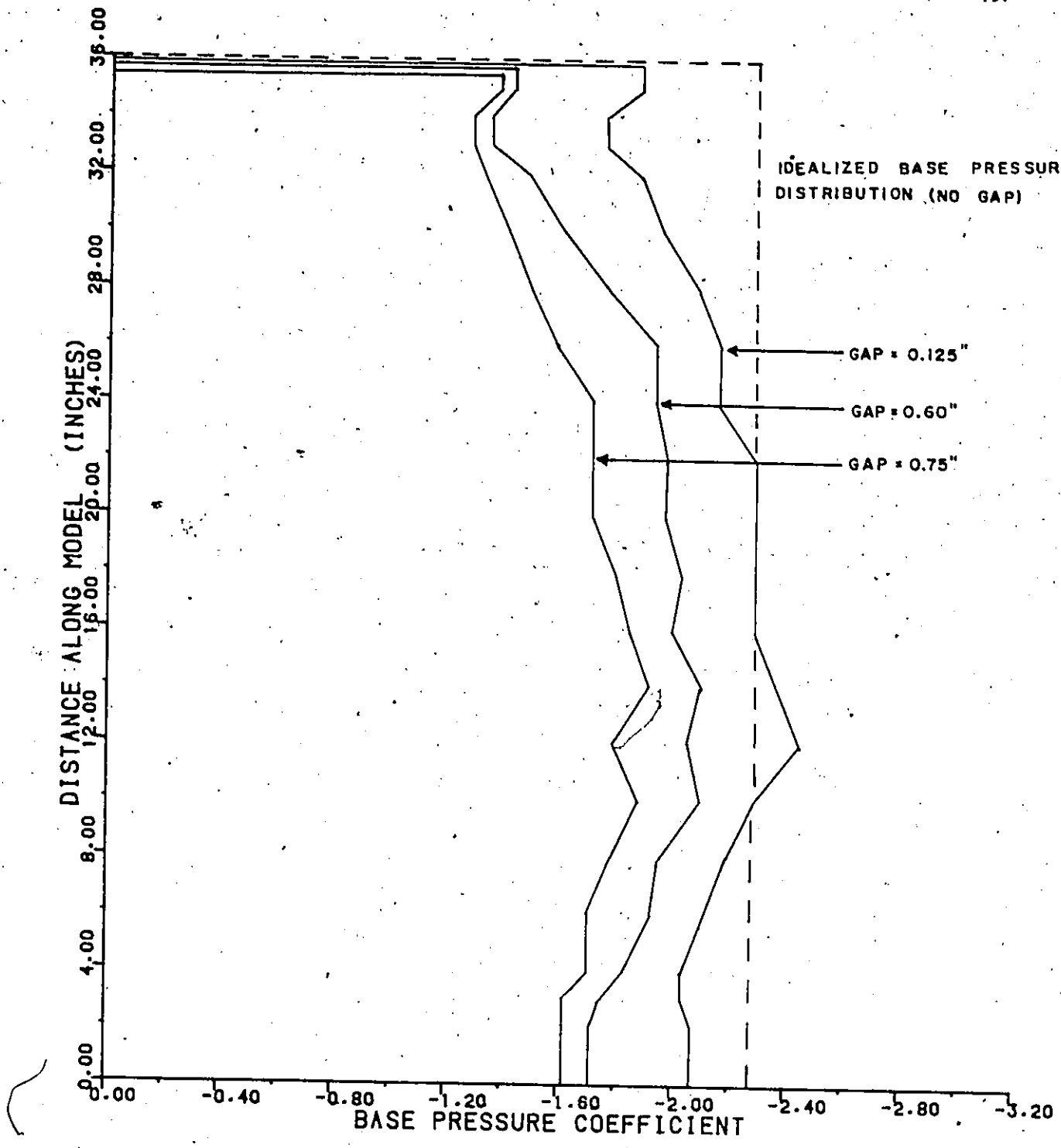

FIGURE 14 - VARIATION OF THE BASE PRESSURE COEFFICIENT FOR MODEL S36T2 FOR DIFFERENT GAP SIZES WITH AN ANGLE OF INCIDENCE OF 0 DEGREES

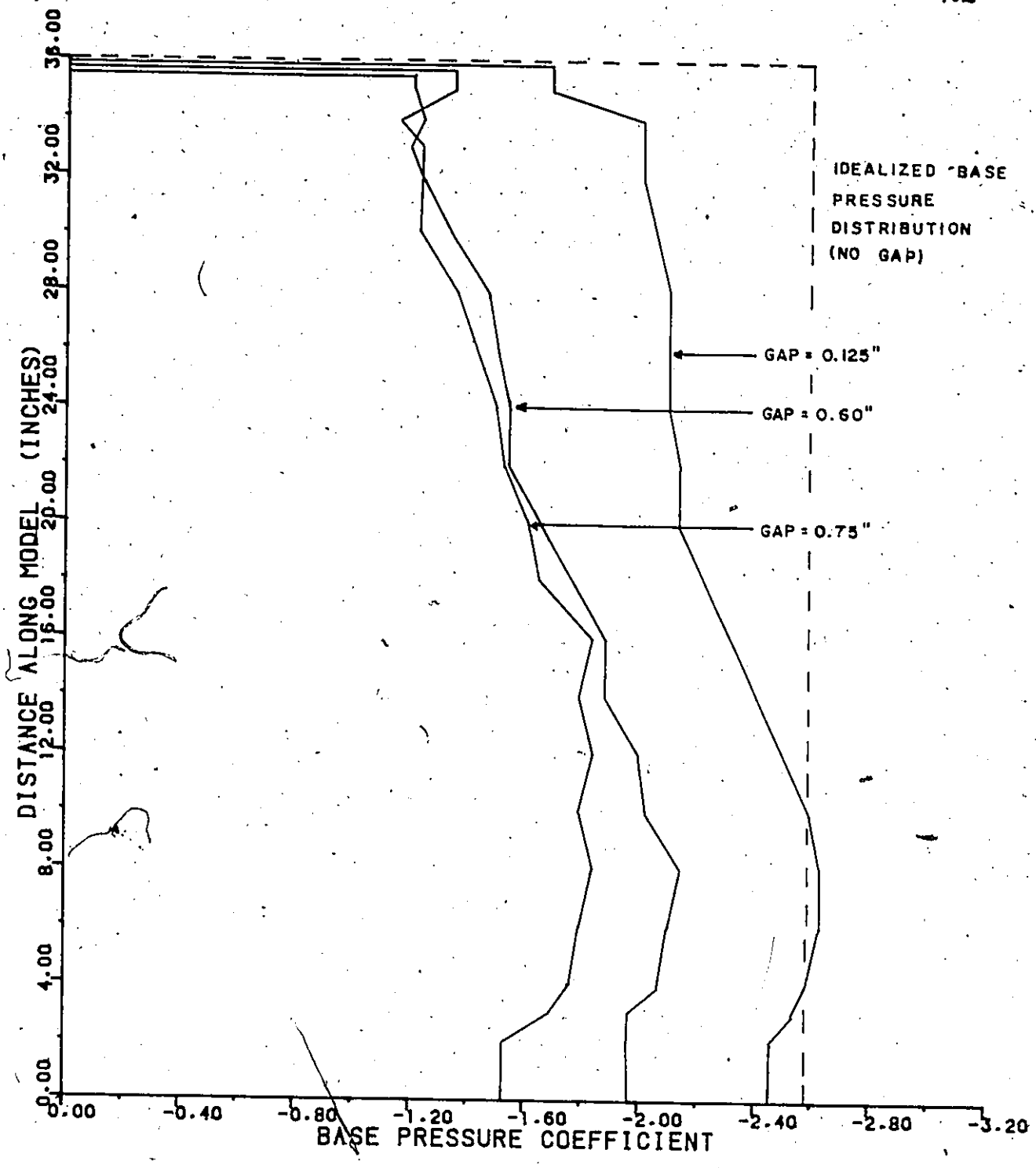

FIGURE 15 - VARIATION OF THE BASE PRESSURE COEFFICIENT FOR MODEL 36S FOR DIFFERENT GAP SIZES WITH AN ANGLE OF INCIDENCE OF 0 DEGREES

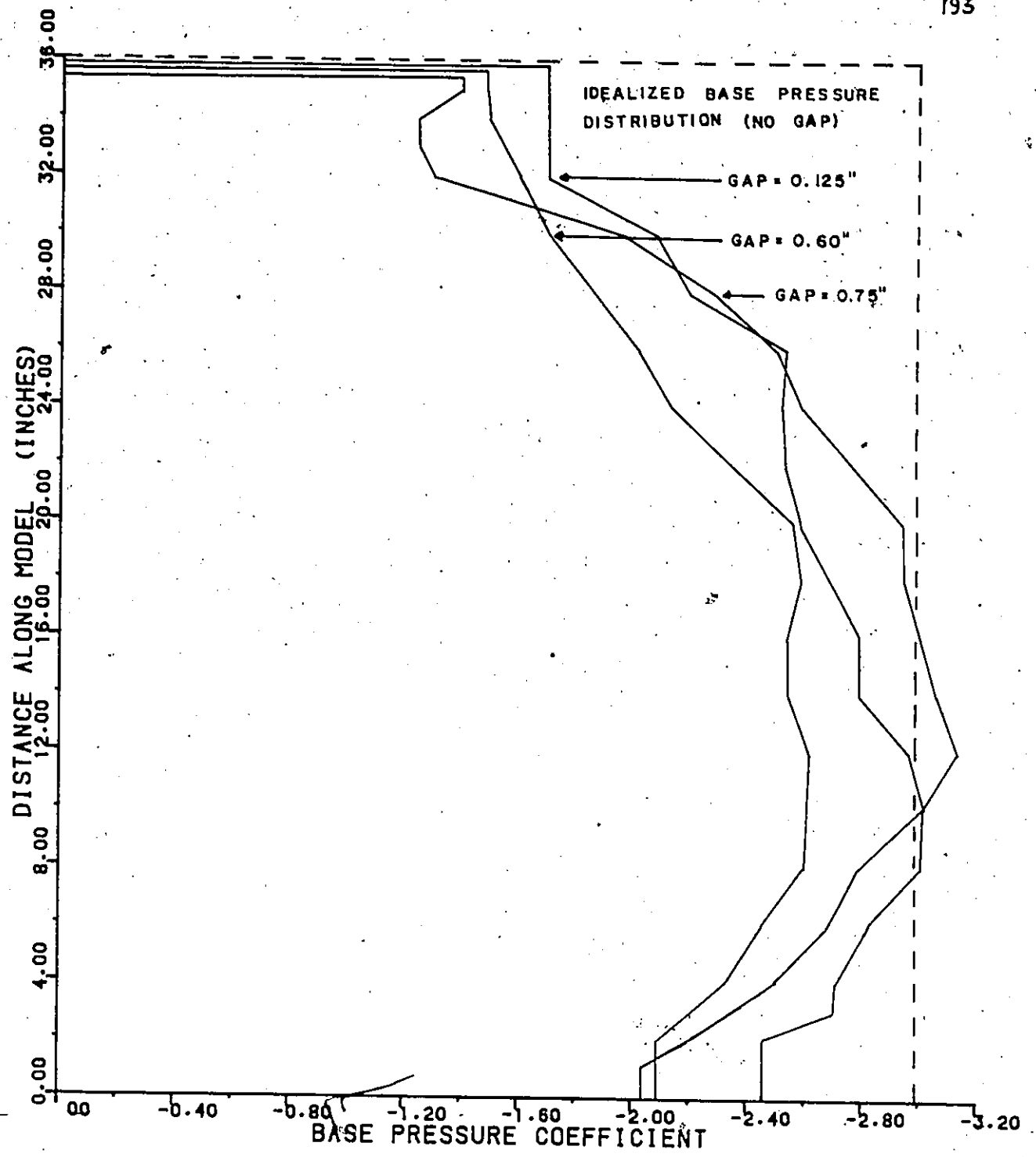

FIGURE 16 - VARIATION OF THE BASE PRESSURE COEFFICIENT FOR MODEL 36T2 FOR DIFFERENT GAP SIZES WITH AN ANGLE OF INCIDENCE OF 0 DEGREES

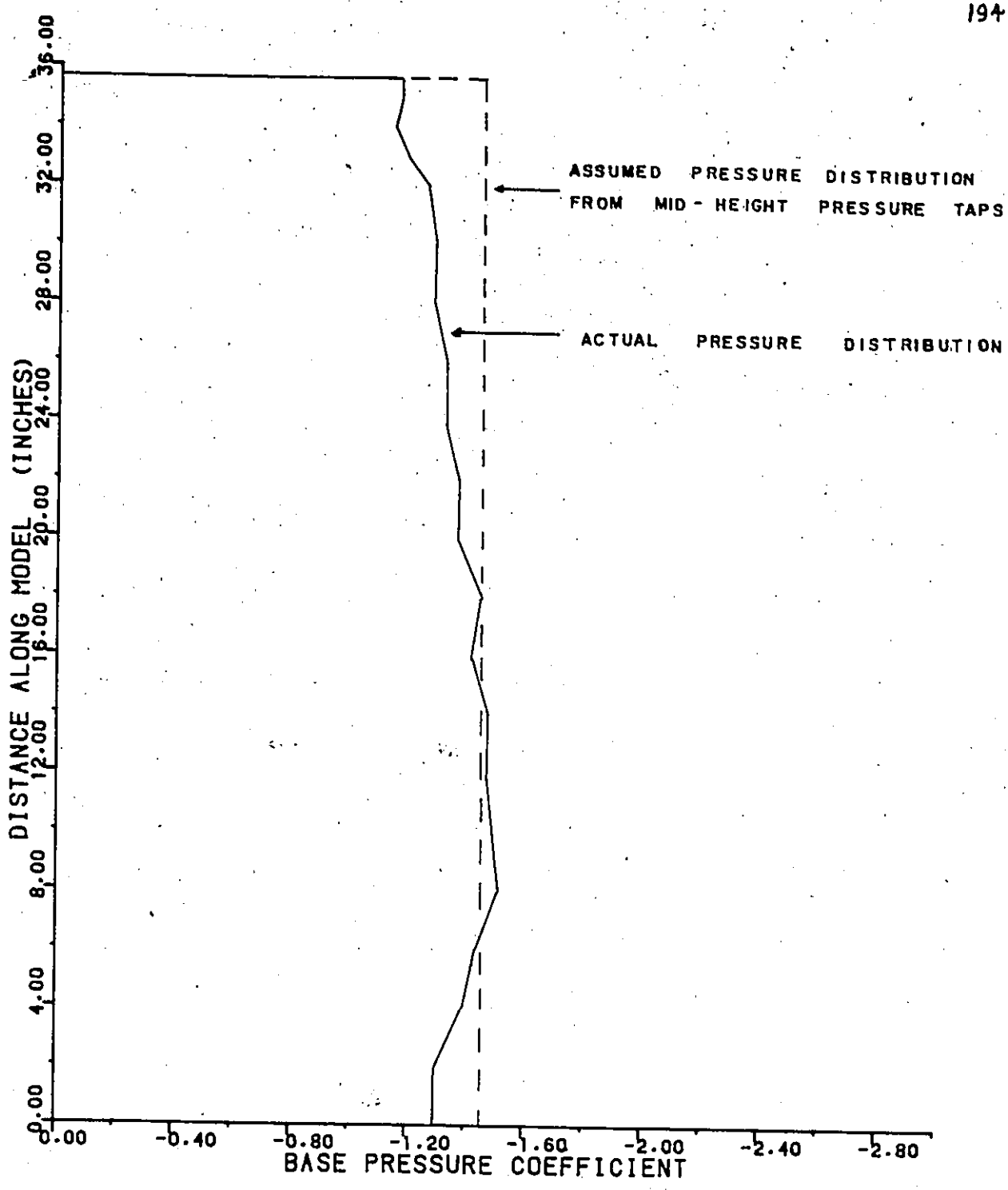

FIGURE 17 - BASE PRESSURE COEFFICIENT DISTRIBUTION FOR MODEL S36S WITH 0.60 INCH GAP AT AN ANGLE OF INCIDENCE OF 0 DEGREES

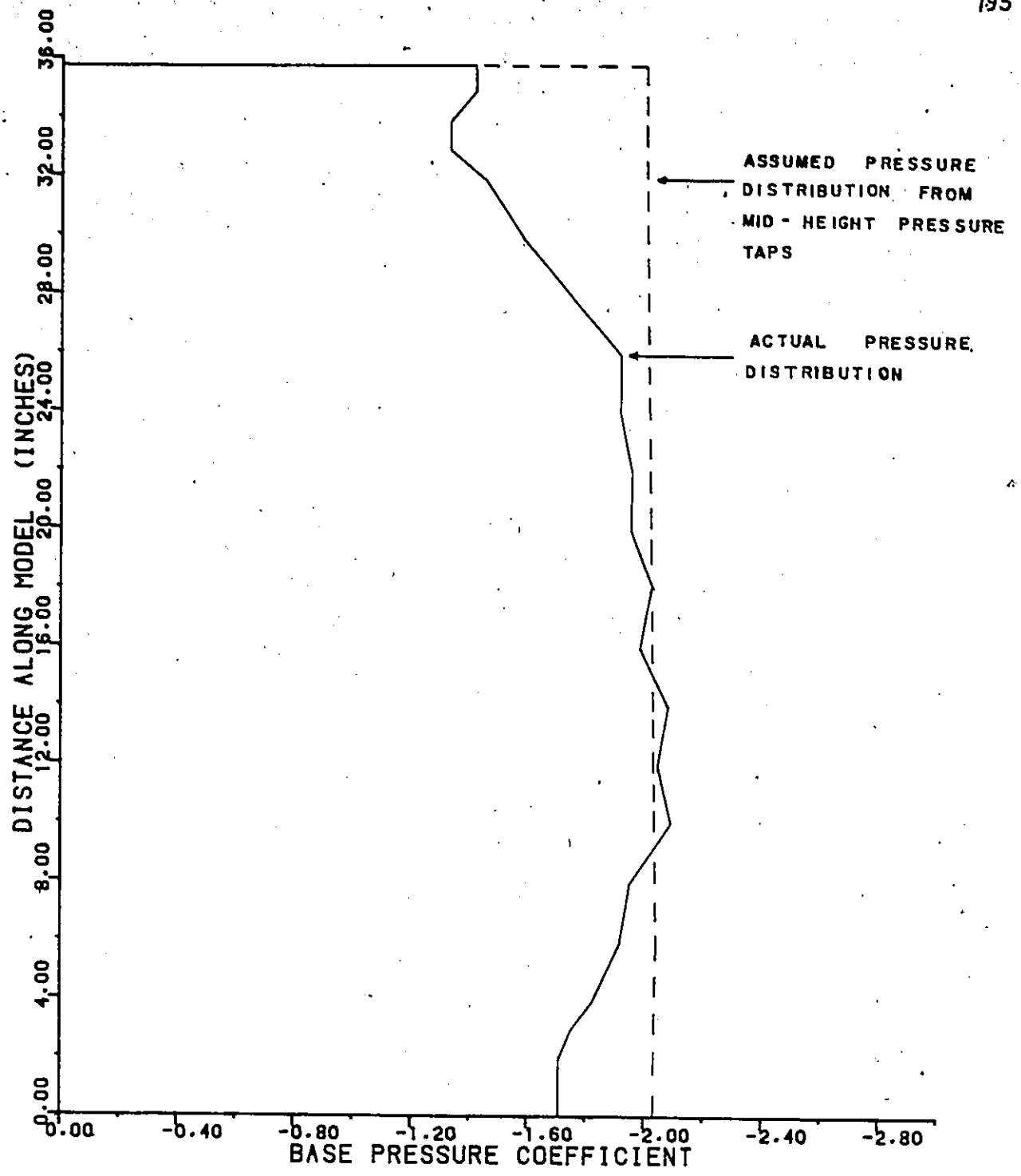

FIGURE 18 - BASE PRESSURE COEFFICIENT DISTRIBUTION FOR MODEL S36T2 WITH 0.60 INCH GAP AT AN ANGLE OF INCIDENCE OF 0 DEGREES

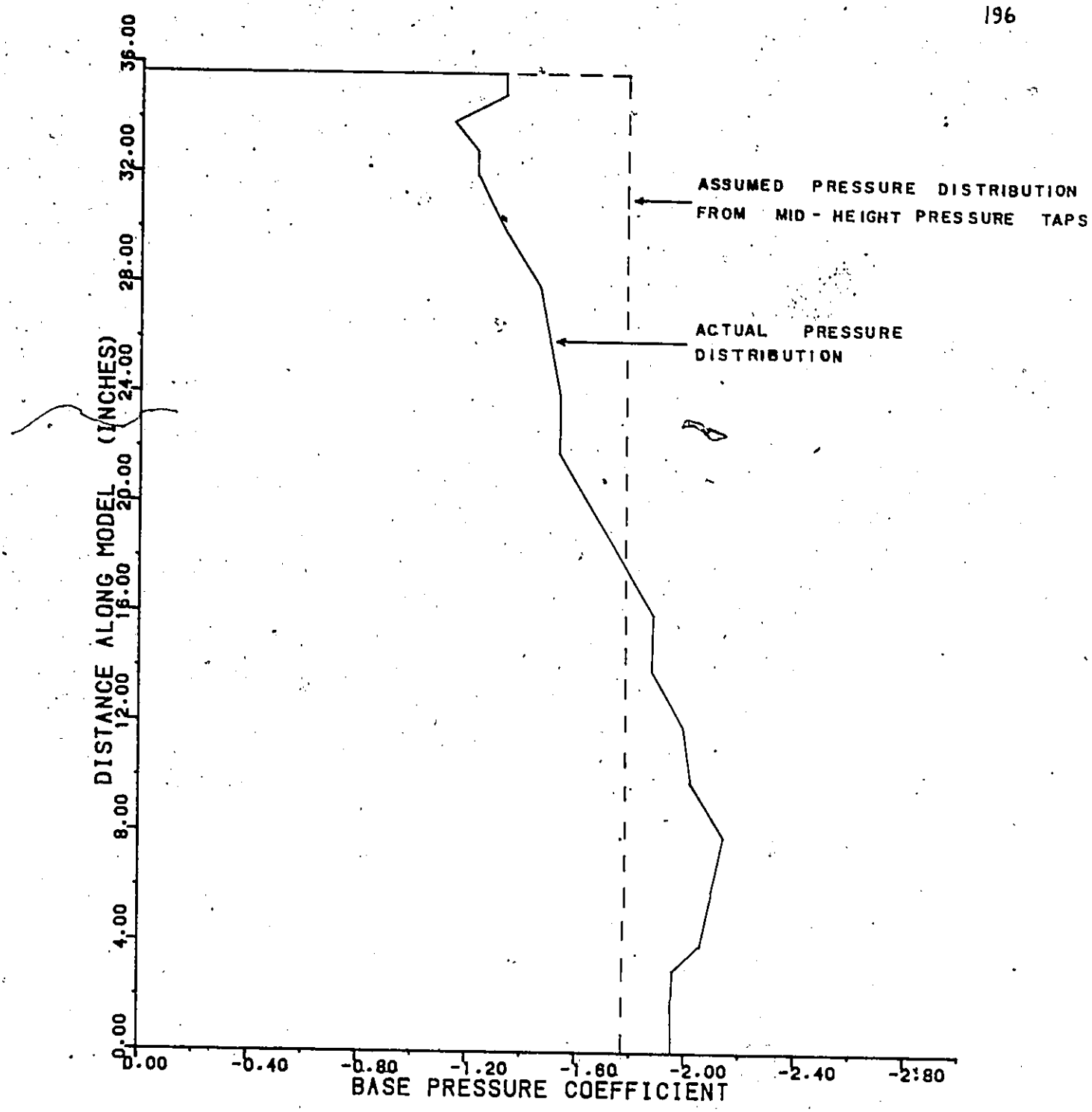

FIGURE 19 - BASE PRESSURE COEFFICIENT DISTRIBUTION FOR MODEL 36S WITH 0.60 INCH GAP AT AN ANGLE OF INCIDENCE OF 0 DEGREES

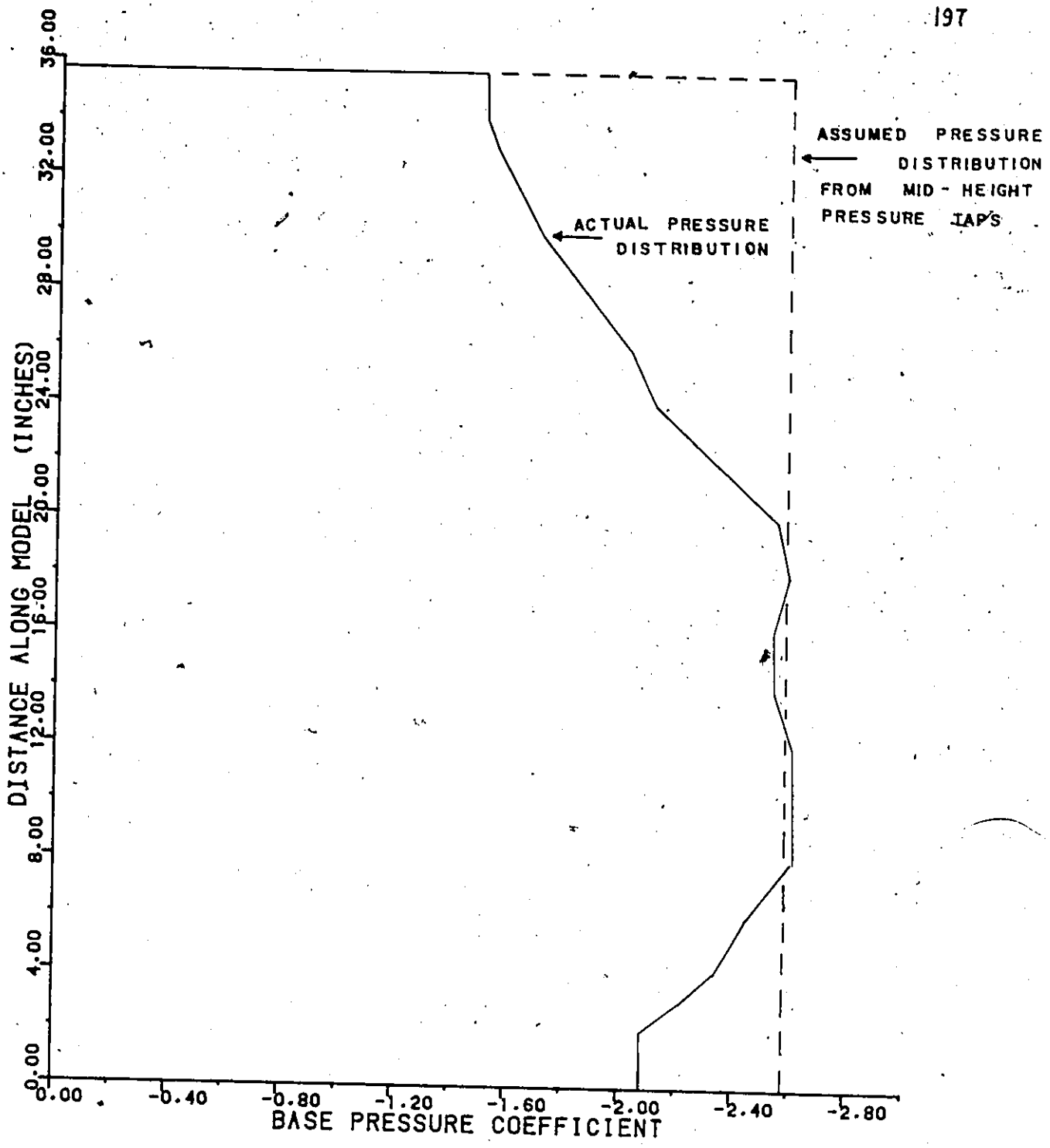

FIGURE 20 - BASE PRESSURE COEFFICIENT DISTRIBUTION FOR MODEL 36T2 WITH 0.60 INCH GAP AT AN ANGLE OF INCIDENCE OF 0 DEGREES

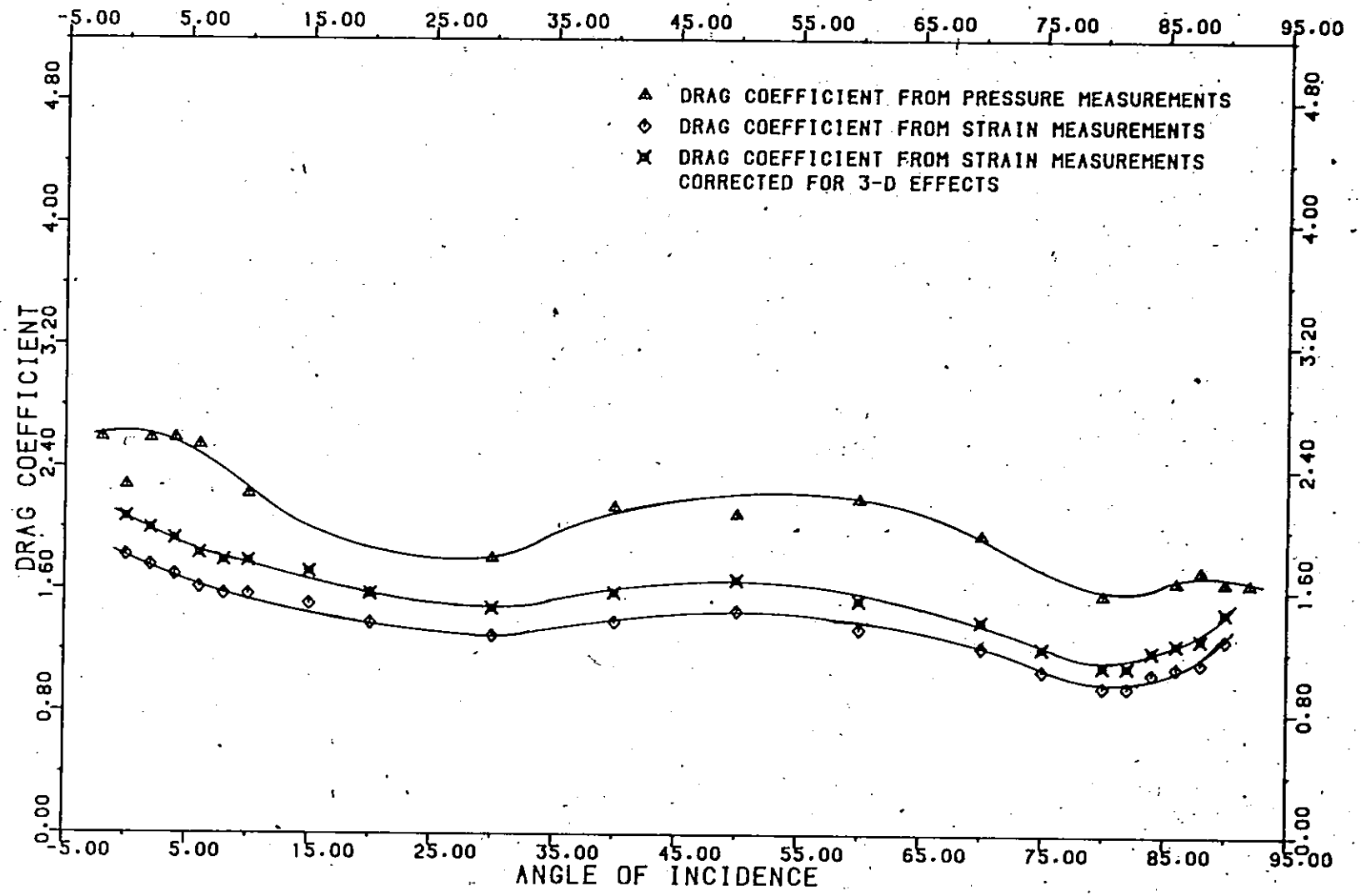

FIGURE 21 - DRAG COEFFICIENT FOR MODEL S36S BY STRAIN AND PRESSURE MEASUREMENTS

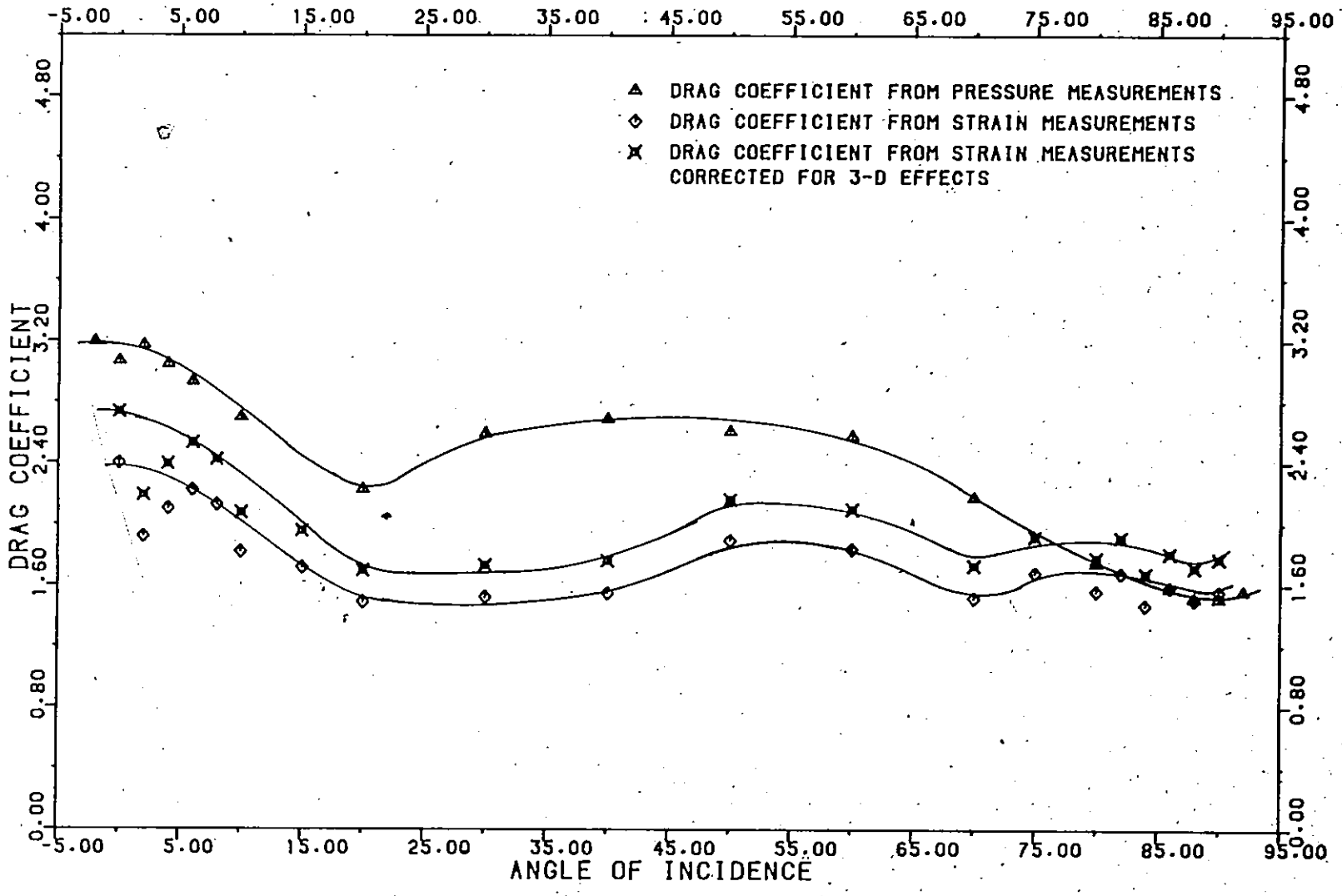

FIGURE 22 - DRAG COEFFICIENT FOR MODEL S36T2 BY STRAIN AND PRESSURE MEASUREMENTS

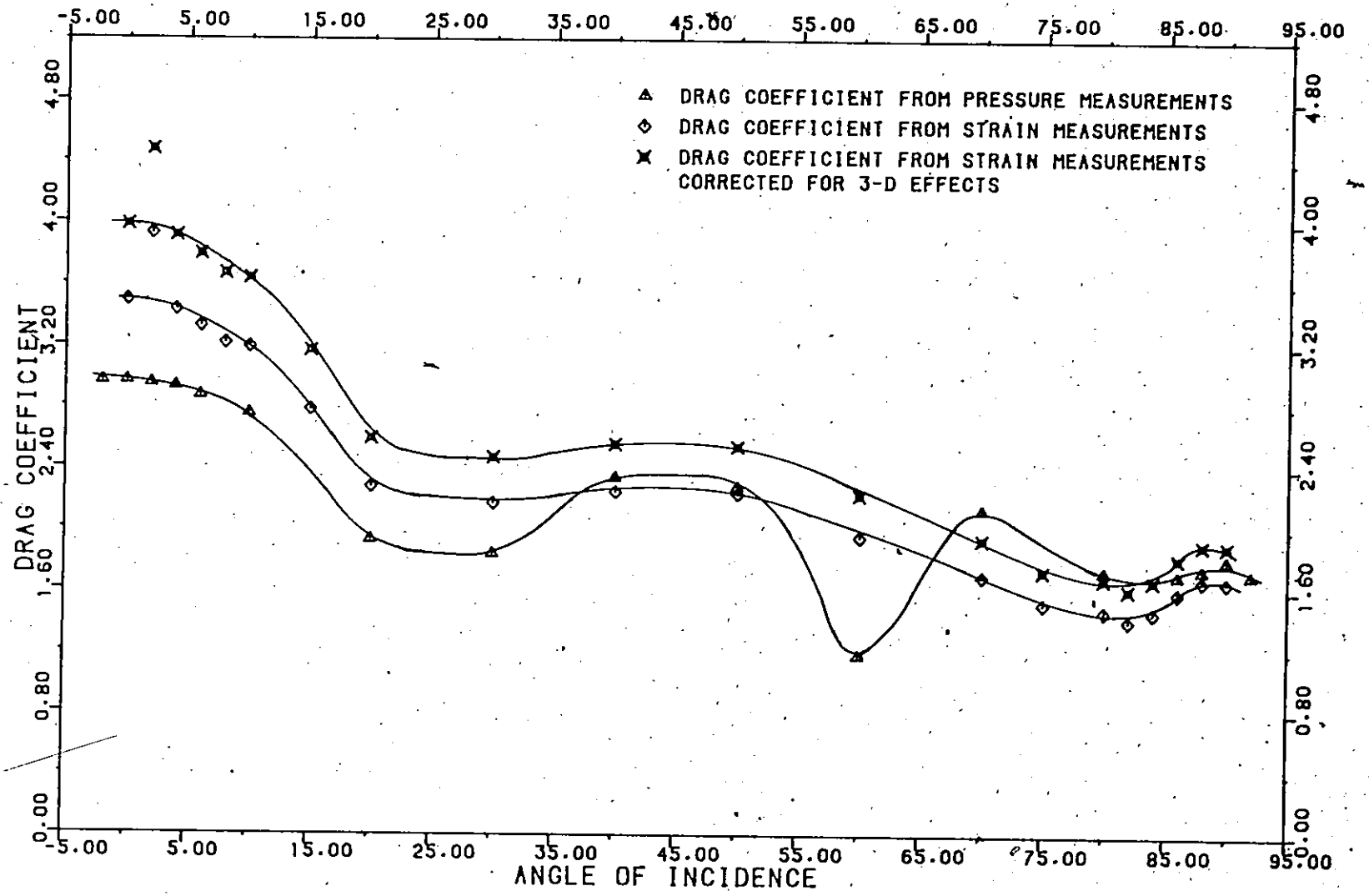

FIGURE 23 - DRAG COEFFICIENT FOR MODEL 36S BY STRAIN AND PRESSURE MEASUREMENTS

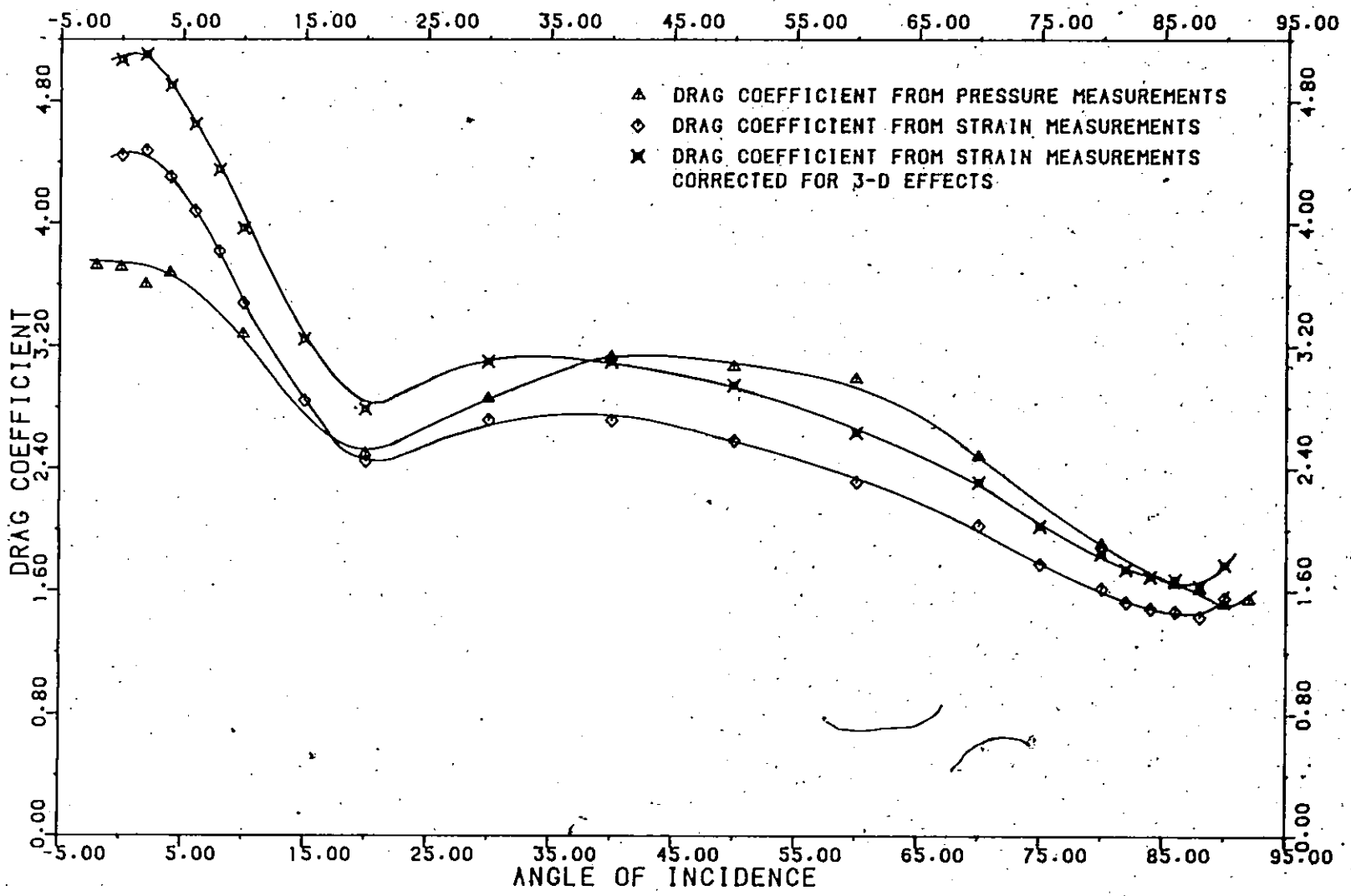

FIGURE 24 - DRAG COEFFICIENT FOR MODEL 36T2 BY STRAIN AND PRESSURE MEASUREMENTS

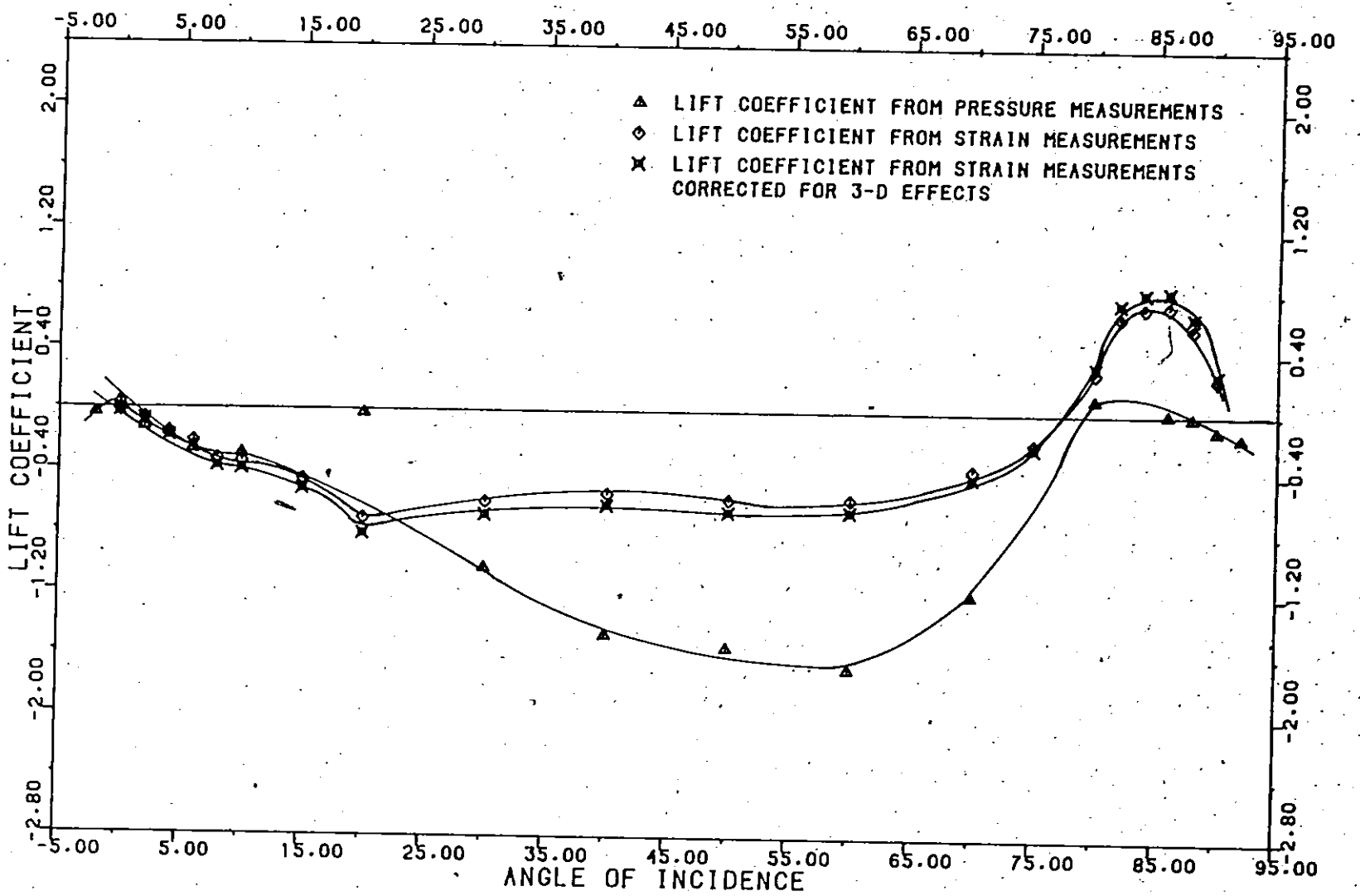

FIGURE 25 - LIFT COEFFICIENT FOR MODEL S36S BY STRAIN AND PRESSURE MEASUREMENTS

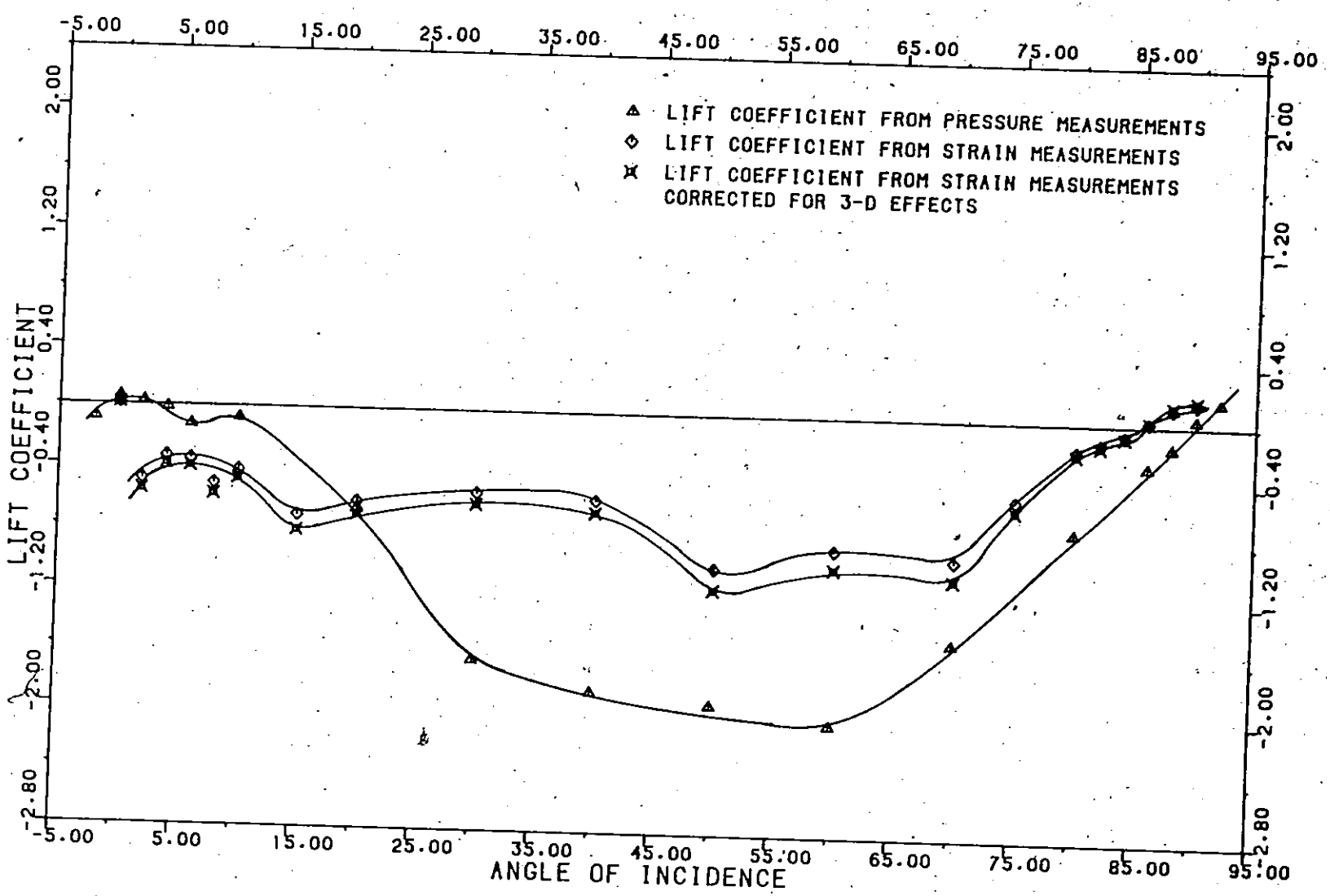

FIGURE 26 - LIFT COEFFICIENT FOR MODEL S36T2 BY STRAIN AND PRESSURE MEASUREMENTS

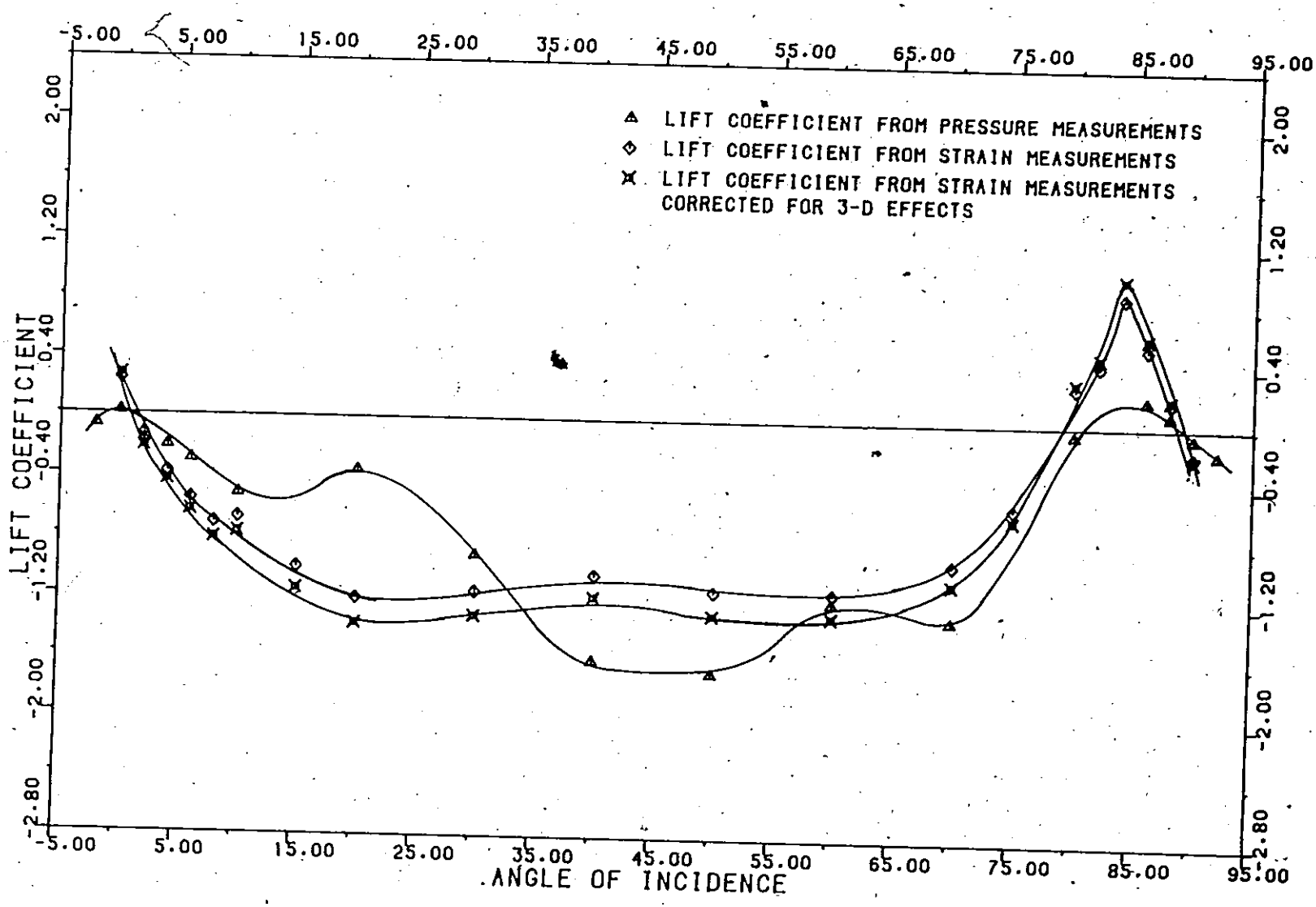

FIGURE 27 - LIFT COEFFICIENT FOR MODEL 36S BY STRAIN AND PRESSURE MEASUREMENTS

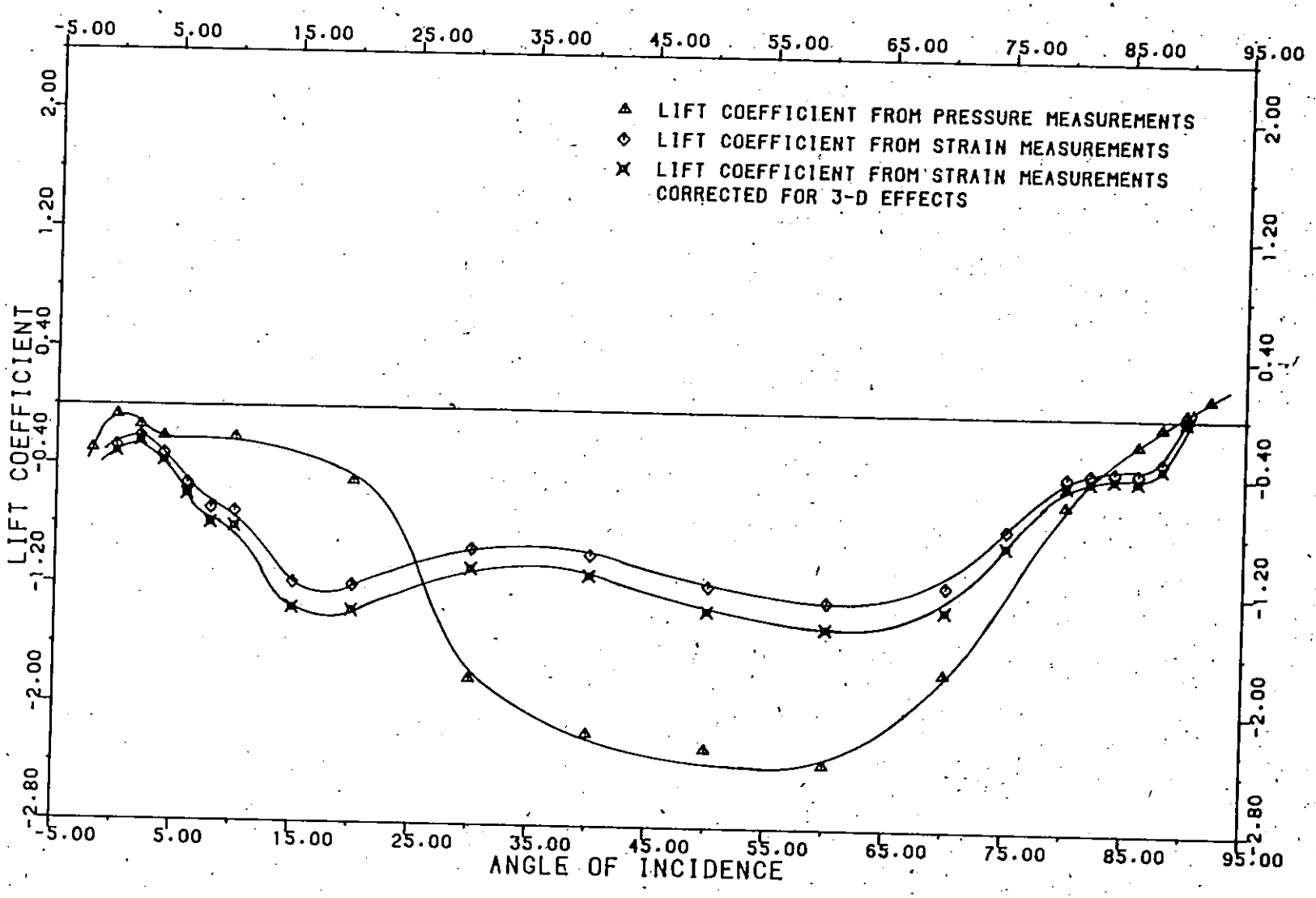

FIGURE 28 - LIFT COEFFICIENT FOR MODEL 36T2 BY STRAIN AND PRESSURE MEASUREMENTS

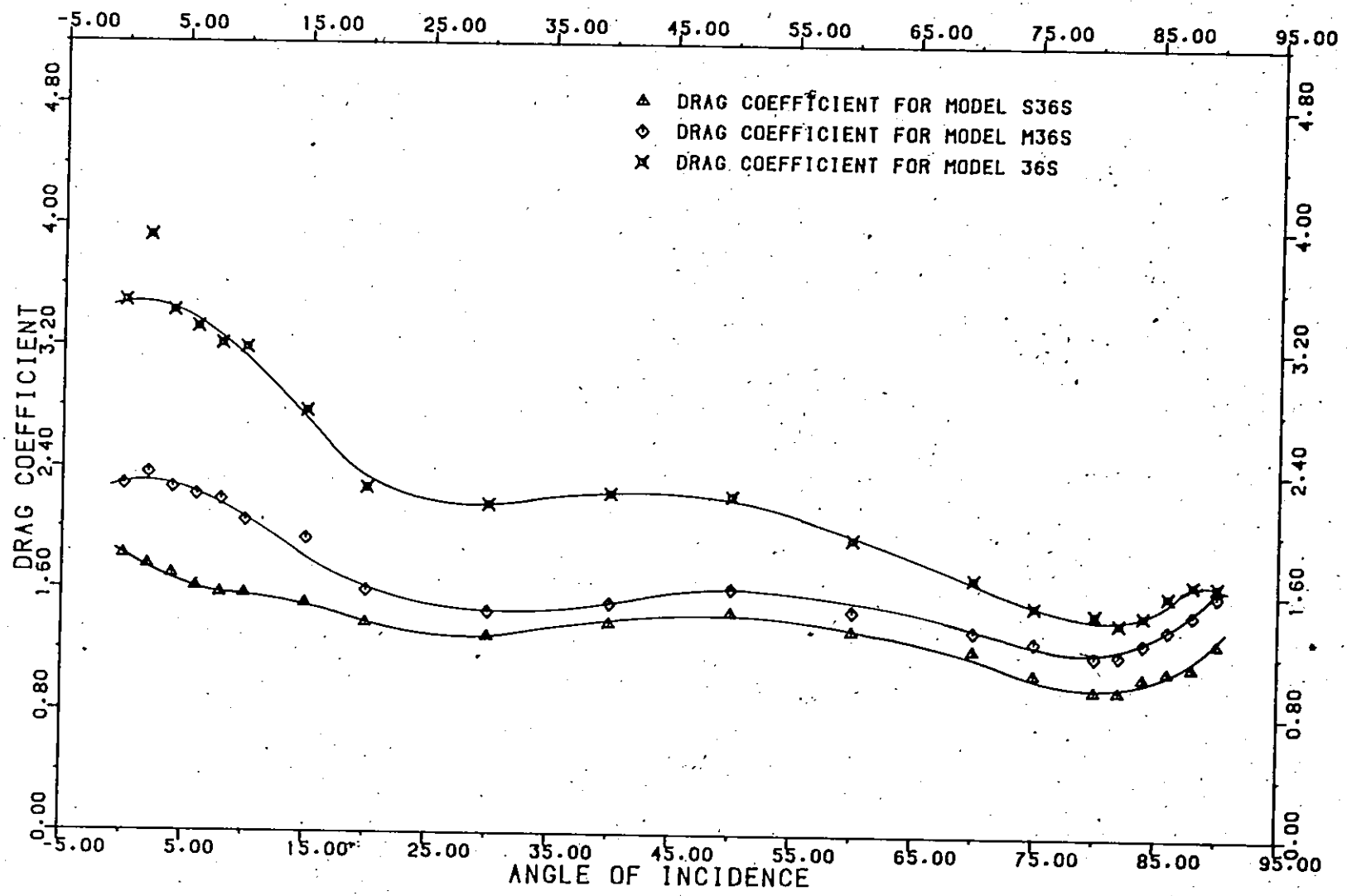

FIGURE 29 - DRAG COEFFICIENT FOR MODELS S36S, M36S AND 36S BY STRAIN MEASUREMENTS

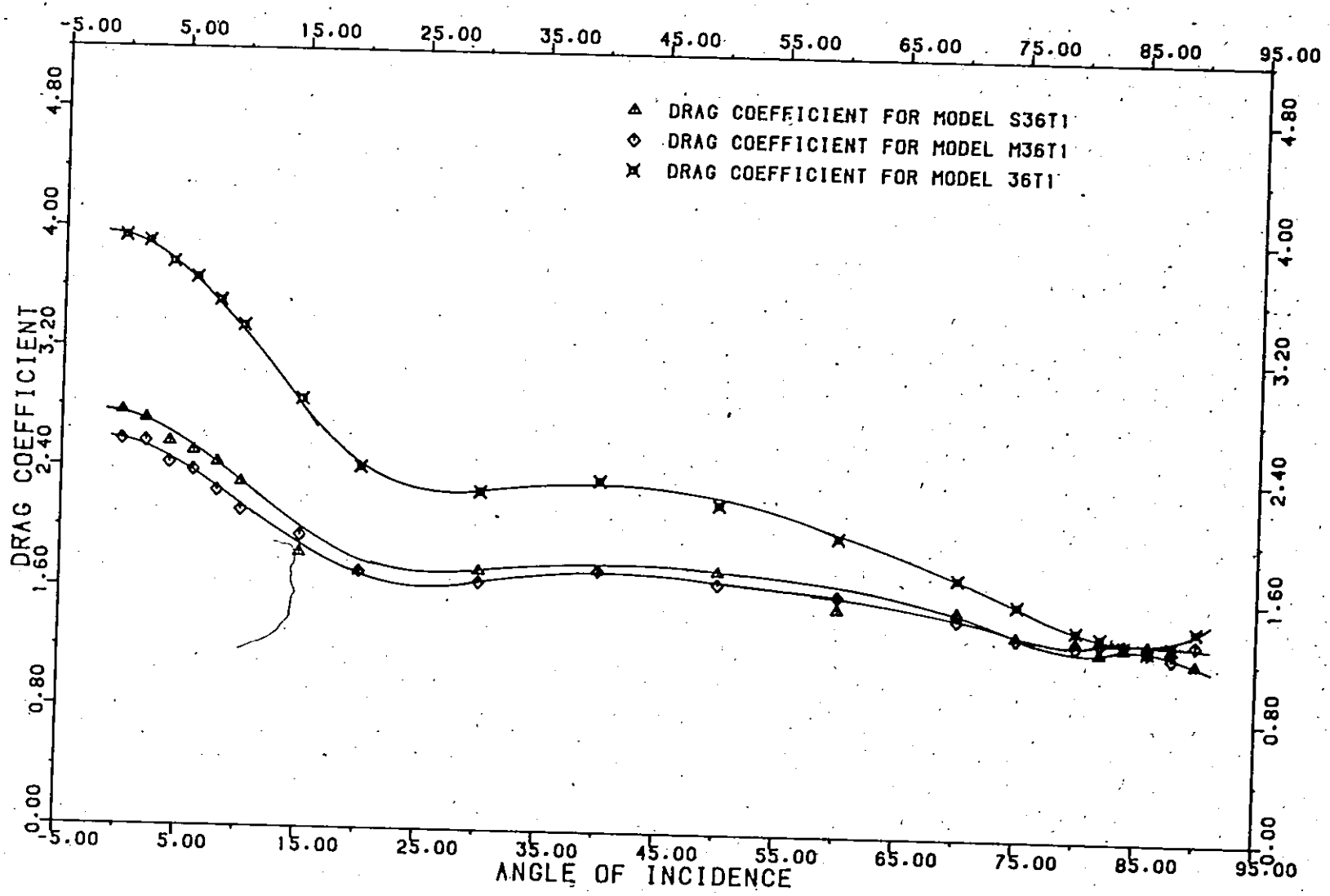

FIGURE 30 - DRAG COEFFICIENT FOR MODELS S36T1, M36T1 AND 36T1 BY STRAIN MEASUREMENTS

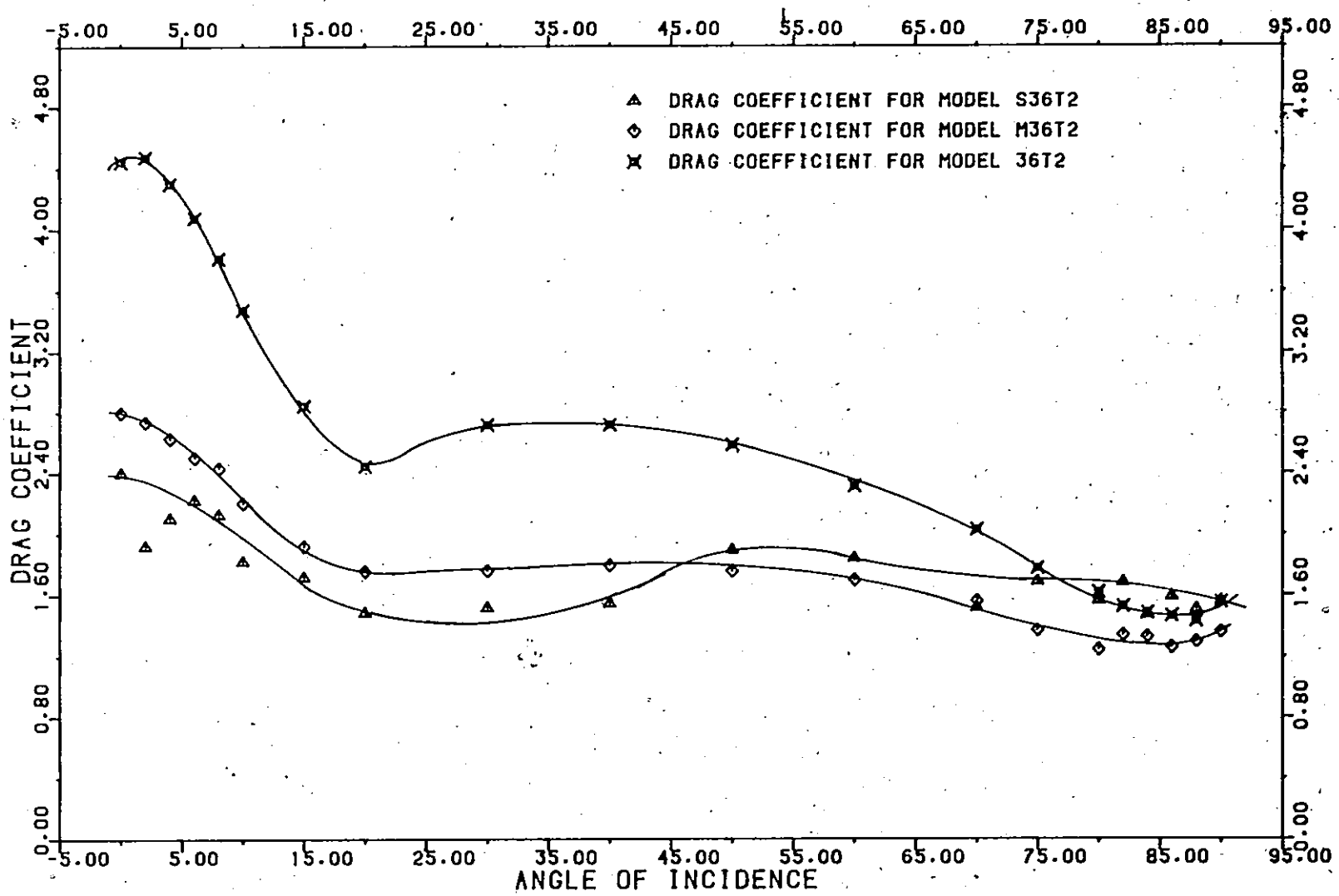

FIGURE 31 - DRAG COEFFICIENT FOR MODELS S36T2, M36T2 AND 36T2 BY STRAIN MEASUREMENTS

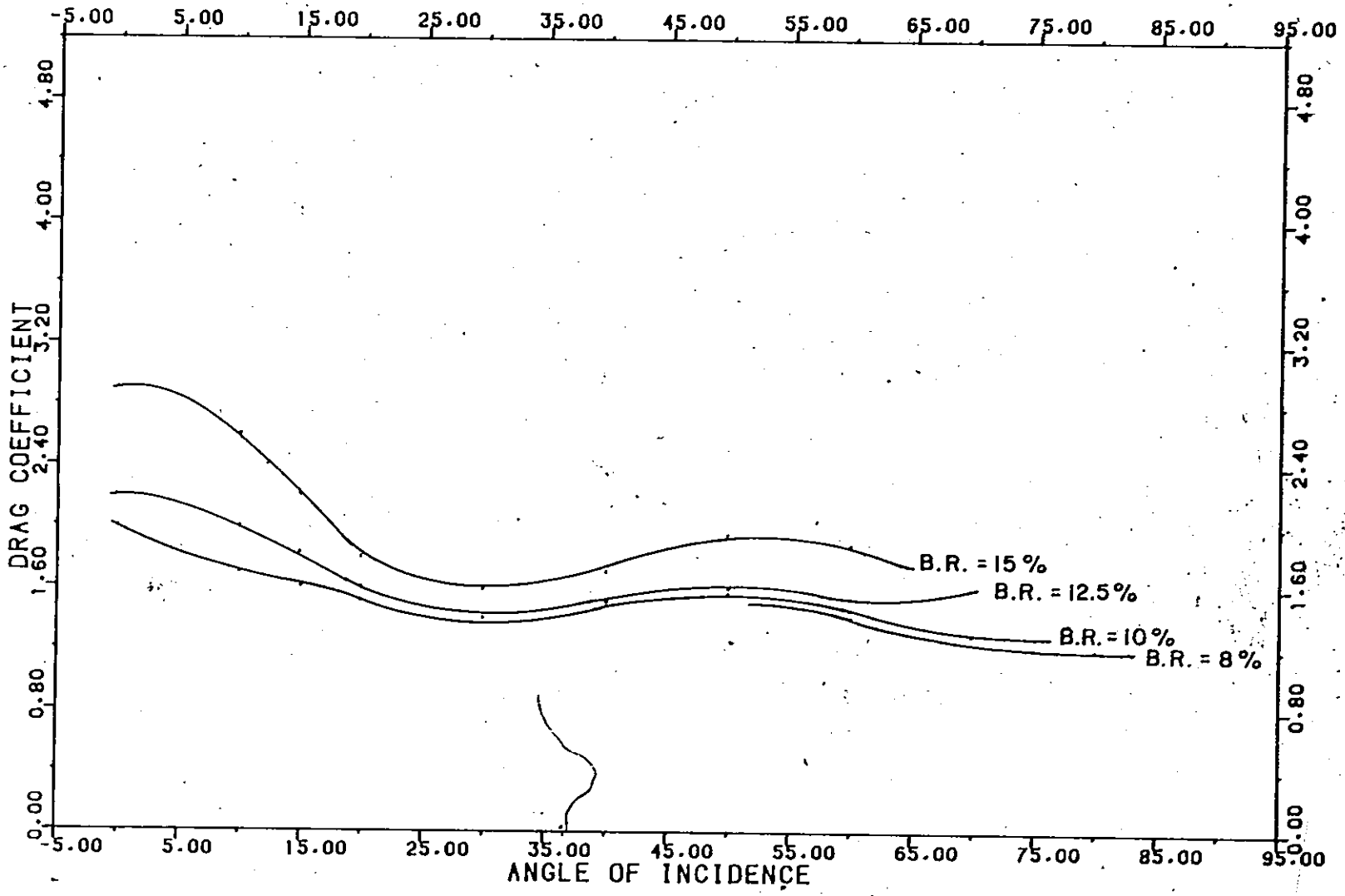

FIGURE 32 - DRAG COEFFICIENT AS A FUNCTION OF BLOCKAGE RATIO VERSUS ANGLE OF INCIDENCE FOR SMOOTH FLOW

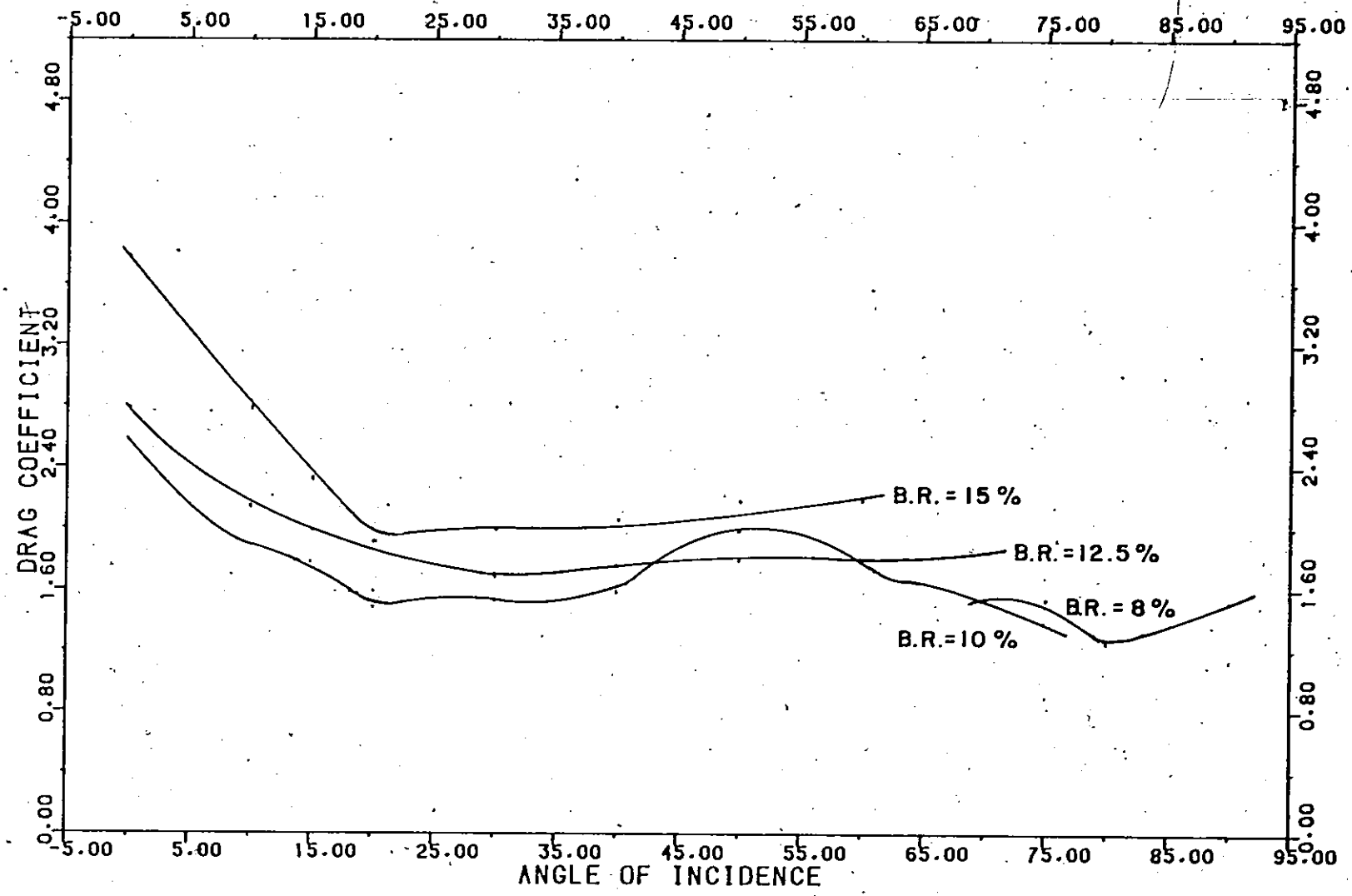

FIGURE 33 - DRAG COEFFICIENT AS A FUNCTION OF BLOCKAGE RATIO VERSUS ANGLE OF INCIDENCE FOR TURBULENT FLOW (GRID 2)

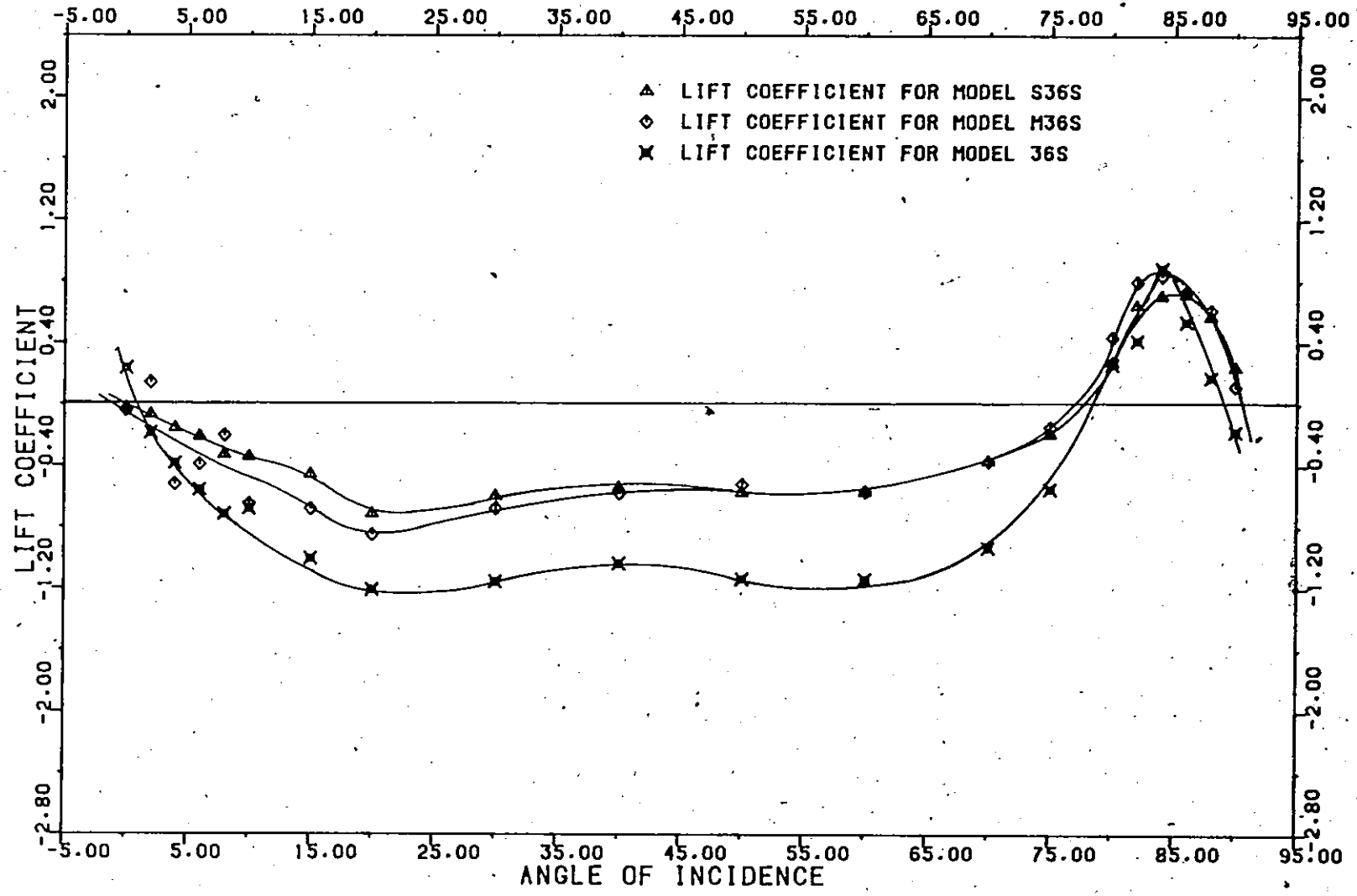

FIGURE 34 - LIFT COEFFICIENT FOR MODELS S36S, M36S AND 36S BY STRAIN MEASUREMENTS

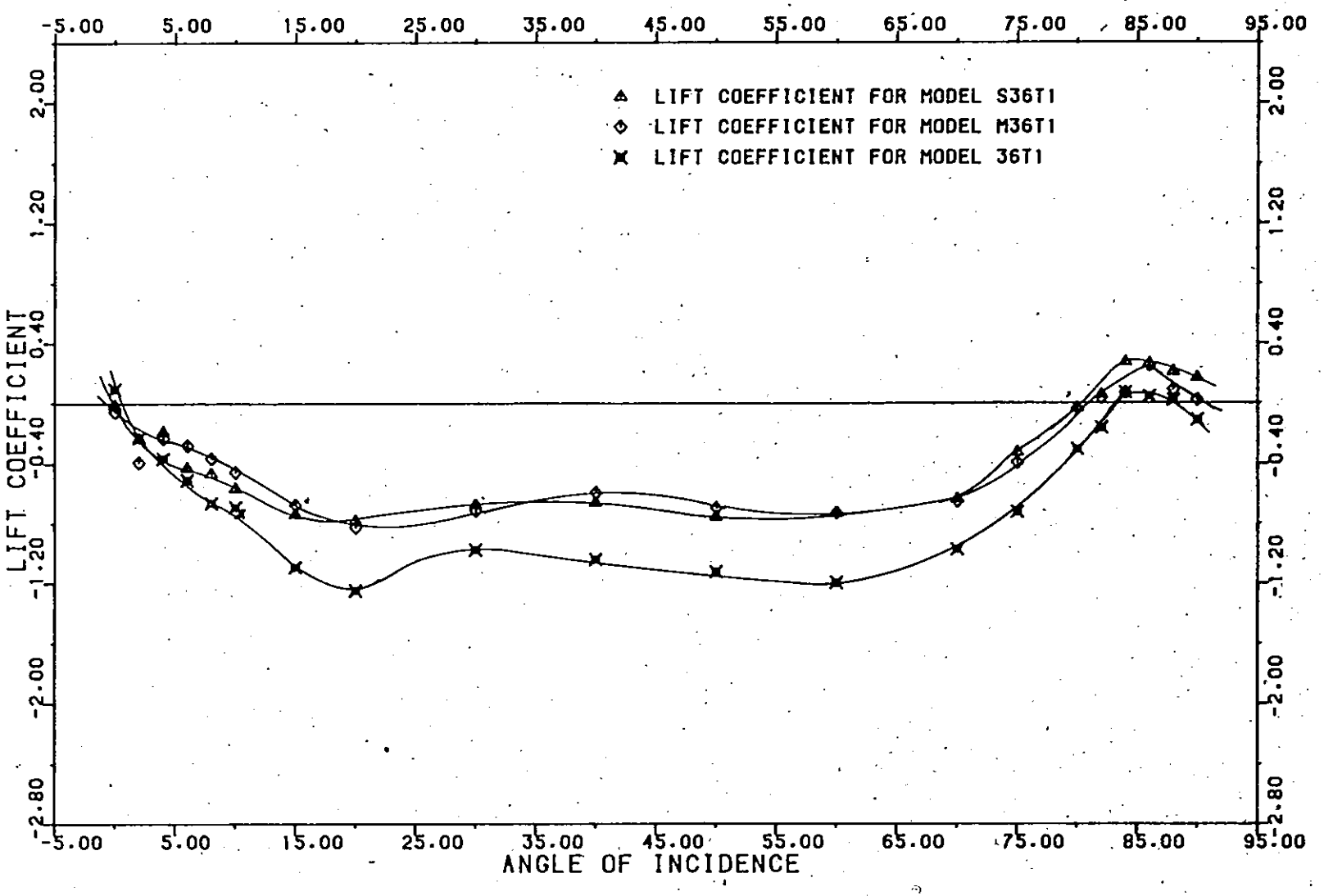

FIGURE 35 - LIFT COEFFICIENT FOR MODELS S36T1, M36T1 AND 36T1 BY STRAIN MEASUREMENTS

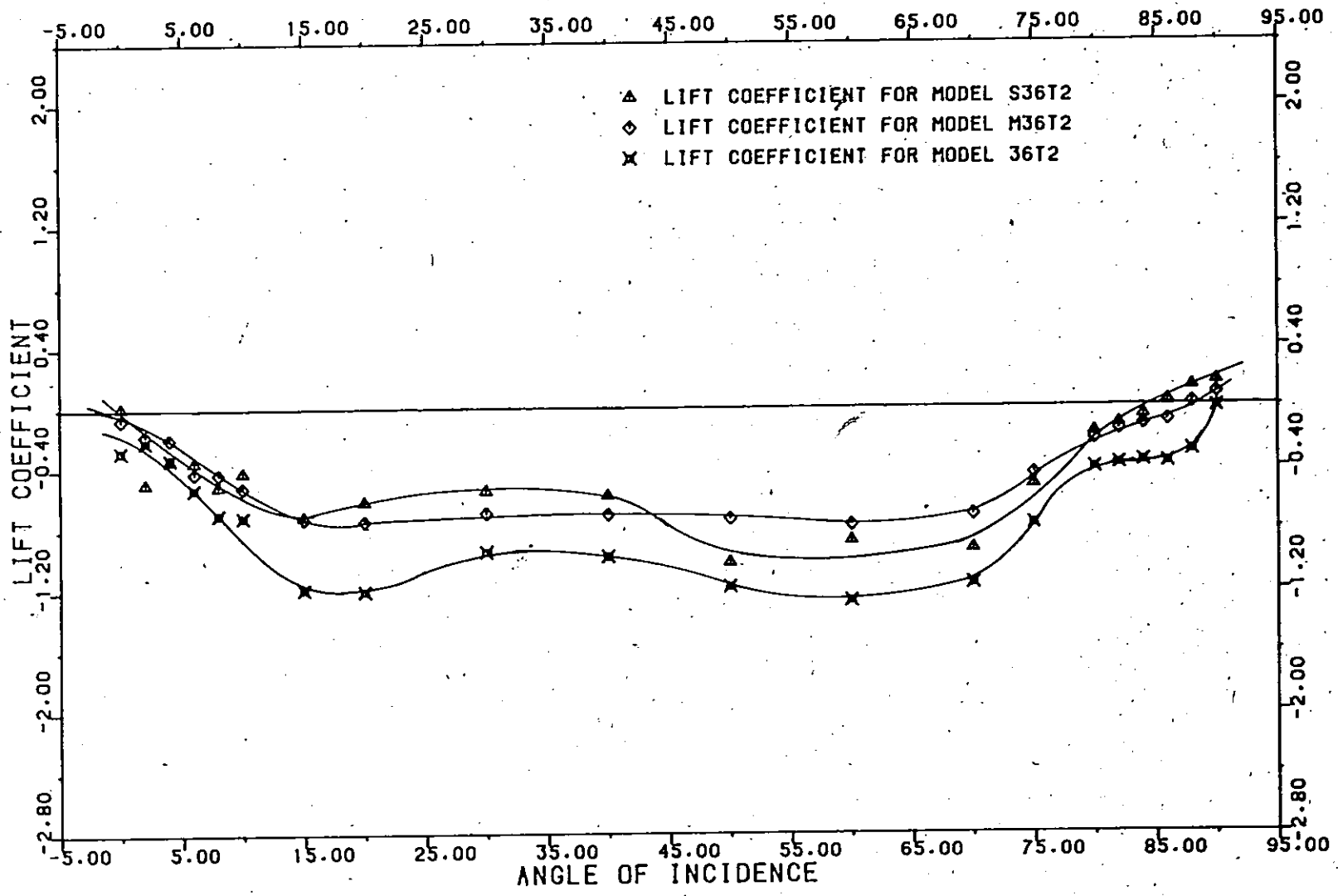

FIGURE 36 - LIFT COEFFICIENT FOR MODELS S36T2, M36T2 AND 36T2 BY STRAIN MEASUREMENTS

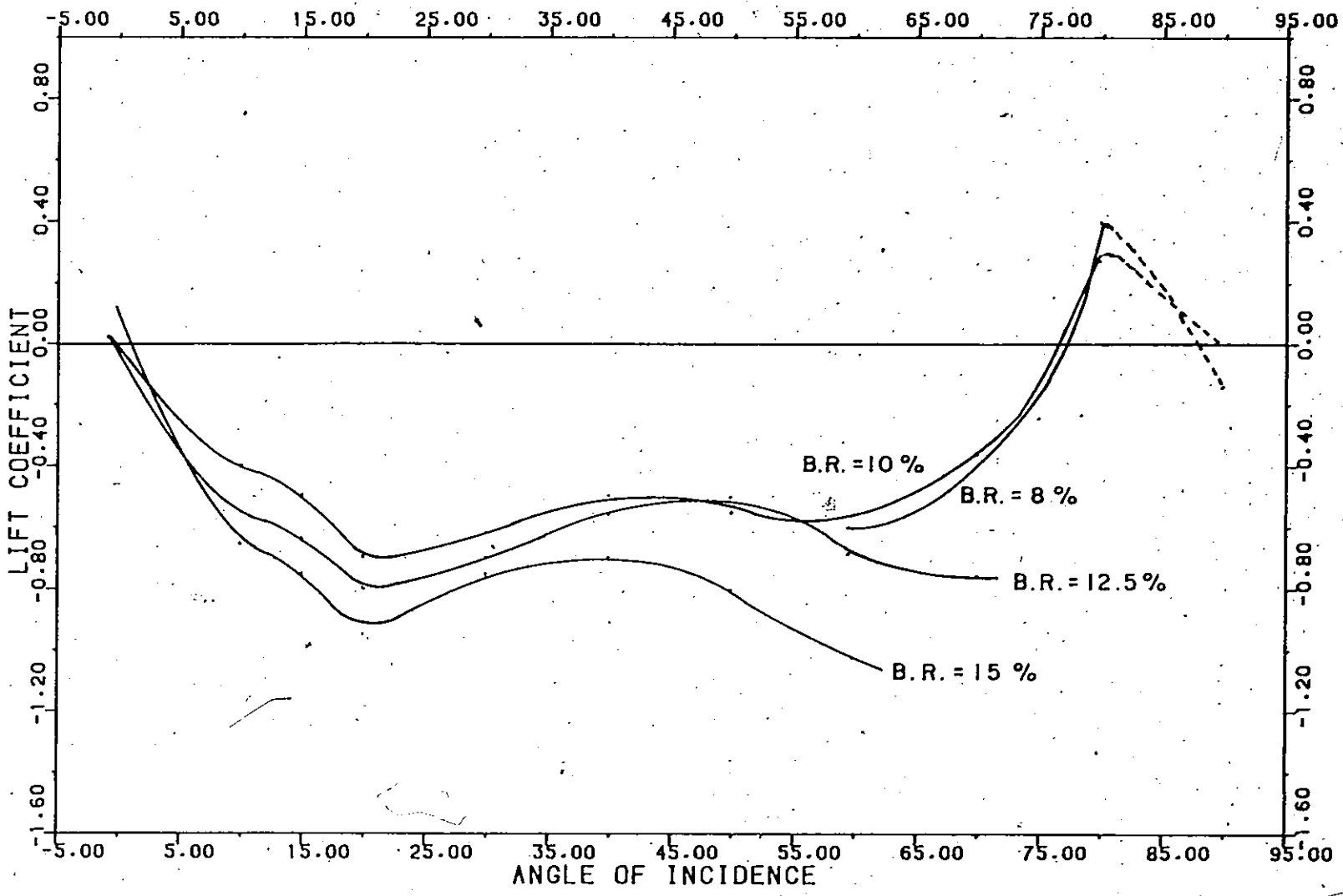

FIGURE 37- LIFT COEFFICIENT AS A FUNCTION OF BLOCKAGE RATIO VERSUS ANGLE OF INCIDENCE FOR SMOOTH FLOW

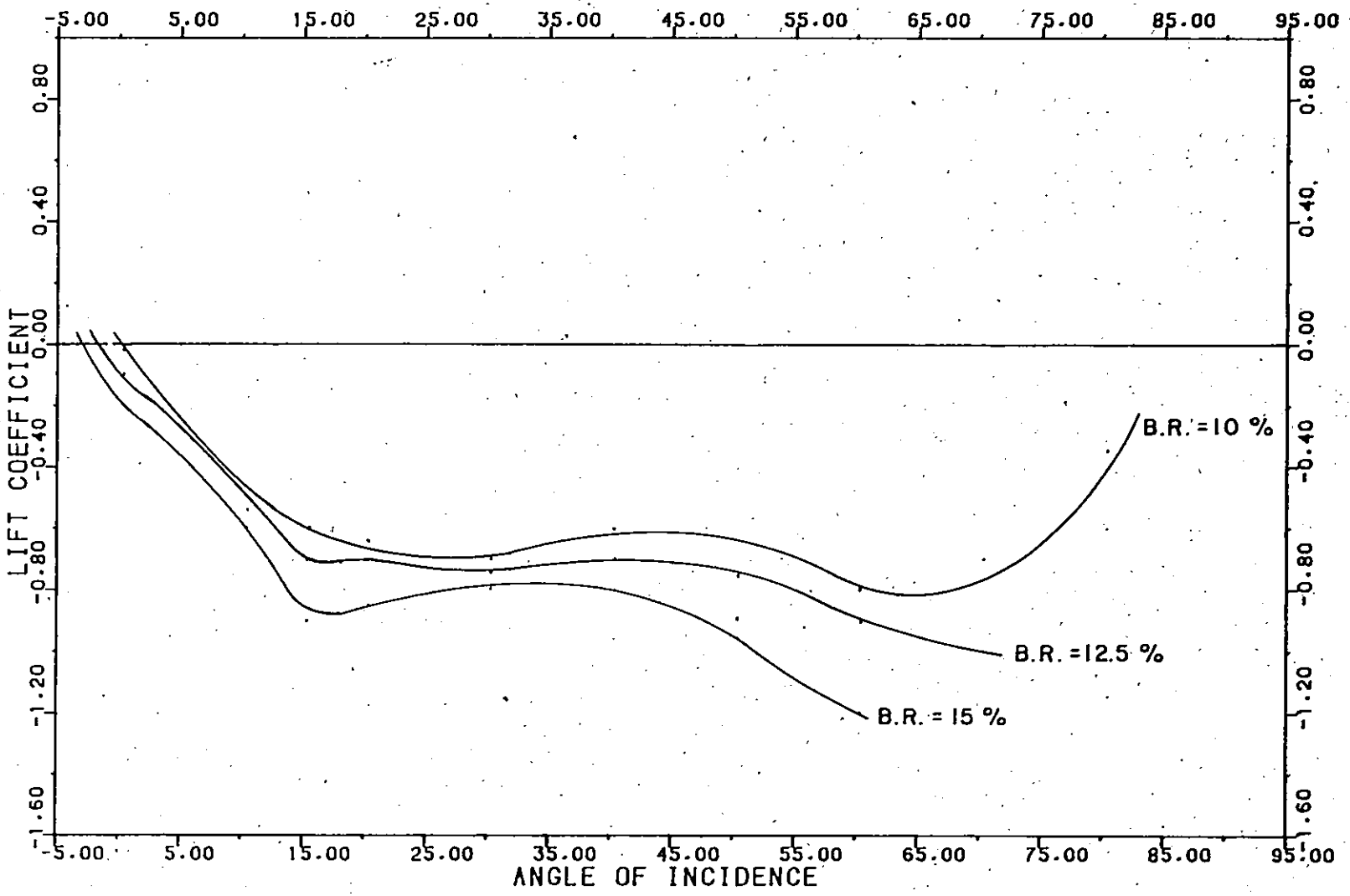

FIGURE 38 - LIFT COEFFICIENT AS A FUNCTION OF BLOCKAGE RATIO VERSUS ANGLE OF INCIDENCE FOR TURBULENT FLOW (GRID 2)

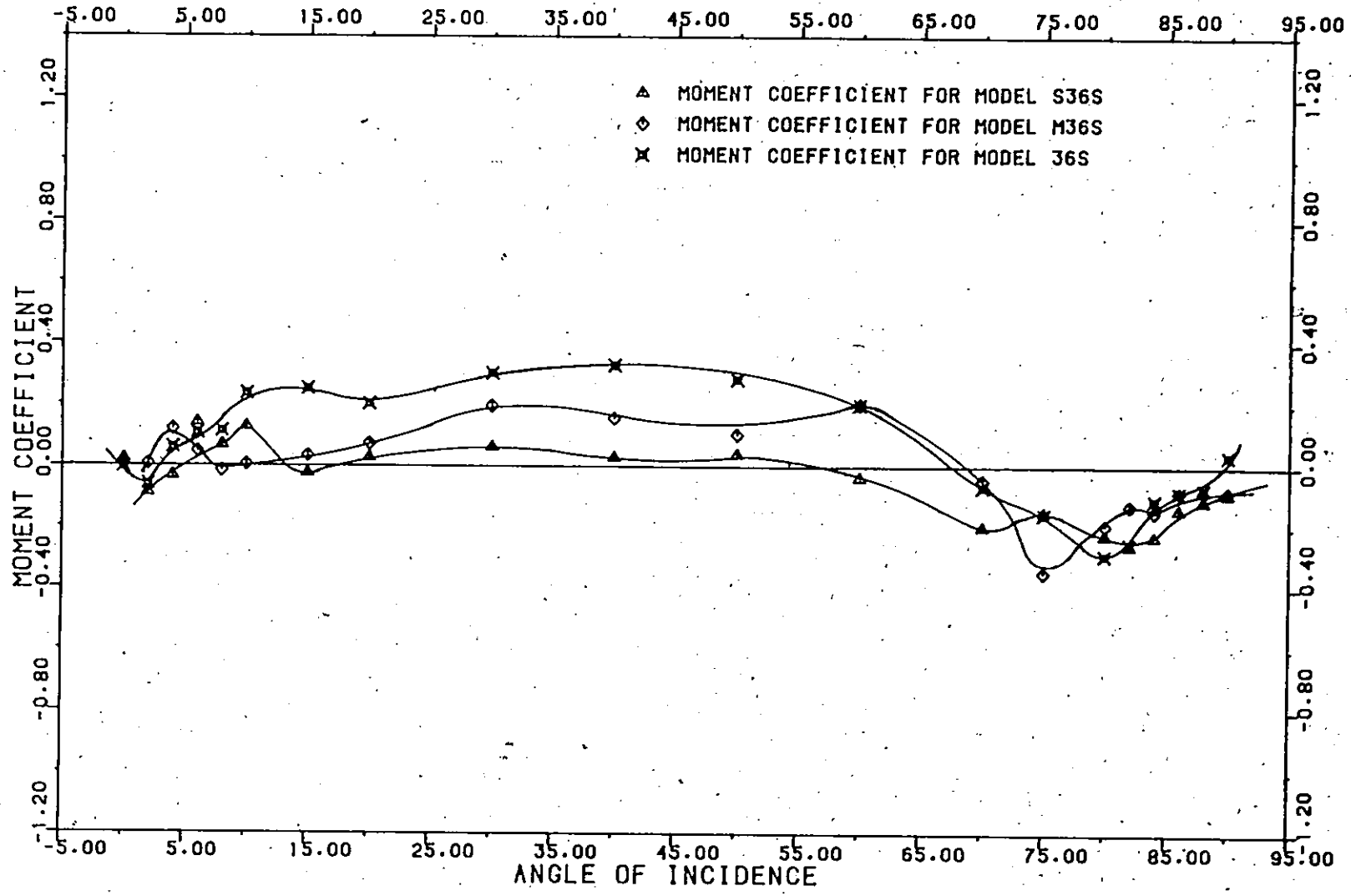

FIGURE 39 - MOMENT COEFFICIENT FOR MODELS S36S, M36S AND 36S BY STRAIN MEASUREMENTS

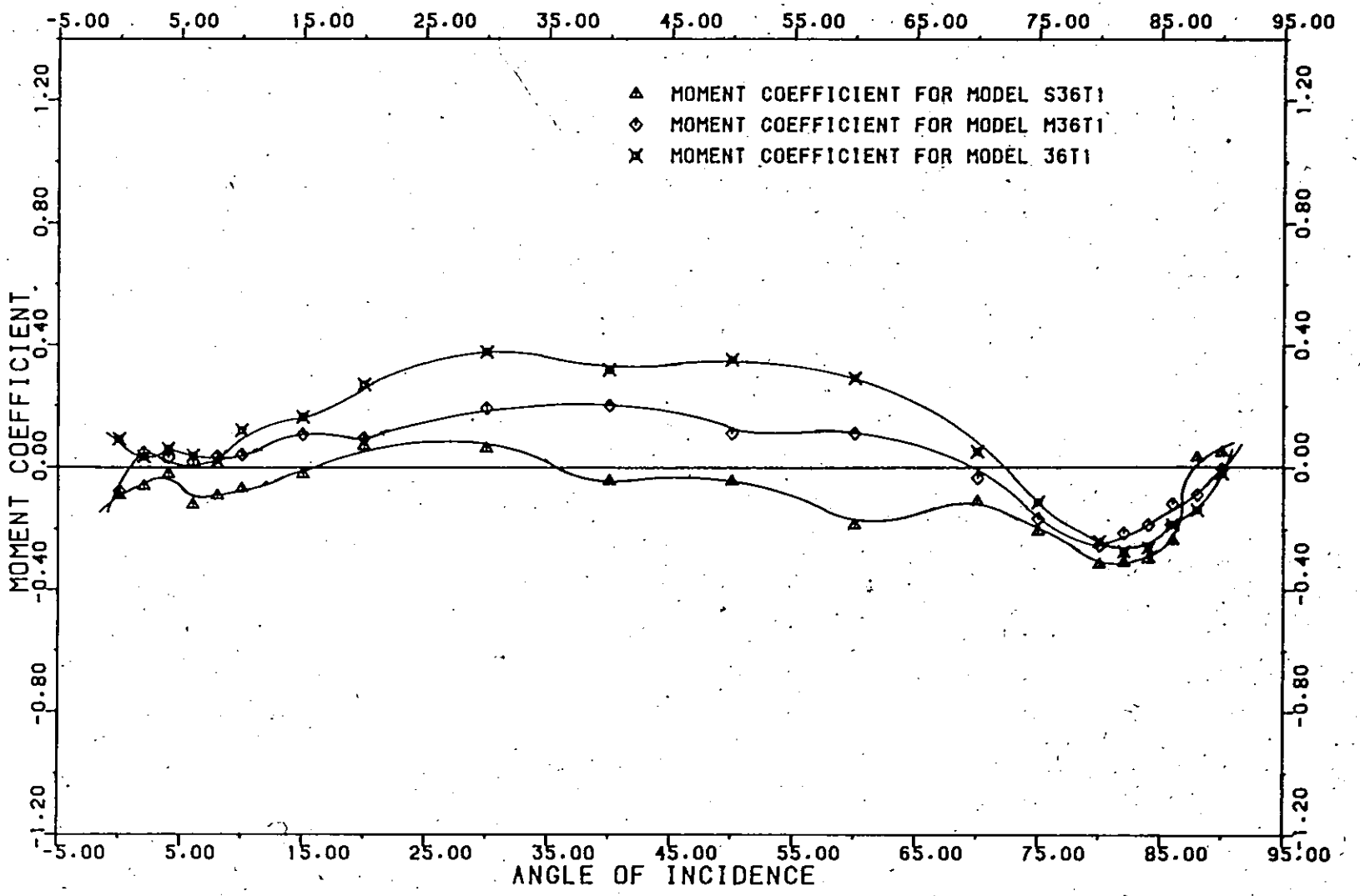

FIGURE 40 - MOMENT COEFFICIENT FOR MODELS S36T1, M36T1 AND 36T1 BY STRAIN MEASUREMENTS

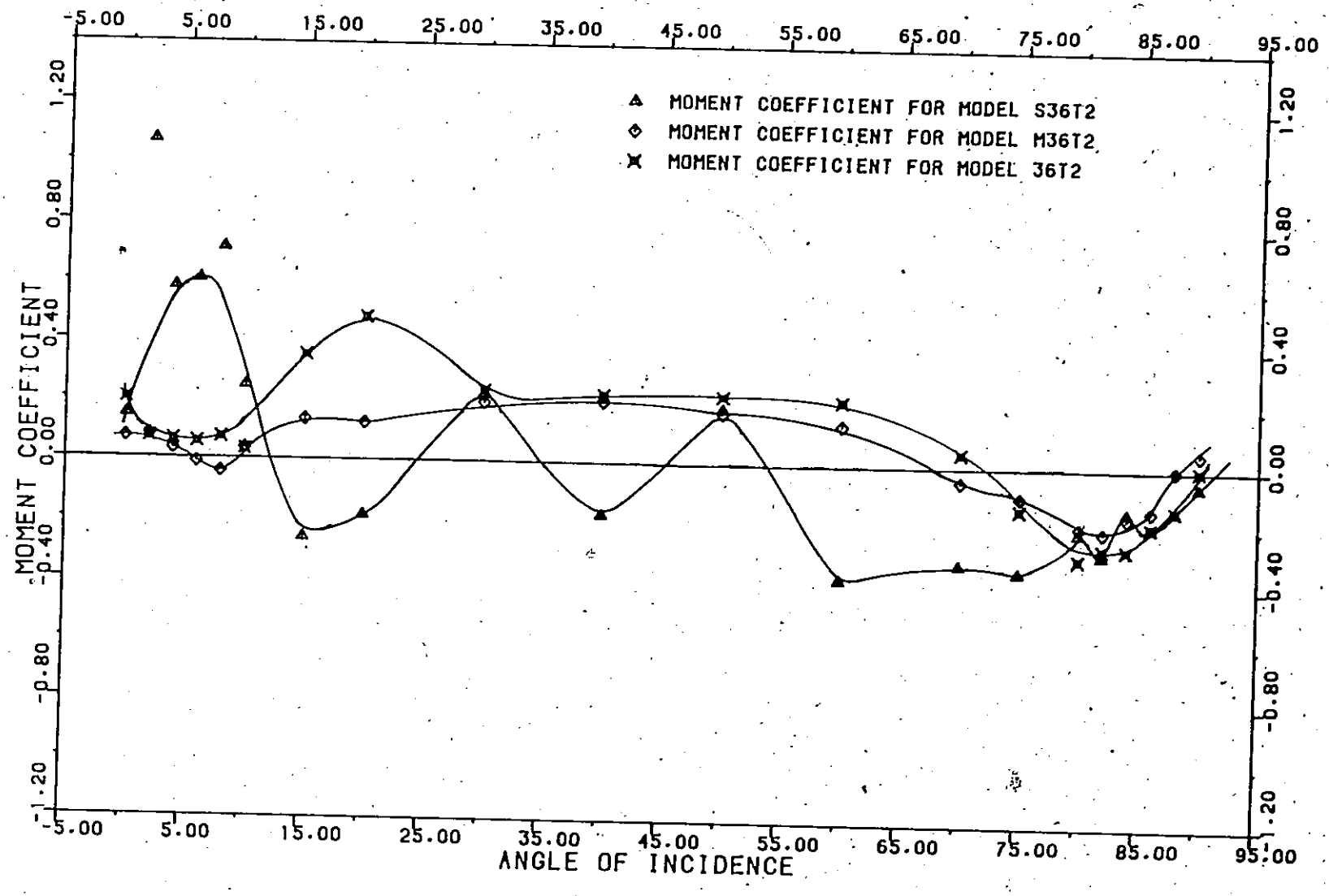

FIGURE 41 - MOMENT COEFFICIENT FOR MODELS S36T2, M36T2 AND 36T2 BY STRAIN MEASUREMENTS

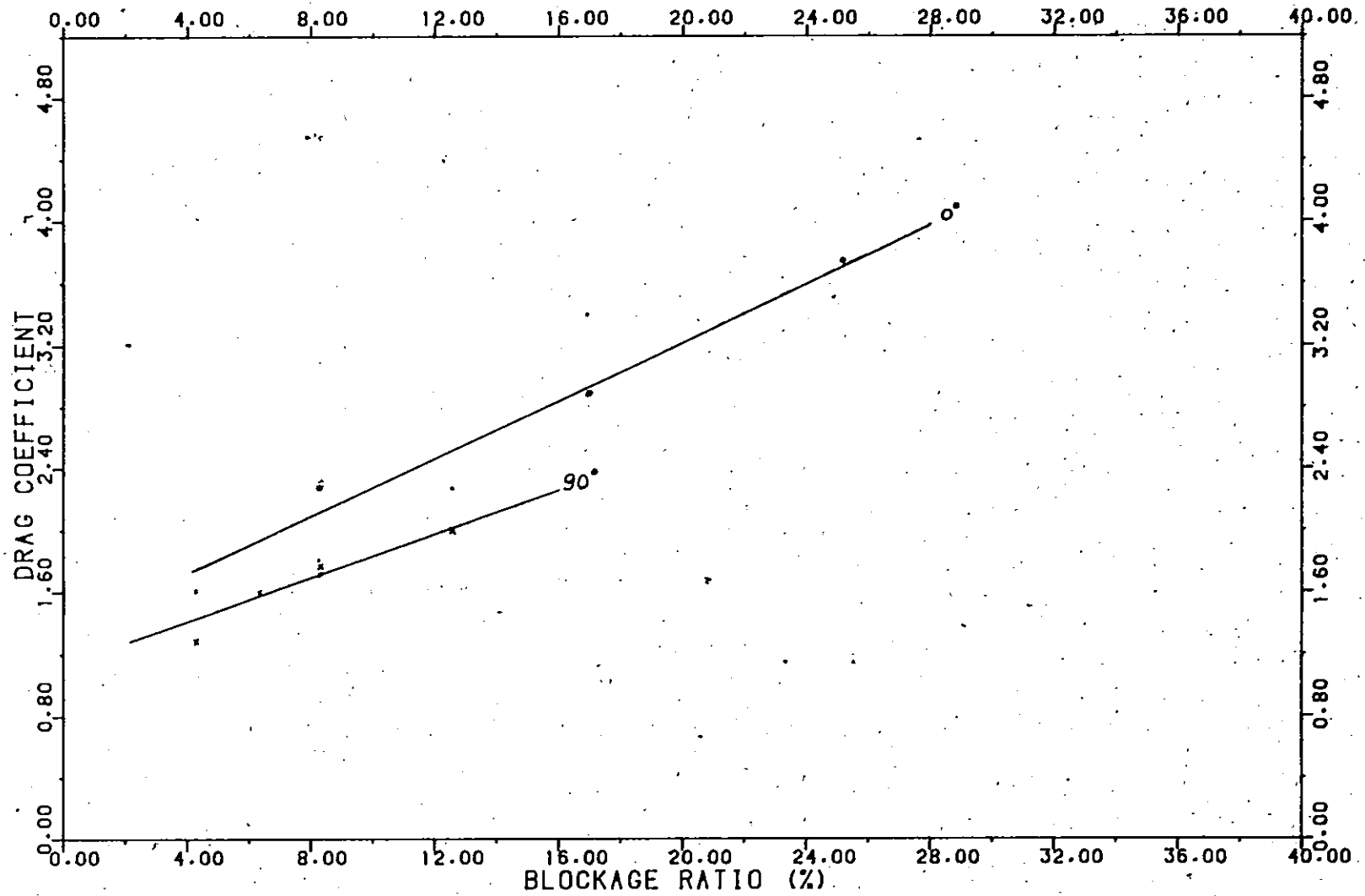

FIGURE 42 - DRAG COEFFICIENT VERSUS BLOCKAGE RATIO FOR SMOOTH FLOW

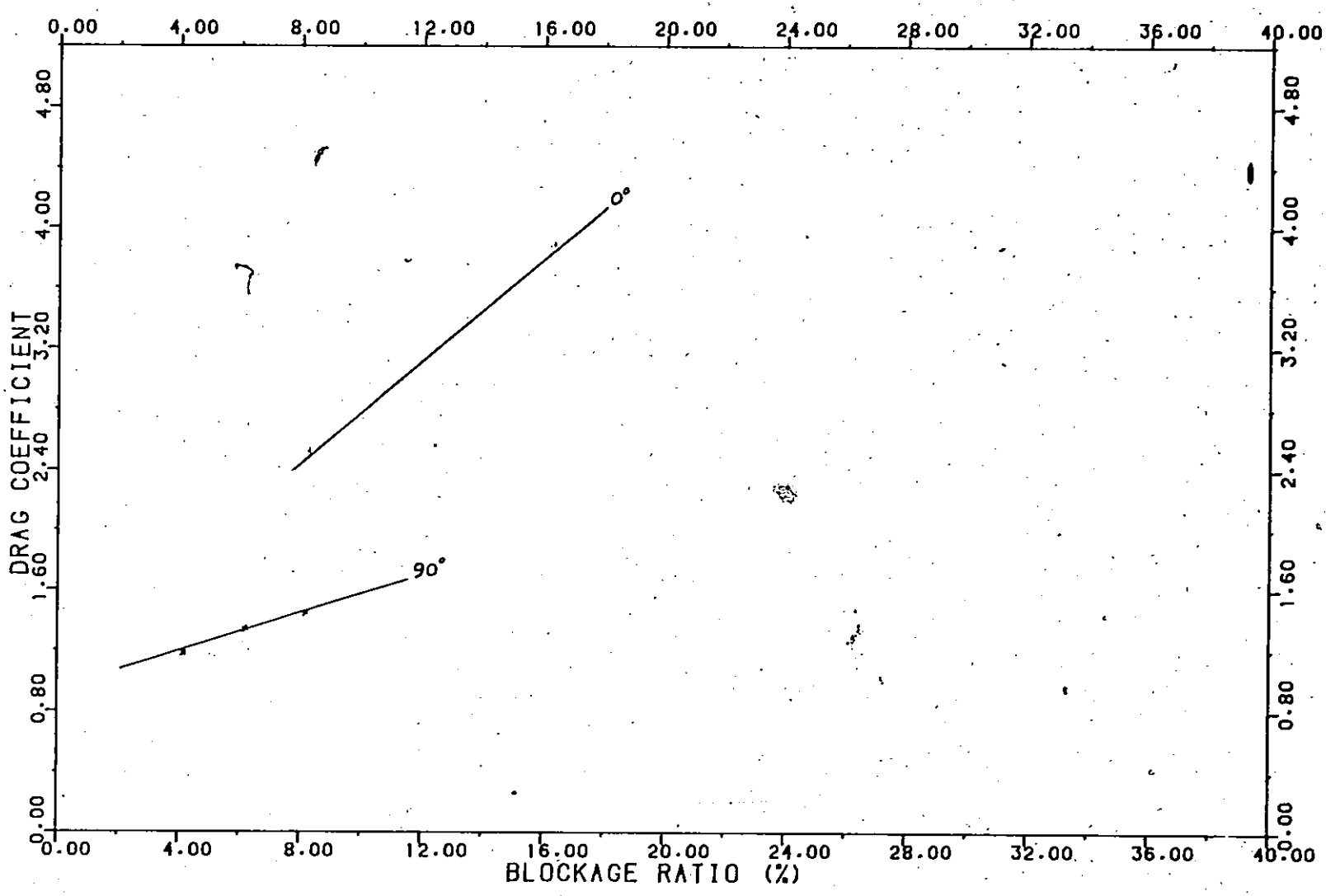

FIGURE 43 - DRAG COEFFICIENT VERSUS BLOCKAGE RATIO FOR TURBULENT FLOW (GRID 1)

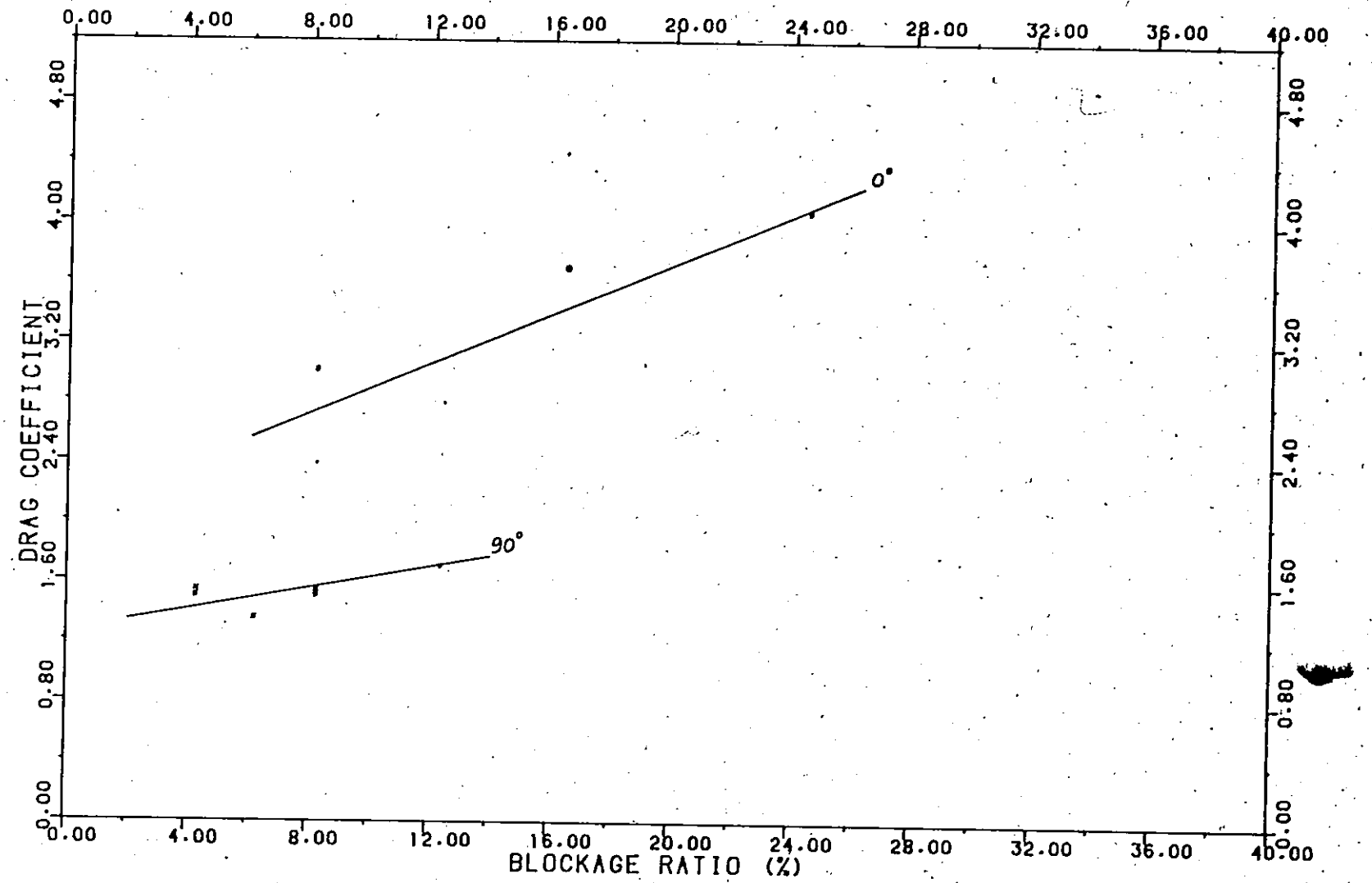

FIGURE 44 - DRAG COEFFICIENT VERSUS BLOCKAGE RATIO FOR TURBULENT FLOW (GRID 2)

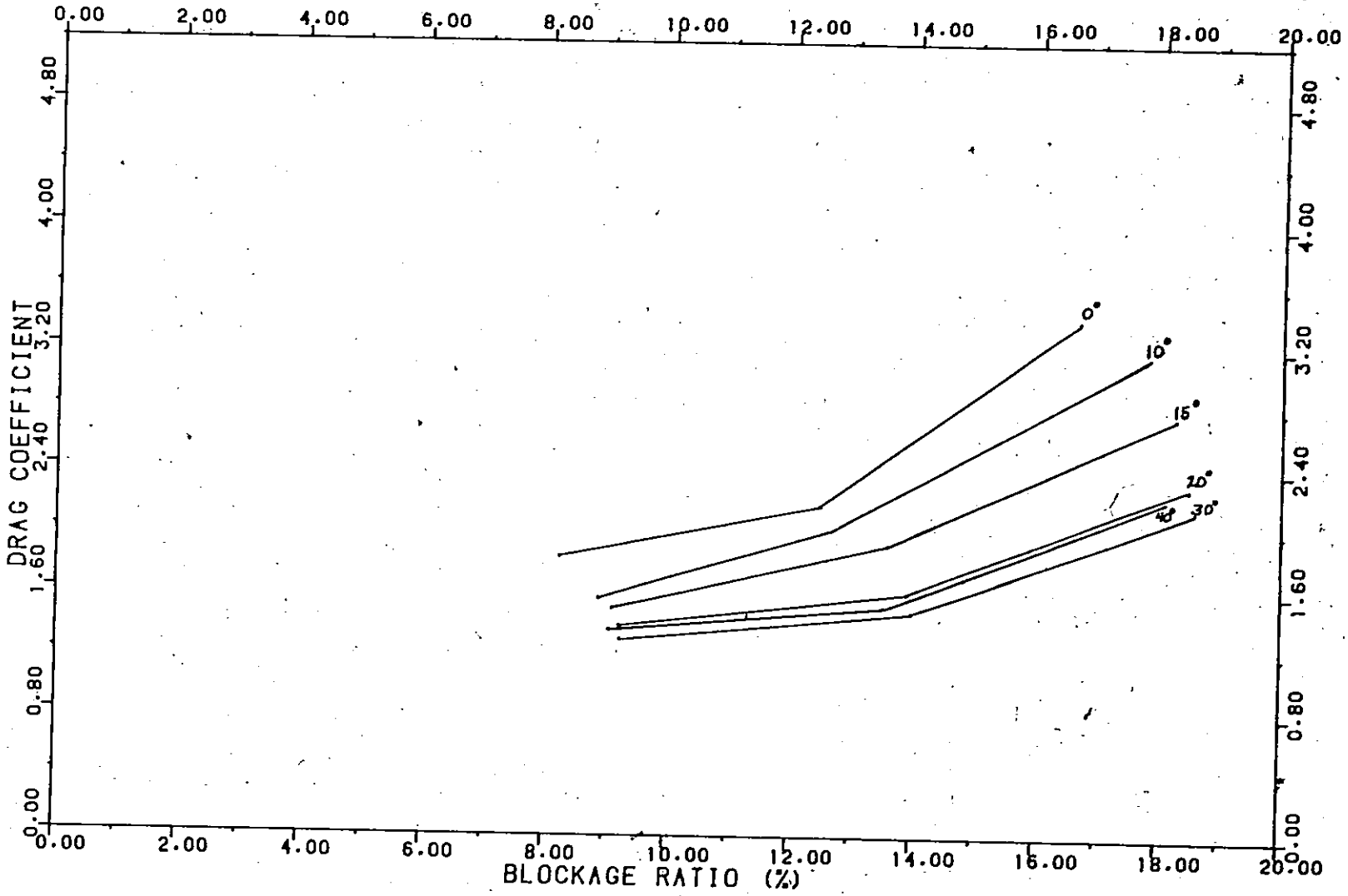

FIGURE 45 - DRAG COEFFICIENT VERSUS BLOCKAGE RATIO FOR SMOOTH FLOW

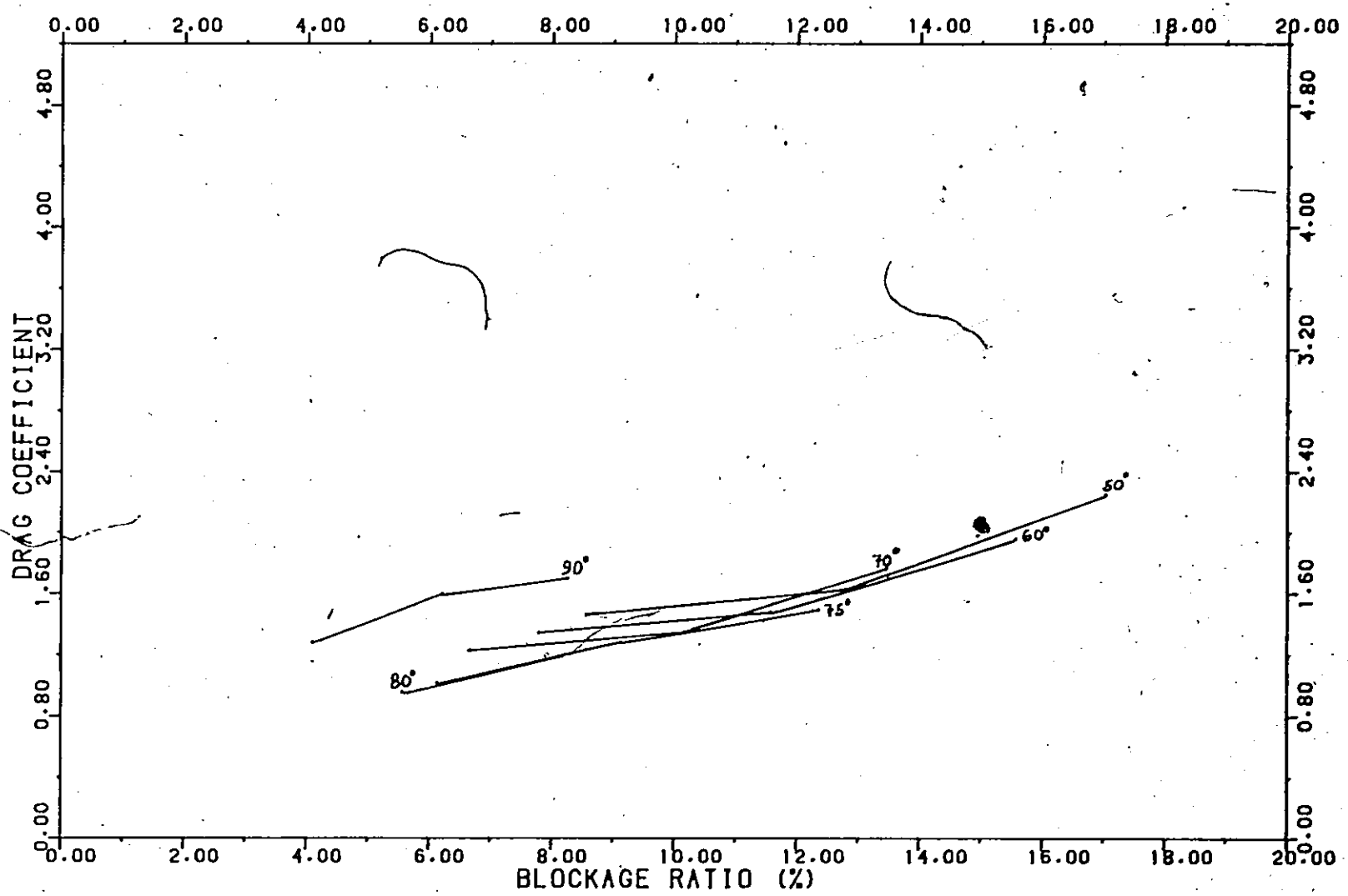

FIGURE 46 - DRAG COEFFICIENT VERSUS BLOCKAGE RATIO FOR SMOOTH FLOW

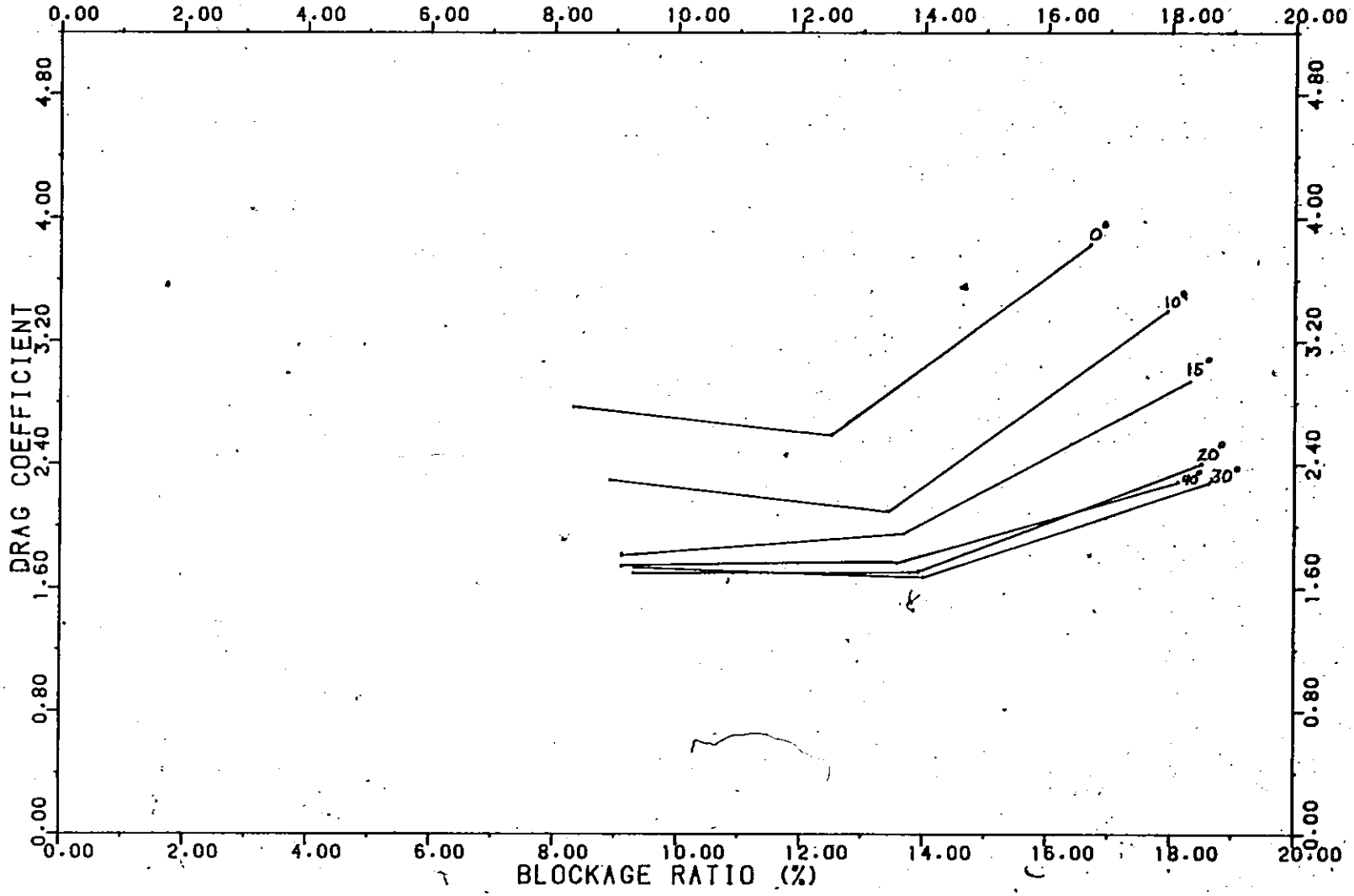

FIGURE 47 - DRAG COEFFICIENT VERSUS BLOCKAGE RATIO FOR TURBULENT FLOW (GRID 1)

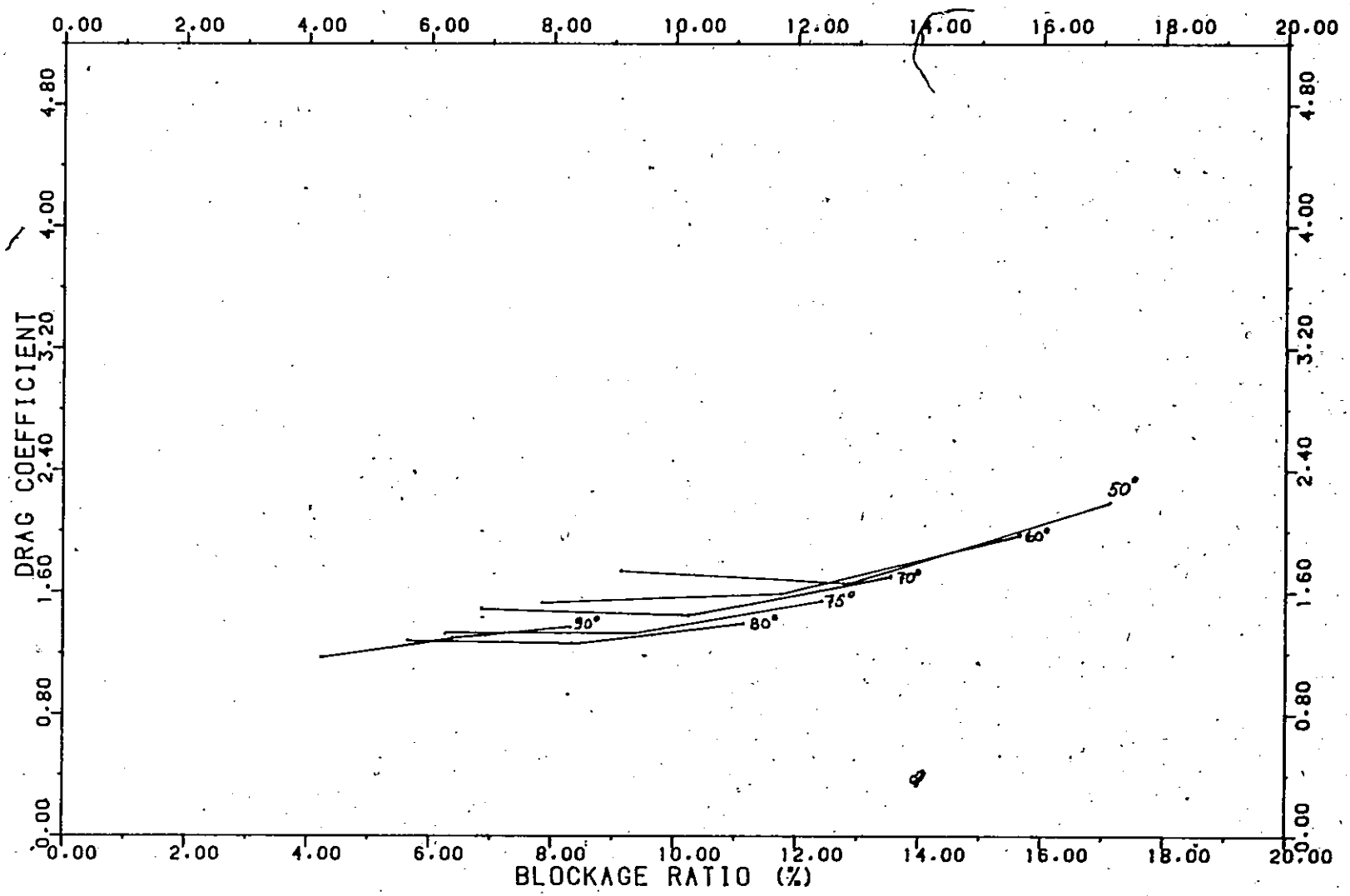

FIGURE 48 - DRAG COEFFICIENT VERSUS BLOCKAGE RATIO FOR TURBULENT FLOW (GRID 1)

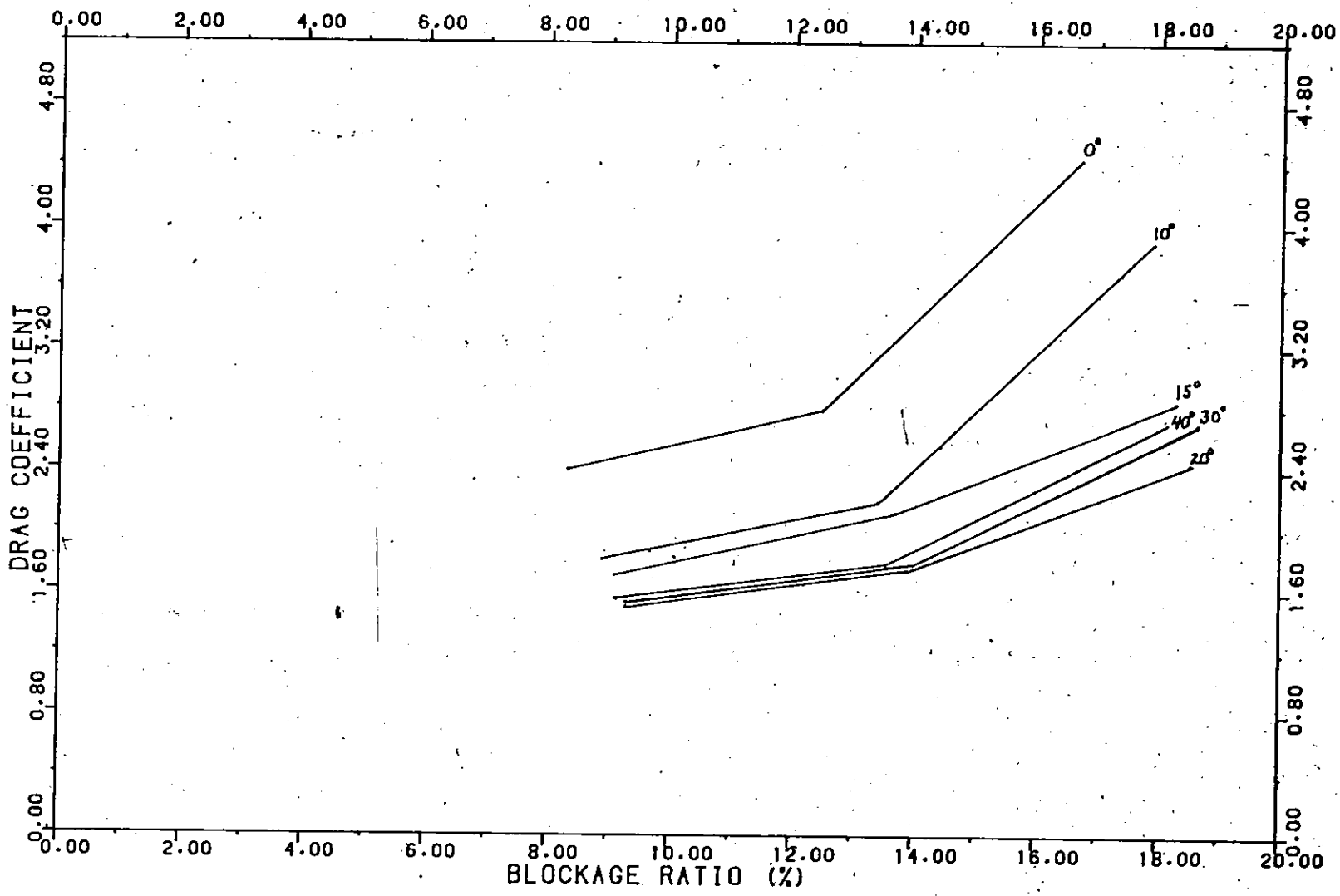

FIGURE 49 - DRAG COEFFICIENT VERSUS BLOCKAGE RATIO FOR TURBULENT FLOW (GRID 2)

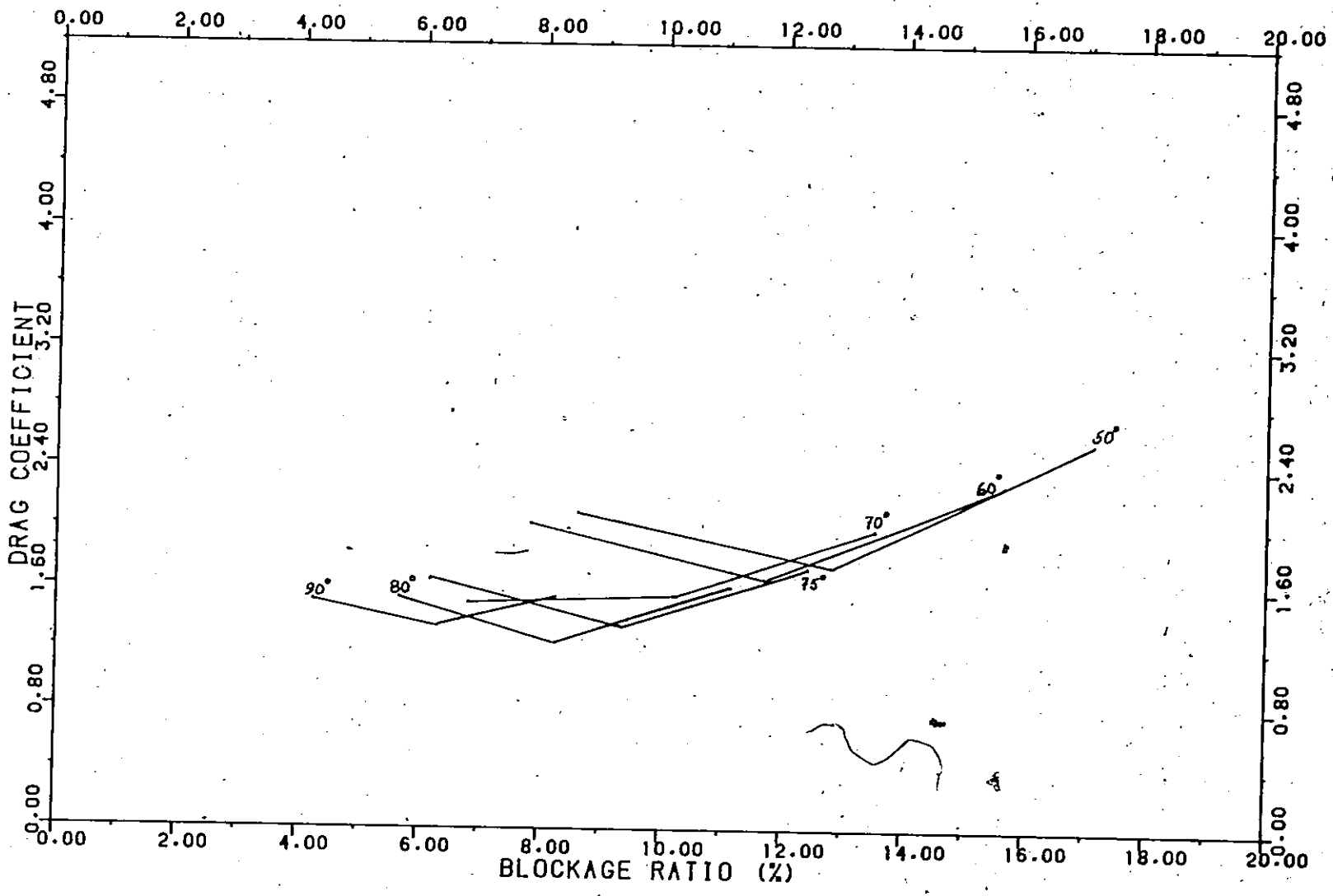

FIGURE 50- DRAG COEFFICIENT VERSUS BLOCKAGE RATIO FOR TURBULENT FLOW (GRID 2)

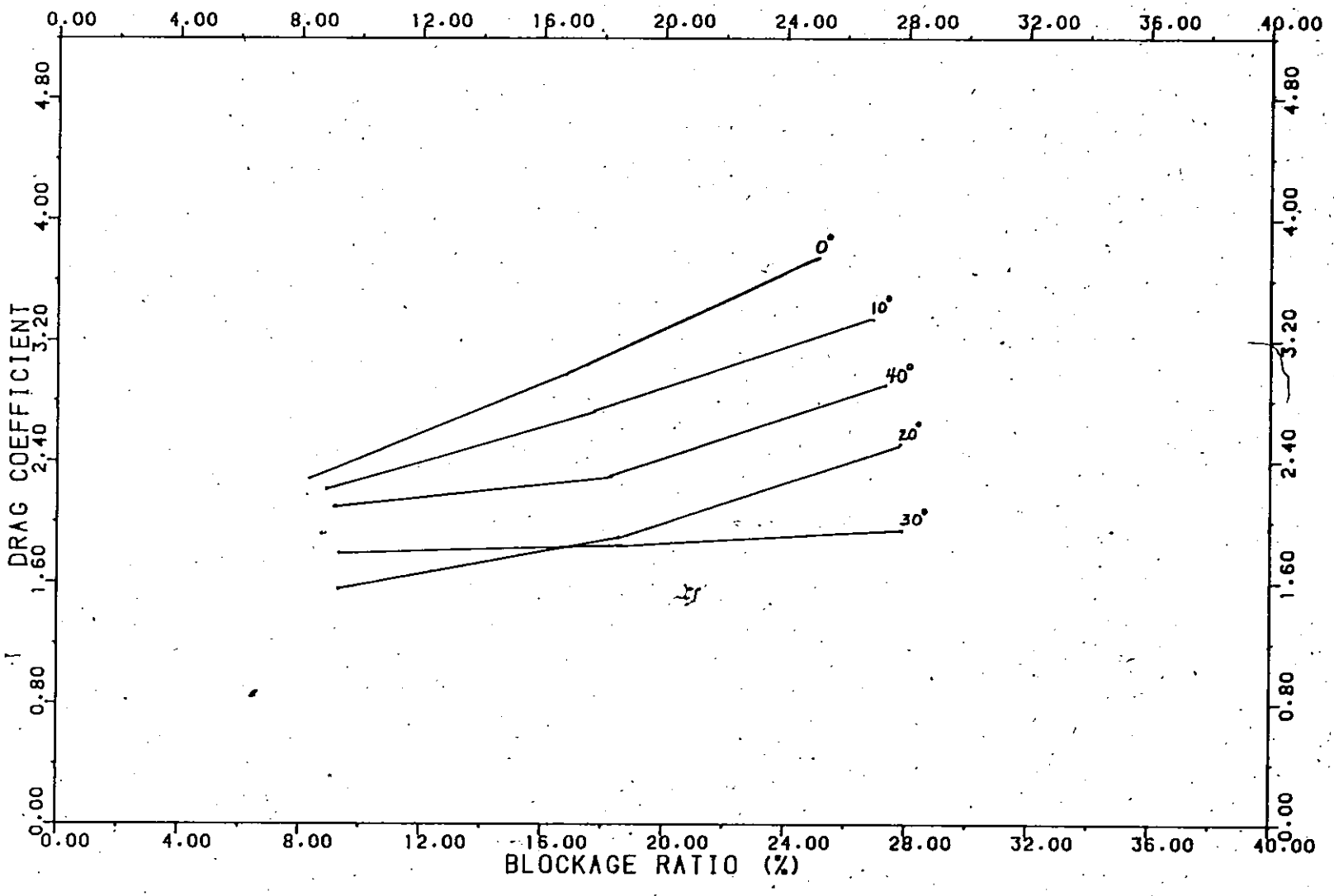

FIGURE 51 - DRAG COEFFICIENT VERSUS BLOCKAGE RATIO FOR SMOOTH FLOW BY PRESSURE MEASUREMENTS

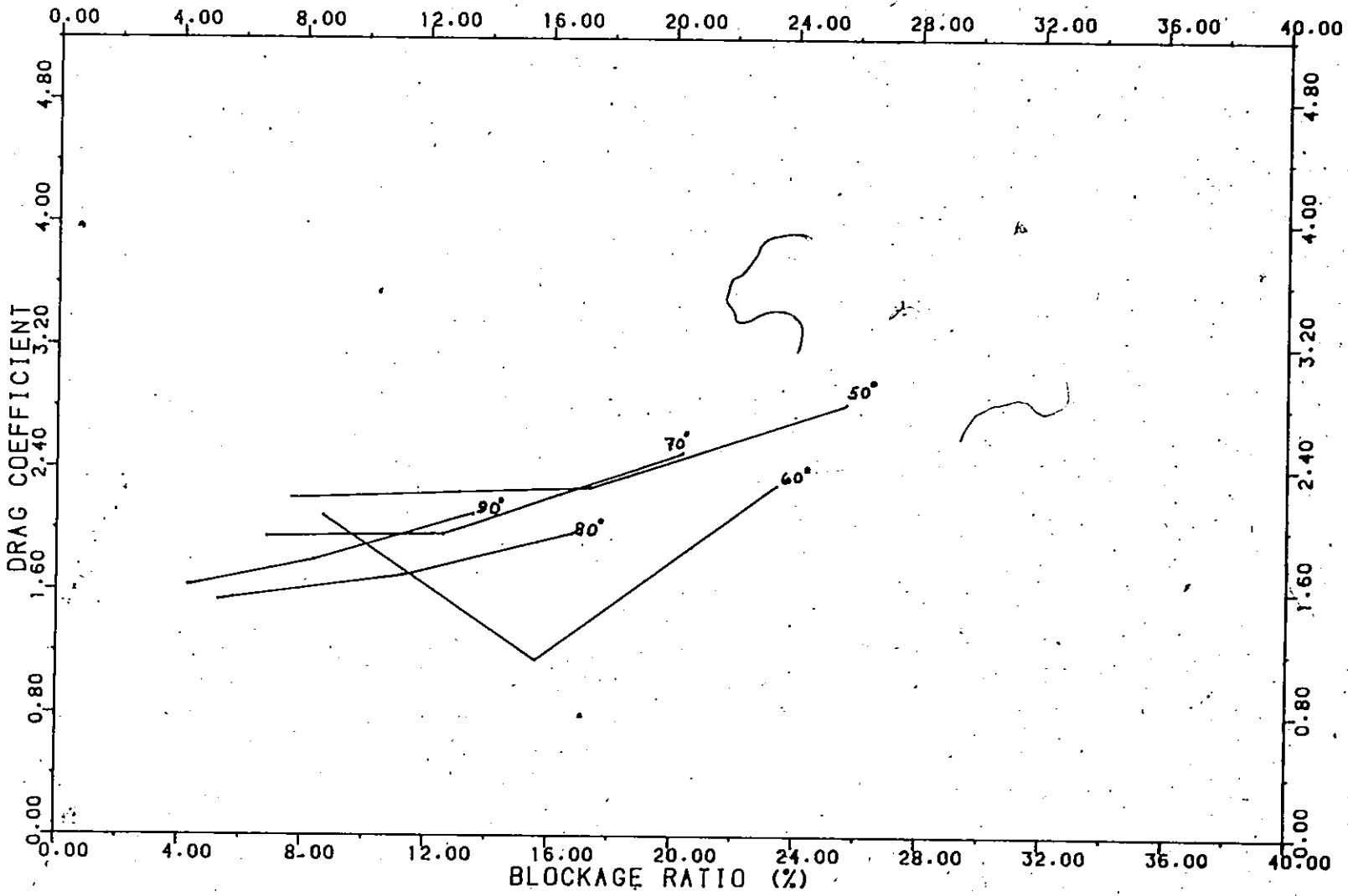

FIGURE 52 - DRAG COEFFICIENT VERSUS BLOCKAGE RATIO FOR SMOOTH FLOW BY PRESSURE MEASUREMENTS

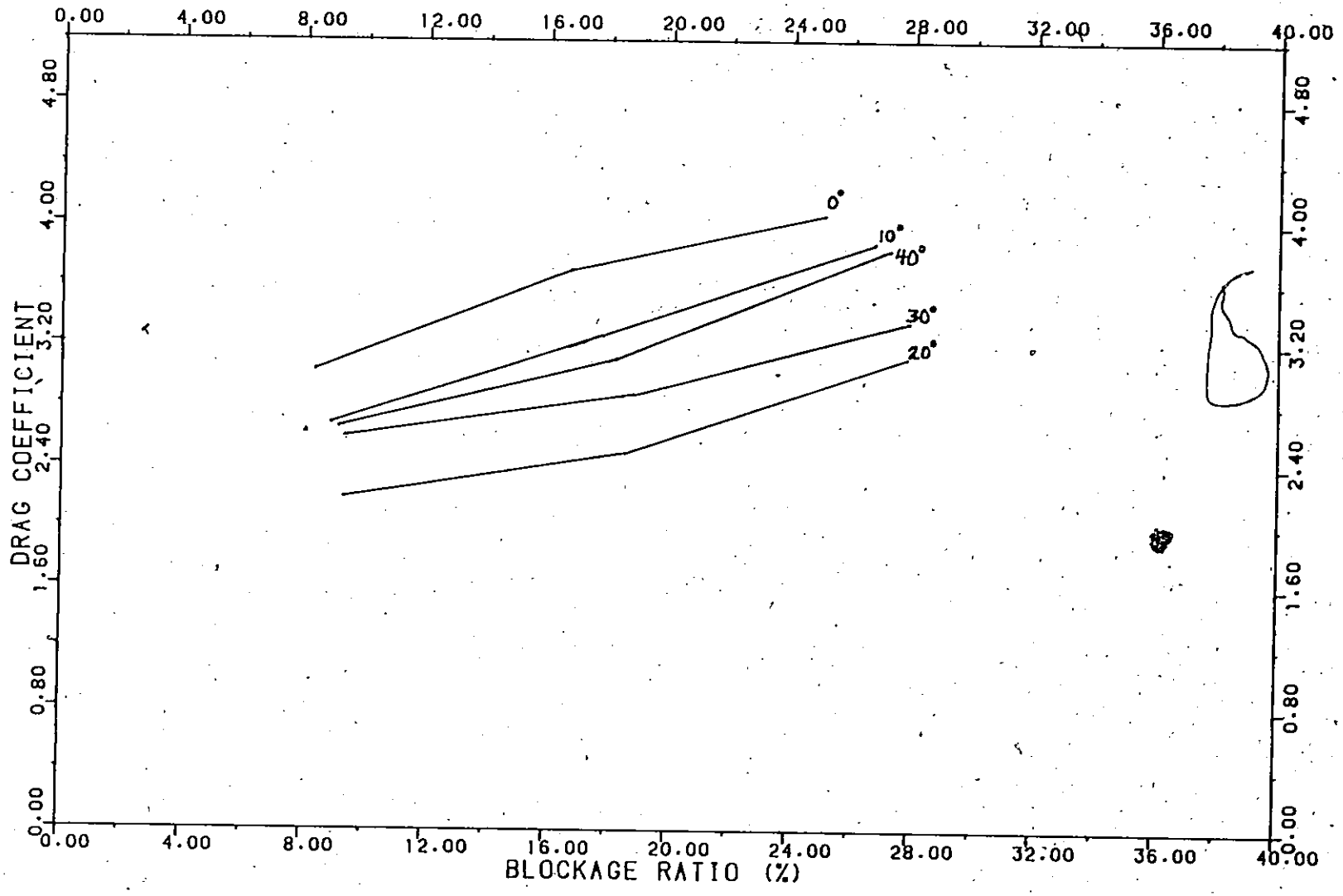

FIGURE 53 - DRAG COEFFICIENT VERSUS BLOCKAGE RATIO FOR TURBULENT FLOW (GRID 2) BY PRESSURE MEASUREMENTS

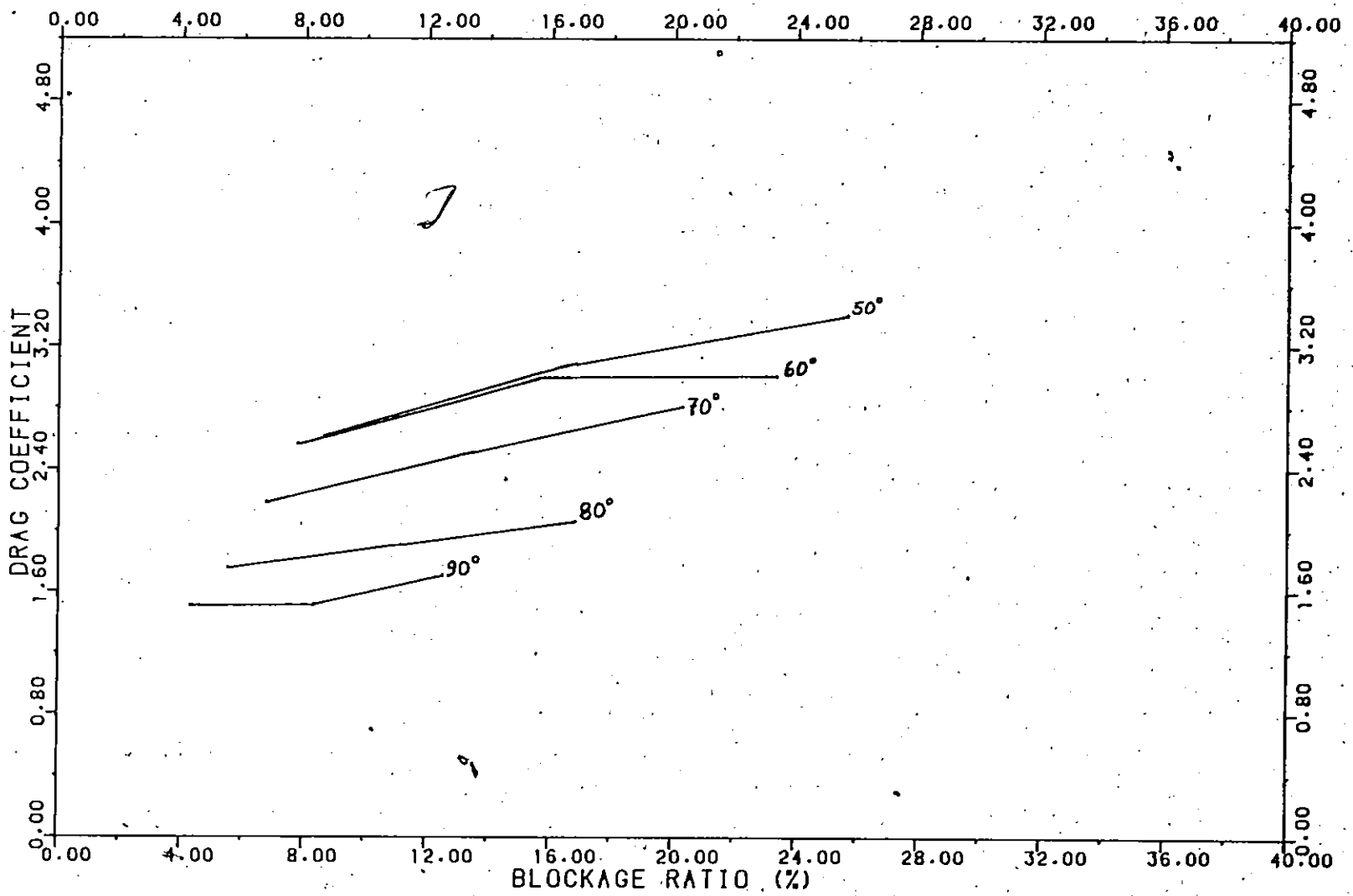

FIGURE 54 - DRAG COEFFICIENT VERSUS BLOCKAGE RATIO FOR TURBULENT FLOW (GRID 2) BY PRESSURE MEASUREMENTS

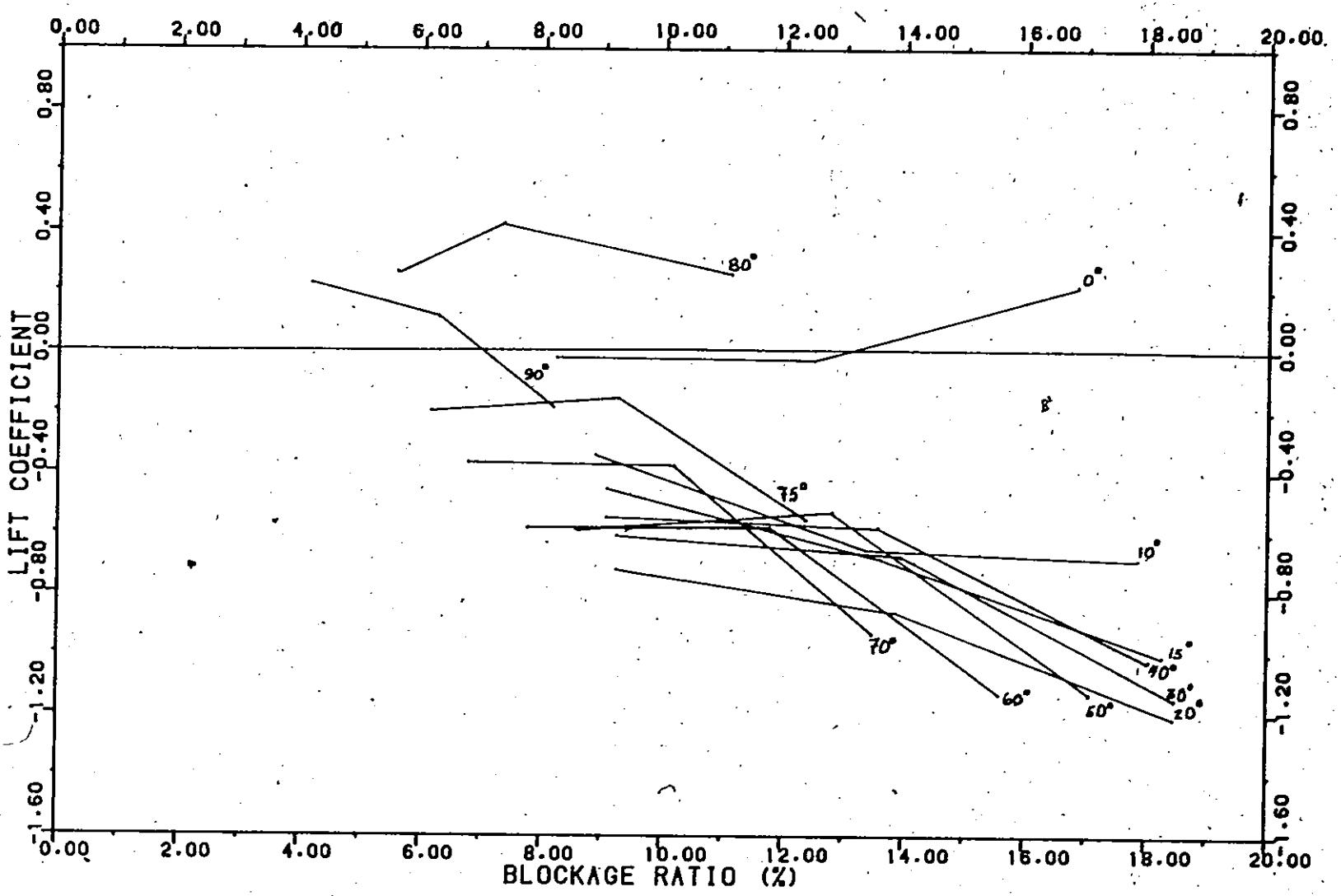

FIGURE 55 - LIFT COEFFICIENT VERSUS BLOCKAGE RATIO FOR SMOOTH FLOW

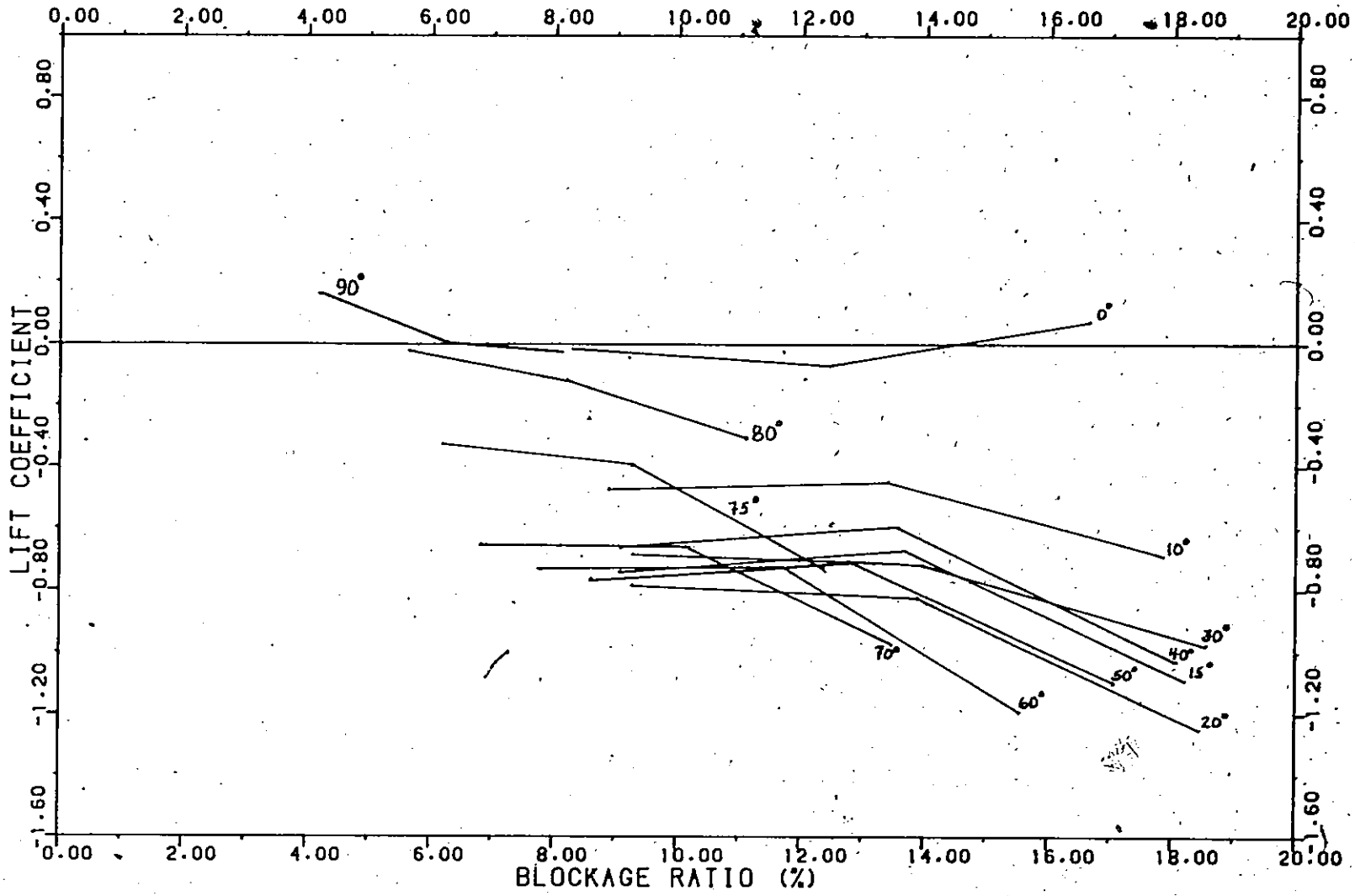

FIGURE 56 - LIFT COEFFICIENT VERSUS BLOCKAGE RATIO FOR TURBULENT FLOW (GRID 1)

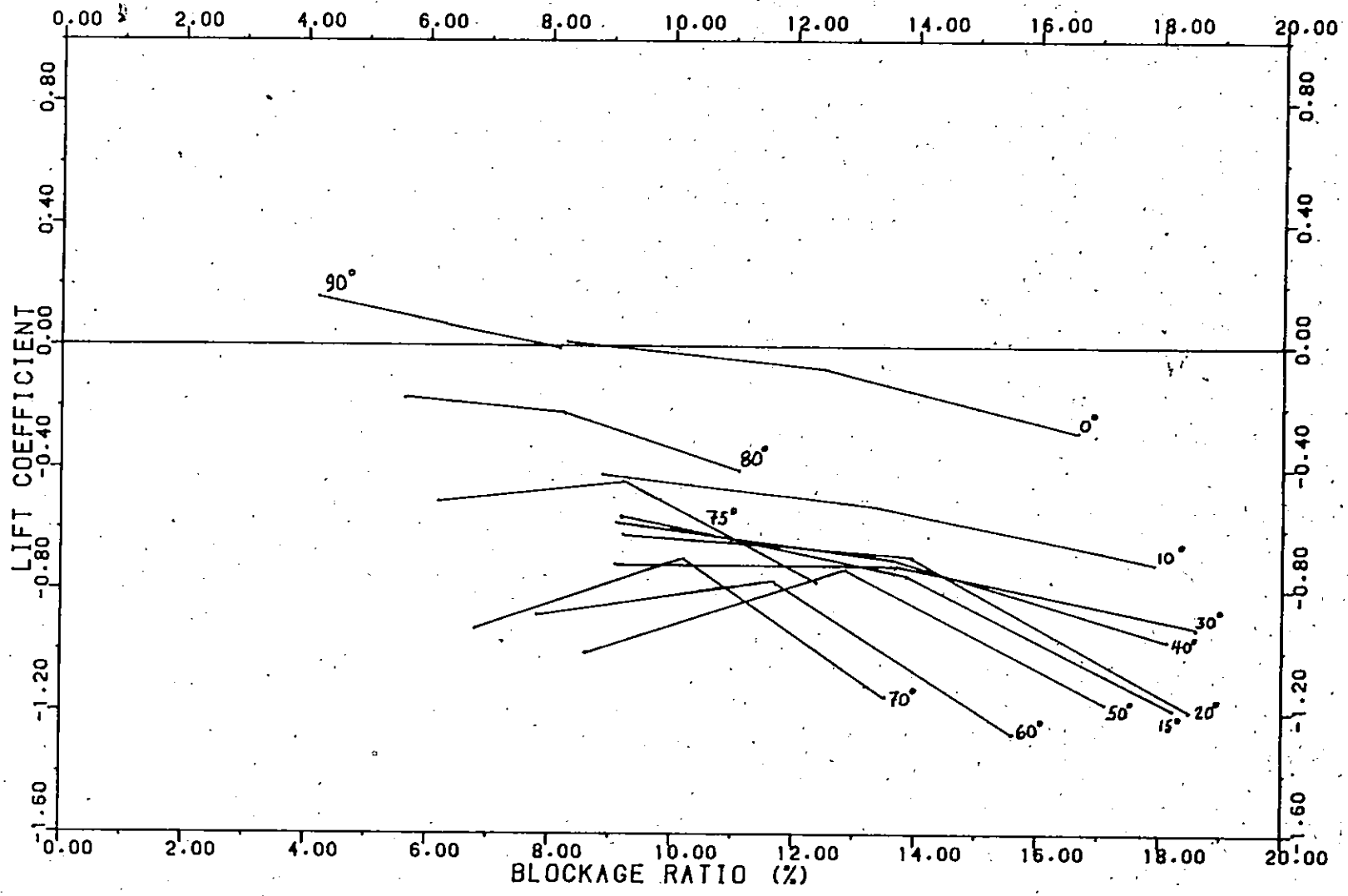

FIGURE 57 - LIFT COEFFICIENT VERSUS BLOCKAGE RATIO FOR TURBULENT FLOW (GRID 2)

TABLE 35

BASE PRESSURE COEFFICIENTS WITH RESPECT TO THE NORMALIZED GAP FOR AN ANGLE OF INCIDENCE OF 0°

	BASE PRESSURE COEFFICIENT					
NORMALIZED GAP	0.03125	0.0625	0.1500	0.1875	0.3000	0.3750
MODEL						
S36S	---	-1.54	---	---	-1.41	-1.33
S36T2	---	-2.33	---	---	-2.00	-1.79
36S	-2.27	---	-1.75	-1.69	---	---
36T2	-2.70	---	-2.48	-2.92	---	---

BASE PRESSURE COEFFICIENTS WITH RESPECT TO THE NORMALIZED GAP FOR AN ANGLE OF INCIDENCE OF 90°

	BASE PRESSURE COEFFICIENT					
NORMALIZED GAP	0.0625	0.1250	0.3000	0.3750	0.6000	0.7500
MODEL						
S36S	---	-0.62	---	---	-0.56	-0.58
S36T2	---	-0.50	---	---	-0.50	-0.46
36S	-0.73	---	-0.68	-0.70	---	---
36T2	-0.58	---	-0.56	-0.60	---	---

TABLE 36

COMPARISON OF BASE PRESSURE COEFFICIENTS OBTAINED FROM PRESSURE TESTS WITH THOSE REGRESSED FOR A ZERO NORMALIZED GAP

ANGLE OF INCIDENCE: $\alpha = 0°$

MODEL	C_{p_b} FROM PRESSURE TESTS	C_{p_b} REGRESSED FOR ZERO NORMALIZED GAP	% DIFFERENCE
S36S	-1.65	-1.61	2.4
S36T2	-2.14	-2.40	12.1
36S	-2.10	-2.05	2.4
36T2	-2.80	-2.76	1.4
		AVERAGE	4.6 %

ANGLE OF INCIDENCE: $\alpha = 90°$

MODEL	C_{p_b} FROM PRESSURE TESTS	C_{p_b} REGRESSED FOR ZERO NORMALIZED GAP	% DIFFERENCE
S36S	-0.69	-0.64	7.3
S36T2	-0.48	-0.51	6.2
36S	-0.84	-0.74	11.9
36T2	-0.56	-0.58	3.5
		AVERAGE	7.2 %

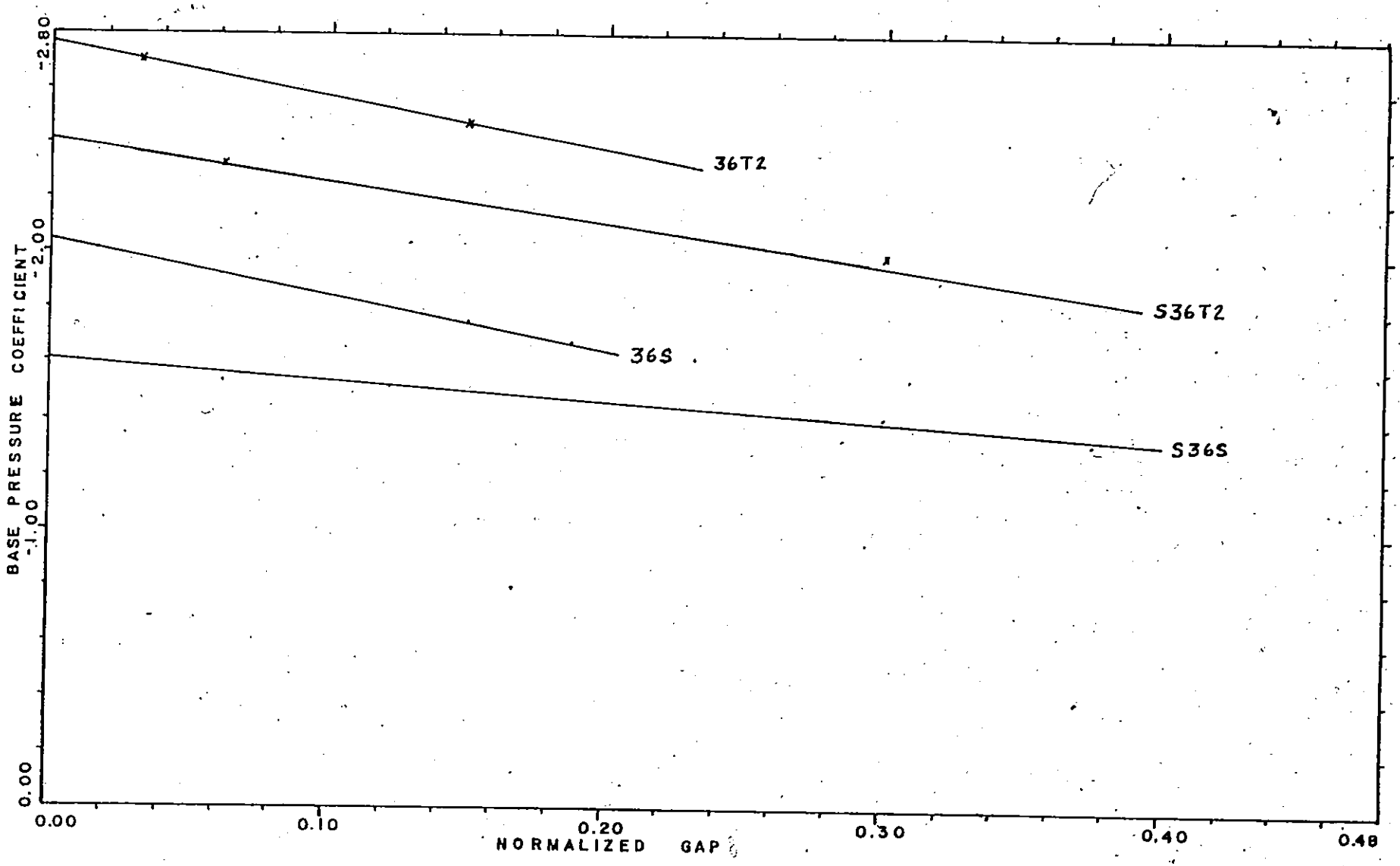

FIGURE 58 - BASE PRESSURE COEFFICIENT VERSUS NORMALIZED GAP FOR AN ANGLE OF INCIDENCE OF 0 DEGREES

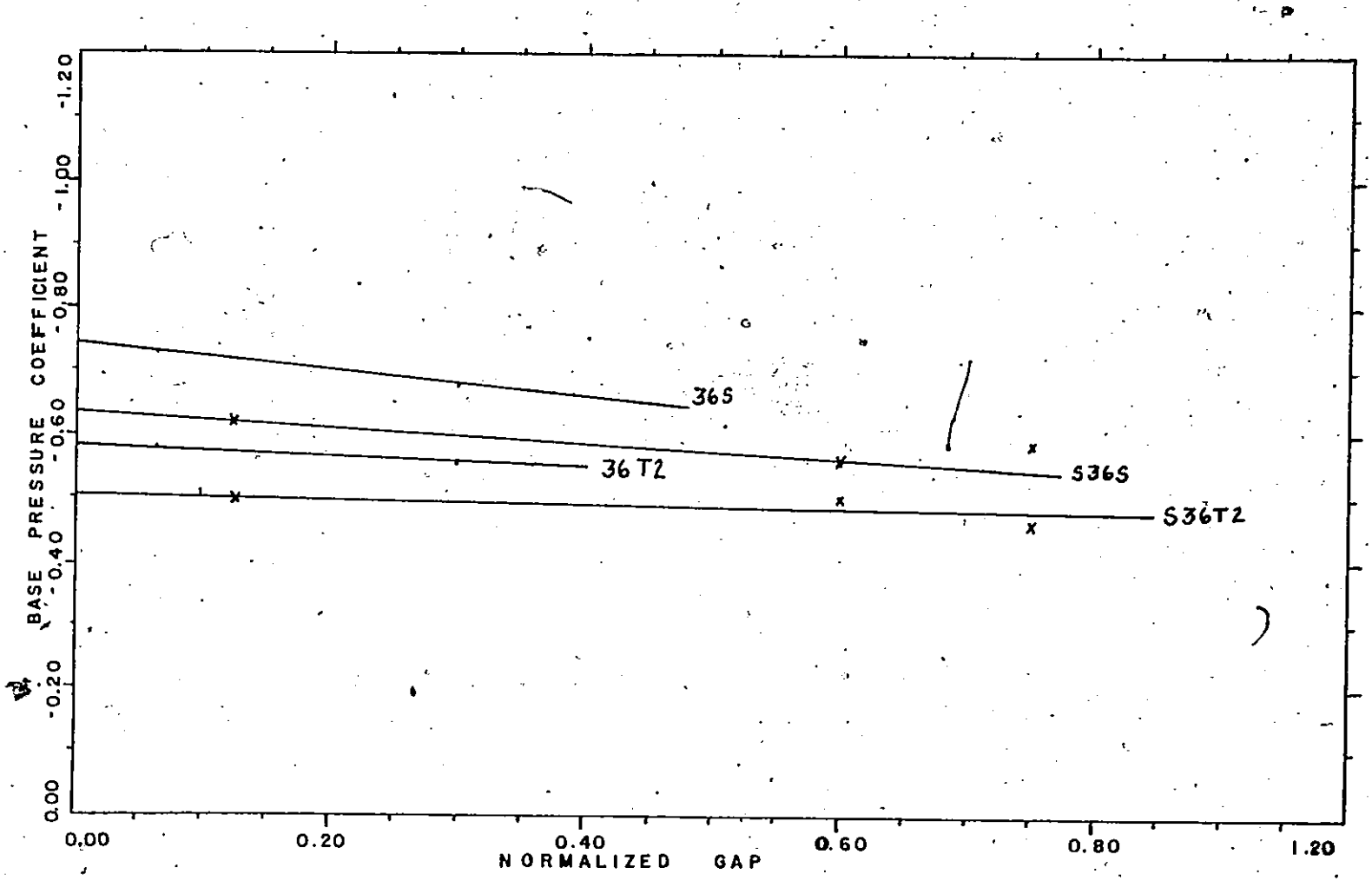

FIGURE 59 - BASE PRESSURE COEFFICIENT VERSUS NORMALIZED GAP FOR AN ANGLE OF INCIDENCE OF 90 DEGREES

TABLE 37

DRAG COEFFICIENT (2-D CASE) FROM STRAIN MEASUREMENTS CORRECTED ACCORDING TO THE DIFFERENT THEORIES AND EQUATIONS FOR MODEL S36S

ANGLE	CD_u	MASKELL	COWDREY	MODI	RAJU	LANEVILLE	DESROSIERS
0	2.073	1.778	1.775	1.814	1.734	1.891	1.915
2	1.998	1.719	1.707	1.745	1.667	1.821	1.842
4	1.930	1.665	1.644	1.682	1.605	1.756	1.775
6	1.834	1.590	1.559	1.595	1.521	1.666	1.683
8	1.788	1.552	1.516	1.551	1.479	1.622	1.636
10	1.785	1.548	1.511	1.547	1.474	1.618	1.631
15	1.716	1.491	1.446	1.482	1.410	1.551	1.562
20	1.573	1.380	1.323	1.356	N/A	N/A	1.428
30	1.479	1.306	1.242	1.273	N/A	N/A	1.341
40	1.582	1.391	1.336	1.368	N/A	N/A	1.442
50	1.667	1.466	1.422	1.454	N/A	N/A	1.534
60	1.533	1.376	1.328	1.355	N/A	N/A	1.432
70	1.399	1.282	1.236	1.257	N/A	N/A	1.331
75	1.225	1.142	1.095	1.112	1.190	1.136	1.179
80	1.106	1.044	1.000	1.014	1.077	1.033	1.076
82	1.105	1.046	1.004	1.017	1.077	1.036	1.080
84	1.207	1.141	1.103	1.117	1.179	1.136	1.186
86	1.254	1.186	1.152	1.165	1.226	1.184	1.238
88	1.287	1.220	1.188	1.201	1.260	1.219	1.277
90	1.463	1.382	1.358	1.372	1.434	1.391	1.458

TABLE 38

DRAG COEFFICIENT (2-D CASE) FROM STRAIN MEASUREMENTS CORRECTED ACCORDING TO THE DIFFERENT THEORIES AND EQUATIONS FOR MODEL S36T1

ANGLE	CD_u	MASKELL	COWDREY	MODI	RAJU	LANEVILLE	DESROSIERS
0	3.150	2.516	2.698	2.757	2.635	2.874	2.911
2	3.093	2.471	2.642	2.701	2.579	2.818	2.851
4	2.918	2.352	2.487	2.543	2.427	2.655	2.683
6	2.853	2.303	2.425	2.481	2.366	2.592	2.618
8	2.769	2.243	2.348	2.403	2.291	2.512	2.535
10	2.621	2.140	2.218	2.271	2.164	2.375	2.395
15	2.096	1.771	1.767	1.810	1.723	1.896	1.908
20	1.957	1.667	1.646	1.687	N/A	N/A	1.777
30	1.981	1.684	1.664	1.706	N/A	N/A	1.798
40	2.001	1.704	1.689	1.730	N/A	N/A	1.823
50	2.003	1.720	1.708	1.747	N/A	N/A	1.844
60	1.735	1.536	1.503	1.533	N/A	N/A	1.620
70	1.731	1.556	1.529	1.555	N/A	N/A	1.647
75	1.552	1.421	1.387	1.408	1.507	1.438	1.492
80	1.520	1.406	1.375	1.394	1.480	1.420	1.478
82	1.434	1.337	1.304	1.321	1.399	1.345	1.402
84	1.476	1.378	1.349	1.366	1.442	1.389	1.450
86	1.506	1.409	1.383	1.399	1.473	1.422	1.486
88	1.473	1.386	1.360	1.375	1.442	1.395	1.461
90	1.362	1.292	1.265	1.277	1.336	1.295	1.358

TABLE 39

DRAG COEFFICIENT (2-D CASE) FROM STRAIN MEASUREMENTS CORRECTED ACCORDING TO THE DIFFERENT THEORIES AND EQUATIONS FOR MODEL S36T2

ANGLE	CD_∞	MASKELL	COWDREY	MODI	RAJU	LANEVILLE	DESROSIERS
0	2.735	2.244	2.343	2.394	2.288	2.496	2.527
2	2.190	1.859	1.871	1.913	1.826	1.995	2.018
4	2.395	2.000	2.041	2.087	1.992	2.179	2.202
6	2.533	2.090	2.153	2.203	2.101	2.301	2.324
8	2.424	2.010	2.055	2.104	2.005	2.199	2.219
10	2.076	1.762	1.757	1.799	1.714	1.881	1.897
15	1.959	1.672	1.651	1.691	1.610	1.771	1.783
20	1.699	1.476	1.428	1.464	N/A	N/A	1.542
30	1.735	1.502	1.458	1.494	N/A	N/A	1.574
40	1.766	1.531	1.491	1.527	N/A	N/A	1.609
50	2.163	1.837	1.845	1.886	N/A	N/A	1.990
60	2.100	1.815	1.819	1.856	N/A	N/A	1.961
70	1.733	1.558	1.531	1.558	N/A	N/A	1.649
75	1.922	1.725	1.718	1.744	1.866	1.782	1.849
80	1.784	1.629	1.614	1.636	1.738	1.667	1.736
82	1.917	1.747	1.743	1.766	1.870	1.798	1.874
84	1.680	1.555	1.535	1.554	1.641	1.581	1.651
86	1.813	1.675	1.665	1.684	1.773	1.711	1.789
88	1.719	1.601	1.587	1.605	1.683	1.629	1.705
90	1.778	1.660	1.651	1.668	1.744	1.691	1.773

TABLE 40

DRAG COEFFICIENT (2-D CASE) FROM STRAIN MEASUREMENTS CORRECTED ACCORDING TO THE DIFFERENT THEORIES AND EQUATIONS FOR MODEL M36S

ANGLE	CD_u	MASKELL	COWDREY	MODI	RAJU	LANEVILLE	DESROSIERS
0	2.607	1.986	2.047	2.120	1.983	2.265	2.219
2	2.697	2.029	2.108	2.185	2.041	2.337	2.286
4	2.586	1.958	2.012	2.087	1.948	2.235	2.183
6	2.531	1.920	1.961	2.036	1.898	2.183	2.128
8	2.495	1.894	1.927	2.001	1.865	2.148	2.092
10	2.338	1.798	1.799	1.870	1.741	2.009	1.954
15	2.204	1.709	1.685	1.753	1.629	1.887	1.830
20	1.816	1.462	1.382	1.439	N/A	N/A	1.502
30	1.662	1.359	1.263	1.315	N/A	N/A	1.373
40	1.731	1.412	1.326	1.379	N/A	N/A	1.440
50	1.845	1.503	1.438	1.491	N/A	N/A	1.560
60	1.684	1.417	1.346	1.390	N/A	N/A	1.458
70	1.541	1.340	1.272	1.307	N/A	N/A	1.375
75	1.465	1.296	1.231	1.262	1.401	1.305	1.330
80	1.362	1.229	1.167	1.193	1.309	1.228	1.259
82	1.374	1.244	1.186	1.211	1.322	1.245	1.279
84	1.463	1.323	1.273	1.298	1.411	1.333	1.372
86	1.569	1.417	1.377	1.402	1.516	1.437	1.483
88	1.680	1.517	1.487	1.512	1.628	1.548	1.601
90	1.821	1.641	1.625	1.650	1.767	1.686	1.749

TABLE 41

DRAG COEFFICIENT (2-D CASE) FROM STRAIN MEASUREMENTS CORRECTED ACCORDING TO THE DIFFERENT THEORIES AND EQUATIONS FOR MODEL M36T1

ANGLE	CD_u	MASKELL	COWDREY	MODI	RAJU	LANEVILLE	DESROSIERS
0	2.935	2.171	2.304	2.387	2.233	2.550	2.499
2	2.923	2.155	2.284	2.368	2.212	2.533	2.477
4	2.763	2.059	2.150	2.230	2.082	2.389	2.333
6	2.710	2.022	2.100	2.180	2.033	2.337	2.279
8	2.556	1.929	1.973	2.050	1.910	2.200	2.142
10	2.412	1.841	1.856	1.929	1.796	2.073	2.016
15	2.228	1.723	1.703	1.772	1.647	1.907	1.850
20	1.963	1.556	1.494	1.556	N/A	N/A	1.624
30	1.892	1.510	1.438	1.498	N/A	N/A	1.563
40	1.997	1.584	1.530	1.591	N/A	N/A	1.662
50	1.908	1.545	1.487	1.543	N/A	N/A	1.614
60	1.834	1.522	1.466	1.514	N/A	N/A	1.588
70	1.670	1.436	1.379	1.417	N/A	N/A	1.490
75	1.536	1.351	1.291	1.323	1.468	1.368	1.394
80	1.484	1.327	1.272	1.300	1.426	1.338	1.372
82	1.510	1.355	1.305	1.331	1.454	1.369	1.407
84	1.508	1.360	1.313	1.339	1.455	1.374	1.415
86	1.458	1.326	1.280	1.303	1.409	1.336	1.379
88	1.406	1.289	1.244	1.265	1.362	1.295	1.340
90	1.513	1.387	1.350	1.371	1.469	1.401	1.453

TABLE 42

DRAG COEFFICIENT (2-D CASE) FROM STRAIN MEASUREMENTS CORRECTED ACCORDING TO THE DIFFERENT THEORIES AND EQUATIONS FOR MODEL M36T2

ANGLE	CD_u	MASKELL	COWDREY	MODI	RAJU	LANEVILLE	DESROSIERS
0	3.191	2.307	2.505	2.595	2.427	2.772	2.716
2	3.119	2.259	2.437	2.526	2.360	2.703	2.644
4	2.995	2.184	2.330	2.417	2.256	2.589	2.528
6	2.852	2.100	2.210	2.294	2.140	2.460	2.399
8	2.774	2.050	2.142	2.224	2.073	2.388	2.325
10	2.513	1.899	1.934	2.009	1.871	2.159	2.099
15	2.192	1.702	1.676	1.743	1.621	1.877	1.820
20	2.005	1.582	1.526	1.589	N/A	N/A	1.658
30	2.010	1.584	1.528	1.591	N/A	N/A	1.660
40	2.050	1.617	1.570	1.633	N/A	N/A	1.706
50	2.005	1.608	1.563	1.621	N/A	N/A	1.696
60	1.938	1.592	1.549	1.600	N/A	N/A	1.678
70	1.783	1.519	1.472	1.512	N/A	N/A	1.591
75	1.564	1.373	1.315	1.347	1.496	1.393	1.420
80	1.419	1.275	1.216	1.243	1.364	1.280	1.312
82	1.528	1.368	1.319	1.347	1.471	1.385	1.423
84	1.515	1.366	1.319	1.345	1.462	1.381	1.422
86	1.436	1.308	1.261	1.284	1.389	1.316	1.358
88	1.479	1.350	1.309	1.331	1.432	1.362	1.409
90	1.552	1.419	1.385	1.407	1.506	1.437	1.490

TABLE 43

DRAG COEFFICIENT (2-D CASE) FROM STRAIN MEASUREMENTS CORRECTED ACCORDING TO THE DIFFERENT THEORIES AND EQUATIONS FOR MODEL 36S

ANGLE	CD_u	MASKELL	COWDREY	MODI	RAJU	LANEVILLE	DESROSIERS
0	3.982	2.432	2.841	2.990	2.740	3.285	3.099
2	4.474	2.589	3.170	3.341	3.058	3.678	3.461
4	3.911	2.376	2.754	2.905	2.656	3.205	3.007
6	3.790	2.319	2.653	2.802	2.559	3.096	2.899
8	3.665	2.260	2.552	2.697	2.461	2.985	2.789
10	3.637	2.240	2.519	2.666	2.430	2.955	2.755
15	3.168	2.037	2.173	2.303	2.096	2.561	2.378
20	2.593	1.775	1.768	1.876	N/A	N/A	1.935
30	2.470	1.714	1.680	1.783	N/A	N/A	1.839
40	2.560	1.771	1.762	1.867	N/A	N/A	1.928
50	2.546	1.795	1.797	1.895	N/A	N/A	1.962
60	2.226	1.671	1.631	1.709	N/A	N/A	1.776
70	1.937	1.548	1.486	1.545	N/A	N/A	1.614
75	1.734	1.438	1.365	1.413	1.632	1.481	1.480
80	1.683	1.427	1.361	1.403	1.594	1.462	1.474
82	1.615	1.388	1.322	1.360	1.534	1.414	1.430
84	1.674	1.441	1.385	1.423	1.594	1.475	1.497
86	1.819	1.561	1.523	1.562	1.738	1.616	1.645
88	1.908	1.641	1.616	1.654	1.828	1.708	1.744
90	1.899	1.649	1.627	1.663	1.825	1.712	1.755

TABLE 44

DRAG COEFFICIENT (2-D CASE) FROM STRAIN MEASUREMENTS CORRECTED ACCORDING TO THE DIFFERENT THEORIES AND EQUATIONS FOR MODEL 36T1

ANGLE	CD_u	MASKELL	COWDREY	MODI	RAJU	LANEVILLE	DESROSIERS
0	4.489	2.613	3.202	3.371	3.089	3.704	3.494
2	4.452	2.582	3.154	3.324	3.042	3.660	3.443
4	4.297	2.513	3.025	3.191	2.918	3.520	3.304
6	4.180	2.459	2.926	3.090	2.822	3.415	3.197
8	4.009	2.387	2.791	2.951	2.692	3.266	3.051
10	3.819	2.308	2.646	2.799	2.551	3.103	2.893
15	3.263	2.076	2.238	2.372	2.158	2.637	2.449
20	2.754	1.849	1.877	1.992	N/A	N/A	2.055
30	2.582	1.767	1.756	1.864	N/A	N/A	1.922
40	2.680	1.828	1.845	1.954	N/A	N/A	2.018
50	2.514	1.780	1.775	1.871	N/A	N/A	1.938
60	2.281	1.702	1.671	1.751	N/A	N/A	1.820
70	1.984	1.577	1.522	1.582	N/A	N/A	1.653
75	1.792	1.478	1.411	1.461	1.687	1.531	1.530
80	1.605	1.371	1.299	1.339	1.521	1.395	1.406
82	1.562	1.348	1.278	1.315	1.484	1.367	1.382
84	1.501	1.312	1.242	1.276	1.430	1.324	1.343
86	1.464	1.292	1.225	1.256	1.398	1.300	1.323
88	1.500	1.330	1.270	1.300	1.437	1.343	1.371
90	1.618	1.432	1.386	1.416	1.554	1.459	1.495

TABLE 45

DRAG COEFFICIENT (2-D CASE) FROM STRAIN MEASUREMENTS CORRECTED ACCORDING TO THE DIFFERENT THEORIES AND EQUATIONS FOR MODEL 36T2

ANGLE	CD_u	MASKELL	COWDREY	MODI	RAJU	LANEVILLE	DESROSIERS
0	5.067	2.798	3.615	3.805	3.487	4.181	3.944
2	5.103	2.788	3.615	3.810	3.487	4.195	3.946
4	4.903	2.709	3.452	3.642	3.329	4.017	3.770
6	4.648	2.613	3.253	3.436	3.137	3.796	3.554
8	4.348	2.503	3.027	3.200	2.919	3.542	3.308
10	3.965	2.360	2.747	2.906	2.649	3.221	3.003
15	3.243	2.068	2.225	2.358	2.145	2.622	2.434
20	2.790	1.865	1.901	2.018	N/A	N/A	2.081
30	3.099	1.995	2.107	2.237	N/A	N/A	2.307
40	3.097	2.013	2.132	2.258	N/A	N/A	2.332
50	2.947	1.986	2.080	2.194	N/A	N/A	2.271
60	2.638	1.893	1.932	2,025	N/A	N/A	2.105
70	2.313	1.779	1.775	1.845	N/A	N/A	1.927
75	2.025	1.632	1.594	1.650	1.905	1.729	1.728
80	1.845	1.542	1.492	1.538	1.747	1.603	1.615
82	1.743	1.481	1.426	1.468	1.656	1.526	1.543
84	1.695	1.457	1.403	1.441	1.615	1.495	1.516
86	1.674	1.452	1.401	1.436	1.599	1.486	1.513
88	1.634	1.433	1.383	1.416	1.565	1.462	1.493
90	1.773	1.553	1.519	1.552	1.703	1.598	1.638

TABLE 46

DRAG COEFFICIENT (2-D CASE) FROM PRESSURE MEASUREMENTS CORRECTED ACCORDING TO THE DIFFERENT THEORIES AND EQUATIONS FOR MODEL B36S

ANGLE	CD_u	MASKELL	COWDREY	MODI	RAJU	LANEVILLE	DESROSIERS
-2	3.628	1.956	2.096	2.297	2.037	2.693	2.323
0	3.748	1.973	2.136	2.347	2.078	2.764	2.371
2	3.742	1.956	2.106	2.320	2.051	2.743	2.339
4	3.694	1.929	2.054	2.269	2.003	2.693	2.284
6	3.614	1.894	1.987	2.200	1.940	2.621	2.212
10	3.370	1.805	1.817	2.020	1.778	2.422	2.026
20	2.474	1.491	1.292	1.447	N/A	N/A	1.445
30	1.954	1.283	1.016	1.139	N/A	N/A	1.137
40	2.910	1.654	1.549	1.727	N/A	N/A	1.729
50	2.834	1.669	1.584	1.747	N/A	N/A	1.761
60	2.302	1.519	1.378	1.499	N/A	N/A	1.523
70	2.452	1.659	1.596	1.708	N/A	N/A	1.753
80	1.979	1.503	1.412	1.486	1.820	1.590	1.541
86	1.866	1.487	1.410	1.469	1.739	1.553	1.532
88	1.923	1.542	1.481	1.539	1.800	1.620	1.608
90	1.966	1.591	1.543	1.599	1.849	1.676	1.674
92	1.873	1.549	1.499	1.548	1.770	1.616	1.623

TABLE 47

DRAG COEFFICIENT (2-D CASE) FROM PRESSURE MEASUREMENTS CORRECTED ACCORDING TO THE DIFFERENT THEORIES AND EQUATIONS FOR MODEL B36T2

ANGLE	CD_a	MASKELL	COWDREY	MODI	RAJU	LANEVILLE	DESROSIERS
-2	4.108	2.087	2.373	2.600	2.306	3.049	2.631
0	4.080	2.061	2.326	2.555	2.262	3.009	2.581
2	4.205	2.075	2.366	2.607	2.305	3.083	2.629
4	4.168	2.050	2.318	2.560	2.260	3.038	2.577
10	3.898	1.947	2.102	2.337	2.057	2.801	2.343
20	3.157	1.714	1.649	1.846	N/A	N/A	1.844
30	3.367	1.770	1.751	1.963	N/A	N/A	1.959
40	3.842	1.918	2.045	2.280	N/A	N/A	2.283
50	3.393	1.849	1.896	2.092	N/A	N/A	2.108
60	3.014	1.800	1.805	1.963	N/A	N/A	1.995
70	2.794	1.809	1.819	1.946	N/A	N/A	1.997
80	2.060	1.550	1.470	1.547	1.894	1.655	1.604
86	1.907	1.513	1.441	1.502	1.777	1.587	1.566
88	1.694	1.392	1.305	1.356	1.586	1.427	1.416
90	1.673	1.393	1.313	1.360	1.573	1.426	1.424
92	1.666	1.405	1.333	1.377	1.574	1.438	1.444

TABLE 48

CORRECTED DRAG COEFFICIENTS ACCORDING TO THE DIFFERENT CORRECTION FORMULAE FOR SMOOTH FLOW

ANGLE OF INCIDENCE: $\alpha = 0°$

MODEL	C_{D_u}	S/C	MASKELL	COWDREY	MODI	RANGA RAJU	LANEVILLE	DESROSIERS
1X2	2.278	0.083	1.928	1.953	1.995	1.906	2.079	1.988
1.5X3	2.607	0.125	1.986	2.048	2.120	1.983	2.265	2.062
2X4	2.962	0.167	2.008	2.111	2.222	2.037	2.443	2.134
3X6	3.748	0.250	1.973	2.136	2.347	2.078	2.764	2.078
4X8	4.730	0.333	1.883	2.021	2.375	2.060	3.076	2.044
			1.956±.045	2.054±.065	2.212±.142	2.013±.062	2.525±.356	2.061±.047

ANGLE OF INCIDENCE: $\alpha = 90°$

MODEL	C_{D_u}	S/C	MASKELL	COWDREY	MODI	RANGA RAJU	LANEVILLE	DESROSIERS
1X2	1.652	0.042	1.542	1.533	1.548	1.620	1.570	1.493
1.5X3	1.821	0.063	1.620	1.624	1.649	1.767	1.686	1.600
2X4	1.805	0.083	1.545	1.547	1.581	1.734	1.628	1.485
3X6	1.966	0.125	1.591	1.543	1.599	1.849	1.676	1.487
4X8	2.162	0.167	1.606	1.541	1.622	1.988	1.736	1.467
			1.581±.032	1.558±.034	1.600±.034	1.792±.123	1.659±.056	1.048±.048

N.B. ALL VALUES OF C_{D_u} ARE OBTAINED FROM THE PRESSURE MEASUREMENTS EXCEPT FOR THE 1.5X3 MODEL WHERE C_{D_u} IS OBTAINED FROM THE STRAIN MEASUREMENTS PLUS 14%.

TABLE 49

CORRECTED DRAG COEFFICIENTS ACCORDING TO THE DIFFERENT CORRECTION FORMULAE FOR TURBULENT FLOW (GRID 2)

ANGLE OF INCIDENCE: $\alpha = 0°$

MODEL	C_{D_u}	S/C	MASKELL	COWDREY	MODI	RANGA RAJU	LANEVILLE	DESROSIERS
1X2	3.064	0.083	2.461	2.627	2.684	2.565	2.797	2.653
1.5X3	3.191	0.125	2.307	2.505	2.595	2.427	2.772	2.462
2X4	3.709	0.167	2.326	2.644	2.783	2.550	3.059	2.561
3X6	4.080	0.250	2.061	2.326	2.555	2.262	3.009	2.315
4X8	5.130	0.333	1.943	2.192	2.576	2.237	3.336	2.312
			2.220±.189	2.459±.175	2.639±.085	2.408±.085	2.995±.205	2.461±.134

ANGLE OF INCIDENCE: $\alpha = 90°$

MODEL	C_{D_u}	S/C	MASKELL	COWDREY	MODI	RANGA RAJU	LANEVILLE	DESROSIERS
1X2	1.515	0.042	1.428	1.406	1.420	1.485	1.440	1.429
1.5X3	1.552	0.063	1.419	1.384	1.406	1.506	1.437	1.413
2X4	1.515	0.083	1.352	1.299	1.327	1.456	1.367	1.335
3X6	1.673	0.125	1.393	1.313	1.360	1.573	1.426	1.367
4X8	1.848	0.167	1.426	1.317	1.387	1.699	1.484	1.352
			1.404±.029	1.344±.043	1.380±.033	1.544±.087	1.431±.038	1.379±.036

N.B. ALL VALUES OF C_{D_u} ARE OBTAINED FROM THE PRESSURE MEASUREMENTS EXCEPT FOR THE 1.5X3 MODEL WHERE C_{D_u} IS OBTAINED FROM THE STRAIN MEASUREMENTS PLUS 14%.

TABLE 50

CORRECTED DRAG COEFFICIENTS ACCORDING TO THE DIFFERENT CORRECTION FORMULAE FOR SMOOTH FLOW

ANGLE OF INCIDENCE: $\alpha = 30°$

MODEL	C_{D_u}	S/C	MASKELL	COWDREY	MODI	RANGA RAJU	LANEVILLE	DESROSIERS
1X2	1.803	0.0930	1.553	1.515	1.552	---	---	1.549
2X4	1.837	0.1860	1.383	1.249	1.326	---	---	1.339
3X6	1.954	0.2790	1.283	1.016	1.139	---	---	1.245
			1.406±.111	1.260±.204	1.339±.169			1.378±.127

ANGLE OF INCIDENCE: $\alpha = 60°$

MODEL	C_{D_u}	S/C	MASKELL	COWDREY	MODI	RANGA RAJU	LANEVILLE	DESROSIERS
1X2	2.197	0.0778	1.887	1.903	1.941	---	---	1.965
2X4	1.185	0.1555	1.007	0.868	0.910	---	---	0.948
3X6	2.302	0.2333	1.519	1.378	1.499	---	---	1.658
			1.703±.184	1.641±.263	1.720±.221			1.812±.154

NEGLECT - PROBABLE ERROR

TABLE 51

CORRECTED DRAG COEFFICIENTS ACCORDING TO THE DIFFERENT CORRECTION FORMULAE FOR TURBULENT FLOW (GRID 2)

ANGLE OF INCIDENCE: $\alpha = 30°$

MODEL	C_{D_u}	S/C	MASKELL	COWDREY	MODI	RANGA RAJU	LANEVILLE	DESROSIERS
1X2	2.592	0.930	2.105	2.177	2.232	---	---	2.157
2X4	2.859	0.1860	1.893	1.944	2.064	---	---	1.975
3X6	3.367	0.2790	1.770	1.751	1.963	---	---	1.911
			1.923±.138	1.957±.174	2.086±.111			2.104±.104

ANGLE OF INCIDENCE: $\alpha = 60°$

MODEL	C_{D_u}	S/C	MASKELL	COWDREY	MODI	RANGA RAJU	LANEVILLE	DESROSIERS
1X2	2.577	0.0778	2.161	2.232	2.277	---	---	2.241
2X4	2.988	0.1555	2.066	2.189	2.293	---	---	2.189
3X6	3.014	0.233	1.799	1.805	1.963	---	---	1.984
			2.009±.153	2.075±.192	2.178±.152			2.138±.111